DESIGN AND PERFORMANCE ANALYSIS OF QUADRATIC-FORM RECEIVERS FOR FADING CHANNELS

LI RONG

M. Eng, Northwestern Polytechnical University, P. R. China

A THESIS SUBMITTED
FOR THE DEGREE OF DOCTOR OF PHILOSOPHY

DEPARTMENT OF ELECTRICAL
AND COMPUTER ENGINEERING

NATIONAL UNIVERSITY OF SINGAPORE

2007

Acknowledgements

I would like to express my deepest appreciation to my supervisor, Prof. Pooi Yuen Kam, for his expert and enlightening guidance in the achievement of this work. He gave me lots of encouragement and constant support throughout my Ph. D studies, and inspired me to learn more about wireless communications and other research areas.

I would also like to thank my colleagues and friends in the Communications Lab and the ECE-I^{2}R Wireless Communication Lab for their generous help and warm friendship during these years.

Finally, I would like to extend my sincere thanks to my family. They have been a constant source of love and support for me all these years.

Contents

Abstract

Quadratic-form receivers (QFRs), which have quadratic-form decision metrics, are commonly used in various detections for fading channels.

As one important type of QFRs, quadratic receivers (QRs) are usually employed when sending additional training signals to acquire channel state information (CSI) at the receiver is infeasible. In multiple-input-multiple-output (MIMO) systems, such a QR is used to perform maximum-likelihood detection for unitary space–time modulation (USTM) which has been widely accepted as a bandwidth-efficient approach to achieving the high capacity promised by MIMO systems. In this dissertation, we first derive some tight bounds on the pairwise error probability (PEP) of the QR for USTM over the Rayleigh block-fading channel, and discuss their implications to constellation design. Then to realize the large performance improvement potential of USTM offered by having perfect CSI at the receiver, we design three generalized quadratic receivers (GQRs) to incorporate channel estimation in detecting various unitary space–time constellations without the help of additional training signals. These GQRs acquire CSI based on the received data signals themselves, and thus conserve bandwidth resources. Their PEP reduces from that of the QR to that of the coherent receiver as the channel memory span exploited in channel estimation increases. A closed-form expression of the PEP is derived for two of the GQRs under certain conditions.

We next turn our attention to the performance analysis of QFRs in general. It is well known that the first-order and the generalized Marcum Q-functions arise very often in such performance analyses. Thus, we study these Marcum

Q-functions in detail by using a geometric approach. For the first-order Marcum Q-function, some finite-integral representations are first derived. Then some closed-form generic bounds and simple bounds are proposed, which involve only exponential functions and/or complementary error functions. Some generic and simple single-integral bounds are also developed. The generic bounds involve an arbitrarily large number of terms, and approach the exact value of the first-order Marcum Q-function as the number of terms involved increases. The simple bounds involve only a few terms, and are tighter than the existing exponential bounds for a wide range of values of the arguments. For the mth-order Marcum Q-function, some closed-form representations are derived for the case of the order m being an odd multiple of 0.5, and some finite-integral representations and closed-form generic bounds are derived for the case of m being an integer. In addition, we prove that this function is an increasing function of its order. Thus, the Marcum Q-function of integer order m can be upper and lower bounded by the Marcum Q-function of orders $(m + 0.5)$ and $(m - 0.5)$, respectively, and these bounds can be evaluated by using our new closed-form representation.

Based on the new representations and bounds for the first-order Marcum Q-function, we obtain a new single-finite-integral expression and some closed-form bounds for the average bit error probability of QFRs over fading channels for a variety of single-channel, differentially coherent and quadratic detections.

List of Figures

List of Tables

List of Abbreviations and Symbols

Abbreviations

ASK	amplitude-shift keying
AUB	asymptotic union bound
AWGN	additive white Gaussian noise
BEP	block error probability
CDF	cumulative distribution function
CF	characteristic function
CR	coherent receiver
CSI	channel state information
CUB	Chernoff upper bound
DPSK	differential phase-shift keying
DQPSK	differential quadrature phase-shift keying
DUSTM	differential unitary space–time modulation
EGC	equal gain combining
FSK	frequency-shift keying
GQR	generalized quadratic receiver
i.i.d.	independent, identically distributed
LRT	likelihood ratio test
MAP	maximum a posteriori probability
MGF	moment generating function

MIMO	multiple-input-multiple-output
MISO	multiple-input-single-output
ML	maximum-likelihood
MMSE	minimum mean-square error
MSE	mean-square error
NOUSTC	nonorthogonal unitary space–time constellations
OUSTC	orthogonal unitary space–time constellations
PDF	probability density function
PEP	pairwise error probability
PSK	phase-shift keying
QFR	quadratic-form receiver
QR	quadratic receiver
RHS	right-hand side
SC	selection combining
SER	symbol error rate
SIMO	single-input-multiple-output
SNR	signal-to-noise ratio
STBC	space–time block codes
STC	space–time coding
STTC	space–time trellis codes
USTC	unitary space–time constellations
USTC-OD	unitary space–time constellations with orthogonal design
USTM	unitary space–time modulation

Symbols

$(\cdot)^*$	the conjugate operation
$(\cdot)^\dagger$	the transpose conjugate operation
$(\cdot)^\top$	the transpose operation
$\det(\mathbf{A})$	the determinant of matrix $\mathbf{A}$
$\Gamma(\cdot)$	the Gamma function

$\jmath$	$\jmath = \sqrt{-1}$
$\mathbb{N}$	the set of all natural numbers
$\mathbf{0}$	the zero column vector or matrix
$\mathbf{0}_N$	the zero matrix of size N
$\mathbf{A} \otimes \mathbf{B}$	the Kronecker product of the matrices $\mathbf{A}$ and $\mathbf{B}$, where each element of $\mathbf{A}$ is multiplied by the matrix $\mathbf{B}$
$\mathbf{I}_N$	the identity matrix of size N
$\mathcal{CN}(u, \sigma^2)$	the circularly symmetric, complex Gaussian distribution with mean u and variance σ^2
$\mathcal{N}(u, \sigma^2)$	the Gaussian distribution with mean u and variance σ^2
$\text{diag}(a_1, a_2, \cdots, a_n)$	the diagonal matrix with the diagonal entries $a_1, a_2, \cdots, a_n$
$\text{erfc}(\cdot)$	the complementary error function
$\exp(\cdot)$	the exponential function
$\text{E}[\cdot]$	the expectation operation
$\Pr(\cdot)$	the probability of the event in the brackets
$\text{Re}\{\cdot\}$	the real part of the quantity in the brackets
$\text{sign}(\cdot)$	the three-valued sign function
$\text{tr}(\mathbf{A})$	the trace of matrix $\mathbf{A}$
$\text{vec}(\mathbf{A})$	the vectorization of the matrix $\mathbf{A}$ formed by stacking the columns of $\mathbf{A}$ into a single column vector
$\lvert \cdot \rvert$	the absolute value of the quantity inside
$\lVert \cdot \rVert$	the Frobenius norm
$I_m(\cdot)$	the mth-order modified Bessel function of the first kind
$J_0(\cdot)$	the zeroth-order Bessel function of the first kind
$Q(\cdot)$	the Gaussian Q function
$Q(\cdot, \cdot)$	the first order Marcum Q function
$Q_m(\cdot, \cdot)$	the generalized Marcum Q function
mod	the modulo operation with $n \bmod n = 0$
modulo	the modulo operation with $n \text{ modulo } n = n$

Chapter 1

Introduction

High data rate communications through wireless channels have become more and more popular during the last two decades. This requires a corresponding improvement in the transmission rate and reliability of wireless communication systems. In single-antenna systems, an obstacle to achieve reliable wireless communications is multipath fading. Multipath fading refers to the random amplitude and phase variations of the received signal, which arise from constructive or destructive additions of multiple delayed and attenuated versions of the transmitted signal received from different paths due to reflection, diffraction and scattering of radio waves by surrounding objects. When destructive addition occurs, the received signal strength is diminished, and this attenuated signal is hard to detect. An effective method to mitigate the negative effect of fading is to use diversity techniques [1]. Diversity techniques provide multiple replicas of the information-bearing signal received from multiple, independent fading channels. Since these fading channels are statistically independent, the probability of all these replicas suffering deep fades at the same time is small. Thus, at each time instant, there is at least one replica whose strength is high enough for the receiver to detect. Diversity can be provided in different domains. In the frequency domain, frequency diversity can be obtained by using multiple carriers or wideband signals. In the temporal domain, time diversity can be obtained by using channel cod-

ing and interleaving. In the spatial domain, space diversity can be obtained by using multiple antennas separated by a few wavelengths. These three types of diversity techniques can be exploited separately or jointly. In a system exploiting space diversity, multiple antennas can be used either at the transmitter, or at the receiver, or both. These various configurations are referred to as multiple-input-single-output (MISO), single-input-multiple-output (SIMO), and multiple-input-multiple-output (MIMO) systems, respectively. It has been shown that MIMO systems have a potential to offer a significant increase in the theoretical channel capacity [2–4].

At the receiver side, various receiver structures can be used to detect the received faded signals. A brief overview of receivers commonly used for fading channels is given in the following section.

1.1 Overview of Receivers for Fading Channels

In a fading environment, the received signals are detected at the receiver according to the modulation scheme used in transmission and the availability of knowledge on channel state information (CSI).

In digital communication systems, digital information data can be transmitted by modulating one or more of the amplitude, phase and frequency of the carrier. The modulation schemes with only one of the carrier attributes being modulated at M levels are called M-ary amplitude-shift keying (ASK), M-ary frequency-shift keying (FSK), and M-ary phase-shift keying (PSK).

In the simpler case that the received signal is only corrupted by additive white Gaussian noise (AWGN), the type of detection techniques used depends on the availability of knowledge of the carrier phase at the receiver [1, 5]. If the receiver has perfect knowledge on the carrier phase as well as the carrier frequency, it can reconstruct the carrier accurately and use this carrier to perform a complex conjugate demodulation of the received signal. Thus, coherent detection

is performed by this coherent receiver (CR). If the receiver has partial knowledge of the carrier phase, and only can reconstruct the carrier with phase errors, then partially coherent detection can be performed. If the receiver has no knowledge of the carrier phase and also makes no attempt to estimate it, the received signals can be demodulated by using a zero-phase carrier reference. Then quadratic detection (also referred to as square-law detection) can be performed by using a quadratic receiver (QR) (also referred to as square-law receiver) to detect only the squared envelopes of the outputs of the matched filters corresponding to all the possible transmitted signals. Envelope detection can also be used, which is performed by using a matched-filter-envelope-detector, and is equivalent to quadratic detection. These energy detections cannot be employed with M-ary PSK modulation, since for M-ary PSK, the information is carried by the carrier phase.

In the case that the received signal is corrupted by channel fading as well as AWGN, the effect of the channel gains should also be taken into account in detections. In this case, the carrier phase can be regarded as a part of the random phase introduced by the channel fading [1, 5]. If the channel gains are perfectly known to the receiver, a CR can be used, in which the channel gains are employed as a coherent reference in data detections [6, 7]. However, the channel gains are in practice not known to the receiver. One solution to this problem is to send training signals, and to estimate the channel gains at the receiver [8, 9]. The estimate of the channel gains can be used as a partially coherent reference, and partially coherent detection can be performed [10–12]. This solution requires additional bandwidth resources for sending training signals. To save bandwidth resources, we can send training signals only at the beginning of a data frame, and then use the decision-feedback method to estimate the channel gains during the rest of the data frame [13–16]. This decision-feedback method has a shortcoming, i.e., undesired error propagation may occur. An alternative solution is to use some detection techniques which do not require channel estimation at the receiver. If the channel fading is slow enough and the channel gains over two successive intervals

are approximately the same, differential transmission and detection can be used [1, 5, 17–19]. The information data to be communicated in the current interval are carried by the transmitted signals in the previous and current intervals, and the receiver takes the received signal in the previous interval as a reference to arrive at the decision on the current information data. When the channel fades rapidly, the performance of differential detection may degrade substantially. Quadratic detection is another common technique, which uses a QR to detect signals without extracting CSI. Since a QR yields decisions based on the squared envelopes, the decision metric of a QR is usually given in terms of the norm squares of complex Gaussian random variables [1, 5, 20, 21].

In addition to quadratic detection, decision metrics of many receivers in coherent, partially coherent and differentially coherent detections can also be cast into a quadratic form of complex Gaussian random variables, and all these receivers can be classified as quadratic-form receivers (QFRs). The concept of the QFR is obviously more general than the QR, because in addition to the norm squares of random variables, a quadratic-form decision metric may also include cross terms. Since QFRs have such wide applications, it is worth putting some effort into the design and performance analysis of QFRs. In the following, a literature review of QFRs and some related topics will be given.

1.2 Review of Quadratic-Form Receivers and Related Topics

The quadratic-form receiver is one of the most common receiver structures used in various detections. In this section, we will first review some important results presented in the literature for general forms of QFRs. Then among all kinds of QFRs, we put emphasis on the QR and its generalization, i.e., the generalized quadratic receiver (GQR), in SIMO systems. Since this GQR has shown some great properties in improving the error performance of the QR, it is desirable to

extend this technique to other systems. To investigate the possibility of extending the idea of the GQR to MIMO systems, we will review some popular schemes used in MIMO systems to determine which scheme can profit from this technique and deserves further study. In addition to extending the GQR concept to MIMO systems, we are also interested in the performance analysis of QFRs in general. Since the Marcum Q-functions are often involved in this performance analysis, it is helpful to learn more about their behavior. We will review some results on the Marcum Q-functions in the last part of this section.

1.2.1 Quadratic-Form Receivers

For single-channel detections, a unified performance analysis for both FSK with quadratic detection and PSK with differentially coherent detection was first given in [22] and presented later in [20]. In the PSK case, a transformation corresponding to a 45° rotation in the coordinate system was used to obtain a decision metric similar to that in quadratic detection. Thus, the decision rule for both the cases was formulated as a comparison between the squared norms of two independent, nonzero-mean, complex Gaussian random variables. The corresponding error probability was given in terms of the first-order Marcum Q-function. A pair of tight upper and lower bounds on this error probability was given in [23].

For multi-channel detections, there are two types of general quadratic-form decision metrics in complex Gaussian variables discussed in the literature. The first type is given by a sum of independent random variables, each of which corresponds to a channel and is a weighted sum of norm squares and cross terms of two correlated, complex Gaussian random variables [24–29]. It applies to various detections if different values are set for the three sets of weights, two sets of real weights for norm squares and one set of complex weights for cross terms. In [24], a simpler case was first considered, in which the values of the weights are independent of the channel index, and the Gaussian random variables have zero means and

channel-independent variances and covariances. The probability density function (PDF) and the characteristic function (CF) of this simpler quadratic form, as well as its probability of being positive or negative, were given in closed form. In [25], the discussion was extended to the nonzero mean case. The CF of the quadratic form was given in closed form, and the probability of the quadratic form being negative was evaluated by using the results in [30]. An alternative expression for this probability was derived similarly in [26]. Compared to these two results, Proakis' result for the same probability derived in [27] and presented in [1, Appendix B] is much more well-known. Proakis' result was given in terms of the first-order Marcum Q-function and the modified Bessel functions of the first kind, and was further rewritten in terms of the generalized Marcum Q-function in [31]. In [28], the PDF and the cumulative distribution function (CDF) of the above quadratic form were given in terms of infinite series. It was also shown in [26, 28] that the above quadratic form in nonzero-mean complex Gaussian variables is equivalent to a weighted sum of two independent, normalized, noncentral chi-square random variables which have the same number of degrees of freedom, i.e., twice the number of independent channels, and different noncentrality parameters. Thus, it is clear that to evaluate the CDF of the above quadratic form at an argument value of zero is equivalent to evaluating the probability of one noncentral chi-square random variable exceeding another with the same number of degrees of freedom. The latter probability was evaluated in [32] as a generalization of the case in [22], but only a two-fold infinite series result was obtained, not as simple as those in [25–28]. In [33], the discussion was further extended to the case of a weighted sum of two independent, noncentral chi-square variables with different numbers of degrees of freedom. The CDF of this quadratic form evaluated at an argument value of zero was given in a form similar to that in [1, Appendix B] or in [31], i.e., given in terms of the generalized Marcum Q-function. In [29], the quadratic form in [24] was extended in the sense that the weights, variances and covariances of zero-mean complex Gaussian variables can be nonidentical for different channels.

The CF of this quadratic form was given in closed form, and the CDF was given in terms of residues.

The second type of general quadratic-form decision metric in complex Gaussian variables is written in terms of an indefinite Hermitian quadratic form of a complex Gaussian random vector [20, 34–38]. This general form applies to various detections by using different definitions for the Gaussian random vector and the Hermitian matrix. The closed-form CF of this quadratic form was first given in [34] for the case that the complex Gaussian random vector has a nonzero mean vector and a nonsingular covariance matrix. Some alternative expressions for this CF were given in [20, Appendix B] and [38]. For the case that the complex Gaussian random vector has a zero mean vector, the CDF of the central quadratic form was evaluated at an argument value of zero in [35] with a closed-form result, and evaluated at an argument value of arbitrary real number in [37] with residue-form results. For the case that the complex Gaussian random vector has a nonzero mean vector, the PDF and the CDF of the noncentral quadratic form were given in [36] in terms of infinite series expansions. In [36] and [20, Appendix B], the indefinite quadratic form of a complex Gaussian random vector with nonzero-mean and correlated elements was shown to be equivalent to a weighted sum of norm squares of independent complex Gaussian random variables with different nonzero means and identical variances. This was further shown in [36] to be a weighted sum of independent, normalized chi-square random variables with different numbers of degrees of freedom and different noncentrality parameters. In [39], an indefinite quadratic form in a real Gaussian random vector was also shown to be equivalent to a weighted sum of independent, normalized chi-square random variables with different numbers of degrees of freedom and different noncentrality parameters. Hence, all the results in [39] and its references for indefinite quadratic forms, or for linear combinations of noncentral chi-square variables can be applied directly to the complex quadratic form.

From the above literature review, we can see that QFRs have a wide range

of usage, and are involved in various detections. Although a lot of work has been done for evaluating the distributions of the general quadratic forms, only for some special cases have the PDF and the CDF been given explicitly in finite closed-form expressions. In the explicit, closed-form expressions of the CDF evaluated at an argument value of zero, the Marcum Q-functions are often involved, which will be discussed later in this section.

Having given a review of the general forms of the QFR, we next concentrate on its special cases, i.e., the QR and the GQR in SIMO systems.

1.2.2 Quadratic Receiver and Generalized Quadratic Receiver in SIMO Systems

In SIMO systems, if the channel gains are unknown to the receiver, the optimal receiver for binary orthogonal signals is a QR [40, ch. 7]. This QR compares the norm squares of the two received signal vectors. Each of these vectors consists of the outputs of the filters matched to one possible transmitted signal for multiple, independent Rayleigh fading channels. In [41], Kam proposed that this QR is identical to a detector–estimator receiver. This is because in the new coordinate system obtained by rotating the original coordinate system counterclockwise 45°, the binary orthogonal signal structure can be considered as the combination of an antipodal signal set and an unmodulated component. The unmodulated component of the received signal can be used as a channel measurement in the estimator to obtain an estimate of the channel gains. This channel estimate then provides a partially coherent reference for the detector in detecting the data carried by the antipodal signaling component of the received signal. Thus, the QR is actually not a noncoherent receiver, and there is no receiver which is completely noncoherent.

An immediate benefit of this new interpretation for the QR is that it shows clearly the possibility of obtaining an error performance much better than that of the QR by improving the accuracy of the channel estimate without consuming any additional bandwidth resource. This possibility was extensively investigated

in [42] by introducing a new concept, i.e., the generalized quadratic receiver. The main idea of the GQR was to exploit the correlation or the memory of the channel between signaling intervals by using also the received signals over the adjacent intervals in the channel estimation. The channel estimation accuracy can thus be improved, and this leads to an improvement in the error performance. Thus, when the channel estimation is just based on the CSI contained in the received signal in the current interval, the GQR shows the same error performance as the QR. When the channel estimation also exploits the CSI contained in the received signals over the adjacent intervals, the GQR will provide a better error performance than the QR. If the channel fading is slow enough, the error performance of the GQR asymptotically approaches that of the CR as the number of signal intervals involved in the channel estimation increases. Since this GQR only extracts the CSI contained in the data signals themselves, it does not require additional bandwidth for sending additional training signals, and in this sense is superior to other partially coherent detections.

Although the GQR has been shown to have many good properties in dealing with binary orthogonal signals in SIMO systems, its extension to MIMO systems has not been investigated in the literature. To extend the GQR concept to MIMO systems, we need to first examine some popular schemes designed for MIMO systems, and determine schemes for which it is possible to design a GQR.

1.2.3 Space–Time Coding and Unitary Space–Time Modulation

Space–time coding (STC) is a technique designed to provide diversity, multiplexing and coding gains and to achieve the capacity of MIMO systems [4, 6, 7, 21, 43–50]. The theoretical capacity of MIMO systems over flat Rayleigh fading channels has been shown to increase linearly with the smaller of the number of transmit and the number of receive antennas in high signal-to-noise ratio (SNR) regime, provided that the channel gains between all pairs of transmit and

receive antennas are statistically independent and known to the receiver [2–4].

To achieve this capacity, Tarokh *et al.* first introduced space–time trellis codes (STTC) in [6], which offer transmit diversity and coding gains without bandwidth expansion. The performance of STTC with or without channel estimation errors, mobility, and multiple paths was investigated in [6, 44]. The famous rank and determinant code design criteria were proposed therein for Rayleigh and Rician channels. Although STTC can simultaneously offer a substantial coding gain, spectral efficiency, and diversity improvement for flat fading channels, this scheme has a potential drawback that the maximum-likelihood (ML) decoding complexity grows exponentially with transmission rate and the required diversity order. Thus, the realizable transmission rate may be limited by the available decoder complexity.

To solve this problem, Alamouti first proposed a much simpler scheme to provide full transmit diversity for systems with two transmit antennas in [43], but this scheme suffers a performance loss compared to STTC. Alamouti's scheme requires no bandwidth expansion and only needs linear decoding because of the orthogonality of the transmitted matrix. Inspired by Alamouti's scheme, Tarokh *et al.* introduced the term space–time block codes (STBC) in [7], and applied the theory of generalized orthogonal designs to the construction of STBC with the maximum diversity order for an arbitrary number of transmit antennas. Like Alamouti's scheme, the orthogonal structure of STBC makes it possible to use a ML decoding algorithm based only on linear processing at the receiver. A shortcoming of STBC is that the coding gain provided by STBC is very limited. Besides, non-full rate STBC will introduce bandwidth expansion.

The good performance of the above space–time schemes is based on the assumption that perfect CSI is available to the receiver and coherent detection is performed. CSI can be obtained at the receiver by performing channel estimation. When channel estimation is imperfect, the performance of STTC and STBC will degrade [4, 44, 51–53]. Since neither coherent detection nor partially coherent

detection employs QRs in data detections, we cannot extend the GQR concept to the schemes STTC and STBC.

In some scenarios, sending training signals to acquire CSI at the receiver is not desirable or feasible, due to the limited bandwidth resources or rapid changes in the channel characteristics. For such scenarios, Hochwald and Marzetta proposed in [21, 45, 54] a scheme called unitary space–time modulation (USTM) which does not require either the receiver or the transmitter to know the channel gains. In the USTM scheme, transmitted signal matrices are orthonormal in time across the antennas. They are selected from unitary space–time constellations (USTC) according to the input information bits, and are transmitted through multiple transmit antennas in a time-block which is composed of a number of coherent symbol periods. The USTM scheme can achieve full channel capacity at high SNR either when combined with channel coding over multiple independent fading intervals [21, 45, 54], or when the length of the coherence interval and the number of transmit antennas are sufficiently large (called autocoding) [55–58]. It was shown in [21] that a QR is required for ML detection in USTM over the flat Rayleigh block-fading channel. This QR seeks to maximize the squared length of the projection of the received matrix onto the complex subspaces spanned by the possible transmitted matrices. Since USTM has been widely accepted as an important, capacity-achieving space–time coding scheme, it is worth investigating the performance of the QR and developing some GQRs for USTM to improve its error performance.

In [21], Hochwald and Marzetta analyzed the error performance of the QR for USTM. The pairwise error probability (PEP) of the QR was given in terms of residues for arbitrary USTC. For the special case that the product of the two unitary signal matrices concerned has equal singular values, this PEP expression can be reduced to a simple closed form. However, for the general case of unequal singular values, this PEP expression requires one to compute residues, and thus cannot give much insight on the performance of USTM. An alternative closed-form

expression was derived in [59] for both the cases of equal and unequal singular values by using Craig's formula for the Gaussian probability integral [60]. However, this PEP expression involves the computation of high-order derivatives, and is not so straightforward and desirable in analytical applications.

Since there is no simple, explicit, closed-form expression for the exact PEP of the QR for USTM available so far, to meet the demands for rapid evaluation of the USTM performance in analytical applications such as signal design, researchers have to resort to bounds on the exact PEP. Hochwald and Marzetta derived in [21] a Chernoff upper bound (CUB) in closed form. From this CUB, two signal design criteria have been developed. The first one is called diversity sum criterion [54, 61, 62], which is valid for low SNR or small singular values. The second one is called diversity product criterion [19, 62], which is valid for high SNR. However, the diversity sum criterion cannot guarantee full diversity, and both of these two criteria cannot guarantee a low symbol error rate (SER). To solve this problem, McCloud *et al.* proposed in [63] an asymptotic union bound (AUB) design criterion for high SNR and correlated channels, based on the asymptotic error probability analysis of QFRs in [37]. Compared with the diversity product and diversity sum criteria, this AUB design criterion can provide signal constellations with a better SER performance, but its form is more complicated and will consume more computation time. Since designing new optimal USTC to provide better error performance with simple encoding and decoding complexity is of great interest [21, 54–59, 61–72], it is still desirable to develop some new, simple and tight bounds on the PEP of the QR for USTM to facilitate signal design.

In addition to the receiver design and error performance analysis for the scenario where CSI is unknown to the receiver, Hochwald and Marzetta also gave in [21] the results for the scenario where CSI is perfectly known to the receiver. The performance advantage for knowing perfect CSI was shown to be a 2 to 4 dB gain in SNR [21, 54]. Although the scheme of USTM was designed mainly for the scenario where neither the transmitter nor the receiver knows the channel

gains, the large performance potential offered by the channel knowledge provides a great motivation to incorporate channel estimation and perform partially coherent detection in USTM. To estimate the channel, sending training signals is a method commonly used [9, 10, 38, 64, 73]. However, this method will reduce the bandwidth efficiency. In the literature, little work has been done in designing and analyzing partially coherent receivers for USTM [10, 38, 73]. No attempt has been made to develop a channel estimation method for USTM, which does not require the help of additional training signals, and which exploits the channel memory to improve the USTM performance. Thus, if it is possible to extend the GQR concept to USTM, we may improve the error performance of USTM significantly without sacrificing bandwidth efficiency.

Another well-known technique used when neither the receiver nor the transmitter has knowledge of CSI is differential transmission and detection. This technique was also extended to MIMO systems employing space–time coding. Differential unitary space–time modulation (DUSTM) was proposed in [18, 19] under the assumption that the channel gains were approximately constant over two consecutive time-blocks. This scheme can be seen as an extension of standard differential PSK to MIMO systems, and has attracted great interest from many researchers [18, 19, 38, 73–97]. In addition to USTM, STBC was also combined with differential technique in [17, 98–102]. Since these differential schemes do not use QRs in their data detections, we cannot extend the GQR concept to them. Thus, we will not discuss them further in this dissertation.

In addition to the performance analysis of QRs and design of GQRs in MIMO systems, we are also interested in the error performance analysis of a general QFR, which takes the general quadratic form in complex Gaussian random variables as the decision metric and is a general form of many QFRs of interest. From the literature review on QFRs in Section 1.2.1, we can see that the first-order Marcum Q-function and the generalized Marcum Q-function are often involved in the expressions of the error performance of the general QFR. Thus, we next review

some important results in the literature for these two Marcum Q-functions.

1.2.4 Marcum Q-Functions

The first-order Marcum Q-function, $Q(\cdot,\cdot)$, was first introduced in [103, 104]. It is the tail probability of a normalized Rician random variable. Similarly, the generalized Marcum Q-function, $Q_m(\cdot,\cdot)$, is the tail probability of a generalized normalized Rician random variable, or equivalently the tail probability of a normalized noncentral chi-square random variable with $2m$ degrees of freedom [1, 5]. The canonical forms of these two functions were given in terms of an infinite integral with an integrand involving the modified Bessel function of the first kind, over an argument-dependent range. While a lot of work has been done for the numerical computation of these Marcum Q-functions [105–112], it is often desirable to have a further analytical handle by which a more detailed evaluation of the system performance can be carried out, providing one with, for instance, insights into optimization of system performance with respect to system parameters. In problems involving transmission over fading channels especially, one often would also need to do statistical averaging over the arguments of the functions, and thus need to evaluate infinite integrals involving the Marcum Q-functions numerically and analytically. In these scenarios, using the canonical forms of the Marcum Q-functions may be unsuitable. Some alternative representations for the Marcum Q-functions were developed in [113–115], which involve only a finite integral over one or two exponential integrands. Another alternative representation was given in [116], which involves the zeroth-order modified Bessel function of the first kind and a finite integral over an integrand involving the exponential function and the complementary error function. The alternative representations in [113, 114] have been used to deal with many performance analysis problems in [5, 31, 117–119]. They can help to reduce some numerical computation problems involving the Marcum Q-functions, and even can lead to some closed-form results in further analytical manipulations of the Marcum Q-functions in some cases.

However, not all problems can be solved by using these alternative representations. Thus, bounding the Marcum Q-functions using some simpler closed-form functions, such as the exponential function, the complementary error function, and the modified Bessel function of the first kind, may be needed to facilitate analytical work involving the Marcum Q-functions. Some exponential bounds were derived in [23, 114, 120, 121]. Some more complicated bounds, which involve the modified Bessel function together with the exponential function and/or the complementary error function, were given in [116, 121, 122]. All the approaches used so far in the references mentioned to obtain representations and bounds for the Marcum Q-functions have been purely mathematical, usually resorting to alternative representations and bounds on the functions involved in defining the Marcum Q-functions. The bounds obtained either are simple enough but not sufficiently tight, or are complicated and not easy to use in theoretical analyses. Thus, bounds which are tight and defined in terms of simple functions, such as the exponential function and the complementary error function, are still of interest. In addition to the closed-form bounds, it may also be helpful to derive some bounds which involve finite integrals but can lead to closed-form results in the further analytical manipulations of the Marcum Q-functions.

1.3 Research Objectives

As addressed in the above section, QFRs have great significance in communication systems. In our study on QFRs, we begin by evaluating the error performance of the QR for USTM. As mentioned in Section 1.2.3, although the USTM scheme is one of important STC techniques and has attracted a great deal of attention, the exact PEP expressions of the QR for USTM over the flat Rayleigh block-fading channel were still given in implicit forms, involving the computation of either residues or high-order derivatives. Thus, one of our objectives here is to develop some new, simple, tight, upper and lower bounds on the PEP of the QR

for USTM, which can be used as better approximations to the PEP and can give some insights into the signal design criteria.

In addition to deriving new bounds on the PEP of the QR, we are also interested in designing new receivers for USTM to improve its error performance further. As mentioned in Section 1.2.3, the error performance of USTM can be significantly improved by learning and using perfect CSI at the receiver. The studies in the literature have all resorted to sending training signals to acquire CSI, and thus require additional bandwidth resources. This motivates us to extend the GQR concept reviewed in Section 1.2.2 to USTM so that the large performance gap between the QR and the CR can be bridged, and at the same time the merit of USTM, i.e., not wasting bandwidth resources for additional training signals, can be kept.

After designing and analyzing the GQRs for USTM, we will extend our work to the performance analysis of QFRs in general. As mentioned in Section 1.2.4, the first-order Marcum Q-function and the generalized Marcum Q-function are frequently involved in the performance analysis of QFRs. All the alternative representations and bounds available in the literature were developed by using mathematical approaches, and these bounds may be either not tight enough in some applications or too complicated to use in further analytical manipulations. Our work here is to use a geometric approach to derive some new, simpler representations and tighter bounds for the first-order and the generalized Marcum Q-functions, which can be used to facilitate the evaluation of the error performance of QFRs.

Furthermore, it is also within our research interests to use newly derived representations and bounds for the first-order Marcum Q-function to derive some new representations and bounds for the average bit error probability of QFRs over fading channels in a variety of single-channel, differentially coherent and quadratic detections.

1.4 Research Contributions

We propose in Chapter 2 two upper bounds and one lower bound on the PEP of the QR for USTM over the flat Rayleigh block-fading channel. Our first upper bound is tighter than the CUB in the literature at high SNR. Our second upper bound is much tighter than the CUB over the entire SNR range. Our lower bound is tighter than the lower bound in the literature at low SNR. Our second upper bound and our lower bound are very close to each other. In some cases, they are even equal, and give the exact expression for the PEP. Implications of these two bounds for the USTM constellation design are discussed. These implications can improve the existing design criteria, and may help in designing some new constellations which have a better error performance than those available in the literature.

To further improve the error performance of USTM, we extend the idea of the GQR to the USTM scheme over the flat Rayleigh block-fading channel in Chapter 3. Three GQRs are designed for various USTC in which signal matrices may or may not contain explicit, inherent training blocks, and may or may not be orthogonal to one another. The newly derived GQRs incorporate a linear minimum mean-square error (MMSE) channel estimator. They extract the CSI inherent in the received data signals themselves, and thus conserve bandwidth resources. They can provide a substantial improvement in error performance over the QR, and in fact, their error performance approaches that of the CR as the channel memory span exploited in channel estimation increases. A closed-form expression of the PEP is derived for two of the GQRs with USTC satisfying certain conditions. This PEP expression is given in terms of the mean-square error of the channel estimate, and thus shows clearly the dependence of the error performance on the channel estimation accuracy. Our simulation results agree well with these theoretical analyses on the error performance. In addition, the GQR designed for a certain class of USTC is simplified, and its complexity for large-sized constellations can be even less than that of the QR or that of the simplified

form of the QR.

To facilitate the error performance analysis of QFRs, we evaluate the first-order Marcum Q-function in Chapter 4 by using a geometric approach. Based on the geometric view of the first-order Marcum Q-function, some new finite-integral representations and some closed-form or single-integral bounds are derived. The new finite-integral representations are simpler than those in the literature. The new bounds include the generic and simple exponential bounds which involve only exponential functions, the generic and simple erfc bounds which involve only complementary error functions, together with exponential functions in some cases, and the generic and simple single-integral bounds which involve finite, single integrals with simple exponential integrands. The generic bounds involve an arbitrarily large number of terms, and approach the exact value of the first-order Marcum Q-function as the number of terms involved increases. The simple exponential bounds and erfc bounds are tighter than the exponential bounds in the literature over a wide range of values of the arguments.

Extensions to the generalized Marcum Q-function are presented in Chapter 5. For the case of the order m being an odd multiple of one half, a new closed-form representation is obtained for $Q_m(\cdot,\cdot)$, which involves only simple exponential functions and simple complementary error functions. For the case of integer order m, some new finite-integral representations, generic exponential bounds and generic erfc bounds are obtained. In addition, we prove that the generalized Marcum Q-function is an increasing function of the order m. Thus, the new closed-form representation for m being an odd multiple of one half can be used to evaluate the upper bound $Q_{m+0.5}(\cdot,\cdot)$ and the lower bound $Q_{m-0.5}(\cdot,\cdot)$ on $Q_m(\cdot,\cdot)$ of integer order m, and the average of these upper and lower bounds is also a good approximation of $Q_m(\cdot,\cdot)$.

By using our new representations, generic exponential bounds and simple erfc bounds for the first-order Marcum Q-function, we also obtain in Chapter 6 a new finite-integral expression and some new, closed-form, upper and lower bounds

for the average bit error probability of a general QFR over fading channels. This general QFR is a general form of QFRs in a variety of single-channel, differentially coherent and quadratic detections. Our new upper performance bounds are tighter than those in the literature for some cases of interest. Although there may be some lower bounds derived in the literature for some special cases of this general QFR, our new lower performance bounds are the first lower bounds available on the average bit error probability of this general QFR, and they are shown to be tight.

1.5 Organization of the Dissertation

In Chapter 2, we first present some background material on STC and USTM. Then we propose some new, tight, upper and lower bounds on the PEP of the QR for USTM over the flat Rayleigh block-fading channel, and discuss the implications of these bounds for the USTM constellation design.

In Chapter 3, we first review the basic idea of the GQR for binary orthogonal signals in the SIMO system. Then we investigate the design and performance analysis of GQRs for USTM over the flat Rayleigh block-fading channel.

In Chapter 4, we present the geometric view of the first-order Marcum Q-function. Then based on this view, we derive some new finite-integral representations and some new upper and lower bounds on the first-order Marcum Q-function.

In Chapter 5, we extend the geometric view to the generalized Marcum Q-function. Based on this view, we give some new, closed-form or finite-integral representations and some new upper and lower bounds on the generalized Marcum Q-function.

In Chapter 6, we illustrate some applications of the new representations and bounds for the first-order Marcum Q-function to the error performance analysis of QFRs in a variety of single-channel, differentially coherent and quadratic detections.

In Chapter 7, we give the conclusions for the current work, and a plan for

our future work.

Chapter 2

Unitary Space–Time Modulation

Space–time coding is a technique designed for approaching the information theoretic capacity limit of MIMO channels. It introduces joint correlation in transmitted signals in both the space and time domains, and has been well documented as an attractive means of achieving high data rate transmissions with diversity and coding gains over spatially uncoded systems. For the scenarios where perfect CSI or the channel estimate is available to the receiver, STTC and STBC were proposed as the coding schemes [6, 7, 43, 44]. For the scenarios where sending additional training signals to extract CSI is infeasible or impractical, Marzetta and Hochwald analyzed the capacity of multiple-antenna links without knowledge of channel gains at both transmitters and receivers [45]. For a flat Rayleigh block-fading channel, they suggested a signal constellation comprising complex-valued unitary signal matrices that are orthonormal with respect to time among the transmit antennas, called USTM. Then they gave further explanations about some issues of USTM in [21, 54] such as modulation, demodulation, error performance and signal design. Interestingly, USTM has been justified not only for the case that the channel is unknown to the receiver, but also for the case that the channel is known to the receiver [21, 74]. Hochwald and Marzetta argued in [21] that when the channel is known to the receiver and the length of coherence interval is sufficiently large, USTM is nearly optimal in the sense of achieving capacity.

Hughes also showed in [74] that when applying the rank and determinant signal design criteria in coherent detection, all optimal full-rank space–time group codes are unitary. These results suggest that USTM may also play an important role when the channel is known. This makes it more meaningful to focus on study on USTM.

In this chapter, a space–time coded system model is first given in Section 2.1. Then some important results in the literature for USTM over flat Rayleigh block-fading channels are summarized in Sections 2.2–2.5 on the issues of capacity-achieving signal structure, ML receiver design, error performance analysis, and signal design. For each issue, the case where the channel is unknown and the case where the channel is known to the receiver are both considered. Finally, in Section 2.6, some new, tight, upper and lower bounds on the PEP of the ML receiver for USTM are derived for the case that the channel is unknown.

2.1 Space–Time Coded System Model

In this section, we present a general STC system model which applies to STTC [6], STBC [7, 43], and USTM [21]. Consider a baseband space–time coded system with N_T transmit antennas and N_R receive antennas over fading channels, as shown in Fig. 2.1. In each time-block which consists of T symbol periods $t = 1, \cdots, T$, a block of information bits is fed into the space–time encoder and mapped into a $T \times N_T$ modulated symbol matrix $\mathbf{S}$. The N_T signals of each row of $\mathbf{S}$ are simultaneously transmitted by N_T different antennas in a symbol period. These N_T parallel signals are denoted by $\{s_m(t), m = 1, \ldots, N_T\}$, and their expected powers obey the power constraint

$$\frac{1}{N_T} \sum_{m=1}^{N_T} \mathrm{E}\left[|s_m(t)|^2\right] = 1, \quad t = 1, \cdots, T. \tag{2.1}$$

Here, E[·] is the expectation operation, and $|\cdot|$ denotes the absolute value of the quantity inside. The expectation in (2.1) is over the input information bits.

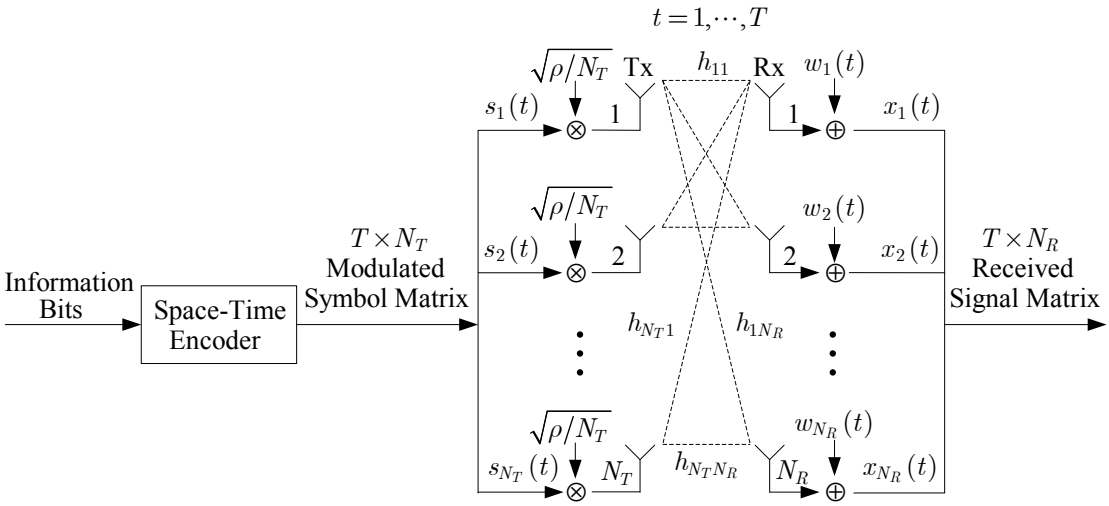

Fig. 2.1: The general baseband space–time coded system model.

The multiple antennas at both transmitter and receiver create a MIMO channel, denoted by an $N_T \times N_R$ matrix $\mathbf{H}$. The channel coherence bandwidth is assumed to be large in comparison with the transmitted signal bandwidth, and the channel gains are assumed to remain constant during one time-block. Thus, $\mathbf{H}$ is a flat block-fading MIMO channel. The element h_{mn} of $\mathbf{H}$ denotes the complex channel gain from transmit antenna m to receive antenna n. In one time block, all the channel gains $\{h_{mn}, m = 1, \cdots, N_T, n = 1, \cdots, N_R\}$ are assumed to be independent, identically distributed (i.i.d.) random variables with the circularly symmetric, complex Gaussian distribution $\mathcal{CN}(\mu, \sigma^2)$ with mean $\mu = 0$ and variance $\sigma^2 = 1$.

The received signal at time t and receive antenna n is given by

$$x_n(t) = \sqrt{\rho/N_T} \sum_{m=1}^{N_T} h_{mn} s_m(t) + w_n(t), \quad t = 1, \cdots, T, \;\; n = 1, \cdots, N_R. \quad (2.2)$$

Here, $w_n(t)$ is the additive receiver noise for receiver antenna n at time t. All the noises $\{w_n(t), n = 1, \cdots, N_R, t = 1, \cdots, T\}$ are modeled as independent, zero-mean, complex, Gaussian random variables with unit variances, i.e., i.i.d. $\mathcal{CN}(0, 1)$ distributed. Thus, it is clear that the quantity ρ is the expected SNR at each receive antenna. To express the received signals in one time-block compactly,

(2.2) can be written in matrix form as

$$\mathbf{X} = \sqrt{\rho/N_T}\mathbf{S}\mathbf{H} + \mathbf{W}. \tag{2.3}$$

Here, $\mathbf{X}$ is the $T \times N_R$ complex received signal matrix, and $\mathbf{W}$ is the $T \times N_R$ additive receiver complex noise matrix. Alternatively, the received signals in (2.2) can also be written in matrix-vector form as

$$\mathbf{x} = \sqrt{\rho/N_T}\bar{\mathbf{S}}\mathbf{h} + \mathbf{w}. \tag{2.4}$$

Here, we have $\mathbf{x} = \text{vec}(\mathbf{X})$, $\bar{\mathbf{S}} = \mathbf{I}_{N_R} \otimes \mathbf{S}$, $\mathbf{h} = \text{vec}(\mathbf{H})$, and $\mathbf{w} = \text{vec}(\mathbf{W})$. The operation $\text{vec}(\mathbf{A})$ denotes the vectorization of the matrix $\mathbf{A}$ formed by stacking the columns of $\mathbf{A}$ into a single column vector. For example, we have $\mathbf{x} = [\mathbf{x}_1^\top\ \mathbf{x}_2^\top\ \cdots\ \mathbf{x}_{N_R}^\top]^\top$, where $(\cdot)^\top$ denotes the transpose operation, and $\mathbf{x}_n$ is the nth column of $\mathbf{X}$, i.e., the received signal column vector at receive antenna n in one time-block. Thus, $\mathbf{h}$ is $\mathcal{CN}(\mathbf{0}, \mathbf{I}_{N_T N_R})$ distributed, and $\mathbf{w}$ is $\mathcal{CN}(\mathbf{0}, \mathbf{I}_{TN_R})$ distributed, where $\mathbf{0}$ is a zero vector, and $\mathbf{I}_N$ is the identity matrix of size N. In addition, $\mathbf{A} \otimes \mathbf{B}$ denotes the Kronecker product of the matrices $\mathbf{A}$ and $\mathbf{B}$, where each element of $\mathbf{A}$ is multiplied by the matrix $\mathbf{B}$.

For STTC, in the tth symbol period of a time-block, a block of R information bits is fed into a space–time trellis encoder [4, 6]. This encoder maps the R information bits into N_T modulated signals chosen from a signal constellation composed of 2^R points. These N_T modulated signals constitute the tth row of the signal matrix $\mathbf{S}$, and are transmitted simultaneously through N_T antennas. Then in one time-block, a block of TR information bits are mapped into the $T \times N_T$ signal matrix $\mathbf{S}$, and $\mathbf{S}$ is transmitted. Thus, the data rate for STTC is R bits per channel use.

For STBC, in each time-block, a block of $T_1 R$ information bits are first mapped into T_1 modulated signals chosen from a signal constellation composed of 2^R points. These T_1 modulated signals are then used as the elements of a $T \times N_T$

space–time block encoding matrix to generate the signal matrix $\mathbf{S}$ [7, 43]. Thus, the data rate for STBC is T_1R/T bits per channel use. It has been shown that for a space–time block code with full transmit diversity, the rate T_1/T is less than or equal to one [4, 7]. If a full rate is achieved, i.e., $T_1/T = 1$, no bandwidth expansion is required. However, if a full rate is not achieved, i.e., $T_1/T < 1$, a bandwidth expansion of T/T_1 is required.

For USTM, in each time-block, a block of TR information bits are mapped into a $T \times N_T$ signal matrix $\mathbf{S}$, and this matrix is chosen from a signal constellation composed of 2^{TR} unitary signal matrices. Thus, the data rate for USTM is R bits per channel use. The rest of this chapter concentrates only on USTM.

2.2 Capacity-Achieving Signal Structure

For the MIMO system with N_T transmit antennas and N_R receive antennas given in (2.4), Marzetta and Hochwald justified USTM in [21, 45] for the scenario where the channel is unknown to both the transmitter and the receiver by arriving at the following theorems.

Theorem 2.1 (Limit on Number of Transmit Antennas) *For any coherence interval T and any fixed number N_R of receive antennas, the capacity obtained with $N_T > T$ transmit antennas equals the capacity obtained with $N_T = T$ transmit antennas. That means there is no benefit obtained by making the number of transmit antennas greater than the length of the coherence interval.*

Theorem 2.2 (Structure of Signal that Achieves Capacity) *A capacity-achieving random signal matrix may be constructed as a product $\mathbf{S} = \mathbf{\Phi V}$, where $\mathbf{\Phi}$ is an isotropically distributed $T \times N_T$ matrix whose columns are orthonormal, and $\mathbf{V} = \mathrm{diag}\,(v_1, v_2, \cdots, v_{N_T})$ is an $N_T \times N_T$ real, nonnegative, diagonal matrix independent of $\mathbf{\Phi}$. Furthermore, we can choose the joint density of the diagonal elements of $\mathbf{V}$ to be unchanged by rearrangements of its arguments.*

An isotropically distributed $T \times N_T$ matrix $\mathbf{\Phi}$ satisfies $\mathbf{\Phi}^\dagger \mathbf{\Phi} = \mathbf{I}_{N_T}$ where $(\cdot)^\dagger$ denotes the transpose conjugate operation, and it has the same PDF as $\mathbf{U\Phi}$ for any $T \times T$ unitary matrix $\mathbf{U}$. That means that its PDF is invariant to all unitary transformations. Thus, $\mathbf{\Phi}$ can be regarded as the matrix counterpart of a complex scalar having unit magnitude and uniformly distributed phase.

Theorem 2.3 (Capacity, Asymptotically in T) *When the length of the coherence interval is significantly greater than the number of transmit antennas, i.e., $T \gg N_T$, setting $v_1 = v_2 = \cdots = v_{N_T} = \sqrt{T}$ attains capacity.*

Theorem 2.4 (Capacity, Asymptotically in ρ) *When the SNR approaches infinity, i.e., $\rho \to \infty$, and the length of the coherence interval is greater than the number of transmit antennas, i.e., $T > N_T$, setting $v_1 = v_2 = \cdots = v_{N_T} = \sqrt{T}$ attains capacity.*

Hence, for the case that the channel is unknown to the receiver, the structure of signals that achieve capacity can be defined as $\mathbf{S} = \sqrt{T}\mathbf{\Phi}$ with $\mathbf{\Phi}^\dagger \mathbf{\Phi} = \mathbf{I}_{N_T}$, which is called unitary space–time modulation. Hughes further proved in [18] that to guarantee full diversity, we must choose $T \geq 2N_T$. According to information theory, if one combines USTM with channel coding over multiple independent fading intervals, it is theoretically possible to transmit information reliably at a rate that is bounded by the channel capacity [21, 45].

For the case that the channel is known to the receiver, Hochwald and Marzetta argued in [21] that when the length of coherence interval T is sufficiently large, USTM is also nearly optimal in the sense of achieving capacity. This is because the channel capacity with perfect CSI at the receiver is achieved by a transmitted signal matrix whose elements are i.i.d. $\mathcal{CN}(0, 1)$. Since as $T \to \infty$, the distributions of the elements of $\mathbf{S} = \sqrt{T}\mathbf{\Phi}$ approach i.i.d. $\mathcal{CN}(0, 1)$, USTM also nearly achieves capacity for this case.

2.3 Maximum-Likelihood Receivers for USTM

As mentioned in Section 2.1, in the USTM scheme, at each time-block, a sequence of TR binary information bits is mapped into a $T \times N_T$ signal matrix $\mathbf{S} = \sqrt{T}\mathbf{\Phi}$, where $\mathbf{\Phi}$ is selected from an $L = 2^{TR}$ unitary space–time constellation $\left\{ \mathbf{\Phi}_l \,\middle|\, \mathbf{\Phi}_l^\dagger \mathbf{\Phi}_l = \mathbf{I}_{N_T} \,,\, l = 1, \cdots, L \right\}$. The received signal vector is given by (2.4) except that $\bar{\mathbf{S}}$ is replaced by $\sqrt{T}\mathbf{\Psi}$, i.e.,

$$\mathbf{x} = \sqrt{\rho T / N_T}\mathbf{\Psi}\mathbf{h} + \mathbf{w}, \tag{2.5}$$

where

$$\mathbf{\Psi} = \mathbf{I}_{N_R} \otimes \mathbf{\Phi}. \tag{2.6}$$

It is easy to see that we have $\mathbf{\Psi}^\dagger \mathbf{\Psi} = \mathbf{I}_{N_T N_R}$. Now, we present the ML receivers for USTM. The ML decision rule leads to a QR for the case of channel unknown to the receiver, and leads to a CR for the case of channel known to the receiver.

2.3.1 Quadratic Receiver

If the channel $\mathbf{h}$ is unknown to the receiver, the received signal vector $\mathbf{x}$ is a zero-mean, circularly symmetric, complex Gaussian vector with covariance matrix

$$\mathbf{\Lambda} = \mathrm{E}\left[\mathbf{x}\mathbf{x}^\dagger\right] = \mathbf{I}_{TN_R} + \frac{\rho T}{N_T}\mathbf{\Psi}\mathbf{\Psi}^\dagger. \tag{2.7}$$

Then the received signal vector has the conditional PDF

$$p\left(\mathbf{x} \,|\, \mathbf{\Psi}_l\right) = \frac{\exp\left\{-\mathbf{x}^\dagger \mathbf{\Lambda}^{-1} \mathbf{x}\right\}}{\pi^{TN_R} \det\left(\mathbf{\Lambda}\right)} = \frac{\exp\left\{-\|\mathbf{x}\|^2 + \dfrac{\rho T / N_T}{\rho T / N_T + 1} \left\| \mathbf{\Psi}_l^\dagger \mathbf{x} \right\|^2 \right\}}{\pi^{TN_R} \left(1 + \rho T / N_T\right)^{N_T N_R}}, \tag{2.8}$$

where $\det(\mathbf{A})$ denotes the determinant of matrix $\mathbf{A}$, and $\|\cdot\|$ denotes the Frobenius norm. Then ML detection leads to a QR, given by [21, eq. (15)]

$$\hat{\mathbf{\Psi}}_{QR} = \arg \max_{\mathbf{\Psi}_l \in \{\mathbf{\Psi}_1,\ldots,\mathbf{\Psi}_L\}} p\left\{\mathbf{x}\,|\mathbf{\Psi}_l\right\} = \arg \max_{\mathbf{\Psi}_l \in \{\mathbf{\Psi}_1,\ldots,\mathbf{\Psi}_L\}} \left\|\mathbf{\Psi}_l^{\dagger}\mathbf{x}\right\|^2. \tag{2.9}$$

Here, the decision $\hat{\mathbf{\Psi}}_{QR}$ on $\mathbf{\Psi}$ is equivalent to the decision $\hat{\mathbf{\Phi}}_{QR}$ on $\mathbf{\Phi}$, since $\mathbf{\Psi}_l$ has a one-to-one correspondence with $\mathbf{\Phi}_l$. We can see that this ML receiver seeks to maximize the squared length of the orthogonal projection of the received signal onto the complex subspace spanned by each of the possible transmitted signals.

2.3.2 Coherent Receiver

If the channel $\mathbf{h}$ is known to the receiver, the received signal vector $\mathbf{x}$ is a circularly symmetric, complex Gaussian vector with mean vector $\sqrt{\rho T/N_T}\mathbf{\Psi}_l\mathbf{h}$ and covariance matrix $\mathbf{I}_{TN_R}$. The conditional PDF of the received signal vector is therefore given by

$$p\left(\mathbf{x}\,|\mathbf{\Psi}_l, \mathbf{h}\right) = \frac{1}{\pi^{TN_R}} \exp\left\{-\left\|\mathbf{x} - \sqrt{\rho T/N_T}\mathbf{\Psi}_l\mathbf{h}\right\|^2\right\}. \tag{2.10}$$

Thus, the CR for ML detection is given by [21, pg. 549]

$$\hat{\mathbf{\Psi}}_{CR} = \arg \max_{\mathbf{\Psi}_l \in \{\mathbf{\Psi}_1,\ldots,\mathbf{\Psi}_L\}} p\left\{\mathbf{x}\,|\mathbf{\Psi}_l, \mathbf{h}\right\} = \arg \min_{\mathbf{\Psi}_l \in \{\mathbf{\Psi}_1,\ldots,\mathbf{\Psi}_L\}} \left\|\mathbf{x} - \sqrt{\rho T/N_T}\mathbf{\Psi}_l\mathbf{h}\right\|^2. \tag{2.11}$$

2.4 Error Performance Analysis for USTM

After arriving at the QR and the CR for USTM, Hochwald and Marzetta derived in [21] the expressions of PEP and CUB for both the receivers. For the special case that the singular values of a certain matrix (i.e., $\mathbf{\Psi}_j^{\dagger}\mathbf{\Psi}_l$ for the QR and $(\mathbf{\Psi}_j - \mathbf{\Psi}_l)$ for the CR) are identical, their PEP expressions were given in an explicit closed form. For a more general case where the singular values may be

distinct, their closed-form PEP expressions require one to compute residues. For such a general case, Lu *et al.* also derived a general, closed-form PEP expression in [59] for both the QR and the CR, by using Craig's formula for the Gaussian probability integral [60]. In this section, we first present the expressions of PEP and CUB for the QR and the CR derived by Hochwald and Marzetta in [21]. Then we give the alternative expressions for the PEPs derived by Lu *et al.* in [59].

2.4.1 PEP and CUB of the Quadratic Receiver

We assume that the unitary signal matrices $\{\mathbf{\Psi}_l, l = 1, \cdots, L\}$ are transmitted with equal probabilities. For the QR in (2.9), the PEP of mistaking $\mathbf{\Psi}_l$ for $\mathbf{\Psi}_j$ when $\mathbf{\Psi}_l$ was sent, or vice versa can be obtained by first deriving the CF of the decision variable, and then integrating over the inversion of the CF. The resultant contour integral can be solved in terms of residues, given by [21, eqs. (B.10) and (17)]

$$\begin{aligned}
&P_e\left(\mathbf{\Psi}_l, \mathbf{\Psi}_j\right) \\
&= \Pr\left\{ \left\| \mathbf{\Psi}_l^\dagger \mathbf{x} \right\|^2 - \left\| \mathbf{\Psi}_j^\dagger \mathbf{x} \right\|^2 < 0 \,|\, \mathbf{\Psi}_l \right\} \\
&= \frac{1}{4\pi} \int_{-\infty}^{\infty} d\omega \frac{1}{\omega^2 + 1/4} \prod_{m=1}^{N_T} \left[1 + \frac{\left(\rho T/N_T\right)^2 \left(1 - d_{m,lj}^2\right) \left(\omega^2 + 1/4\right)}{1 + \rho T/N_T} \right]^{-N_R} \\
&= \sum_n \mathrm{Res}_{\omega = \jmath \alpha_{n,lj}} \left\{ -\frac{1}{\omega + \jmath/2} \prod_{\substack{m=1 \\ d_{m,lj}<1}}^{N_T} \left[\frac{1 + \rho T/N_T}{\left(\rho T/N_T\right)^2 \left(1 - d_{m,lj}^2\right) \left(\omega^2 + \alpha_{m,lj}^2\right)} \right]^{N_R} \right\}.
\end{aligned} \tag{2.12}$$

Here, $\Pr(\cdot)$ denotes the probability of the event in the brackets; $1 \geq d_{1,lj} \geq \cdots \geq d_{N_T,lj} \geq 0$ are the singular values of the matrix $\mathbf{\Phi}_j^\dagger \mathbf{\Phi}_l$, $\jmath = \sqrt{-1}$, and

$$\alpha_{m,lj} = \sqrt{\frac{1}{4} + \frac{1 + \rho T/N_T}{\left(\rho T/N_T\right)^2 \left(1 - d_{m,lj}^2\right)}}. \tag{2.13}$$

The PEP in (2.12) decreases as any $d_{m,lj}$ decreases.

The CUB on the PEP in (2.12) can be obtained by setting ω inside the square brackets in the second equation in (2.12) to zero, i.e., [21, eq. (18)]

$$P_e\left(\mathbf{\Psi}_l, \mathbf{\Psi}_j\right) \leq \frac{1}{2} \prod_{m=1}^{N_T} \left[1 + \frac{\left(\rho T/N_T\right)^2 \left(1 - d_{m,lj}^2\right)}{4\left(1 + \rho T/N_T\right)}\right]^{-N_R}. \tag{2.14}$$

For the special case that the singular values $\{d_{m,lj}\}_{m=1}^{N_T}$ of the matrix $\mathbf{\Phi}_j^\dagger \mathbf{\Phi}_l$ satisfy

$$0 \leq d_{1,lj} = \cdots = d_{N_T,lj} = d_{lj} \leq 1, \tag{2.15}$$

the PEP in (2.12) can be simplified as [21, eq. at bottom of pg. 562]

$$P_e\left(\mathbf{\Psi}_l, \mathbf{\Psi}_j\right) = \left(\frac{1 - \lambda_{lj,QR}}{2}\right)^{N_T N_R} \sum_{i=0}^{N_T N_R - 1} \binom{N_T N_R - 1 + i}{i} \left(\frac{1 + \lambda_{lj,QR}}{2}\right)^i, \tag{2.16}$$

where

$$\lambda_{lj,QR} = \frac{\rho T}{N_T} \sqrt{\frac{1 - d_{lj}^2}{(2 + \rho T/N_T)^2 - (d_{lj}\rho T/N_T)^2}}. \tag{2.17}$$

From the above results, we can see that orthogonal unitary space–time constellations (OUSTC), in which signal matrices are orthogonal to one another, i.e., given by $\{\mathbf{\Phi}_l \big| \mathbf{\Phi}_l^\dagger \mathbf{\Phi}_l = \mathbf{I}_{N_T}, \mathbf{\Phi}_l^\dagger \mathbf{\Phi}_j = \mathbf{0}_{N_T}, l, j = 1, \ldots, L, l \neq j\}$, are optimal for the case that the channel is unknown to the receiver. This is because the singular values for any pair of $\mathbf{\Phi}_l$ and $\mathbf{\Phi}_j$ of OUSTC are equal to zero, and thus $P_e\left(\mathbf{\Psi}_l, \mathbf{\Psi}_j\right)$ is minimized.

2.4.2 PEP and CUB of the Coherent Receiver

For the CR in (2.11), the PEP of mistaking $\mathbf{\Psi}_l$ for $\mathbf{\Psi}_j$ when $\mathbf{\Psi}_l$ was sent, or vice versa can also be obtained by integrating over the inversion of the CF of the decision variable. The resultant contour integral can be solved in terms of

residues, given by [21, eqs. (C.3) and (19)]

$$\begin{aligned}
&P_e\left(\mathbf{\Psi}_l, \mathbf{\Psi}_j\right) \\
&= \Pr\left\{ \left\| \mathbf{x} - \sqrt{\rho T/N_T}\mathbf{\Psi}_j \mathbf{h} \right\|^2 - \left\| \mathbf{x} - \sqrt{\rho T/N_T}\mathbf{\Psi}_l \mathbf{h} \right\|^2 < 0 \,|\, \mathbf{\Psi}_l \right\} \\
&= \frac{1}{4\pi} \int_{-\infty}^{\infty} d\omega \frac{1}{\omega^2 + 1/4} \prod_{m=1}^{N_T} \left[1 + \left(\rho T/N_T\right) \delta_{m,lj}^2 \left(\omega^2 + 1/4\right) \right]^{-N_R} \\
&= \sum_n \mathrm{Res}_{\omega = \jmath\beta_{n,lj}} \left\{ -\frac{1}{\omega + \jmath/2} \prod_{\substack{m=1 \\ \delta_{m,lj}>0}}^{N_T} \left[\left(\rho T/N_T\right) \delta_{m,lj}^2 \left(\omega^2 + \beta_{m,lj}^2\right) \right]^{-N_R} \right\}. \quad (2.18)
\end{aligned}$$

Here, $2 \geq \delta_{1,lj} \geq \cdots \geq \delta_{N_T,lj} \geq 0$ are the singular values of the matrix $(\mathbf{\Phi}_j - \mathbf{\Phi}_l)$, and $\beta_{m,lj}$ is given by

$$\beta_{m,lj} = \sqrt{\frac{1}{4} + \frac{1}{\left(\rho T/N_T\right) \delta_{m,lj}^2}}. \quad (2.19)$$

The PEP in (2.18) decreases as any $\delta_{m,lj}$ increases.

The CUB on the PEP in (2.18) can be obtained by setting ω inside the square brackets in the second equation in (2.18) to zero, i.e., [21, eq. (20)]

$$P_e\left(\mathbf{\Psi}_l, \mathbf{\Psi}_j\right) \leq \frac{1}{2} \prod_{m=1}^{N_T} \left[1 + \frac{\rho T}{4N_T} \delta_{m,lj}^2 \right]^{-N_R}. \quad (2.20)$$

For the special case that the singular values $\{\delta_{m,lj}\}_{m=1}^{N_T}$ of the matrix $(\mathbf{\Phi}_j - \mathbf{\Phi}_l)$ satisfy

$$\delta_{1,lj} = \cdots = \delta_{N_T,lj} = \delta_{lj}, \quad (2.21)$$

the PEP in (2.18) can be simplified as [21, eq. at bottom of pg. 563]

$$P_e\left(\mathbf{\Psi}_l, \mathbf{\Psi}_j\right) = \left(\frac{1 - \lambda_{lj,CR}}{2} \right)^{N_T N_R} \sum_{i=0}^{N_T N_R - 1} \binom{N_T N_R - 1 + i}{i} \left(\frac{1 + \lambda_{lj,CR}}{2} \right)^i, \quad (2.22)$$

where

$$\lambda_{lj,CR} = \sqrt{\frac{\delta_{lj}^2 \rho T/N_T}{4 + \delta_{lj}^2 \rho T/N_T}}. \tag{2.23}$$

For OUSTC, we have

$$d_{1,lj} = \cdots = d_{N_T,lj} = d = 0, \tag{2.24}$$

and

$$\delta_{1,lj} = \cdots = \delta_{N_T,lj} = \delta = \sqrt{2}. \tag{2.25}$$

At high SNR, the CUB in (2.14) for the QR approximates to [21]

$$P_e\left(\mathbf{\Psi}_l, \mathbf{\Psi}_j\right) \lesssim \frac{1}{2}\left(\frac{4N_T}{\rho T}\right)^{N_T N_R}, \tag{2.26}$$

and the CUB in (2.20) for the CR approximates to [21]

$$P_e\left(\mathbf{\Psi}_l, \mathbf{\Psi}_j\right) \lesssim \frac{1}{2}\left(\frac{2N_T}{\rho T}\right)^{N_T N_R}. \tag{2.27}$$

We can see that knowledge of perfect CSI at the receiver yields a 3-dB gain in SNR for OUSTC. For nonorthogonal unitary space–time constellations (NOUSTC) in which signal matrices may not be orthogonal to one another, Hochwald *et al.* have shown that when we use 1 to 3 transmit antennas, we can obtain a 2 to 4 dB gain in SNR by using the CR instead of the QR.

2.4.3 Alternative Expressions of the PEPs

In the second equations in (2.12) and (2.18), if we use the coordinate transformation

$$\omega = \frac{1}{2}\tan\theta,$$

the PEPs for the QR and the CR can be rewritten in a unified form, given by [59, eqs. (5)–(9)]

$$\begin{aligned} P_e\left(\mathbf{\Psi}_l, \mathbf{\Psi}_j\right) &= \frac{1}{\pi}\int_0^{\pi/2}\prod_{i=1}^{N_T}\left(\frac{\cos^2\theta}{\cos^2\theta+\eta\zeta_i}\right)^{N_R}d\theta \\ &= \frac{1}{\pi}\int_0^{\pi/2}\prod_{i=1}^{N_T}\left(\frac{\sin^2\theta}{\sin^2\theta+\eta\zeta_i}\right)^{N_R}d\theta \\ &= \frac{1}{\pi}\int_0^{\pi/2} f^{-N_R}\left(\frac{\eta}{\sin^2\theta}\right)d\theta. \end{aligned} \tag{2.28}$$

Here, we have

$$\eta = \begin{cases} \dfrac{\left(\rho T/N_T\right)^2}{4\left(1+\rho T/N_T\right)}, & \text{for the QR,} \\ \dfrac{\rho T}{4N_T}, & \text{for the CR,} \end{cases} \tag{2.29}$$

and

$$\zeta_i = \begin{cases} 1-d_i^2, & \text{for the QR,} \\ \delta_i^2, & \text{for the CR.} \end{cases} \tag{2.30}$$

The function $f\left(x\right)$ is defined as

$$f\left(x\right) = \prod_{i=1}^{N_d}\left(1+\zeta_i x\right)^{e_i}, \tag{2.31}$$

where N_d is the number of distinct nonzero ζ_i's, i.e., $\{\zeta_i\}_{i=1}^{N_d}$ are distinct and nonzero, and e_i denotes the multiplicity of $(1+\zeta_i x)$ as a factor of $f\left(x\right)$. Thus, we have $\sum_{i=1}^{N_d} e_i \leq N_T$. By using the partial-fraction expansion

$$f^{-N_R}\left(x\right) = \prod_{i=1}^{N_d}\left(1+\zeta_i x\right)^{-m_i} = \sum_{i=1}^{N_d}\sum_{n=1}^{m_i}\frac{\kappa_{ni}}{\left(1+\zeta_i x\right)^n}, \tag{2.32}$$

where

$$m_i = N_R e_i,$$

$$\kappa_{ni} = \frac{\left\{ \frac{d^{m_i-n}}{dx^{m_i-n}} \left(1+\zeta_i x\right)^{m_i} f^{-N_R}(x) \right\} \Big|_{x=-\zeta_i^{-1}}}{(m_i-n)!\zeta_i^{m_i-n}}.$$

Using (2.32) in (2.28) gives [59, eq. (16)]

$$P_e(\boldsymbol{\Psi}_l, \boldsymbol{\Psi}_j) = \frac{1}{2}\left\{1 - \sum_{i=1}^{N_d} \mu_i \sum_{n=1}^{m_i} \kappa_{ni} \sum_{q=0}^{n-1} \binom{2q}{q} \left(\frac{1-\mu_i^2}{4}\right)^q \right\}, \tag{2.33}$$

where

$$\mu_i = \sqrt{\frac{\eta\zeta_i}{1+\eta\zeta_i}}.$$

We can see that (2.33) still requires one to compute high-order derivatives.

2.5 Signal Design for USTM

Given expressions of the PEP and CUB, researchers have put a lot of efforts to design optimal constellations which minimize the error probability of USTM. Signal design usually requires a design criterion and a constellation construction. Constellations with this construction are optimized to satisfy the criterion. In this section, we will give some important signal design criteria and constellation constructions proposed in the literature for USTM.

2.5.1 Design Criteria

As we mentioned in Section 2.2, the USTM scheme has been justified for the case that CSI is known to the receiver and the CR is used, and also for the case that CSI is unknown to the receiver and the QR is used. Therefore, we list signal design criteria for both the CR and the QR here.

2.5.1.1 Design Criteria for the CR

The design criteria for the CR were given by Tarokh *et al.* in [6] for STTC. These design criteria also apply to USTM when the CR is used in detecting USTC, as presented in the following. The CUB on the PEP of the CR in (2.20) can be rewritten as

$$P_e\left(\mathbf{\Psi}_l, \mathbf{\Psi}_j\right) \leq \frac{1}{2} \prod_{m=1}^{N_d} \left[1 + \frac{\rho T}{4N_T} \delta_{m,lj}^2\right]^{-N_R}, \tag{2.34}$$

where N_d is the rank of $\mathbf{C}\left(\mathbf{\Phi}_l, \mathbf{\Phi}_j\right) = \left(\mathbf{\Phi}_j - \mathbf{\Phi}_l\right)^{\dagger}\left(\mathbf{\Phi}_j - \mathbf{\Phi}_l\right)$, i.e., the number of nonzero singular values $\delta_{m,lj}$ of $\left(\mathbf{\Phi}_j - \mathbf{\Phi}_l\right)$. At high SNR, the CUB in (2.34) approximates to

$$P_e\left(\mathbf{\Psi}_l, \mathbf{\Psi}_j\right) \lesssim \frac{1}{2} \left(\prod_{m=1}^{N_d} \delta_{m,lj}^2\right)^{-N_R} \left(\frac{\rho T}{4N_T}\right)^{-N_d N_R}. \tag{2.35}$$

In (2.35), the diversity gain is defined as the absolute value of the power of SNR, i.e., $N_d N_R$ [4, 6, 18, 74]. It represents the gain in SNR obtained by the system with space diversity over the system without diversity at the same error probability. The coding gain is defined as $\prod_{m=1}^{N_d} \delta_{m,lj}^2 / d_{uncoded}^2$ where $d_{uncoded}^2$ is the squared Euclidian distance of the reference uncoded system [4, 6, 18, 74]. It represents the gain in SNR obtained by the coded system over an uncoded system operating with the same diversity at the same error probability. Thus, in a plot of the error probability versus SNR, the slope of the curve is determined by the diversity gain, and the horizontal shift of the curve for the uncoded system to the curve for the coded system with the same diversity is determined by the coding gain.

From (2.35), the signal design criteria for the CR can be given by [6]:

The Rank Criterion: To achieve the maximum diversity $N_T N_R$, the matrix $\mathbf{C}\left(\mathbf{\Phi}_l, \mathbf{\Phi}_j\right)$ has to be of full rank for any pair of codewords $\mathbf{\Phi}_l$ and $\mathbf{\Phi}_j$. If $\mathbf{C}\left(\mathbf{\Phi}_l, \mathbf{\Phi}_j\right)$ has minimum rank N_d over the set of two distinct codewords, then a diversity of $N_d N_R$ is achieved.

The Determinant Criterion: The minimum of the determinant of $\mathbf{C}(\mathbf{\Phi}_l, \mathbf{\Phi}_j), \prod_{m=1}^{N_d} \delta_{m,lj}^2$, taken over all possible pairs of distinct codewords needs to be maximized. This measures the coding advantage.

The above design criteria were proposed for the case that perfect CSI was available at the receiver. In a practical scenario, we have to estimate the channel gains at the receiver, and channel estimation errors exist. Tarokh *et al.* studied the effect of channel estimation errors in [44]. Based on the assumption that the constellations have constant energy, they proved that in the absence of ideal CSI, the above design criteria are still valid, and standard channel estimation techniques can be used in conjunction with space–time codes provided that the number of transmit antennas is small.

2.5.1.2 Design Criteria for the QR

Design Criterion for Low SNR or Small Singular Values (Diversity Sum Criterion): From the CUB expression in (2.14) for the QR in (2.9), Hochwald *et al.* found that the sum of the squares of the singular values can be used as a simple error performance indicator [54]. Independently, Agrawal *et al.* also found that either for small singular values or for a low SNR, the CUB on the PEP was dominated by the sum of the squares of the singular values [61]. Hence, a signal design criterion was proposed to minimize the diversity sum, i.e., to minimize

$$\xi = \max_{1 \le l < j \le L} \sqrt{\frac{1}{N_T} \sum_{m=1}^{N_T} d_{m,lj}^2} = \max_{1 \le l < j \le L} \sqrt{\frac{1}{N_T} \mathrm{tr}\left(\mathbf{\Phi}_l^\dagger \mathbf{\Phi}_j \mathbf{\Phi}_j^\dagger \mathbf{\Phi}_l\right)}. \tag{2.36}$$

Here, $\mathrm{tr}(\mathbf{A})$ denotes the trace of $\mathbf{A}$. However, this design criterion does not guarantee that full transmit diversity is achieved.

Design Criterion for High SNR (Diversity Product Criterion): From the CUB expression in (2.14) for the QR, Hochwald *et al.* also defined the diversity product

as [19, eq. (9)],[54]

$$\xi = \min_{1<l<j\leq L} \left[\prod_{m=1}^{N_T} \left(1 - d_{m,lj}^2\right) \right]^{\frac{1}{2N_T}} = \min_{1<l<j\leq L} \det \left(\mathbf{I}_{N_T} - \mathbf{\Phi}_l^\dagger \mathbf{\Phi}_j \mathbf{\Phi}_j^\dagger \mathbf{\Phi}_l \right)^{\frac{1}{2N_T}}. \quad (2.37)$$

This signal design criterion is to maximize ξ. Full transmit diversity is achieved if ξ is nonzero. We can see that this design criterion can also be interpreted as a rank-determinant criterion, but with different definitions of the rank and the determinant [18]. Here, the rank N_d is defined as the rank of $\mathbf{C}\left(\mathbf{\Phi}_l, \mathbf{\Phi}_j\right) = \mathbf{I}_{N_T} - \mathbf{\Phi}_l^\dagger \mathbf{\Phi}_j \mathbf{\Phi}_j^\dagger \mathbf{\Phi}_l$, and the determinant is defined as $\prod_{m=1}^{N_d} \left(1 - d_{m,lj}^2\right)$. Only when $N_d = N_T$, can full transmit diversity be achieved. For the case of small $\{d_{m,lj}\}_{m=1}^{N_T}$, it has been shown in [54] that the diversity product criterion is roughly the same as the diversity sum criterion, since we have $\prod_{m=1}^{N_T} \left(1 - d_{m,lj}^2\right) \approx 1 - \sum_{m=1}^{N_T} d_{m,lj}^2$.

Design Criterion Based on the Asymptotic Union Bound (AUB Criterion) : Since the diversity sum criterion in [54, 61] cannot guarantee a full diversity order, and optimizing the worst case cannot promise a good performance in the SEP, McCloud *et al.* proposed in [63] a design criterion based on the asymptotic value of the union bound at high SNR. This criterion is to minimize

$$\xi = \sum_{l=1}^{L} \sum_{j\neq l} \frac{1}{\det \left(\mathbf{I}_{N_T} - \mathbf{\Phi}_l^\dagger \mathbf{\Phi}_j \mathbf{\Phi}_j^\dagger \mathbf{\Phi}_l \right)^{N_R}}. \quad (2.38)$$

This design criterion guarantees the full diversity order, minimizes the SEP, and is independent of the correlation structure of the fading channel.

From above three design criteria, we can also see that OUSTC are optimal for the QR. This is because OUSTC provide the maximum value 1 for (2.37), the minimum value 0 for (2.36), and the minimum value $L\left(L-1\right)$ for (2.38).

2.5.2 Constellation Constructions

Constellations with Block-Circulant Structure: Hochwald *et al.* proposed a systematic method for creating constellations of USTM in [54]. Constellations

obtained have a block-circulant correlation structure, namely,[54, eq. (19)]

$$\mathbf{\Phi}_l^\dagger \mathbf{\Phi}_j = \mathbf{P}_{(j-l) \bmod L}, \qquad l, j = 1, \cdots, L, \tag{2.39}$$

which means that for a given constellation, the value of $\mathbf{\Phi}_l^\dagger \mathbf{\Phi}_j$ only depends on $(j-l)$. Here, "mod" denotes the modulo operation with $n \bmod n = 0$; $\mathbf{P}_l$'s are $N_T \times N_T$ matrices, and are different from constellations to constellations. It is clear we have $\mathbf{P}_0 = \mathbf{I}_{N_T}$ and $\mathbf{P}_{-l} = \mathbf{P}_l^\dagger$. This correlation structure implies that the conditional error probability $P_{e|\mathbf{\Phi}_l}$ when $\mathbf{\Phi}_l$ was transmitted is the same for any $l \in [1, L]$. In this construction, signal matrices are constructed as [54, eq. (25)]

$$\mathbf{\Phi}_l = \mathbf{\Theta}^{l-1} \mathbf{\Phi}_1, \qquad l = 2, \cdots, L, \tag{2.40}$$

where $\mathbf{\Theta} = \mathrm{diag}\left(e^{j2\pi u_1/L} \ \cdots \ e^{j2\pi u_T/L}\right)$ and $0 \le u_1, \cdots, u_T \le L-1$, and $\mathbf{\Phi}_1$ consists of N_T different columns of the $T \times T$ discrete Fourier transform matrix. For $N_T = 1$, $\mathbf{\Phi}_1$ is $1/\sqrt{T}$ times a vector of all ones. For $N_T = 2$, $\mathbf{\Phi}_1$ is given by

$$\mathbf{\Phi}_1 = \frac{1}{\sqrt{T}} \begin{pmatrix} 1 & 1 & \cdots & 1 \\ 1 & e^{\jmath \frac{2\pi}{T}} & \cdots & e^{\jmath \frac{2\pi(T-1)}{T}} \end{pmatrix}^\top. \tag{2.41}$$

The optimum value of $\mathbf{u} = [1 \ \mathbf{u}'] = [1 \ u_2 \ \cdots \ u_T]$ is determined by computer search to satisfy the design criteria.

This construction was also extended to have a multiple index block-circulant structure, namely,

$$\mathbf{\Phi}_{l_1 \cdots l_K}^\dagger \mathbf{\Phi}_{l_1' \cdots l_K'} = \mathbf{P}_{(l_1'-l_1) \bmod L_1 \cdots (l_K'-l_K) \bmod L_K}, \ l_i, l_i' = 1, \cdots, L_i, \ i = 1, \cdots, K. \tag{2.42}$$

A K-indexed constellation of size $L = \prod_{i=1}^K L_i$ is given by [54, eq. (29)]

$$\mathbf{\Phi}_{l_1 \cdots l_K} = \mathbf{\Theta}_1^{l_1-1} \mathbf{\Theta}_2^{l_2-1} \cdots \mathbf{\Theta}_K^{l_K-1} \mathbf{\Phi}_1, \qquad l_i = 1, \cdots, L_i, \ i = 1, \cdots, K, \tag{2.43}$$

where $\mathbf{\Theta}_i$ is a diagonal unitary matrix that is the L_ith root of $\mathbf{I}_T$, with arguments

$0 \leq u_{i1}, \cdots, u_{iT} \leq L_i - 1$. Thus, the $K \times T$ argument matrix $\mathbf{U}$, whose elements are $u_{it}, i = 1, \cdots, K, t = 1, \cdots, T$, needs to be optimized. This matrix can be restricted to $\mathbf{U} = [\mathbf{I}_K \ \mathbf{U}']$, and only $K \times (T-K)$ matrix $\mathbf{U}'$ needs to be optimized.

Constellations with Orthogonal Design: Another class of important and useful signal constellations, unitary space–time constellations with orthogonal design (USTC-OD), was designed by Zhao *et al.* in [66, 67] by using an algebraic method. This construction was inspired by Alamouti's scheme [43], and provides full diversity. For the case of $N_T = 2$ and $L = q^2$, $q \in \mathbb{N}$ where $\mathbb{N}$ denotes the set of all natural numbers, their constellations are given by $C_a = \left\{ \mathbf{\Phi}_{i,l} \middle| i, l \in \{0, \ldots, q-1\} \right\}$, where

$$\mathbf{\Phi}_{i,l} = \frac{1}{2} \begin{pmatrix} 1 & -1 & r^i & -r^{-l} \\ 1 & 1 & r^l & r^{-i} \end{pmatrix}^\top, \tag{2.44}$$

and where $r = e^{\jmath 2\pi/q}$. Constellations of size $L = 2^{2n-1}, n \in \mathbb{N}$ can be obtained by extracting the subsets of the constellations of size $L = 2^{2n}$ [66]. For the case of $N_T = 4$ and $L = q^3$, $q \in \mathbb{N}$, their constellations are given by $C_a = \left\{ \mathbf{\Phi}_{i,l,j} \middle| i, l, j \in \{0, \ldots, q-1\} \right\}$, where

$$\mathbf{\Phi}_{i,l,j} = \frac{1}{\sqrt{6}} \begin{pmatrix} 1 & -1 & -1 & 0 & r^i & -r^{-l} & -r^{-j} & 0 \\ 1 & 1 & 0 & 1 & r^l & r^{-i} & 0 & r^{-j} \\ 1 & 0 & 1 & -1 & r^j & 0 & r^{-i} & -r^{-l} \\ 0 & -1 & 1 & 1 & 0 & -r^j & r^l & r^i \end{pmatrix}^\top. \tag{2.45}$$

Constellations with $N_T = 3$ can be obtained by deleting one column from the design of $N_T = 4$. We can see that these signal matrices consist of a training block and a data block, and this data block is a complex orthogonal design for STBC [7]. This class of constellations has some good properties. For example, the inner product and the difference of any two signal matrices for $N_T = 2$ and 4 have equal singular values. For the USTC-OD in (2.44) with $N_T = 2$, it was shown that all the singular values of $\mathbf{\Phi}_{i,l}^\dagger \mathbf{\Phi}_{i',l'}$, $\forall \mathbf{\Phi}_{i,l}, \mathbf{\Phi}_{i',l'} \in C_a$ are identical, given

by [67]

$$d_{i,l;i',l'} = \frac{1}{2}\sqrt{2 + \cos\frac{2\pi}{q}(i-i') + \cos\frac{2\pi}{q}(l-l')}. \tag{2.46}$$

Similarly, since we have

$$(\mathbf{\Phi}_{i,l} - \mathbf{\Phi}_{i',l'})^{\dagger}(\mathbf{\Phi}_{i,l} - \mathbf{\Phi}_{i',l'}) = \left[1 - \frac{1}{2}\left(\cos\frac{2\pi}{q}(i-i') + \cos\frac{2\pi}{q}(l-l')\right)\right]\mathbf{I}_2,$$

we can also show that all the singular values of $(\mathbf{\Phi}_{i,l} - \mathbf{\Phi}_{i',l'})$ are identical, and given by

$$\delta_{i,l;i',l'} = \sqrt{1 - \frac{1}{2}\left(\cos\frac{2\pi}{q}(i-i') + \cos\frac{2\pi}{q}(l-l')\right)}. \tag{2.47}$$

It can easily be shown that similar results hold for the case of $N_T = 4$. Thus, the PEPs of the USTC-OD with $N_T = 2$ or 4 for the QR (2.9) and the CR (2.11) can be given, respectively, in explicit, closed forms in (2.16) and (2.22). In addition, the orthogonal design of the signal matrices in USTC-OD allows for detecting on the indexes of the signal matrices separately [67, pgs. 1321–1322], and thus, the QR in (2.9) can be reduced to have a much lower complexity. The error performance of USTC-OD has been shown in [66, 67] to be comparable to that of constellations with block-circulant structure in (2.40).

Tarokh *et al.* also presented two constellation constructions in [65]. One construction is based on a generalization of PSK constellations, and the other is similar to that given in [66, 67], i.e, it is a concatenation of a training block and a real or complex orthogonal design block. Both of these two constructions do not require any computer search, and enable simple encoding and decoding algorithms with complexity independent of their transmission rates.

Other Constructions: In [61, 63], the Grassmanian manifold, the space of all N_T-dimensional subspaces of the complex T-dimensional vector space $\mathbb{C}^T$, was used to be a USTC construction, with no extra structure imposed. Optimization was performed by using a cumbersome computer search.

A more promising constellation design method was proposed by Jing *et al.* in [64] based on the Cayley transform. These Cayley codes, designed for any number of transmit and receive antennas, are simple to encode, and can be decoded in a variety of ways, including simple polynomial-time linear-algebraic techniques such as successive nulling and cancelling, or sphere decoding.

2.6 New Tight Bounds on the PEP of the QR

In [123], Byun and Lee proposed some tight bounds on the PEP of the CR in (2.11) for STC. In this section, we use similar techniques to derive some new bounds on the PEP of the QR in (2.9) for USTM. The two new upper bounds are the tightest available so far, and the new lower bound is the tightest at low SNR. Some implications for USTM constellation design are also pointed out.

2.6.1 New Bounds on the PEP

As given in (2.28), by letting $\omega = \tan(\theta)/2$, the PEP expression in (2.12) for the QR in (2.9) can be rewritten as

$$P_e\left(\mathbf{\Psi}_l, \mathbf{\Psi}_j\right) = \frac{1}{\pi}\int_0^{\pi/2}\prod_{m=1}^{N_d}\left[1+\frac{\varrho\left(1-d_{m,lj}^2\right)}{4\sin^2\theta}\right]^{-N_R} d\theta, \tag{2.48}$$

where $0 < N_d \leq N_T$ is the number of non-unity singular values, and $\varrho = \left(\rho T/N_T\right)^2/\left(1+\rho T/N_T\right)$. This expression leads to the following new bounds on the PEP.

2.6.1.1 Tight Upper Bound-1 (TUB1)

Applying the inequality $(1+x)^{-1} \leq x^{-1}, x > 0$ to the integrand in (2.48), we can upper bound the PEP by

$$P_e\left(\mathbf{\Psi}_l, \mathbf{\Psi}_j\right) \leq \frac{1}{\pi}\int_0^{\pi/2}\prod_{m=1}^{N_d}\left[\frac{\varrho\left(1-d_{m,lj}^2\right)}{4\sin^2\theta}\right]^{-N_R} d\theta. \tag{2.49}$$

Using the integral formula in [124, eq. 2.513 1], i.e.,

$$\int \sin^{2n} x dx = \frac{1}{2^{2n}}\binom{2n}{n}x + \frac{(-1)^n}{2^{2n-1}}\sum_{k=0}^{n-1}(-1)^k\binom{2n}{k}\frac{\sin 2(n-k)x}{2(n-k)}, \quad (2.50)$$

the upper bound in (2.49) can be reduced to

$$P_e\left(\mathbf{\Psi}_l, \mathbf{\Psi}_j\right) \leq \left(\varrho \overline{d}_{gm,lj}\right)^{-N_d N_R}\binom{2N_d N_R - 1}{N_d N_R}. \quad (2.51)$$

Here, $\overline{d}_{gm,lj}$ is the geometric mean of the singular values, defined as

$$\overline{d}_{gm,lj} = \left[\prod_{m=1}^{N_d}\left(1 - d_{m,lj}^2\right)\right]^{1/N_d}. \quad (2.52)$$

The right-hand side (RHS) of (2.51) is our new, tight, upper bound-1, abbreviated as TUB1, on the PEP of the QR. Since $\{d_{m,lj}\}_{m=1}^{N_T}$ are the singular values of $\mathbf{\Phi}_j^\dagger\mathbf{\Phi}_l$, it is clear that $\left\{\left(1 - d_{m,lj}^2\right)\right\}_{m=1}^{N_T}$ are the eigenvalues of the matrix $\left(\mathbf{I} - \mathbf{\Phi}_l^\dagger\mathbf{\Phi}_j\mathbf{\Phi}_j^\dagger\mathbf{\Phi}_l\right)$, and their product equals the determinant of this matrix [125]. Thus, when we have full diversity, i.e., $N_d = N_T$, $\overline{d}_{gm,lj}$ can be obtained by

$$\overline{d}_{gm,lj} = \left[\det\left(\mathbf{I} - \mathbf{\Phi}_l^\dagger\mathbf{\Phi}_j\mathbf{\Phi}_j^\dagger\mathbf{\Phi}_l\right)\right]^{1/N_T}, \quad (2.53)$$

which does not require one to compute singular values. For this special case, [63] has shown that the RHS of (2.51) is an approximation of the PEP at high SNR, i.e., $\rho \to \infty$, by applying the asymptotic error probability analysis in [37]. However, our simpler derivation here shows that (2.51) is actually an upper bound on the PEP for all SNR, irrespective of whether or not the diversity order is full.

At high SNR, $\rho \gg 1$, which implies $\varrho \gg 1$, the CUB in (2.14) can be approximated by

$$\begin{aligned} P_e\left(\mathbf{\Psi}_l, \mathbf{\Psi}_j\right) &\lesssim \frac{1}{2}\prod_{m=1}^{N_d}\left[\varrho\left(1 - d_{m,lj}^2\right)/4\right]^{-N_R} \\ &= \left(\varrho\overline{d}_{gm,lj}\right)^{-N_d N_R} 2^{2N_d N_R - 1}. \end{aligned} \quad (2.54)$$

It can easily be shown that [124, eqs. (0.151 2) and (0.151 3)]

$$\binom{2N_dN_R-1}{N_dN_R} < \sum_{i=0}^{2N_dN_R-1}\binom{2N_dN_R-1}{i} = 2^{2N_dN_R-1}, \tag{2.55}$$

and thus, from (2.51), (2.54), and (2.55), we can see that our bound in (2.51) is tighter than the CUB in (2.14) at high SNR.

2.6.1.2 Tight Upper Bound-2 (TUB2)

Using the well-known arithmetic mean-geometric mean inequality, Byun and Lee obtained in [123] the following inequality:

$$\prod_{i=1}^{N_d}(1+x_i) \geq (1+x_{gm})^{N_d} \tag{2.56}$$

where $x_i > 0, \forall i$, and $x_{gm} = \left(\prod_{i=1}^{N_d} x_i\right)^{1/N_d}$ is the geometric mean of the x_i's. We apply this inequality to (2.48), and obtain

$$P_e\left(\mathbf{\Psi}_l, \mathbf{\Psi}_j\right) \leq \frac{1}{\pi}\int_0^{\pi/2}\left(1+\frac{\varrho\overline{d}_{gm,lj}}{4\sin^2\theta}\right)^{-N_dN_R} d\theta. \tag{2.57}$$

The RHS of (2.57) can be regarded as an equal-singular-value case of the PEP expression in (2.48), whose closed-form result for this case is given in (2.16) and (2.17). Therefore, a closed-form expression for the upper bound in (2.57) can be obtained by replacing $(1-d_{lj}^2)$ in (2.16) and (2.17) with $\overline{d}_{gm,lj}$, and thus is given by

$$P_e\left(\mathbf{\Psi}_l, \mathbf{\Psi}_j\right) \leq \left(\frac{1-\mu_{lj}}{2}\right)^{N_dN_R}\sum_{n=0}^{N_dN_R-1}\binom{N_dN_R-1+n}{n}\left(\frac{1+\mu_{lj}}{2}\right)^n \tag{2.58}$$

where

$$\mu_{lj} = \sqrt{\varrho\overline{d}_{gm,lj}/\left(\varrho\overline{d}_{gm,lj}+4\right)}.$$

This is our new, tight, upper bound-2, abbreviated as TUB2. Equality in (2.58) holds when all non-unity singular values are equal. The more distinct the singular values are from one another, the looser the upper bound becomes. For a given N_d, this bound is a decreasing function of $\overline{d}_{gm,lj}$.

Applying the formula [124, eq. 0.151 1], i.e.,

$$\binom{n+m+1}{n+1} = \sum_{k=0}^{m} \binom{n+k}{n} = \sum_{k=0}^{m} \binom{n+k}{k}, \tag{2.59}$$

the upper bound in (2.51) can be rewritten as

$$P_e\left(\mathbf{\Psi}_l, \mathbf{\Psi}_j\right) \leq \sum_{n=0}^{N_d N_R - 1} \binom{N_d N_R - 1 + n}{n} \left(\varrho \overline{d}_{gm,lj}\right)^{-N_d N_R}. \tag{2.60}$$

Since $\varrho \overline{d}_{gm,lj} \geq 0$ and $0 \leq \mu_{lj} \leq 1$, it can easily be shown that

$$\left(\frac{1-\mu_{lj}}{2}\right)^{N_d N_R} \left(\frac{1+\mu_{lj}}{2}\right)^{n} \leq \left(\frac{1-\mu_{lj}}{2}\right)^{N_d N_R} < \left(\varrho \overline{d}_{gm,lj}\right)^{-N_d N_R}. \tag{2.61}$$

Therefore, from (2.58), (2.60) and (2.61), we can see that the bound (2.58) is always tighter than the bound (2.51). From our numerical results in Section 2.6.2, we will see that the upper bound (2.58) is actually the tightest upper bound so far for all SNR.

2.6.1.3 Tight Lower Bound-1 (TLB1)

By applying Jensen's inequality to $\log(1+x)$, Byun and Lee obtained in [123] the following inequality

$$\prod_{i=1}^{N_d} (1 + x_i) \leq (1 + x_{am})^{N_d}, \tag{2.62}$$

where $x_i > 0, \forall i$, and $x_{am} = \sum_{i=1}^{N_d} x_i/N_d$ is the arithmetic mean of the x_i's. Applying this result to (2.48), we obtain the lower bound

$$P_e\left(\mathbf{\Psi}_l, \mathbf{\Psi}_j\right) \geq \frac{1}{\pi}\int_0^{\pi/2}\left(1+\frac{\varrho\overline{d}_{am,lj}}{4\sin^2\theta}\right)^{-N_dN_R} d\theta. \tag{2.63}$$

The RHS of (2.63) can also be solved in closed form by using $\overline{d}_{am,lj}$ to replace $(1-d_{lj}^2)$ in the PEP expression in (2.16) and (2.17) for the equal-singular-value case. Thus, a closed-form expression for (2.63) is given by

$$P_e\left(\mathbf{\Psi}_l, \mathbf{\Psi}_j\right) \geq \left(\frac{1-\nu_{lj}}{2}\right)^{N_dN_R}\sum_{n=0}^{N_dN_R-1}\binom{N_dN_R-1+n}{n}\left(\frac{1+\nu_{lj}}{2}\right)^n \tag{2.64}$$

where

$$\nu_{lj} = \sqrt{\varrho\overline{d}_{am,lj}/\left(\varrho\overline{d}_{am,lj}+4\right)},$$

and $\overline{d}_{am,lj}$ is the arithmetic mean of the singular values, defined as

$$\overline{d}_{am,lj} = \frac{1}{N_d}\left[\sum_{m=1}^{N_d}\left(1-d_{m,lj}^2\right)\right] = \frac{1}{N_d}\mathrm{tr}\left(\mathbf{I}-\mathbf{\Phi}_l^\dagger\mathbf{\Phi}_j\mathbf{\Phi}_j^\dagger\mathbf{\Phi}_l\right). \tag{2.65}$$

The second equality in (2.65) follows the fact that the trace of a matrix equals the sum of its eigenvalues [125, eq. (7.1.7)]. The RHS of (2.64) is our new, tight, lower bound-1, abbreviated as TLB1, which is a decreasing function of $\overline{d}_{am,lj}$. Equality in (2.64) holds when all non-unity singular values are equal. This new lower bound will be seen in Section 2.6.2 to be the tightest at low SNR.

When ρ is sufficiently large and thus $\varrho\overline{d}_{am,lj} \gg 4$, we can obtain an approximation of the RHS of (2.64) by using the approximations used in [1, eq. (14.4–18)], that is, we can use the approximations $(1+\nu_{lj})/2 \approx 1$ and $(1-\nu_{lj})/2 \approx 1/\left(\varrho\overline{d}_{am,lj}\right)$ and the equality [1, eq. (14.4–17)]

$$\sum_{n=0}^{N_dN_R-1}\binom{N_dN_R-1+n}{n} = \binom{2N_dN_R-1}{N_dN_R} \tag{2.66}$$

in (2.64), and obtain

$$P_e^{ATLB}\left(\mathbf{\Psi}_l, \mathbf{\Psi}_j\right) = \left(\varrho \overline{d}_{am,lj}\right)^{-N_d N_R} \binom{2N_d N_R - 1}{N_d N_R}. \tag{2.67}$$

This approximation to the RHS of (2.64) is easier to compute.

2.6.1.4 Tight Lower Bound-2 (TLB2)

For comparison, we also include here another tight lower bound, abbreviated as TLB2, given in [59, eq. (20)], i.e.,

$$P_e\left(\mathbf{\Psi}_l, \mathbf{\Psi}_j\right) \geq \binom{2N_d N_R - 1}{N_d N_R - 1} \prod_{m=1}^{N_d} \left[4 + \varrho\left(1 - d_{m,lj}^2\right)\right]^{-N_R}. \tag{2.68}$$

This bound was obtained by applying the inequality $1 \leq \sin^{-2}\theta$ to the integrand in (2.48). We can see that the TLB2 in the RHS of (2.68) equals the CUB in the RHS of (2.14) times the constant $\binom{2N_d N_R}{N_d N_R}/4^{N_d N_R}$ [59]. The TLB2 can be tighter than the TLB1 in (2.64) at high SNR if the singular values are sufficiently distinct.

2.6.2 Numerical Results

Here we provide some comparisons among the CUB in (2.14), TUB1 in (2.51), TUB2 in (2.58), TLB1 in (2.64), its approximation at high SNR in (2.67), and TLB2 in (2.68), on the PEP of the QR. Figs. 2.2 and 2.3 give the numerical results for the constellation of size seventeen in [54, Table II] which has unequal singular values. At low SNR as shown in Fig. 2.2, the TUB2 in (2.58) and TLB1 in (2.64) on the PEP are the tightest, and they are very close to each other. Hence, they can provide a very good prediction for the PEP. The TUB1 in (2.51) is tighter than the CUB in (2.14) for SNR above 3.8 dB. At high SNR as shown in Fig. 2.3, the TUB1 in (2.51), TUB2 in (2.58) and TLB2 in (2.68) are very close. They can be seen to be a very good approximation to the PEP. We can also see that at high SNR, the expression in (2.67) is a good approximation to both the lower bounds in (2.64) and (2.68).

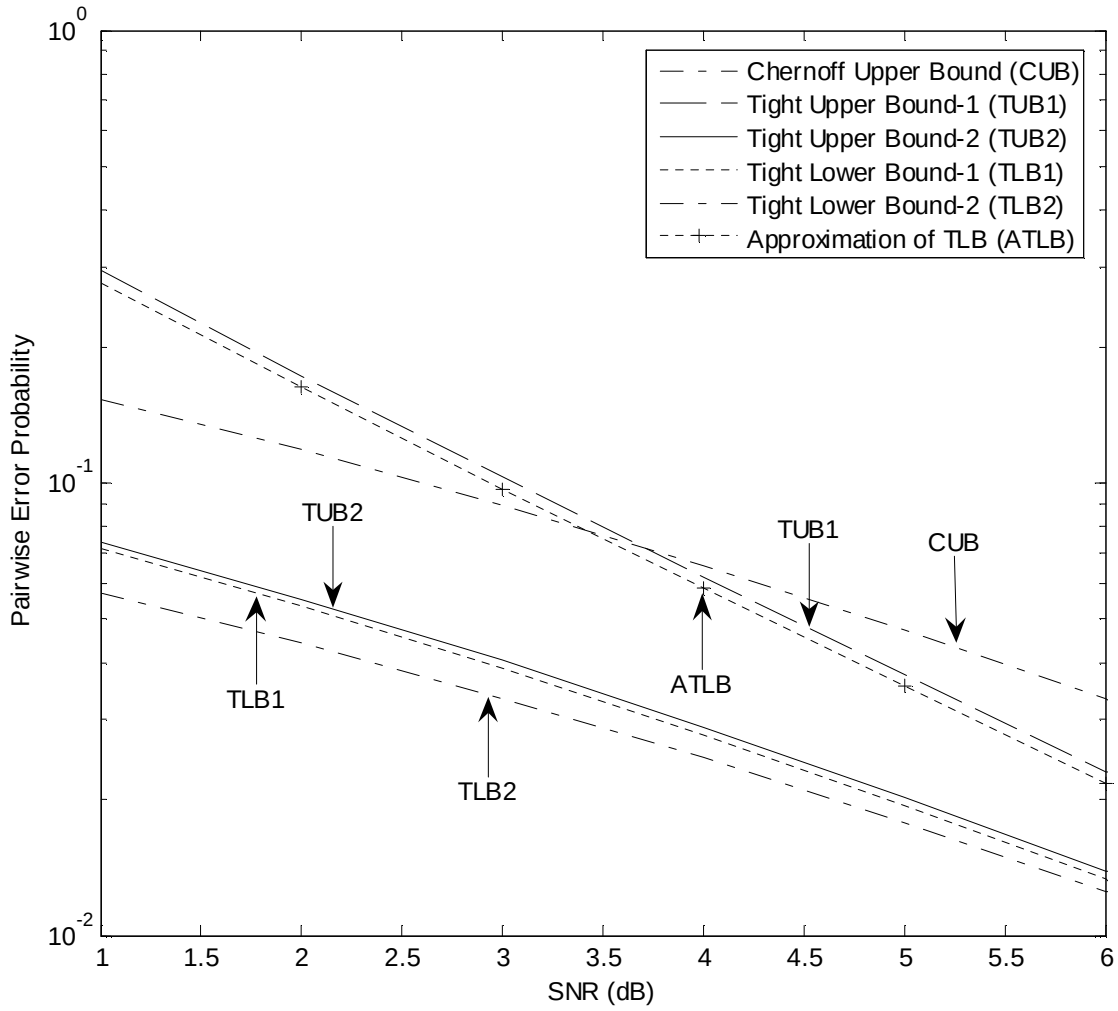

Fig. 2.2: Bounds on the PEP of the QR for the constellation in [54, Table II] at low SNR, $N_T = 2$, $N_R = 1$, $T = 8$, $L = 17$, $d_{1,12} = 0.6366$, $d_{2,12} = 0.1628$.

2.6.3 Implications for Signal Design

The TUB2 in (2.58) on the PEP provides a refinement to the diversity product criterion in (2.37) for USTM constellation design. The diversity product criterion, which is valid for high SNR [19, 54, 62], seeks to minimize the worst PEP by maximizing the minimum of the geometric means $\overline{d}_{gm,lj}$ over all pairs of signal matrices. Thus, we first choose constellations with full diversity, i.e., $N_d = N_T$, and then pick from among them the one whose minimum geometric mean $\overline{d}_{gm,lj}$ over all pairs of l and j is maximum. This ensures that the value of the RHS of (2.58) for the pair of signal matrices with the minimum geometric mean is

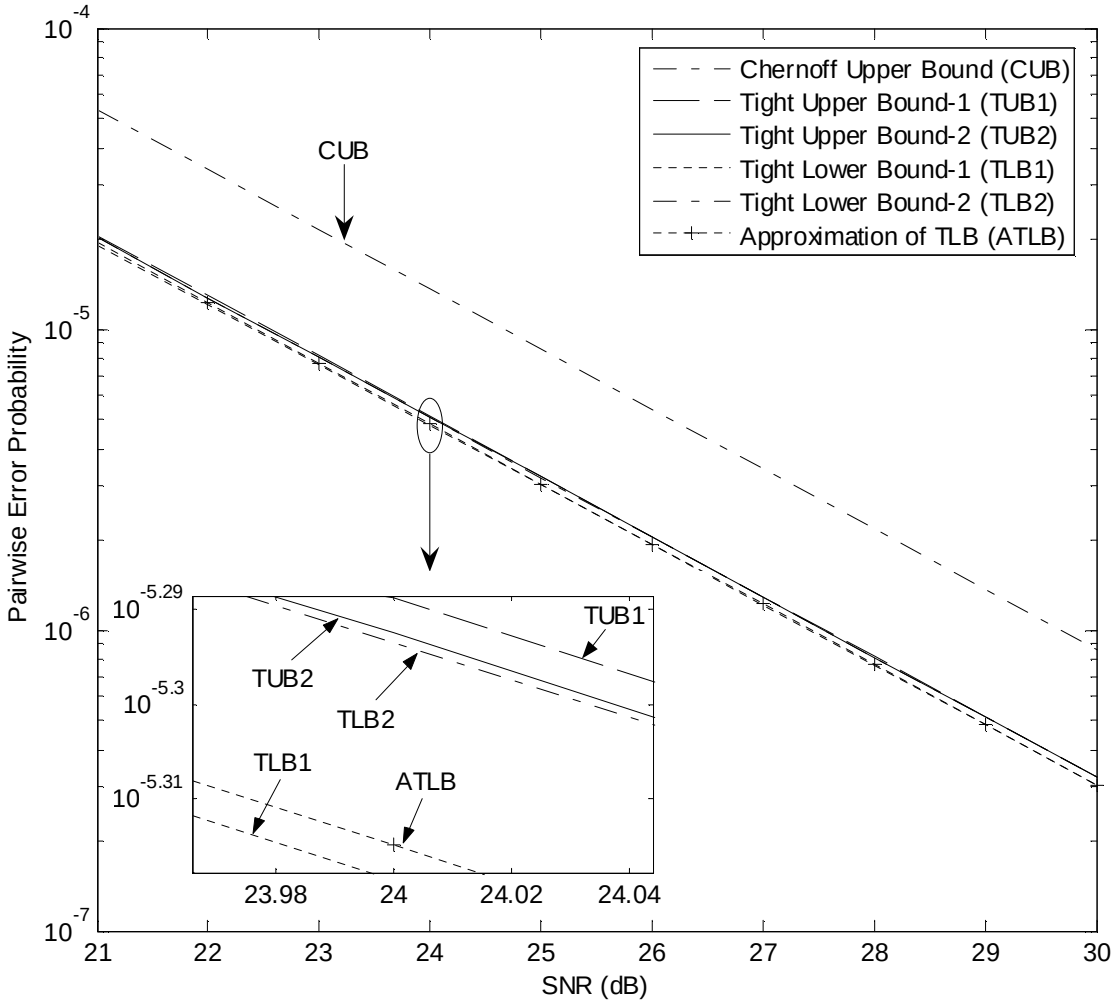

Fig. 2.3: Bounds on the PEP of the QR for the constellation in [54, Table II] at high SNR, $N_T = 2$, $N_R = 1$, $T = 8$, $L = 17$, $d_{1,12} = 0.6366$, $d_{2,12} = 0.1628$.

minimized, since the RHS of (2.58) is a decreasing function of $\overline{d}_{gm,lj}$. The above step gives a result similar to the original diversity product criterion in (2.37). Our new finding is that if from the above step, we obtain more than one constellation, then from these constellations obtained, we should choose the one whose singular values for any pair of signal matrices are as distinct from one another as possible, because this ensures that the PEPs are furthest away from the values of the RHS of (2.58), thus minimizing the PEPs and improving the SEP. Similarly, the AUB criterion in (2.38) can also be refined, since it is also determined only by the geometric means of singular values. From the constellations obtained by using

the AUB criterion, we should choose those whose singular values are as distinct from one another as possible. This is because for the constellations with the same geometric means, those with distinct singular values give lower PEPs than those with similar singular values.

The TLB1 in (2.64) also provides a refinement to the diversity sum criterion in (2.36). The diversity sum criterion in (2.36), which is valid for low SNR or small singular values [54, 61, 62], is equivalent to maximizing the minimum of the arithmetic means $\overline{d}_{am,lj}$ over all pairs of signal matrices. It does not guarantee full diversity, as was shown in [19, 63]. In our proposed approach, we first choose constellations for which $N_d = N_T$, so that we already have full diversity. Then from these constellations, we pick the one whose minimum arithmetic mean $\overline{d}_{am,lj}$ is maximum, since it gives the minimum value of the RHS of (2.64) for the pair of signal matrices with the minimum arithmetic mean. If we obtain more than one constellation, then from the constellations obtained, we finally choose the one whose non-unity singular values for any pair of signal matrices are the closest together. This is because for a given value of the RHS of (2.64), the PEP attains this lower bound only when non-unity singular values are equal.

2.7 Summary

In this chapter, we have presented a general space–time coded system model. Based on this model, some important results for USTM in the literature have been reviewed, concentrating in particular on the issues of capacity-achieving signal structure, ML receiver design, performance analysis, and signal design. Both the case where the channel is unknown to the receiver and the case where the channel is known to the receiver have been discussed. From these results, we can see that in the sense of achieving capacity, the USTM scheme has been shown to be optimal when the receiver does not know the channel, and nearly optimal when the receiver knows the channel perfectly. We can also see that ML detection leads

to a QR for the case that the channel is unknown, and a CR for the case that the channel is known. For both the QR and the CR, expressions for the PEP have been given in terms of residues or high-order derivatives. Only for the special case that singular values are identical can the expressions for the PEP be given explicitly in a simple closed form. The performance gain for having perfect CSI and using the CR has been shown to be 2–4 dB in SNR over using the QR. Based on the CUBs, some popular signal design criteria and constellation constructions have been given.

In addition to these existing results, we have also proposed and examined some simple, tight, upper and lower bounds on the PEP of the QR for USTM over the Rayleigh block-fading channel. Our analytical and numerical results have shown that these simple bounds can provide a very accurate prediction for the error performance. They have also led to some refinements for the USTM constellation design criteria.

Chapter 3

Generalized Quadratic Receivers for Unitary Space–Time Modulation

In this chapter, we propose the generalized quadratic receivers for USTM over the flat Rayleigh block-fading channel. The GQRs realize the performance improvement potential, known to be approximately 2–4 dB in SNR, between the QR and the CR, by performing channel estimation without the help of additional training signals that consume additional bandwidth. They are designed for various USTC in which signal matrices may or may not contain explicit inherent training blocks, and may or may not be orthogonal to one another. As the channel memory span exploited for channel estimation increases, the error probability of the GQRs reduces from that of the QR to that of the CR. The GQRs work well for both slow and fast fading channels, and the performance improvement increases as the channel fade rate decreases. For a class of USTC with the orthogonal design structure, the GQR can be simplified to a form whose complexity can be less than the complexity of the QR or even that of the simplified form of the QR.

3.1 Introduction

For the scenarios where sending training signals to acquire CSI at the receiver is undesirable or infeasible, due to the limited bandwidth resources or rapid changes in the channel characteristics, the USTM scheme has been proposed in [21, 45, 54] to enable data detection to be done by using a QR without CSI at the receiver. However, a notable result therein is that a CR with perfect CSI can bring about a 2 to 4 dB gain in SNR over a QR [21, 54]. This result carries the exciting implication that for the scenarios where we have to employ the USTM scheme to avoid sending additional training signals, if there exist some robust channel estimation methods for USTM, which require no additional training signals and which give accurate channel estimates, the error performance of USTM can be significantly improved without consuming additional bandwidth. This motivates us to develop the concept of GQR for USTM, which incorporates channel estimation without the help of additional training signals and which bridges the performance gap between the QR and the CR.

The concept of GQR was originally proposed for binary orthogonal signaling in [42], based on a new detector–estimator interpretation of the original optimum QR [41]. This GQR exploits the implicit, but extractable pilot components inherent in the binary orthogonal data signals to estimate the channel. It guarantees an error performance at least as good as that of the QR, and leads to a substantial performance improvement over the QR when the channel memory is exploited to improve the channel estimation accuracy.

We generalize the idea of the GQR to USTM. We first derive the GQR for a class of USTC-OD proposed in [65–67], and reviewed in Section 2.5.2. Each signal matrix in USTC-OD consists of a training block and a real or complex orthogonal design block for STBC [7]. We only focus on the complex orthogonal design case, and this class of constellations has been designed and fully justified in [67] for two to four transmit antennas. For the case of two or four transmit antennas, simply using the inherent training blocks to estimate the channel can already achieve our

aim given above, but this is not true for the case of three antennas. Thus, we start with the former simpler case to build up the concepts and to facilitate the derivations of the GQRs for the more complicated cases. The case of three transmit antennas will be discussed later. The GQR for the USTC-OD with two or four transmit antennas can be simplified to have a complexity less than that of the QR in [21] and that of the simplified form of the QR in [67]. This simplified GQR can also be interpreted as a mismatched receiver[1] for the corresponding STBC, with channel estimation based on additional training signals, and the latter was discussed in [10–12, 126]. However, our GQR improves the error performance by exploiting the channel memory in channel estimation, not by varying the training signal power as was done in [10–12, 126]. Next, we derive the GQR for OUSTC in which the signal matrices are orthogonal to one another, such as some constellations designed in [54]. Since signal matrices in OUSTC contain no explicit training blocks, similar to the binary orthogonal signaling case in [42], we have to exploit their implicit, but extractable pilot components to estimate the channel. An explicit, exact, closed-form expression for the PEP of the GQRs for the USTC-OD with two or four transmit antennas and for OUSTC is derived in terms of the channel estimation accuracy. Finally, we consider the most difficult case, i.e., deriving the GQR for general NOUSTC in which signal matrices may be nonorthogonal to one another. This GQR uses a novel approach to estimate the channel. It applies to constellations which contain no explicit or implicit extractable pilot components, such as most of the constellations in [54]. It also applies to constellations which contain training blocks, but whose conventional mismatched receiver is suboptimal and gives an error performance worse than that of the QR when only the current received training block is used in channel estimation, such as the USTC-OD for three transmit antennas in [67]. Our theoretical and simulation results show that the error performance of the three GQRs improves from that

[1] In [12], the term "mismatched receiver" was used to refer to the receiver which uses the channel estimate to replace the true value of the channel in the CR. Here, we follow this usage. This mismatched receiver was also called an estimator–detector receiver in [10].

of the QR to that of the CR when a wider channel memory span is exploited in channel estimation. Compared to the trained modulation for USTM in [73] which used additional training signals, and which did not exploit the channel memory to improve the channel estimation accuracy, our GQRs use less bandwidth, and can provide a better error performance with a small increase in receiver complexity.

We first review the concept of the GQR for binary orthogonal signals over the flat Rayleigh fading channel in SIMO systems in Section 3.2. Then in Section 3.3, we derive the GQRs and their performance for the USTC-OD with two or four transmit antennas, OUSTC and general NOUSTC.

3.2 Generalized Quadratic Receiver for Binary Orthogonal Signals in SIMO Systems

In this section, we review the main idea of the GQR for binary orthogonal signals over the slow, flat, Rayleigh fading channel in SIMO systems [41, 42]. The structure of the GQR is actually based on a new detector–estimator interpretation of the well-known QR for binary orthogonal signals [41]. This new interpretation shows that it is wrong to refer to the QR as a noncoherent receiver. The QR actually performs partially coherent detection, and uses half of the energy per bit to estimate the channel. This new interpretation also provides an access to the generalization of the QR to achieve substantial performance gains by exploiting the channel memory to improve the channel estimation accuracy [42]. Thus here, we first review the detector–estimator interpretation of the QR, and then generalize it to obtain the GQR. This section serves as a starting point of the main contribution of this chapter, i.e., design and performance analysis of the GQRs for USTM.

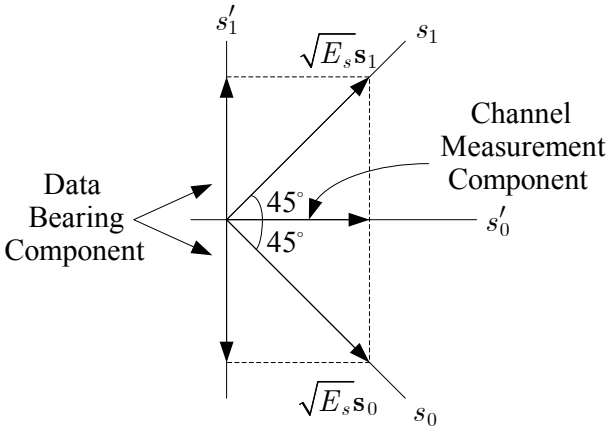

Fig. 3.1: The binary orthogonal signal structure.

3.2.1 Detector–Estimator Receiver for Binary Orthogonal Signals

As shown in Fig. 3.1, after rotating the coordinate system, the orthogonal signal structure can be considered as the combination of an antipodal signal set and a pilot component for channel measurement [41]. In the original $s_0 s_1$-space, the transmitted signal can be given in vector notation by

$$\mathbf{s} = \begin{cases} \sqrt{E_s}\mathbf{s}_0 = \sqrt{E_s}\begin{pmatrix} 1 \\ 0 \end{pmatrix}, & \text{on hypothesis } H_0, \quad (3.1a) \\ \sqrt{E_s}\mathbf{s}_1 = \sqrt{E_s}\begin{pmatrix} 0 \\ 1 \end{pmatrix}, & \text{on hypothesis } H_1. \quad (3.1b) \end{cases}$$

Here, E_s is the energy per bit, and $\mathbf{s}_0$ and $\mathbf{s}_1$ are orthonormal vectors corresponding to orthonormal waveforms $s_0(t)$ and $s_1(t)$ over $[0,\ T_s]$. Then we define the rotated coordinate system as $s_0' s_1'$-space in which the orthonormal vectors $\mathbf{s}_0'$ and $\mathbf{s}_1'$ are defined by

$$\begin{cases} \mathbf{s}_0' = \dfrac{1}{\sqrt{2}}\left[\mathbf{s}_0 + \mathbf{s}_1\right], & (3.2a) \\ \mathbf{s}_1' = \dfrac{1}{\sqrt{2}}\left[\mathbf{s}_1 - \mathbf{s}_0\right]. & (3.2b) \end{cases}$$

In this new $s'_0 s'_1$-space, the transmitted signal is given by

$$\mathbf{s} = \begin{cases} \sqrt{\frac{E_s}{2}} \left[\mathbf{s}'_0 - \mathbf{s}'_1\right] = \sqrt{\frac{E_s}{2}} \begin{pmatrix} 1 \\ -1 \end{pmatrix}, & \text{on hypothesis } H_0, \quad (3.3a) \\ \sqrt{\frac{E_s}{2}} \left[\mathbf{s}'_0 + \mathbf{s}'_1\right] = \sqrt{\frac{E_s}{2}} \begin{pmatrix} 1 \\ 1 \end{pmatrix}, & \text{on hypothesis } H_1. \quad (3.3b) \end{cases}$$

Thus, from the $s_0 s_1$-space to the $s'_0 s'_1$-space, the rotation matrix $\mathbf{A}_r$ is given by

$$\mathbf{A}_r = \frac{1}{\sqrt{2}} \begin{pmatrix} 1 & 1 \\ -1 & 1 \end{pmatrix}. \quad (3.4)$$

From (3.3) and Fig. 3.1, we can see that after the coordinate system rotation, the two orthogonal signals have the same value on the s'_0-axis and the opposite values on the s'_1-axis. Hence, $\sqrt{E_s/2}\mathbf{s}'_0$ is an unmodulated component, which is independent of the hypothesis and can be used to estimate the channel. The antipodal signal set, i.e., $\sqrt{E_s/2}\mathbf{s}'_1$ and $-\sqrt{E_s/2}\mathbf{s}'_1$, is data bearing component and can be used to detect signals.

Suppose we employ a diversity reception over N_R i.i.d. flat Rayleigh fading channels. Then in the $s_0 s_1$-space, the complex received signal over the ith channel is given in vector notation by

$$\mathbf{r}_i = c_i \mathbf{s} + \mathbf{v}_i, \quad i = 1, \cdots, N_R. \quad (3.5)$$

Here, $\mathbf{s}$ is defined by (3.1); E_s is now the energy per bit per diversity channel, and $N_R E_s = E_b$ is the energy per bit. The received signal vector is $\mathbf{r}_i = [r_{0i}\ r_{1i}]^\top$. Its elements are given by $r_{ji} = \int_0^{T_s} r_i(t) s_j^*(t)\, dt$ for $j = 0, 1$, where $r_i(t)$, $0 \le t < T_s$, is the received signal over the ith channel, and $(\cdot)^*$ denotes the conjugate operation. The additive white Gaussian noise vector is given by $\mathbf{v}_i = [v_{0i}\ v_{1i}]^\top$, where we have $v_{ji} = \int_0^{T_s} v_i(t) s_j^*(t)\, dt$ for $j = 0, 1$, and $v_i(t)$, $0 \le t < T_s$, is the noise over the ith channel. The noise variables $\{v_{0i}, v_{1i}\}_{i=1}^{N_R}$ are i.i.d. $\mathcal{CN}(0, N_0)$ distributed. The parameters $\{c_i\}_{i=1}^{N_R}$ are the unknown complex channel gains which are independent

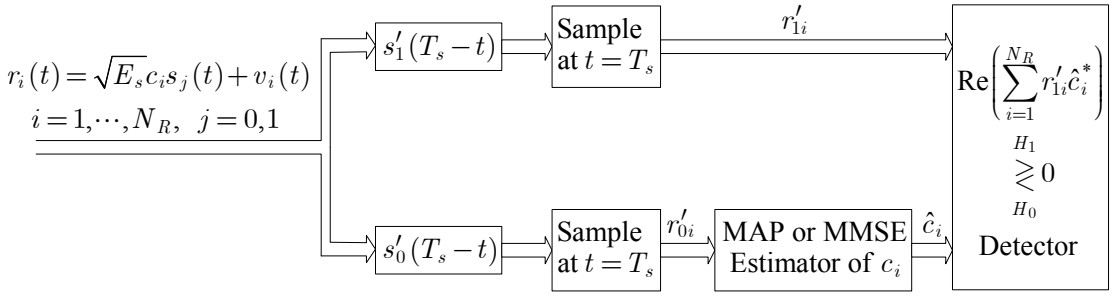

Fig. 3.2: The detector–estimator receiver structure for binary orthogonal signals.

of the hypothesis as well as the noise set $\{\mathbf{v}_i\}_{i=1}^{N_R}$. In Rayleigh fading channels, $\{c_i\}_{i=1}^{N_R}$ are i.i.d. $\mathcal{CN}(0, 2\sigma^2)$ distributed variables.

Then we transform the received signal in (3.5) into $s_0's_1'$-space. In $s_0's_1'$-space, the received signal vector $\mathbf{r}_i' = [r_{0i}'\ r_{1i}']^\top$ is given by

$$\mathbf{r}_i' = \begin{pmatrix} r_{0i}' \\ r_{1i}' \end{pmatrix} = \mathbf{A}_r \mathbf{r}_i = \frac{1}{\sqrt{2}} \begin{pmatrix} 1 & 1 \\ -1 & 1 \end{pmatrix} \begin{pmatrix} r_{0i} \\ r_{1i} \end{pmatrix} = \frac{1}{\sqrt{2}} \begin{pmatrix} r_{0i} + r_{1i} \\ r_{1i} - r_{0i} \end{pmatrix}. \quad (3.6)$$

Thus we have [41, eq. (13)]

$$\begin{cases} r_{0i}' = c_i\sqrt{\dfrac{E_s}{2}} + v_{0i}', & i = 1, \cdots, N_R, \quad (3.7a) \\ r_{1i}' = qc_i\sqrt{\dfrac{E_s}{2}} + v_{1i}', & i = 1, \cdots, N_R, \quad (3.7b) \end{cases}$$

where $q = 1$ on hypothesis H_1, and $q = -1$ on hypothesis H_0; and $\mathbf{v}_i' = [v_{0i}'\ v_{1i}']^\top = \mathbf{A}_r\mathbf{v}_i$ is AWGN with $\{v_{0i}', v_{1i}'\}_{i=1}^{N_R}$ being i.i.d. $\mathcal{CN}(0, N_0)$ distributed. From (3.7), it is clear that r_{0i}' is a hypothesis-independent noisy observation on the unknown channel gain c_i, and only r_{1i}' contains the data information. Thus, a detector–estimator receiver can be used to detect the data carried by r_{1i}', as shown in Fig. 3.2 [41]. The maximum a posteriori probability (MAP) or conditional mean estimate $\hat{c}_i$ of c_i based on r_{0i}' is given by [41, eq. (14)]

$$\hat{c}_i = E\left[c_i \,|r_{0i}'\right] = \frac{2\sigma^2\sqrt{E_s/2}}{E_s\sigma^2 + N_0} r_{0i}', \qquad i = 1, \cdots, N_R. \quad (3.8)$$

Then the detector–estimator receiver in Fig. 3.2 treats the $\hat{c}_i$'s as if they were equal to c_i's and uses them to remove the unknown gains c_i's from the decision statistics r'_{1i}'s. The data decision is made using the likelihood ratio test (LRT) [41, eq. (15)]:

$$\mathrm{Re}\left\{\sum_{i=1}^{N_R} r'_{1i}\hat{c}_i^*\right\} \underset{H_0}{\overset{H_1}{\gtrless}} 0 \tag{3.9}$$

or equivalently

$$\mathrm{Re}\left\{\sum_{i=1}^{N_R} r'_{1i}r'^*_{0i}\right\} \underset{H_0}{\overset{H_1}{\gtrless}} 0. \tag{3.10}$$

Here, $\mathrm{Re}\{\cdot\}$ denotes the real part of the quantity in the brackets. Using (3.6), the receiver (3.10) can be rewritten as

$$\mathrm{Re}\left\{\sum_{i=1}^{N_R} r'_{1i}r'^*_{0i}\right\} = \frac{1}{2}\sum_{i=1}^{N_R}\left[|r_{1i}|^2 - |r_{0i}|^2\right] \underset{H_0}{\overset{H_1}{\gtrless}} 0. \tag{3.11}$$

Thus, the detector–estimator receiver in (3.9) or (3.10) is equivalent to a QR in the sense that they produce identical symbol decisions, and the QR has been shown in [40, ch. 7] to be the optimum receiver.

3.2.2 Generalized Quadratic Receiver for Binary Orthogonal Signals

Since the detector–estimator receiver in $s'_0s'_1$-space produces identical symbol decisions as the optimum QR in s_0s_1-space, as shown in (3.11), the error probability of the former should be the same as that of the latter, given by the well-known result in [1, eqs. (14.4–15) and (14.4–30)]. One important consequence of this new interpretation of the QR is that we can further improve the error performance by exploiting the correlation or the memory of the channel between signaling intervals. As a natural extension of the detector–estimator receiver in (3.9) or (3.10), Kam *et al.* proposed in [42] to use the signals received over all the symbol intervals

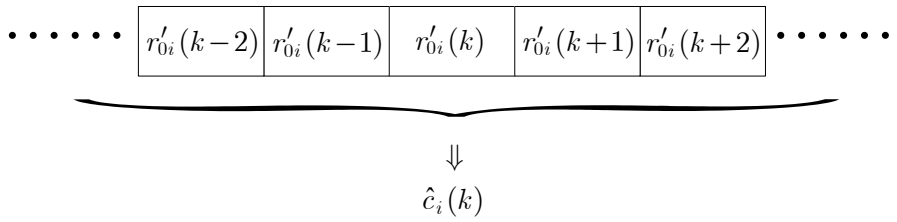

Fig. 3.3: Channel estimation in the GQR for binary orthogonal signals.

or a subset of these intervals to estimate the channel gain in each symbol interval, as shown in Fig. 3.3. By doing so, the accuracy of the channel gain estimate can be improved. This, in turn, leads to an improvement in the error probability performance in data detection.

We now consider to detect the data in the kth symbol interval. The received signal vector over the ith channel during the kth symbol interval is given by

$$\mathbf{r}_i(k) = c_i(k)\,\mathbf{s} + \mathbf{v}_i(k), \quad i = 1, \cdots, N_R. \tag{3.12}$$

Here, the noise vectors $\mathbf{v}_i(k) = [v_{0i}(k)\; v_{1i}(k)]^\top$ for $k = 0, 1, \cdots, \infty$ and $i = 1, \cdots, N_R$ are i.i.d. $\mathcal{CN}(0, N_0\mathbf{I}_2)$. Each variable of the channel gain sequence $\{c_i(k)\}_{k=0}^{\infty}$ is assumed to remain constant within each symbol interval with $\mathcal{CN}(0, 2\sigma^2)$ distribution, and is assumed to be correlated with the one in another symbol interval with the correlation function $R_c(m) = \mathrm{E}[c_i(k+m)\,c_i^*(k)]$. The channel gain sequence $\{c_i(k)\}_{k=0}^{\infty}$ is independent of $\{c_j(k)\}_{k=0}^{\infty}$ for $i \neq j$, and is independent of the noise sequence $\{v_j(k)\}_{k=0}^{\infty}$ for all i and j.

According to (3.9), (3.10), and (3.11), the conventional QR is equivalent to the following detector–estimator receiver [42, eq. (19)]

$$-\sqrt{2}\mathrm{Re}\left\{\sum_{i=1}^{N_R} r'_{1i}(k)\,\hat{c}_i^*(k)\right\} = \mathrm{Re}\left\{\sum_{i=1}^{N_R}\left[r_{0i}(k) - r_{1i}(k)\right]\hat{c}_i^*(k)\right\} \underset{H(k)=H_1}{\overset{H(k)=H_0}{\gtrless}} 0. \tag{3.13}$$

Here,

$$\hat{c}_i(k) = \mathrm{E}[c_i(k)\,|r'_{0i}(k)] = \mathrm{E}[c_i(k)\,|r_{0i}(k) + r_{1i}(k)] \tag{3.14}$$

is the MMSE or MAP or conditional mean estimate of $c_i(k)$ based on $(r_{0i}(k) + r_{1i}(k))$ for each $i = 1, \cdots, N_R$.

Generalizing (3.13) then leads to the GQR for binary orthogonal signals, namely [42, eq. (20)]

$$\mathrm{Re}\left\{\sum_{i=1}^{N_R}\left[r_{0i}(k) - r_{1i}(k)\right]\hat{c}_{i|Z}(k)\right\} \underset{H(k)=H_1}{\overset{H(k)=H_0}{\gtrless}} 0. \tag{3.15}$$

Here,

$$\hat{c}_{i|Z}(k) = \mathrm{E}\left[c_i(k)\,|Z_i(k)\right], \qquad i = 1, \cdots, N_R, \tag{3.16}$$

is the MMSE or MAP or conditional mean estimate of $c_i(k)$ based on the information set

$$Z_i(k) = \{r_{0i}(m) + r_{1i}(m)\}_{m=k-M}^{k+M}, \qquad i = 1, \cdots, N_R. \tag{3.17}$$

The error probability of this GQR is given by [42, eqs. (24) and (25)]

$$P_e = \left(\frac{1-\mu}{2}\right)^{N_R}\sum_{i=0}^{N_R-1}\binom{N_R-1+i}{i}\left(\frac{1+\mu}{2}\right)^{i} \tag{3.18}$$

where

$$\mu = \sqrt{\frac{1 - v_c^2/(2\sigma^2)}{1 + 2/\gamma_c}}. \tag{3.19}$$

Here, $\gamma_c = 2\sigma^2 E_s/N_0$ is the mean received SNR per channel per bit, and v_c^2 is the mean-square error (MSE) in the estimate $\hat{c}_{i|Z}(k)$, given by

$$v_c^2 = \mathrm{E}\left[\left|c_i(k) - \hat{c}_{i|Z}(k)\right|^2 \Big| \{Z_i(k)\}_{i=1}^{N_R}\right]. \tag{3.20}$$

Since the channels are identical, the MSE v_c^2 is identical for all the channels, i.e., independent of the channel index i.

For finite memory sets, the estimator for each channel is a Wiener filter which

generates $\hat{c}_{i|Z}(k)$ as a linear weighted sum of the signals in $Z_i(k)$, namely [14, eq. (24)]

$$\hat{c}_{i|Z}(k) = \sum_{m=-M}^{M} \alpha(m) \left[r_{0i}(k+m) + r_{1i}(k+m) \right]. \tag{3.21}$$

The weights $\alpha(m)$'s are chosen to minimize the MSE v_c^2. According to the orthogonality property, $\alpha(m)$'s are the solutions of the following equations [14, eq. (25)]

$$\sum_{m=-M}^{M} \alpha(m) \left[E_s R_c(j-m) + 2N_0 \delta_{mj} \right] = \sqrt{E_s} R_c(j), \ j = -M, \cdots, M \tag{3.22}$$

where

$$\delta_{mj} = \begin{cases} 1, & m = j, \\ 0, & m \neq j. \end{cases}$$

The corresponding MMSE is given by

$$v_c^2 = R_c(0) - \sqrt{E_s} \sum_{m=-M}^{M} \alpha(m) R_c(m) = 2\sigma^2 - \sqrt{E_s} \sum_{m=-M}^{M} \alpha(m) R_c(m). \tag{3.23}$$

Kam *et al.* have shown in [42] that when the information set $Z_i(k)$ only involves $\{r_{0i}(k) + r_{1i}(k)\}$, i.e., only the received signals in the current interval are used to estimate channels, the MMSE in (3.23) reduces to $v_c^2 = 4\sigma^2/(\gamma_c + 2)$. Thus, the parameter μ in (3.19) of the error probability for the GQR reduces to $\mu = \gamma_c/(\gamma_c+2)$, which turns out to be the same as that in [1, eq. (14.4–30)] for the conventional QR. As the channel memory span exploited in channel estimation increases, the error probability of the GQR decreases. In the limit of perfect channel estimation, i.e., $v_c^2 = 0$, the parameter μ in (3.19) for the GQR reduces to $\mu = \sqrt{\gamma_c/(\gamma_c + 2)}$, which turns out to be the same as that in [1, eq. (14.4–21)] for the CR. The simulation results in [42] have shown that the performance gain of the GQR over the QR is larger for a slower channel, and is also larger for a higher order of diversity. For a finite memory receiver, most of the potential performance gain

can be obtained by using signal observations in just a few immediately adjacent symbol intervals. Hence, the additional computational requirement is not great in most cases of practical interest.

3.3 Generalized Quadratic Receiver for Unitary Space–Time Modulation

In this section, we extend the concept of the GQR to the USTM system over the flat Rayleigh block-fading channel. In Section 3.3.1, we first give the USTM system model which takes into account the channel memory. Then in Section 3.3.2, we derive the GQR for the USTC-OD with two or four transmit antennas in [67]. In Section 3.3.3, we derive the GQR for OUSTC in [54]. In Section 3.3.4, we give a unified derivation of the PEP for the above two GQRs. In Section 3.3.5, we derive the GQR for general NOUSTC. Finally, in Section 3.3.6, we present some numerical and simulation results.

3.3.1 System Model

Consider a system with N_T transmit antennas and N_R receive antennas. The Rayleigh fading channels are assumed to remain constant in one time-block of T symbol intervals, and we assume $T > N_T$. Thus, at the kth time-block, the received signal vector is given by

$$\mathbf{x}(k) = \sqrt{\rho T/N_T}\mathbf{\Psi}_l\mathbf{h}(k) + \mathbf{w}(k). \tag{3.24}$$

To make the discussion concise, the time-block index k is omitted when only the signals in the current kth time-block are considered, and is only used to avoid confusion when the signals in the adjacent time-blocks are also involved. In each individual time-block, $\mathbf{x}$, ρ, $\mathbf{\Psi}_l$, $\mathbf{h}$, and $\mathbf{w}$ in (3.24) have the same definitions as those in (2.5). We review these definitions here for easy reference.

The $TN_R \times 1$ complex received signal vector is defined as $\mathbf{x} = [\mathbf{x}_1^\top \ \mathbf{x}_2^\top \ \cdots \ \mathbf{x}_{N_R}^\top]^\top$, where $\mathbf{x}_n = [x_n((k-1)T+1) \ x_n((k-1)T+2) \ \cdots \ x_n(kT)]^\top$ is the received signal vector at receive antenna n and time-block k. The quantity ρ is the mean SNR at each receive antenna. The $TN_R \times N_T N_R$ transmitted signal matrix is defined as $\mathbf{\Psi}_l = \mathbf{I}_{N_R} \otimes \mathbf{\Phi}_l$, where the $T \times N_T$ unitary matrix $\mathbf{\Phi}_l$, chosen from the constellation $\{\mathbf{\Phi}_l \big| \mathbf{\Phi}_l^\dagger \mathbf{\Phi}_l = \mathbf{I}_{N_T}, l = 1, \ldots, L\}$, is transmitted from N_T transmit antennas at time-block k. The $N_T N_R \times 1$ complex channel gain vector is defined as $\mathbf{h} = [\mathbf{h}_1^\top \ \mathbf{h}_2^\top \ \cdots \ \mathbf{h}_{N_R}^\top]^\top$, where $\mathbf{h}_n = [h_{1n} \ h_{2n} \ \cdots \ h_{N_T n}]^\top$. Each h_{mn} is the path gain from transmit antenna m to receive antenna n at time-block k, and $\mathbf{h}$ is $\mathcal{CN}(\mathbf{0}, \mathbf{I}_{N_T N_R})$ distributed. The $TN_R \times 1$ complex noise vector is defined as $\mathbf{w} = [\mathbf{w}_1^\top \ \mathbf{w}_2^\top \ \cdots \ \mathbf{w}_{N_R}^\top]^\top$, where $\mathbf{w}_n = [w_n((k-1)T+1) \ w_n((k-1)T+2) \ \cdots \ w_n(kT)]^\top$ is the noise vector at receive antenna n and time-block k, and $\mathbf{w}$ is $\mathcal{CN}(\mathbf{0}, \mathbf{I}_{TN_R})$ distributed.

In addition, we assume that the path gains over different branches are always independent, but those over the same branch are correlated from one time-block to another with the correlation $R_h(\tau) = \mathrm{E}[h_{mn}(k+\tau)h_{mn}^*(k)]$. The correlation $R_h(\tau)$ is assumed to be identical for all branches, i.e., $R_h(\tau)$ is independent of m and n, and thus we have $\mathrm{E}[\mathbf{h}(k+\tau)\mathbf{h}^\dagger(k)] = R_h(\tau)\mathbf{I}_{N_T N_R}, \forall \tau$. We also assume that the noise vectors are independent with respect to both time and space, i.e., $\mathrm{E}[\mathbf{w}(k+\tau)\mathbf{w}^\dagger(k)] = \mathbf{0}_{TN_R}, \forall \tau \neq 0$, and are independent of $\mathbf{h}$, i.e., $\mathrm{E}[\mathbf{w}(k+\tau)\mathbf{h}^\dagger(k)] = \mathbf{0}, \forall \tau$.

As we have mentioned in Chapter 2, if the channel $\mathbf{h}$ is unknown, the ML receiver is the QR in (2.9), while if the channel $\mathbf{h}$ is known, the ML receiver is the CR in (2.11). When the singular values $\{d_{m,lj}\}_{m=1}^{N_T}$ of the matrix $\mathbf{\Phi}_j^\dagger \mathbf{\Phi}_l$ are equal, i.e., they satisfy (2.15), and the singular values $\{\delta_{m,lj}\}_{m=1}^{N_T}$ of the matrix $(\mathbf{\Phi}_j - \mathbf{\Phi}_l)$ are equal, i.e., they satisfy (2.21), the closed-form expressions for the PEP of mistaking $\mathbf{\Psi}_l$ for $\mathbf{\Psi}_j$ when $\mathbf{\Psi}_l$ was sent for the QR and the CR can be written in the same form, given by

$$P_e(\lambda_{lj}) = \left(\frac{1-\lambda_{lj}}{2}\right)^{N_T N_R} \sum_{i=0}^{N_T N_R - 1} \binom{N_T N_R - 1 + i}{i} \left(\frac{1+\lambda_{lj}}{2}\right)^i. \tag{3.25}$$

For the QR in (2.9), the parameter $\lambda_{lj} = \lambda_{lj,QR}$ is given by (2.17), while for the CR in (2.11), the parameter $\lambda_{lj} = \lambda_{lj,CR}$ is given by (2.23). The QR bases its current decision only on the received signals in the current time-block. In Sections 3.3.2–3.3.5, we develop the GQRs which also extract CSI inherent in the received signals over the adjacent time-blocks. The GQRs bridge the performance gap between the QR and the CR, and as will be shown, their PEP expressions are also given in the form of (3.25) when the conditions in (2.15) and (2.21) are both satisfied.

3.3.2 Generalized Quadratic Receiver for Unitary Space–Time Constellations with Orthogonal Design

We now consider the USTC-OD for $N_T = 2$ and 4, and $T = 2N_T$ proposed in [67]. For the case of $N_T = 2$ and $L = q^2$, $q \in \mathbb{N}$, their constellations are given by (2.44). For the case of $N_T = 2$ and $L = 2^{2n-1}, n \in \mathbb{N}$, their constellations are obtained by extracting the subsets of the constellations of size $L = 2^{2n}$ [66]. For the case of $N_T = 4$ and $L = q^3$, $q \in \mathbb{N}$, their constellations are given by (2.45). We can see that these signal matrices consist of a training block and a data block, and this data block is a square complex orthogonal design for STBC [7]. We let $\mathbf{C}_p$ and $\mathbf{C}_d$ denote, respectively, the $N_T \times N_T$ training block and the $N_T \times N_T$ data block, and $\mathbf{w}_p$ and $\mathbf{w}_d$ denote the corresponding $N_T N_R \times 1$ noise vectors. Thus, the received signals in the training block session are given by

$$\mathbf{x}_p = \sqrt{\rho T/N_T}(\mathbf{I}_{N_R} \otimes \mathbf{C}_p)\mathbf{h} + \mathbf{w}_p, \tag{3.26}$$

and the received signals in the data block session are given by

$$\mathbf{x}_d = \sqrt{\rho T/N_T}(\mathbf{I}_{N_R} \otimes \mathbf{C}_d)\mathbf{h} + \mathbf{w}_d. \tag{3.27}$$

As shown in [67, pgs. 1321–1322], by exploiting the property of orthogonal designs, the QR in (2.9) can be simplified to a receiver that decides on the indexes of the signal matrices separately. For example, for the constellations in (2.44) with

$N_T = 2$ and $L = q^2$, $q \in \mathbb{N}$, the QR in (2.9) can be simplified as

$$\begin{cases} \hat{i}_{ML} = \arg \max\limits_{i=0,\ldots,q-1} \|\mathbf{\Psi}_{i,0}^{\dagger}\mathbf{x}\|^2, & \text{(3.28a)} \\ \hat{l}_{ML} = \arg \max\limits_{l=0,\ldots,q-1} \|\mathbf{\Psi}_{0,l}^{\dagger}\mathbf{x}\|^2. & \text{(3.28b)} \end{cases}$$

For the constellations in (2.45) with $N_T = 4$ and $L = q^3$, $q \in \mathbb{N}$, the QR in (2.9) can be simplified as

$$\begin{cases} \hat{i}_{ML} = \arg \max\limits_{i=0,\ldots,q-1} \|\mathbf{\Psi}_{i,0,0}^{\dagger}\mathbf{x}\|^2, & \text{(3.29a)} \\ \hat{l}_{ML} = \arg \max\limits_{l=0,\ldots,q-1} \|\mathbf{\Psi}_{0,l,0}^{\dagger}\mathbf{x}\|^2, & \text{(3.29b)} \\ \hat{j}_{ML} = \arg \max\limits_{j=0,\ldots,q-1} \|\mathbf{\Psi}_{0,0,j}^{\dagger}\mathbf{x}\|^2. & \text{(3.29c)} \end{cases}$$

As will be shown in Section 3.3.2.4, our GQR can also be simplified similarly.

3.3.2.1 GQR Structure

We now derive the GQR for the USTC-OD given above. As was done for space–time decoding in [10–12, 126], when the channel estimate $\hat{\mathbf{h}}$, instead of $\mathbf{h}$ itself, is available to the receiver, we can replace $\mathbf{h}$ in the CR (2.11) by $\hat{\mathbf{h}}$ to obtain a mismatched receiver for USTM. It is clear that for the USTC-OD, the CR in (2.11) for USTM is equivalent to the CR only for the data block, which can be obtained by replacing $\mathbf{x}$ and $\mathbf{\Psi}_l$ in (2.11) with $\mathbf{x}_d$ and $(\mathbf{I}_{N_R} \otimes \mathbf{C}_{d,l})$, respectively, namely

$$\hat{\mathbf{C}}_{d,CR} = \arg \min_{\mathbf{C}_{d,l} \in \{\mathbf{C}_{d,1},\ldots,\mathbf{C}_{d,L}\}} \left\| \mathbf{x}_d - \sqrt{\rho T / N_T}(\mathbf{I}_{N_R} \otimes \mathbf{C}_{d,l})\mathbf{h} \right\|^2. \quad \text{(3.30)}$$

Here, $\mathbf{C}_{d,l}$ is the data block of $\mathbf{\Phi}_l$ for $l = 1, \cdots, L$, and $\mathbf{C}_{d,l}^{\dagger}\mathbf{C}_{d,l} = \frac{1}{2}\mathbf{I}_{N_T}$. Thus, we can also obtain a mismatched receiver for the data block by using $\hat{\mathbf{h}}$ to replace $\mathbf{h}$ in the CR (3.30) for the data block, as was done in [10, eq. (13)]. These two mismatched receivers are equivalent. Here, we first present the GQR derived from the mismatched receiver for USTM, since this GQR has a structure similar to that of the GQR designed in Section 3.3.3 for OUSTC, and we can derive their PEP

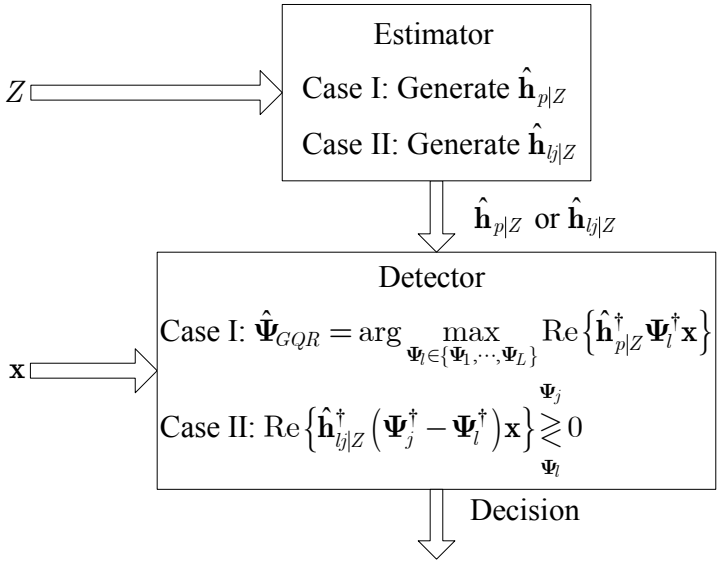

Fig. 3.4: GQR structure for Case I where the channel estimate is the same for all the hypotheses, and Case II where the channel estimate is the same for the two hypotheses concerned.

expressions together in Section 3.3.4. We will discuss the equivalent GQR derived from the mismatched receiver for the data block in Sections 3.3.2.4 and 3.3.2.5.

We define the general information set as

$$Z = \{\mathbf{x}_p(k+m)\}_{m=-M_1}^{M_2}, \qquad M_1, M_2 \geq 0. \tag{3.31}$$

Then we use $\hat{\mathbf{h}}_{p|Z} = \mathrm{E}\big[\mathbf{h}\big|Z\big]$, the MMSE channel estimate based on Z, to replace $\mathbf{h}$ in the CR in (2.11), and obtain the mismatched receiver for USTM, i.e.,

$$\hat{\mathbf{\Psi}} = \arg \min_{\mathbf{\Psi}_l \in \{\mathbf{\Psi}_1, \ldots, \mathbf{\Psi}_L\}} \left\| \mathbf{x} - \sqrt{\rho T / N_T} \mathbf{\Psi}_l \hat{\mathbf{h}}_{p|Z} \right\|^2. \tag{3.32}$$

Since both $\mathbf{\Psi}_l^{\dagger}\mathbf{\Psi}_l = \mathbf{I}_{N_T N_R}$ and $\hat{\mathbf{h}}_{p|Z}$ are independent of the hypothesis, we can reduce (3.32) further to obtain our GQR, namely

$$\hat{\mathbf{\Psi}}_{GQR} = \arg \max_{\mathbf{\Psi}_l \in \{\mathbf{\Psi}_1, \ldots, \mathbf{\Psi}_L\}} \mathrm{Re}\Big\{\hat{\mathbf{h}}_{p|Z}^{\dagger} \mathbf{\Psi}_l^{\dagger} \mathbf{x}\Big\}. \tag{3.33}$$

The GQR in (3.33) is shown in Fig. 3.4 as Case I. Its structure is similar to that of (3.15). This receiver first obtains the channel estimate $\hat{\mathbf{h}}_{p|Z}$ based on Z, which

provides a partially coherent reference in detecting the data carried by $\mathbf{\Psi}_l^\dagger \mathbf{x}$, the projection of the received signal onto the complex subspace spanned by each of the possible transmitted signal matrices. As will be shown in Section 3.3.2.3, by using MMSE channel estimation, we can ensure that the GQR in (3.33) has the same error performance as the QR in (2.9) when we set $M_1 = M_2 = 0$ in (3.31). Since we can further improve the channel estimation accuracy, as shown in [42], by exploiting the channel memory and using also the received signals over the adjacent time-blocks to estimate the channel, we expect a better error performance by setting $M_1 > 0$ and/or $M_2 > 0$.

3.3.2.2 Error Performance

For the USTC-OD in (2.44) with $N_T = 2$, it has been shown that all the singular values of $\mathbf{\Phi}_{i,l}^\dagger \mathbf{\Phi}_{i',l'}$, $\forall \mathbf{\Phi}_{i,l}, \mathbf{\Phi}_{i',l'} \in C_a$ are identical, given by (2.46), and all the singular values of $(\mathbf{\Phi}_{i,l} - \mathbf{\Phi}_{i',l'})$ are identical, given by (2.47). It can easily be shown that similar results hold for the case of $N_T = 4$. Thanks to this nice property, the PEPs of the USTC-OD for the QR and the CR are given explicitly and exactly by the PEP function in (3.25) with the parameters defined in (2.17) and (2.23), respectively.

We now discuss the PEP of the GQR in (3.33). We let h_n and $\hat{h}_{n|Z}$ denote the nth element of $\mathbf{h}$ and its MMSE estimate, respectively. Then the MSE v_h^2 of the channel estimate is defined as

$$v_h^2 = \mathrm{E}\left[\left|h_n - \hat{h}_{n|Z}\right|^2\right], \forall n \in \{1, \ldots, N_T N_R\}. \tag{3.34}$$

Here, since the channels are statistically identical, v_h^2 is independent of n. As will be shown in Section 3.3.4, when the conditions in (2.15) and (2.21) are both satisfied, for the GQR in (3.33), the PEP of mistaking $\mathbf{\Psi}_l$ for $\mathbf{\Psi}_j$ when $\mathbf{\Psi}_l$ was

sent is given by the PEP function $P_e(\lambda_{lj,GQR})$ in (3.25) with

$$\lambda_{lj,GQR} = \left(\sqrt{1 + \frac{4v_h^2(d_{lj}^2 - 1) + 4\left[v_h^2 + N_T/(\rho T)\right]\delta_{lj}^2}{\delta_{lj}^4\left(1 - v_h^2\right)}} \right)^{-1}. \tag{3.35}$$

From (3.25) together with (3.35), we can see that $P_e(\lambda_{lj,GQR})$ is an increasing function of the MSE v_h^2. Hence, if we can exploit the channel correlation better to obtain a more accurate channel estimate, we will have a smaller $P_e(\lambda_{lj,GQR})$. When $v_h^2 = 0$, i.e., the channel estimation is perfect, the error performance parameter $\lambda_{lj,GQR}$ in (3.35) for the GQR reduces to $\lambda_{lj,CR}$ in (2.23) for the CR.

3.3.2.3 Channel Estimation

Now we discuss channel estimation for the USTC-OD in (2.44) and (2.45), by using a Wiener filter to estimate the channel $\mathbf{h}(k)$ based on the received signals over successive time-blocks. We define the channel measurement components $\mathbf{b}(k+m)$ for time-blocks $\{k+m\}_{m=-M_1}^{M_2}$ as

$$\begin{aligned}\mathbf{b}(k+m) &= \left(\rho T/N_T\right)^{-1/2}\mathbf{F}_p\mathbf{x}_p(k+m) \\ &= \mathbf{h}(k+m) + \left(\rho T/N_T\right)^{-1/2}\mathbf{F}_p\mathbf{w}_p(k+m), m = -M_1, \ldots, M_2, \end{aligned} \tag{3.36}$$

where $\mathbf{F}_p = (\mathbf{I}_{N_R} \otimes \mathbf{C}_p)^{-1}$. It is clear that $\mathbf{b}(k+m)$ is a noisy observation on the channel gain $\mathbf{h}(k+m)$, and $\{\mathbf{b}(k+m)\}_{m=-M_1}^{M_2}$ is a one-to-one function of Z in (3.31). Thus, we have $\hat{\mathbf{h}}_{p|Z} = \mathrm{E}\left[\mathbf{h}(k)\middle|\{\mathbf{b}(k+m)\}_{m=-M_1}^{M_2}\right]$. We define $b_n(k+m)$ as the nth element of $\mathbf{b}(k+m)$, and $\mathbf{b}_n(k) = \left[b_n(k-M_1)\ b_n(k-M_1+1)\ \cdots\ b_n(k+M_2)\right]^\top$. Then the MMSE estimate of $h_n(k)$ based on $\mathbf{b}_n(k)$ is

$$\hat{h}_{n|Z} = \mathbf{a}^\dagger\mathbf{b}_n(k), \qquad n = 1, \ldots, N_T N_R, \tag{3.37}$$

where $\mathbf{a} = [a(-M_1)\ a(-M_1+1)\ \cdots\ a(M_2)]^\top$ is the Wiener filter weight vector. According to the orthogonality property, the vector $\mathbf{a}$ is the solution of the Wiener-

Hopf equation [127], given by

$$\mathbf{a} = \mathbf{R}_{bb}^{-1}\mathbf{r}_{hb}, \tag{3.38}$$

where $\mathbf{R}_{bb} = \mathrm{E}\big[\mathbf{b}_n(k)\mathbf{b}_n^{\dagger}(k)\big]$ is the autocorrelation matrix and $\mathbf{r}_{hb} = \mathrm{E}\big[\mathbf{b}_n(k)h_n^*(k)\big]$ is the cross correlation vector. Since we have $\mathrm{E}[h_n(k+s)h_n^*(k+t)] = R_h(s-t)$ and the noise samples are independent of one another and also independent of the channel gains, the (s,t)th entry of $\mathbf{R}_{bb}$ for the USTC-OD is given by

$$r_{st} = \begin{cases} 1 + 2(\rho T/N_T)^{-1}, & s = t \\ R_h(s-t), & s \neq t \end{cases} \tag{3.39}$$

and $\mathbf{r}_{hb}$ is given by

$$\mathbf{r}_{hb} = [R_h(-M_1)\ R_h(-M_1+1)\ \cdots\ R_h(M_2)]^{\top}. \tag{3.40}$$

From (3.38)–(3.40), we can see that $\mathbf{a}$ is real-valued and independent of the channel branch number n and the time-block number k. Thus, $\mathbf{a}$ can be computed in advance, and (3.37) becomes

$$\hat{\mathbf{h}}_{p|Z} = \mathbf{B}\mathbf{a}, \tag{3.41}$$

where

$$\mathbf{B} = [\mathbf{b}(k-M_1)\ \mathbf{b}(k-M_1+1)\ \cdots\ \mathbf{b}(k+M_2)] = [\mathbf{b}_1(k)\ \mathbf{b}_2(k)\ \cdots\ \mathbf{b}_{N_TN_R}(k)]^{\top}. \tag{3.42}$$

The MMSE v_h^2 in (3.34) becomes [127]

$$v_h^2 = 1 - \mathbf{a}^{\top}\mathbf{r}_{hb} = 1 - \sum_{m=-M_1}^{M_2} a(m)R_h(m). \tag{3.43}$$

The expression (3.43) shows that a smaller v_h^2 can be obtained if more adjacent time-blocks are used in channel estimation, provided the channel gains over these

time-blocks are correlated with that being estimated. Hence, if the channel fading is slow enough, v_h^2 is expected to approach zero when we exploit a longer channel memory. This results in the performance of our GQR approaching that of the CR. The expression (3.43) also shows that slower fading will result in a smaller v_h^2 and in turn a better error performance even if the same number of time-blocks is used in channel estimation, since each element $R_h(m)$ is larger for slower fading.

We now examine the worst case where only the received signals in the current time-block are used to acquire the CSI, i.e., $M_1 = M_2 = 0$. From (3.38)–(3.43), we obtain

$$a(0) = \frac{\rho T/N_T}{\rho T/N_T + 2} \tag{3.44}$$

and

$$v_h^2 = \frac{2}{\rho T/N_T + 2}. \tag{3.45}$$

For the USTC-OD in (2.44), substituting this value of v_h^2 and the singular values in (2.46) and (2.47) into the PEP expressions of the GQR in (3.35) and the QR in (2.17), we see that the PEP of our GQR reduces to that of the QR. Similar results hold for the case of $N_T = 4$.

3.3.2.4 Simplified GQR

The GQR in (3.33) can be simplified so that it has a complexity less than that of the QR in (2.9) and even that of the simplified QR in (3.28) and (3.29). We illustrate this for the case of $N_T = 2$ and $L = q^2$, $q \in \mathbb{N}$. It is easy to see that the GQR in (3.33) can be simplified to the following form

$$\hat{\mathbf{\Psi}}_{GQR} = \arg \max_{i,l \in \{0,\ldots,q-1\}} \mathrm{Re}\Big\{ \hat{\mathbf{h}}_{p|Z}^{\dagger} \mathbf{D}_{i,l}^{\dagger} \mathbf{x}_d \Big\}, \tag{3.46}$$

where $\mathbf{D}_{i,l} = \mathbf{D}_i + \mathbf{D}_l$, and

$$\mathbf{D}_i = \mathbf{I}_{N_R} \otimes \frac{1}{2} \begin{bmatrix} r^i & 0 \\ 0 & r^{-i} \end{bmatrix}, \qquad \mathbf{D}_l = \mathbf{I}_{N_R} \otimes \frac{1}{2} \begin{bmatrix} 0 & r^l \\ -r^{-l} & 0 \end{bmatrix}.$$

The GQR in (3.46) can also be derived directly from the mismatched receiver for the data block. As described in Section 3.3.2.1, we can replace $\mathbf{h}$ in the CR (3.30) with $\hat{\mathbf{h}}_{p|Z}$ when $\mathbf{h}$ is not available, and obtain the mismatched receiver for the data block, namely

$$\hat{\mathbf{C}}_d = \arg \min_{\{i,l\} \in \{0,\ldots,q-1\}} \left\| \mathbf{x}_d - \sqrt{\rho T / N_T} \left(\mathbf{I}_{N_R} \otimes \mathbf{C}_{d,(i,l)} \right) \hat{\mathbf{h}}_{p|Z} \right\|^2. \tag{3.47}$$

Here, $\mathbf{C}_{d,(i,l)}$ is the data block of $\mathbf{\Phi}_{i,l}$ for $\{i,l\} \in \{0,\cdots,q-1\}$. This receiver is equivalent to [10, eq. (18)] when $M_1 = M_2 = 0$. Since $\mathbf{C}_{d,(i,l)}$ has a one-to-one correspondence with $\mathbf{\Psi}_{i,l}$, the decision $\hat{\mathbf{C}}_d$ on $\mathbf{C}_{d,(i,l)}$ is equivalent to the decision $\hat{\mathbf{\Psi}}$ on $\mathbf{\Psi}_{i,l}$. Thus, simplifying (3.47) leads to (3.46).

By exploiting the property of orthogonal designs, the GQR in (3.46) can be further simplified to decide on $\hat{\mathbf{\Psi}}_{\hat{i}_{GQR},\hat{l}_{GQR}}$, i.e.,

$$\hat{\mathbf{\Psi}}_{GQR} = \arg \max_{\mathbf{\Psi}_{i,l}} \mathrm{Re}\left\{ \hat{\mathbf{h}}_{p|Z}^{\dagger} \left(\mathbf{D}_i^{\dagger} + \mathbf{D}_l^{\dagger} \right) \mathbf{x}_d \right\} = \hat{\mathbf{\Psi}}_{\hat{i}_{GQR},\hat{l}_{GQR}}, \tag{3.48}$$

where

$$\begin{cases} \hat{i}_{GQR} = \arg \max\limits_{i \in \{0,\ldots,q-1\}} \mathrm{Re}\left\{ \hat{\mathbf{h}}_{p|Z}^{\dagger} \mathbf{D}_i^{\dagger} \mathbf{x}_d \right\}, & \text{(3.49a)} \\ \hat{l}_{GQR} = \arg \max\limits_{l \in \{0,\ldots,q-1\}} \mathrm{Re}\left\{ \hat{\mathbf{h}}_{p|Z}^{\dagger} \mathbf{D}_l^{\dagger} \mathbf{x}_d \right\}. & \text{(3.49b)} \end{cases}$$

It is clear that this detector needs to use only the received signals in the current orthogonal-design session, as shown in Fig. 3.5. To detect the signals at time-block k, the simplified GQR in (3.36), (3.41) and (3.48) needs to calculate the quantities $\mathbf{F}_p \mathbf{x}_p(k + M_2)$ ($\{\mathbf{F}_p \mathbf{x}_p(k+m)\}_{m=-M_1}^{M_2-1}$ are computed in the previous time-blocks) and $\mathbf{Ba}$ each once, and the quantities $\mathrm{Re}\left\{ \hat{\mathbf{h}}_{p|Z}^{\dagger} \mathbf{D}_i^{\dagger} \mathbf{x}_d \right\}$ and $\mathrm{Re}\left\{ \hat{\mathbf{h}}_{p|Z}^{\dagger} \mathbf{D}_l^{\dagger} \mathbf{x}_d \right\}$ each q times. By contrast, the original QR in (2.9) needs to calculate the quantity

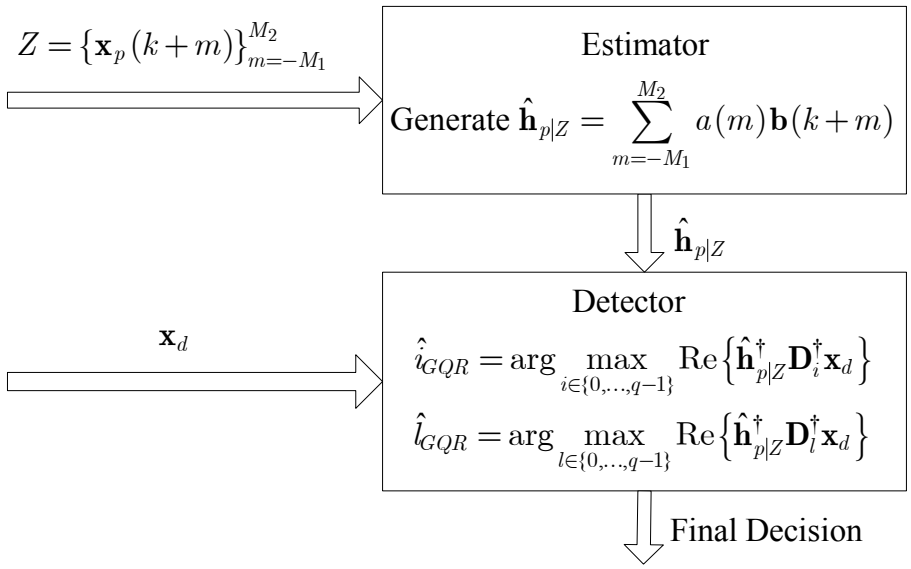

Fig. 3.5: Simplified GQR structure for the USTC-OD with $N_T = 2, 4$.

$\left\|\mathbf{\Psi}_{i,l}^{\dagger}\mathbf{x}\right\|^2$, q^2 times. We can see that if M_1 and M_2 are small enough, the simplified GQR, including the detector and the estimator, can involve less computational complexity than the QR in (2.9). Even compared with the simplified form of the QR in (3.28), which calculates the quantities $\left\|\mathbf{\Psi}_{i,0}^{\dagger}\mathbf{x}\right\|^2$ and $\left\|\mathbf{\Psi}_{0,l}^{\dagger}\mathbf{x}\right\|^2$ each q times, our simplified GQR can still involve less computational complexity, since the sizes of matrices $\mathbf{D}_i$, $\mathbf{D}_l$ and $\mathbf{x}_d$ are only half of those of $\mathbf{\Psi}_{i,0}$, $\mathbf{\Psi}_{0,l}$ and $\mathbf{x}$, respectively. For large-sized constellations, the complexity of the simplified GQR is much less than those of the QR and the simplified form of the QR.

3.3.2.5 Discussion

Our work here is motivated by designing a receiver which exploits pilot components inherent in the data signals themselves to provide a better performance than that of the QR. When $M_1 = M_2 = 0$, the simplified GQR in (3.48) is equivalent to the mismatched receiver for orthogonal STBC that uses the current received training block to obtain the MMSE channel estimate. The latter receiver has also been discussed in [10, 12, 126]. In [10], the performance of general training codes, which consist of one training block and one or more data blocks, was evaluated for

the mismatched receiver with MMSE channel estimation based on the current received training block. *Proposition 1* therein shows that this mismatched receiver is equivalent to the QR if and only if the training codes, which consist of one training block with orthonormal columns and one data block with orthonormal rows, are transmitted over block-wise constant, i.i.d. Rayleigh fading channels. This proposition holds for any power distribution between the training and data blocks. It verifies our result in Section 3.3.2.3, i.e., for the USTC-OD with $N_T = 2$ or 4, our GQR gives the same PEP as the QR when $M_1 = M_2 = 0$. It also indicates that for the USTC-OD with $N_T = 3$, which can be obtained by deleting one column from the design of $N_T = 4$ [67], the mismatched receiver is suboptimal, i.e., its error performance is worse than that of the QR when $M_1 = M_2 = 0$, since the rows of the data block are not orthogonal. This indication is consistent with our results, so we will use the GQR designed in Section 3.3.5 for general NOUSTC to process the USTC-OD with $N_T = 3$ to provide a performance at least as good as that of the QR.

In [10–12, 126], the error performance is improved by increasing or optimizing the power of the training block, while in our work, the error performance is improved by exploiting the channel memory to increase the channel estimation accuracy. For a given training code which satisfies the conditions in *Proposition 1* in [10] mentioned above, optimizing the power distribution between the training and data blocks, as was done in [10, 12], can give a better error performance for the mismatched receiver, or equivalently, for the QR. Even after obtaining the optimal power distribution, one can further improve the error performance by using our GQR to exploit the channel memory.

In addition, the PEP expression in (3.25) together with (3.35) is given in terms of the MSE v_h^2, and shows clearly the effect of the channel estimation accuracy on the error performance. This PEP expression has more flexibility than those in the literature. It holds for the mismatched receivers with different MMSE channel estimation accuracies, since it is independent of the exact expression of the MMSE

channel estimate. It is also valid for various unitary constellations, including not only training codes, but also OUSTC, as will be shown in Section 3.3.3.

3.3.3 Generalized Quadratic Receiver for Orthogonal Unitary Space–Time Constellations

We now derive the GQR for OUSTC which are defined by $\{\mathbf{\Phi}_l \big| \mathbf{\Phi}_l^\dagger \mathbf{\Phi}_l = \mathbf{I}_{N_T}, \mathbf{\Phi}_l^\dagger \mathbf{\Phi}_j = \mathbf{0}_{N_T}, l, j = 1, \ldots, L, l \neq j\}$. Some examples of this class of constellations can be found in [54]. Signal matrices in OUSTC do not contain explicit training blocks, but we can extend the channel estimation method for binary orthogonal signals in [42] to OUSTC.

We first consider the case where only the received signals in the current time-block are involved in channel estimation, i.e., $M_1 = M_2 = 0$. When we decide between two signal matrices $\mathbf{\Psi}_l$ and $\mathbf{\Psi}_j$, we can reexpress the QR in (2.9) as

$$\left\| \mathbf{\Psi}_j^\dagger \mathbf{x} \right\|^2 - \left\| \mathbf{\Psi}_l^\dagger \mathbf{x} \right\|^2 = \mathrm{Re}\left\{ \mathbf{x}^\dagger \left(\mathbf{\Psi}_j + \mathbf{\Psi}_l \right) \left(\mathbf{\Psi}_j^\dagger - \mathbf{\Psi}_l^\dagger \right) \mathbf{x} \right\} \underset{\mathbf{\Psi}_l}{\overset{\mathbf{\Psi}_j}{\gtrless}} 0. \tag{3.50}$$

For OUSTC, the value of the first half of the terms in the curly brackets in (3.50) is independent of the two hypotheses concerned, i.e., the vector

$$\mathbf{b} = \left(\rho T / N_T \right)^{-1/2} \left(\mathbf{\Psi}_j^\dagger + \mathbf{\Psi}_l^\dagger \right) \mathbf{x} = \mathbf{h} + \left(\rho T / N_T \right)^{-1/2} \left(\mathbf{\Psi}_j^\dagger + \mathbf{\Psi}_l^\dagger \right) \mathbf{w} \tag{3.51}$$

has the same value irrespective of whether $\mathbf{\Psi}_l$ or $\mathbf{\Psi}_j$ was transmitted at time-block k. We can see that $\mathbf{b}$ in (3.51) is a noisy observation on $\mathbf{h}$, and thus can be defined as the channel measurement component. The MMSE estimate of $\mathbf{h}$ based on $\mathbf{b}$ when either $\mathbf{\Psi}_l$ or $\mathbf{\Psi}_j$ was sent in time-block k is given by

$$\hat{\mathbf{h}}_{lj} = \mathrm{E}\left[\mathbf{h} \big| \mathbf{\Psi}_l, \mathbf{\Psi}_j, \mathbf{b} \right] = a(0) \mathbf{b}, \tag{3.52}$$

where the Wiener filter weight is

$$a(0) = \frac{\rho T/N_T}{\rho T/N_T + 2} \tag{3.53}$$

by (3.38). Since $a(0)$ and $\left(\rho T/N_T\right)^{-1/2}$ are real positive numbers, the receiver

$$\mathrm{Re}\Big\{\hat{\mathbf{h}}_{lj}^{\dagger}\left(\boldsymbol{\Psi}_j^{\dagger} - \boldsymbol{\Psi}_l^{\dagger}\right)\mathbf{x}\Big\} \underset{\boldsymbol{\Psi}_l}{\overset{\boldsymbol{\Psi}_j}{\gtrless}} 0 \tag{3.54}$$

gives the same decisions on $\boldsymbol{\Psi}$ as the QR in (3.50), and thus they have the same error performance.

We can improve the channel estimation accuracy further in the receiver (3.54) by exploiting the channel memory, and obtain a better error performance over the QR. In the limit of perfect channel estimation, i.e., $\hat{\mathbf{h}}_{lj} = \mathbf{h}$, (3.54) becomes

$$\mathrm{Re}\Big\{\mathbf{h}^{\dagger}\left(\boldsymbol{\Psi}_j^{\dagger} - \boldsymbol{\Psi}_l^{\dagger}\right)\mathbf{x}\Big\} = \frac{1}{2}\left[\left\|\mathbf{x} - \sqrt{\rho T/N_T}\boldsymbol{\Psi}_l\mathbf{h}\right\|^2 - \left\|\mathbf{x} - \sqrt{\rho T/N_T}\boldsymbol{\Psi}_j\mathbf{h}\right\|^2\right] \underset{\boldsymbol{\Psi}_l}{\overset{\boldsymbol{\Psi}_j}{\gtrless}} 0, \tag{3.55}$$

which shows that in this limit, our GQR gives the same decisions on $\boldsymbol{\Psi}$ as the CR in (2.11).

To exploit the channel memory and obtain the channel estimate with higher accuracy, we define the general information set Z for OUSTC as

$$Z = \{\mathbf{b}(k+m)\}_{m=-M_1}^{M_2}, \qquad M_1, M_2 \geq 0. \tag{3.56}$$

Here, the channel measurement components $\{\mathbf{b}(k+m)\}_{m=-M_1}^{M_2}$ are defined by

$$\mathbf{b}(k+m) = \left(\rho T/N_T\right)^{-1/2}\mathbf{F}_o(m)\mathbf{x}(k+m), \quad m = -M_1, \ldots, M_2, \tag{3.57}$$

where

$$\mathbf{F}_o(m) = \begin{cases} \boldsymbol{\Psi}_j^{\dagger} + \boldsymbol{\Psi}_l^{\dagger}, & m = 0, \qquad (3.58a) \\ \displaystyle\sum_{i=1}^{L} \boldsymbol{\Psi}_i^{\dagger}, & m = -M_1, \ldots, M_2, \text{ and } m \neq 0. \qquad (3.58b) \end{cases}$$

For the case of $m = 0$, if either $\mathbf{\Psi}_l$ or $\mathbf{\Psi}_j$ was sent at time-block k, $\mathbf{b}(k)$ has the same value given by (3.51). For the case of $m \neq 0$, regardless of which signal matrix was sent at time-block $(k+m)$, $\mathbf{b}(k+m)$ has the same value, given by

$$\mathbf{b}(k+m) = \mathbf{h}(k+m) + (\rho T/N_T)^{-1/2} \sum_{i=1}^{L} \mathbf{\Psi}_i^{\dagger} \mathbf{w}(k+m). \tag{3.59}$$

Then similar to the case of the USTC-OD in Section 3.3.2.3, the MMSE channel estimate based on Z when either $\mathbf{\Psi}_l$ or $\mathbf{\Psi}_j$ was sent at time-block k is given by

$$\hat{\mathbf{h}}_{lj|Z} = \mathrm{E}\big[\mathbf{h}\big|\mathbf{\Psi}_l, \mathbf{\Psi}_j, Z\big] = \sum_{m=-M_1}^{M_2} a(m)\mathbf{b}(k+m) = \mathbf{B}\mathbf{a}, \tag{3.60}$$

where $\mathbf{B} = [\mathbf{b}(k-M_1)\ \mathbf{b}(k-M_1+1)\ \cdots\ \mathbf{b}(k+M_2)]$. The values of the Wiener filter weight vector $\mathbf{a} = [a(-M_1)\ a(-M_1+1)\ \cdots\ a(M_2)]^{\top}$ and the MMSE v_h^2 can be obtained by using the formulas in (3.38) and (3.43), respectively. The (s,t)th entry of the autocorrelation matrix $\mathbf{R}_{bb}$ for OUSTC becomes

$$r_{o,st} = \begin{cases} 1 + L\,(\rho T/N_T)^{-1}, & s = t \neq M_1 + 1, \quad \text{(3.61a)} \\ 1 + 2\,(\rho T/N_T)^{-1}, & s = t = M_1 + 1, \quad \text{(3.61b)} \\ R_h(s-t), & s \neq t. \quad \text{(3.61c)} \end{cases}$$

The cross correlation vector $\mathbf{r}_{hb}$ for OUSTC has the same value as that in (3.40). We can see that the values of $\mathbf{a}$ and v_h^2 are independent of the channel branch number n and the time-block number k, and also independent of the values of l and j.

Now, we use $\hat{\mathbf{h}}_{lj|Z}$ in (3.60) to replace $\hat{\mathbf{h}}_{lj}$ in the receiver (3.54), and obtain the GQR for OUSTC:

$$\mathrm{Re}\Big\{\hat{\mathbf{h}}_{lj|Z}^{\dagger}\left(\mathbf{\Psi}_j^{\dagger} - \mathbf{\Psi}_l^{\dagger}\right)\mathbf{x}\Big\} \underset{\mathbf{\Psi}_l}{\overset{\mathbf{\Psi}_j}{\gtrless}} 0. \tag{3.62}$$

In this GQR, for any pair of $\mathbf{\Psi}_l$ and $\mathbf{\Psi}_j$, we just apply the same weight vector $\mathbf{a}$, computed in advance by using the values of $\mathbf{R}_{bb}$ in (3.61) and $\mathbf{r}_{hb}$ in (3.40), to

$\{\mathbf{b}(k+m)\}_{m=-M_1}^{M_2}$ in (3.57) to obtain $\hat{\mathbf{h}}_{lj|Z}$, and apply the decision rule in (3.62). We can choose an arbitrary pair of the signal matrices to start the comparisons. If neither of the alternatives $\mathbf{\Psi}_l$ and $\mathbf{\Psi}_j$ is the actual signal matrix sent at time-block k, $\mathbf{b}(k)$ in (3.57) for the case of $m = 0$ just contains noise, and thus, it does not matter which of the alternatives is selected. We just move on to the next comparison between this interim survivor and the next possible signal matrix. An error event can only occur when the actual signal matrix sent is involved in the comparison. We can see that the GQR for OUSTC needs to estimate the channel and use the decision rule in (3.62) $(L-1)$ times to come to a final decision. This GQR structure is shown in Fig. 3.4 as Case II where the channel estimate is the same for the two hypotheses concerned.

For OUSTC, the singular values $\{d_{m,lj}\}_{m=1}^{N_T}$ of $\mathbf{\Phi}_j^\dagger \mathbf{\Phi}_l$ satisfy the condition in (2.15), and are all given by $d = 0$. The singular values $\{\delta_{m,lj}\}_{m=1}^{N_T}$ of $(\mathbf{\Phi}_j - \mathbf{\Phi}_l)$ satisfy the condition in (2.21), and are all given by $\delta = \sqrt{2}$. We can see that the values of these singular values are independent of the values of l and j. As will be shown in Section 3.3.4, the PEP of the GQR for OUSTC for any pair of $\mathbf{\Psi}_l$ and $\mathbf{\Psi}_j$ is also given by the PEP function in (3.25), and the parameter $\lambda_{lj,GQR}$ in (3.35) reduces to λ_{GQR}, given by

$$\lambda_{GQR} = \sqrt{\frac{(1 - v_h^2)\rho T/N_T}{2 + \rho T/N_T}}. \tag{3.63}$$

For the worst case where only the received signals in the current time-block are used to estimate the channel, i.e., $M_1 = M_2 = 0$, we substitute the value of the MMSE

$$v_h^2 = \frac{2}{\rho T/N_T + 2} \tag{3.64}$$

into (3.63), and find that the PEP parameter of the GQR for OUSTC reduces to that of the QR in (2.17), the same result as our analysis for the special case of the GQR in (3.54). Similar to the case of the USTC-OD in Section 3.3.2, as M_1 and

M_2 increase, the value of v_h^2 for OUSTC decreases, and the PEP of the GQR for OUSTC drops lower and lower toward that of the CR.

3.3.4 PEP of the GQRs for the USTC-OD and OUSTC

In this section, we give a unified derivation of the PEP for the GQRs for the USTC-OD in Section 3.3.2 and for OUSTC in Section 3.3.3.

For both the GQRs in (3.33) and in (3.62), the conditional PEP of mistaking $\mathbf{\Psi}_l$ for $\mathbf{\Psi}_j$ when $\mathbf{\Psi}_l$ was sent, or vice versa in the kth time-block is given by

$$P_e\left(\mathbf{\Psi}_l, \mathbf{\Psi}_j \middle| Z\right) = \Pr\left[\mathrm{Re}\left\{\hat{\mathbf{h}}^\dagger \left(\mathbf{\Psi}_j^\dagger - \mathbf{\Psi}_l^\dagger\right)\mathbf{x}\right\} > 0 \middle| \mathbf{\Psi}_l, Z\right]. \tag{3.65}$$

For the GQR in (3.33), we have $\hat{\mathbf{h}} = \hat{\mathbf{h}}_{p|Z}$, and for the GQR in (3.62), we have $\hat{\mathbf{h}} = \hat{\mathbf{h}}_{lj|Z}$. We define

$$f = \mathrm{Re}\left\{\hat{\mathbf{h}}^\dagger \left(\mathbf{\Psi}_j^\dagger - \mathbf{\Psi}_l^\dagger\right)\mathbf{x}\right\}. \tag{3.66}$$

Then f is a Gaussian random variable given Z, $\mathbf{\Psi}_l$ and $\mathbf{\Psi}_j$, with conditional mean

$$\hat{f} = -\sqrt{\frac{\rho T}{4N_T}}\hat{\mathbf{h}}^\dagger \left[\left(\mathbf{\Psi}_l^\dagger - \mathbf{\Psi}_j^\dagger\right)\left(\mathbf{\Psi}_l - \mathbf{\Psi}_j\right)\right]\hat{\mathbf{h}} \tag{3.67}$$

and conditional variance

$$\begin{aligned} v_f^2 = \frac{1}{2}\hat{\mathbf{h}}^\dagger \Bigg\{ & \frac{v_h^2 \rho T}{N_T}\left(\mathbf{\Psi}_j^\dagger \mathbf{\Psi}_l \mathbf{\Psi}_l^\dagger \mathbf{\Psi}_j - \mathbf{I}_{N_T N_R}\right) \\ & + \left(\frac{v_h^2 \rho T}{N_T} + 1\right)\left(\mathbf{\Psi}_l^\dagger - \mathbf{\Psi}_j^\dagger\right)\left(\mathbf{\Psi}_l - \mathbf{\Psi}_j\right)\Bigg\}\hat{\mathbf{h}}. \end{aligned} \tag{3.68}$$

Here, the quantity v_h^2 is the MSE in the estimate $\hat{\mathbf{h}}$, and is identical for all branches. The conditional PEP is thus given by

$$P_e\left(\mathbf{\Psi}_l, \mathbf{\Psi}_j \middle| Z\right) = Q\left(-\frac{\hat{f}}{v_f}\right), \tag{3.69}$$

where $Q(\cdot)$ is the Gaussian Q-function. It follows that the PEP is given by

$$P_e\left(\mathbf{\Psi}_l, \mathbf{\Psi}_j\right) = \mathrm{E}_{\hat{\mathbf{h}}}\left[Q\left(-\frac{\hat{f}}{v_f}\right)\right]. \tag{3.70}$$

When all the singular values of $\mathbf{\Phi}_j^\dagger \mathbf{\Phi}_l$ are equal to d_{lj}, i.e., the condition in (2.15) is satisfied, we have $\mathbf{\Psi}_j^\dagger \mathbf{\Psi}_l \mathbf{\Psi}_l^\dagger \mathbf{\Psi}_j = d_{lj}^2 \mathbf{I}_{N_T N_R}$. When all the singular values of $(\mathbf{\Phi}_j - \mathbf{\Phi}_l)$ are equal to δ_{lj}, i.e., the condition in (2.21) is satisfied, we have $\left(\mathbf{\Psi}_l^\dagger - \mathbf{\Psi}_j^\dagger\right)(\mathbf{\Psi}_l - \mathbf{\Psi}_j) = \delta_{lj}^2 \mathbf{I}_{N_T N_R}$. Thus, when the conditions in (2.15) and (2.21) are both satisfied, the PEP expression in (3.70) can be reduced to

$$P_e\left(\mathbf{\Psi}_l, \mathbf{\Psi}_j\right) = \mathrm{E}_{\hat{\mathbf{h}}}\left[Q\left(\sqrt{\frac{\delta_{lj}^4 \left\|\hat{\mathbf{h}}\right\|^2}{2v_h^2(d_{lj}^2 - 1) + 2\left[v_h^2 + N_T/(\rho T)\right]\delta_{lj}^2}}\right)\right]. \tag{3.71}$$

Now, we define $g = \left\|\hat{\mathbf{h}}\right\|^2 = \sum_{n=1}^{N_T N_R} \left|\hat{h}_n\right|^2$, where $\hat{h}_n$ is the nth element of $\hat{\mathbf{h}}$. Each $\hat{h}_n$ is a complex Gaussian random variable with mean zero and variance

$$\mathrm{E}\left[\left|\hat{h}_n\right|^2\right] = \mathrm{E}\left[|h_n|^2\right] - \mathrm{E}\left[\left|h_n - \hat{h}_n\right|^2\right] = 1 - v_h^2 \triangleq \sigma_{\hat{h}}^2. \tag{3.72}$$

Thus, g is a $chi^2_{2N_T N_R}$ distributed random variable with probability density function [1, eq. 2.1–110]

$$p_g(g) = \frac{1}{\sigma_{\hat{h}}^{2N_T N_R}\Gamma(N_T N_R)} g^{N_T N_R - 1} e^{-g/\sigma_{\hat{h}}^2}, \qquad g \geq 0 \tag{3.73}$$

where $\Gamma(\cdot)$ is the Gamma function, defined as [124, eq. (8.310 1)]

$$\Gamma(x) = \int_0^\infty t^{x-1} e^{-t} dt, \qquad \mathrm{Re}(x) > 0. \tag{3.74}$$

Then (3.71) becomes [1, pg. 825]

$$P_e\left(\mathbf{\Psi}_l, \mathbf{\Psi}_j\right) = \int_0^\infty P_e\left(\mathbf{\Psi}_l, \mathbf{\Psi}_j \middle| g\right) p_g(g) dg$$
$$= \left(\frac{1-\lambda_{lj,GQR}}{2}\right)^{N_T N_R} \sum_{i=0}^{N_T N_R - 1} \binom{N_T N_R - 1 + i}{i} \left(\frac{1+\lambda_{lj,GQR}}{2}\right)^i, \tag{3.75}$$

where

$$\lambda_{lj,GQR} = \left(\sqrt{1 + \frac{4v_h^2(d_{lj}^2 - 1) + 4\left[v_h^2 + N_T/(\rho T)\right]\delta_{lj}^2}{\delta_{lj}^4(1 - v_h^2)}}\right)^{-1}.$$

The closed-form expression in (3.75) for the PEP applies to the GQR in (3.33) for the USTC-OD with two or four transmit antennas, and also applies to the GQR in (3.62) for OUSTC.

When the conditions in (2.15) and (2.21) are both satisfied, we can also obtain a CUB on $P_e\left(\mathbf{\Psi}_l, \mathbf{\Psi}_j\right)$. We first bound the Gaussian Q-function in the RHS of (3.69) by using the Chernoff bound: $Q(x) < e^{-x^2/2}/2$, and obtain

$$P_e\left(\mathbf{\Psi}_l, \mathbf{\Psi}_j \middle| g\right) < \frac{1}{2}\exp\left\{-\frac{\delta_{lj}^4 g}{4v_h^2(d_{lj}^2 - 1) + 4\left[v_h^2 + N_T/(\rho T)\right]\delta_{lj}^2}\right\}. \tag{3.76}$$

Then using the formula in [124, eq. 3.351 3], i.e.,

$$\int_0^\infty x^n e^{-ax} dx = n! a^{-n-1}, \quad \mathrm{Re}(a) > 0, \tag{3.77}$$

we obtain the CUB on $P_e\left(\mathbf{\Psi}_l, \mathbf{\Psi}_j\right)$ as

$$P_e\left(\mathbf{\Psi}_l, \mathbf{\Psi}_j\right) < \frac{1}{2}\left\{1 + \frac{\delta_{lj}^4(1 - v_h^2)}{4v_h^2(d_{lj}^2 - 1) + 4\left[v_h^2 + N_T/(\rho T)\right]\delta_{lj}^2}\right\}^{-N_T N_R}. \tag{3.78}$$

Since the exact expression for the PEP in (3.75) is already simple to use, we will not discuss the CUB in (3.78) further here.

3.3.5 Generalized Quadratic Receiver for General Nonorthogonal Unitary Space–Time Constellations

Thus far, we have developed the GQR for the USTC-OD with $N_T = 2, 4$ and the GQR for OUSTC, and have derived a closed-form expression for their PEP. We now consider a more general case, i.e., NOUSTC which are defined by $\{\mathbf{\Phi}_l \big| \mathbf{\Phi}_l^\dagger \mathbf{\Phi}_l = \mathbf{I}_{N_T}, \exists \{\mathbf{\Phi}_l, \mathbf{\Phi}_j\}$ s.t. $\mathbf{\Phi}_l^\dagger \mathbf{\Phi}_j \neq \mathbf{0}_{N_T}, l, j = 1, \ldots, L, l \neq j\}$. These NOUSTC may contain an explicit training block in each $\mathbf{\Phi}_l$, such as the USTC-OD with $N_T = 3$ in [67], and may also not contain any explicit training blocks, such as the constellations in [54] (except those OUSTC). For this general case, we can still give a form of the GQR and analyze its error performance. However, it is difficult to obtain the PEP expression precisely for this GQR.

In NOUSTC, the two alternatives, $\mathbf{\Psi}_l$ and $\mathbf{\Psi}_j$, can be orthogonal or nonorthogonal to each other. In our derivation here, we treat them as a nonorthogonal pair in general. All the results also apply to an orthogonal pair. For NOUSTC, the reexpressed form of the QR in (3.50) still holds. However, under the assumption that either $\mathbf{\Psi}_l$ or $\mathbf{\Psi}_j$ was sent at time-block k, the vector $\mathbf{b}$ in (3.51) becomes

$$\mathbf{b} = \left(\rho T / N_T\right)^{-1/2} \left(\mathbf{\Psi}_j^\dagger + \mathbf{\Psi}_l^\dagger\right) \mathbf{x} = \mathbf{A}_{lj}\mathbf{h} + \mathbf{b}', \tag{3.79}$$

where

$$\mathbf{A}_{lj} = \begin{cases} \mathbf{\Psi}_j^\dagger \mathbf{\Psi}_l, & \text{if } \mathbf{\Psi}_l \text{ was sent,} \\ \mathbf{\Psi}_l^\dagger \mathbf{\Psi}_j, & \text{if } \mathbf{\Psi}_j \text{ was sent,} \end{cases}$$

and

$$\mathbf{b}' = \mathbf{h} + \left(\rho T / N_T\right)^{-1/2} \left(\mathbf{\Psi}_j^\dagger + \mathbf{\Psi}_l^\dagger\right) \mathbf{w}. \tag{3.80}$$

Comparing (3.79) with (3.51), we can see that there is one additional term for NOUSTC which is dependent on the hypothesis. Thus, we cannot regard $\mathbf{b}$ as

the channel measurement component for NOUSTC anymore. However, the second term $\mathbf{b}'$ has the same form as $\mathbf{b}$ in (3.51) for OUSTC, and can be made to be closer to $\mathbf{h}$ by using the same method in Section 3.3.3. Therefore, instead of obtaining the channel estimate directly, we first obtain the Wiener filter weight vector $\mathbf{a}$ for the MMSE estimate of $\mathbf{h}$ based on $\mathbf{b}'$ as if $\mathbf{b}'$ were available, and then apply $\mathbf{a}$ to $\mathbf{b}$, since we cannot separate $\mathbf{b}'$ from $\mathbf{b}$.

We now define the general information set Z for NOUSTC as

$$Z = \{\mathbf{b}'(k+m)\}_{m=-M_1}^{M_2}, \qquad M_1, M_2 \geq 0. \tag{3.81}$$

Here, the vector $\mathbf{b}'(k+m)$ is defined by

$$\mathbf{b}'(k+m) = \mathbf{h}(k+m) + (\rho T/N_T)^{-1/2}\,\mathbf{F}_{no}(m)\mathbf{w}(k+m), \tag{3.82}$$

where $\mathbf{F}_{no}(m)$ is chosen to be a function of the unitary signal matrices, and $\mathbf{F}_{no}(m)$, $m \neq 0$ should be independent of all the hypotheses. For some NOUSTC, the value of $\sum_{i=1}^{L} \mathbf{\Psi}_i^\dagger \mathbf{\Psi}_j$ is independent of $j \in \{1, \ldots, L\}$, and $\left(\sum_{i=1}^{L} \mathbf{\Psi}_i^\dagger \mathbf{\Psi}_j\right)^{-1}$ exists. Thus, we can define $\mathbf{F}_{no}(m)$ as

$$\mathbf{F}_{no}(m) = \begin{cases} \mathbf{\Psi}_j^\dagger + \mathbf{\Psi}_l^\dagger, & m = 0, \qquad (3.83a) \\ \left(\sum_{i=1}^{L} \mathbf{\Psi}_i^\dagger \mathbf{\Psi}_j\right)^{-1} \sum_{i=1}^{L} \mathbf{\Psi}_i^\dagger, & m = -M_1, \ldots, M_2, \text{ and } m \neq 0. \qquad (3.83b) \end{cases}$$

For other NOUSTC, we have to employ past decisions $\{\hat{\mathbf{\Psi}}(k+m)\}_{m=-M_1}^{-1}$ to estimate the channel, i.e., we have $M_2 = 0$ and define $\mathbf{F}_{no}(m)$ as

$$\mathbf{F}_{no}(m) = \begin{cases} \mathbf{\Psi}_j^\dagger + \mathbf{\Psi}_l^\dagger, & m = 0, \qquad (3.84a) \\ \hat{\mathbf{\Psi}}^\dagger(k+m), & m = -M_1, \ldots, -1. \qquad (3.84b) \end{cases}$$

For this decision-feedback method, in the first time-block, we just set $M_1 = M_2 = 0$, and make a decision without the aid of past decisions. Then in the following time-blocks, we can set $M_1 > 0$ to use past decisions in channel estimation. The

channel estimate based on Z is thus given by

$$\hat{\mathbf{h}}_{lj|Z} = \sum_{m=-M_1}^{M_2} a_{lj}(m)\mathbf{b}'(k+m). \tag{3.85}$$

Here, the Wiener filter weight vector $\mathbf{a} = [a_{lj}(-M_1)\ a_{lj}(-M_1+1)\ \cdots\ a_{lj}(M_2)]^\top$ and the corresponding MMSE v_h^2 can be obtained, respectively, by using the formulas in (3.38) and (3.43), and replacing $\mathbf{b}(k+m)$ therein with $\mathbf{b}'(k+m)$. The cross correlation vector $\mathbf{r}_{hb'}$ for NOUSTC has the same value as that in (3.40), while the (s,t)th entry of the autocorrelation matrix $\mathbf{R}_{b'b'}$ for NOUSTC becomes

$$r_{no,st} = \begin{cases} 1 + \|\mathbf{f}(-1)\|^2 (\rho T/N_T)^{-1}, & s = t \neq M_1+1, \quad \text{(3.86a)} \\ 1 + \|\mathbf{f}(0)\|^2 (\rho T/N_T)^{-1}, & s = t = M_1+1, \quad \text{(3.86b)} \\ R_h(s-t), & s \neq t. \quad \text{(3.86c)} \end{cases}$$

In (3.86), $\mathbf{f}(m)$ can be any row of $\mathbf{F}_{no}(m)$, since for the constellations with the structures defined in [54, 67], the value of $\|\mathbf{f}(m)\|$ is independent of the row number. Besides, $\mathbf{f}(-1)$ in (3.86a) can be any $\mathbf{f}(m), m = -M_1, \cdots, M_2,\ m \neq 0$, because in (3.83) or (3.84), $\|\mathbf{f}(m)\|$'s for all $m \neq 0$ are the same. We also can see that the value of $\|\mathbf{f}(0)\|$ is dependent on $\{l, j\}$. Thus, the value of $\mathbf{a}$ should be computed for each pair $\{l, j\}$, and this can be done in advance. We now define

$$\mathbf{b}(k+m) = (\rho T/N_T)^{-1/2}\, \mathbf{F}_{no}(m)\mathbf{x}(k+m), \quad m = -M_1, \cdots, M_2, \tag{3.87}$$

and $\mathbf{B} = [\mathbf{b}(k-M_1)\ \mathbf{b}(k-M_1+1)\ \cdots\ \mathbf{b}(k+M_2)]$. Then we obtain the GQR for NOUSTC:

$$\mathrm{Re}\left\{ \left(\sum_{m=-M_1}^{M_2} a_{lj}(m)\mathbf{b}^\dagger(k+m) \right) \left(\mathbf{\Psi}_j^\dagger - \mathbf{\Psi}_l^\dagger \right) \mathbf{x} \right\} = \mathrm{Re}\left\{ \mathbf{a}^\top \mathbf{B}^\dagger \left(\mathbf{\Psi}_j^\dagger - \mathbf{\Psi}_l^\dagger \right) \mathbf{x} \right\} \underset{\mathbf{\Psi}_l}{\overset{\mathbf{\Psi}_j}{\gtrless}} 0. \tag{3.88}$$

Here, we need to apply the decision rule in (3.88) $(L-1)$ times to reach a final decision.

For the worst case of $M_1 = M_2 = 0$, we have

$$a_{lj}(0) = \frac{\rho T/N_T}{\rho T/N_T + \|\mathbf{f}(0)\|^2}$$

and

$$a_{lj}(0)\mathbf{b} = \frac{(\rho T/N_T)^{1/2}}{\rho T/N_T + \|\mathbf{f}(0)\|^2} \left(\mathbf{\Psi}_j^\dagger + \mathbf{\Psi}_l^\dagger\right) \mathbf{x}.$$

We can see that in this case, the GQR for NOUSTC in (3.88) gives the same decision on $\mathbf{\Psi}$ as the QR in (3.50). Then we evaluate the error performance of the GQR for the case where we exploit the channel memory. Similar to the case of OUSTC, only the comparisons where one of the alternatives is the true hypothesis affect the error performance of the GQR. Thus, under the assumption that either $\mathbf{\Psi}_l$ or $\mathbf{\Psi}_j$ was sent at time-block k and the assumption that past decisions $\{\hat{\mathbf{\Psi}}^\dagger(k+m)\}_{m=-M_1}^{-1}$ in the decision-feedback method are all correct, we can expand $\mathbf{b}(k+m)$ in (3.87) as

$$\mathbf{b}(k+m) = \begin{cases} \mathbf{A}_{lj}\mathbf{h}(k) + \mathbf{b}'(k), & m = 0, \\ \mathbf{b}'(k+m), & m \neq 0, \end{cases} \tag{3.89}$$

and the GQR in (3.88) becomes

$$\mathrm{Re}\left\{ \left(a_{lj}(0)\mathbf{h}^\dagger \mathbf{A}_{lj}^\dagger + \hat{\mathbf{h}}_{lj|Z}^\dagger\right) \left(\mathbf{\Psi}_j^\dagger - \mathbf{\Psi}_l^\dagger\right) \mathbf{x} \right\} \underset{\mathbf{\Psi}_l}{\overset{\mathbf{\Psi}_j}{\gtrless}} 0. \tag{3.90}$$

From this expression, we can see that when M_1 and/or M_2 increase, the value of $\mathbf{Ba}$ in (3.88) approaches $\mathbf{h}$. This is because as the channel memory span exploited increases, $\hat{\mathbf{h}}_{lj|Z}$ in (3.85) becomes more and more accurate, and at the same time, the decrease in the value of $a_{lj}(0)$ makes the effect of the term $\mathbf{A}_{lj}\mathbf{h}$ decrease. Thus, the error probability of the GQR for NOUSTC reduces from that of the QR and comes closer to that of the CR.

3.3.6 Numerical and Simulation Results

We now show some numerical and simulation results to prove the effectiveness of our GQRs. Here, we assume that the fading process on each link is correlated according to Jakes' model [128] with autocorrelation function $R_h(\triangle t) = J_0(2\pi f_d T_s \triangle t)$, where $J_0(\cdot)$ is the zeroth-order Bessel function of the first kind, f_d is the maximum Doppler frequency, and T_s is the symbol interval. In the theoretical analyses, we assume a block-fading channel model for simplicity, i.e., $\triangle t = \tau T$ and τ is an integer, while in the simulations, we use a more realistic symbol-wise constant fading channel model, i.e., $\triangle t$ can be any integer.

We first show the performance of the GQR designed in Section 3.3.2 for the USTC-OD with $N_T = 2, 4$ [67]. Fig. 3.6 shows the numerical results for the USTC-OD in (2.44) with $N_T = 2$ and $L = 16$ and the USTC-OD in (2.45) with $N_T = 4$ and $L = 27$ versus the value of $M_1 = M_2 = M$. The normalized fade rate is set to be $f_d T_s = 0.0025$. These results are computed by using (3.25) together with (3.35), (3.43), (3.38)–(3.40) for the GQR, with (2.17) for the QR, and with (2.23) for the CR. It is clear that the PEP of our GQR reduces from that of the QR and approaches that of the CR as the channel memory span increases. About half of the potential improvement is obtained by increasing $M_1 = M_2 = M$ from 0 to 1, and the incremental improvement decreases as M increases further. This means that we can obtain most of the potential performance improvement by exploiting the channel correlation over just a few adjacent time-blocks. This quality, in addition to the other merits such as having closed-form PEP expressions, enabling low-complexity detections, and enjoying full antenna diversity, makes the USTC-OD with $N_T = 2, 4$ as well as its GQR more attractive and more important. Fig. 3.7 shows the theoretical and simulated values of the PEPs for the USTC-OD with $f_d T_s = 0.0025$ versus SNR. We can see that the simulation results agree very well with the theoretical predictions. However, at higher SNR's, the simulation results are slightly higher than the theoretical predictions. This is due to the mismatch between the approximate block-fading channel model used in the theoretical anal-

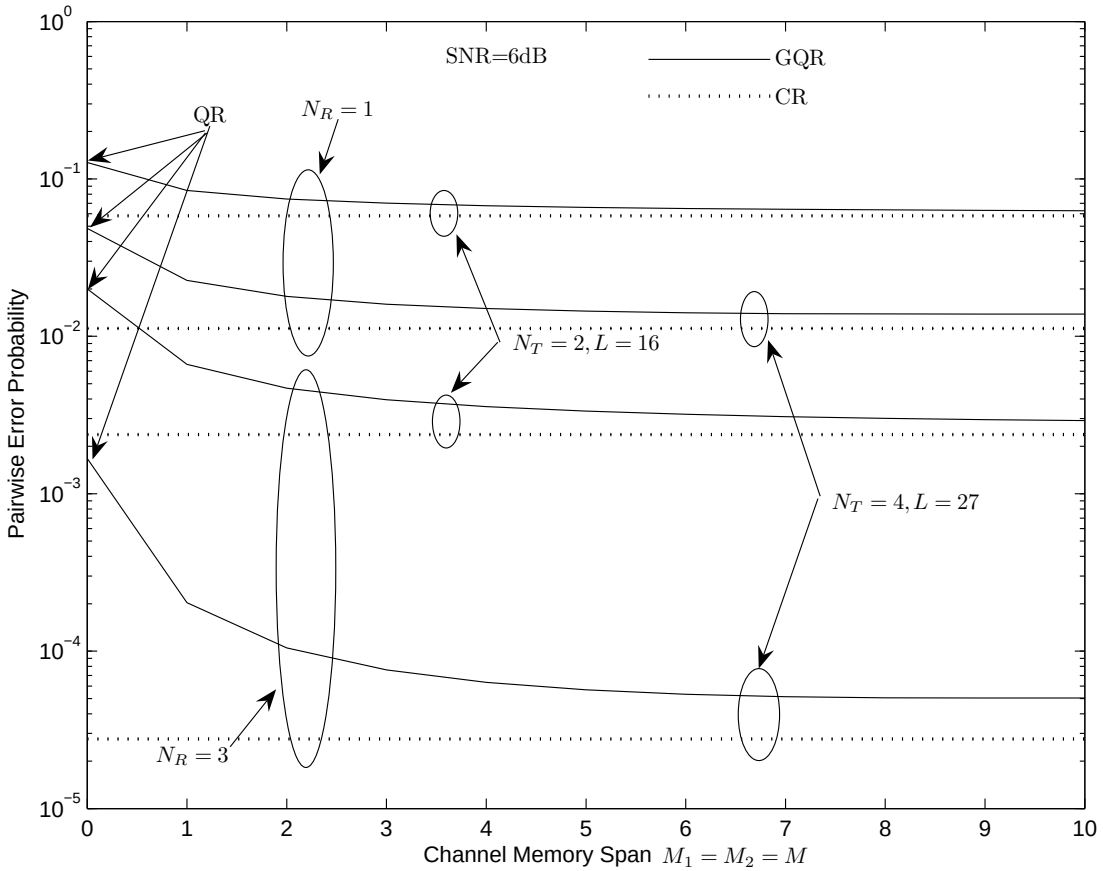

Fig. 3.6: Theoretical PEPs of the QR, the CR and the GQR for the USTC-OD in [67] of Case 1 where $N_T = 2$, $L = 16$, $d_{0,0;0,1} = 0.8660$, $\delta_{0,0;0,1} = 0.7071$ and Case 2 where $N_T = 4$, $L = 27$, $d_{0,0,0;0,0,1} = 0.8660$, $\delta_{0,0,0;0,0,1} = 0.7071$. The normalized fade rate is $f_d T_s = 0.0025$.

yses and the symbol-wise constant fading channel model used in the simulations. The performance is dominated by the errors due to noise at lower SNR's, and the effect of the mismatch between the channel models is more visible at higher SNR's. This mismatch increases with the fade rate. Figs. 3.8 and 3.9 show the simulated block error probabilities (BEPs) for $f_d T_s = 0.0025$ and 0.01, respectively. We can see that our GQR is effective for both slow and fast fading channels. By setting $M = 1$, more than fifty percent of the potential gain is obtained in slow fading, while a smaller percentage is obtained in fast fading. Fig. 3.10 shows the simulated BEPs for the USTC-OD in (2.44) with $N_T = 2$, $L = 16$ and $f_d T_s$ ranging from 0.0025 to 0.01. We can see that at low SNR ($\rho = 2$dB), the channel fade rate

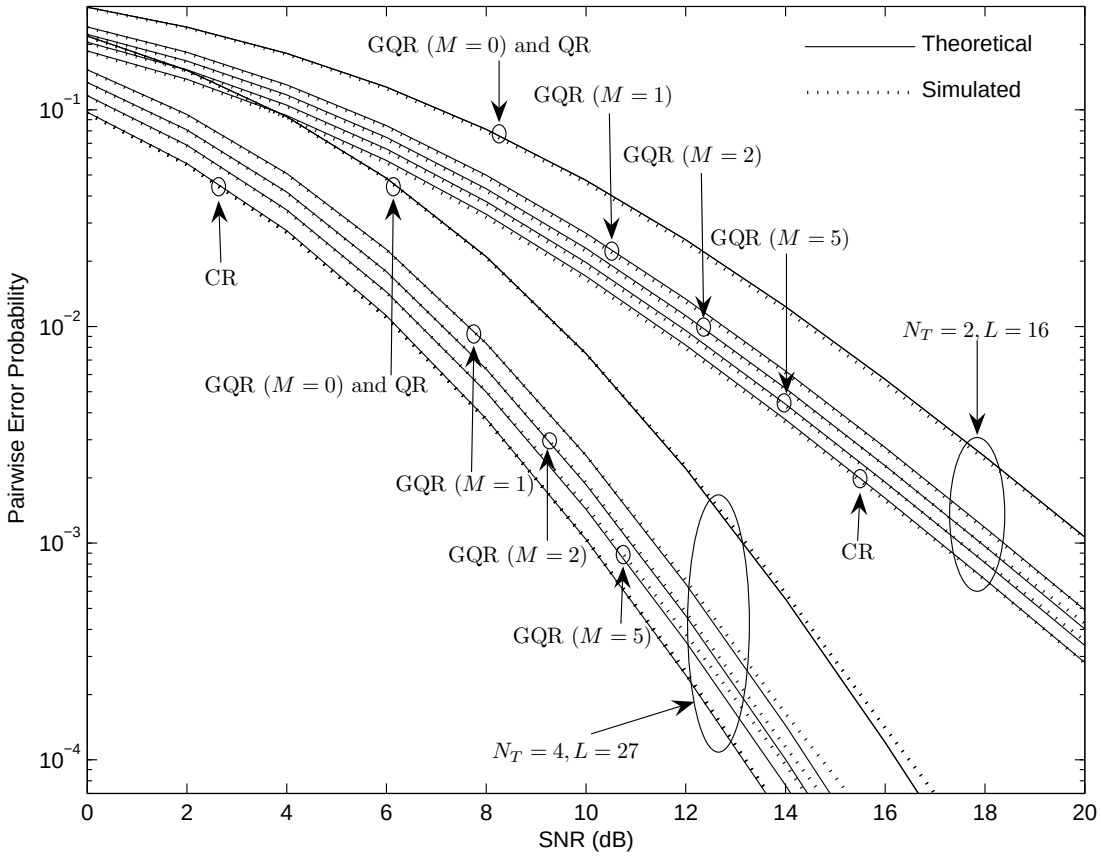

Fig. 3.7: PEPs of the QR, the CR and the GQR for the USTC-OD in [67] of Case 1 where $N_T = 2$, $L = 16$, $d_{0,0;0,1} = 0.8660$, $\delta_{0,0;0,1} = 0.7071$ and Case 2 where $N_T = 4$, $L = 27$, $d_{0,0,0;0,0,1} = 0.8660$, $\delta_{0,0,0;0,0,1} = 0.7071$ with $N_R = 1$ and $f_d T_s = 0.0025$. The channel memory span is $M_1 = M_2 = M = 0, 1, 2, 5$.

has a negligible effect on the error performance, but at high SNR ($\rho = 20$dB), the improvement brought about by exploiting more channel memory decreases as the fade rate increases.

Next, we show the error performance of the GQR designed in Section 3.3.3 for OUSTC [54]. Fig. 3.11 shows the results for the OUSTC with $N_T = 1$ and $L = 8$ in [54, Table I]. This constellation is generated by using the construction in (2.40) with $\mathbf{u}' = [3\ 7\ 6\ 5\ 0\ 4\ 2]$. The numerical results are computed by using (3.25) together with (3.63), (3.43), (3.38), (3.61), and (3.40) for the GQR. Although increasing M from 0 to 1 gives less gain than that in the case of the USTC-OD, the PEP of the GQR reduces steadily toward that of the CR as M increases. Since OUSTC usually have a small size ($L \leq T/N_T$), they cannot provide a high data

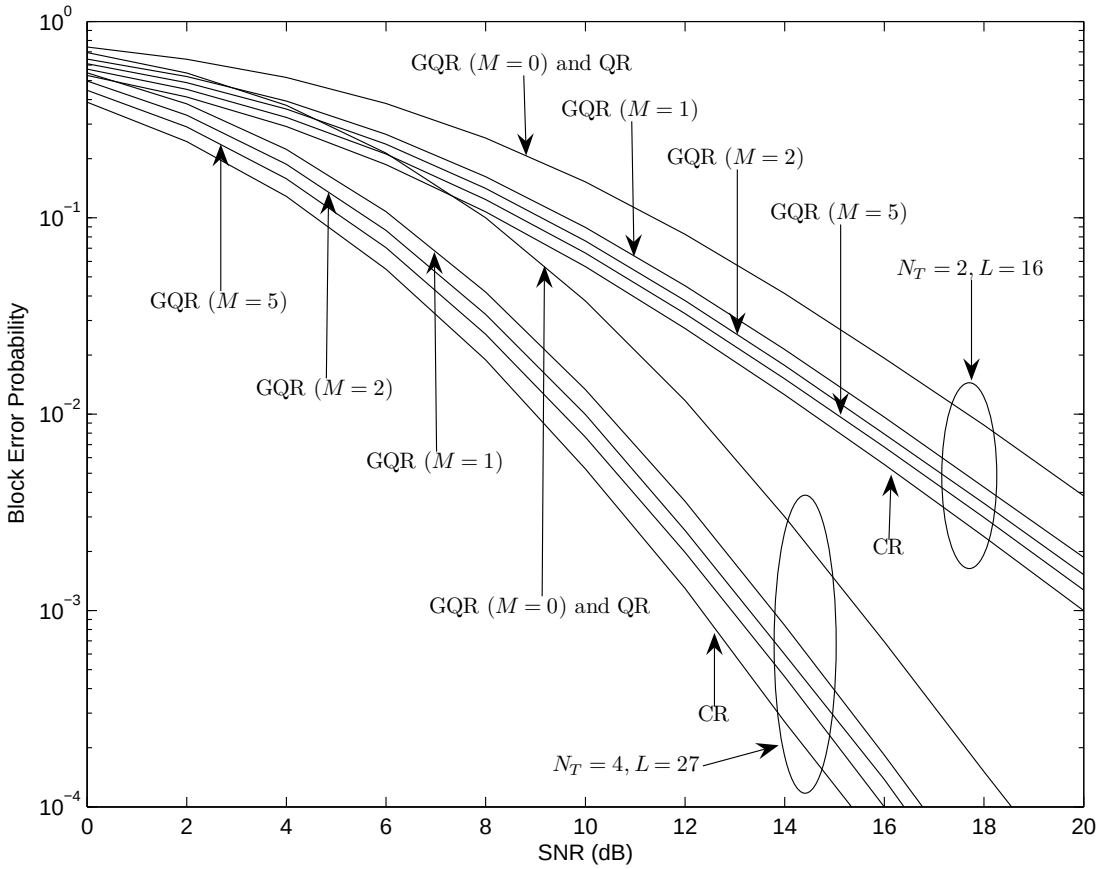

Fig. 3.8: BEPs of the QR, the CR and the GQR for the USTC-OD in [67] of Case 1 where $N_T = 2$, $L = 16$ and Case 2 where $N_T = 4$, $L = 27$ with $N_R = 1$ and $f_d T_s = 0.0025$. The channel memory span is $M_1 = M_2 = M = 0, 1, 2, 5$.

rate. This limits the importance of OUSTC and also of this GQR.

Finally, we show the performance of the GQR designed in Section 3.3.5 for general NOUSTC. This GQR applies to a wide range of the constellations designed for USTM. Here, we apply this GQR to the USTC-OD with $N_T = 3$ in [67] and the NOUSTC with block-circulant structure in [54]. For the case of the USTC-OD with $N_T = 3$, as we have mentioned in Section 3.3.2.5, we do not recommend using the GQR designed in Section 3.3.2, since this GQR is suboptimal for this case and gives an error performance worse than that of the QR when $M_1 = M_2 = 0$. Instead, we recommend the GQR for NOUSTC in (3.88) together with $\mathbf{F}_{no}(m)$ in (3.83), because this GQR can guarantee an error performance at least as good as that of the QR for the USTC-OD with $N_T = 3$, and can provide a large

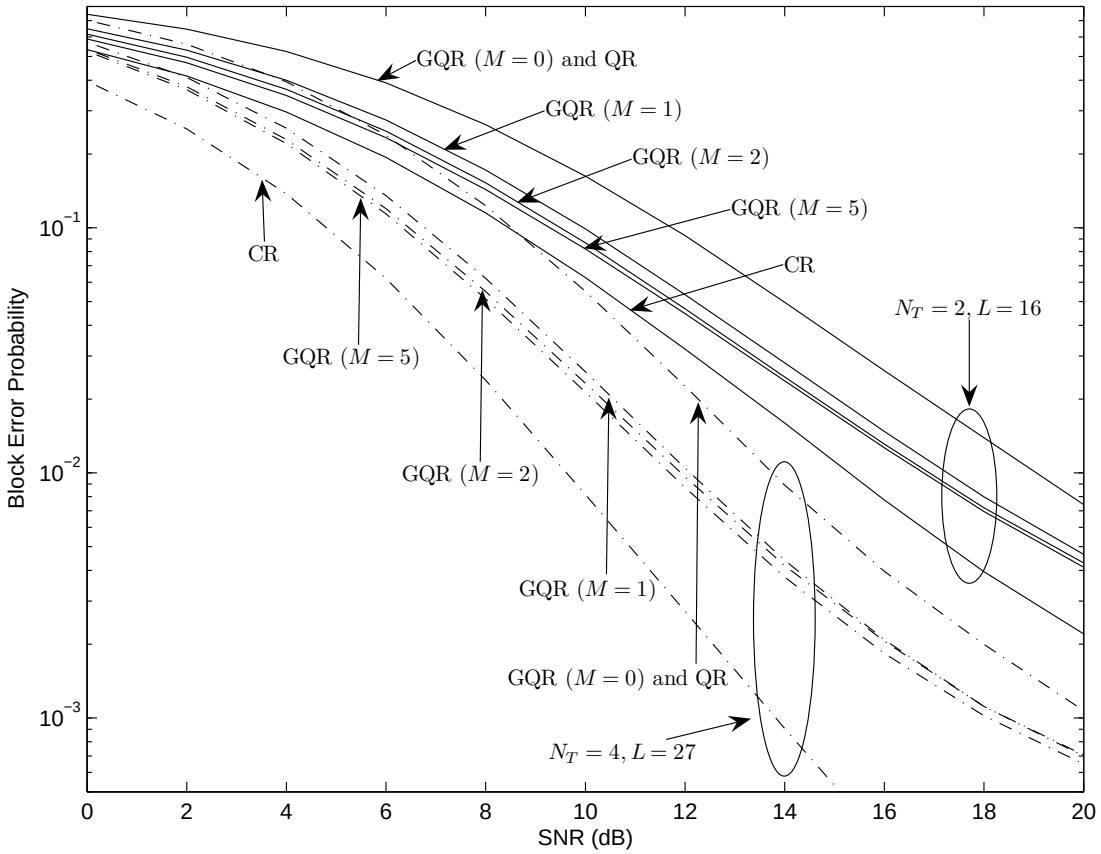

Fig. 3.9: BEPs of the QR, the CR and the GQR for the USTC-OD in [67] of Case 1 where $N_T = 2$, $L = 16$ and Case 2 where $N_T = 4$, $L = 27$ with $N_R = 1$ and $f_d T_s = 0.01$. The channel memory span is $M_1 = M_2 = M = 0, 1, 2, 5$.

performance gain when $M_1, M_2 > 0$. Fig. 3.12 shows the performance of the GQR in (3.88) for the USTC-OD with $N_T = 3$ which is obtained by deleting the fourth column of the constellation in (2.45) with $N_T = 4$ and $L = 27$. Two channel estimation methods are used for comparison. Method 1 employs $\mathbf{F}_{no}(m)$ in (3.83) which does not involve past decisions, and Method 2 employs $\mathbf{F}_{no}(m)$ in (3.84) which requires past decisions. We can see that for a given positive value of $(M_1 + M_2)$, Method 1 provides a better performance than Method 2. This is because Method 2 has the error propagation problem, and thus is not as robust as Method 1. In addition, the received signals in the immediate past M_1 and the immediate succeeding M_2 time-blocks are more correlated with the channel gains being estimated than are those in the past $(M_1 + M_2)$ time-blocks. Fig. 3.13 shows

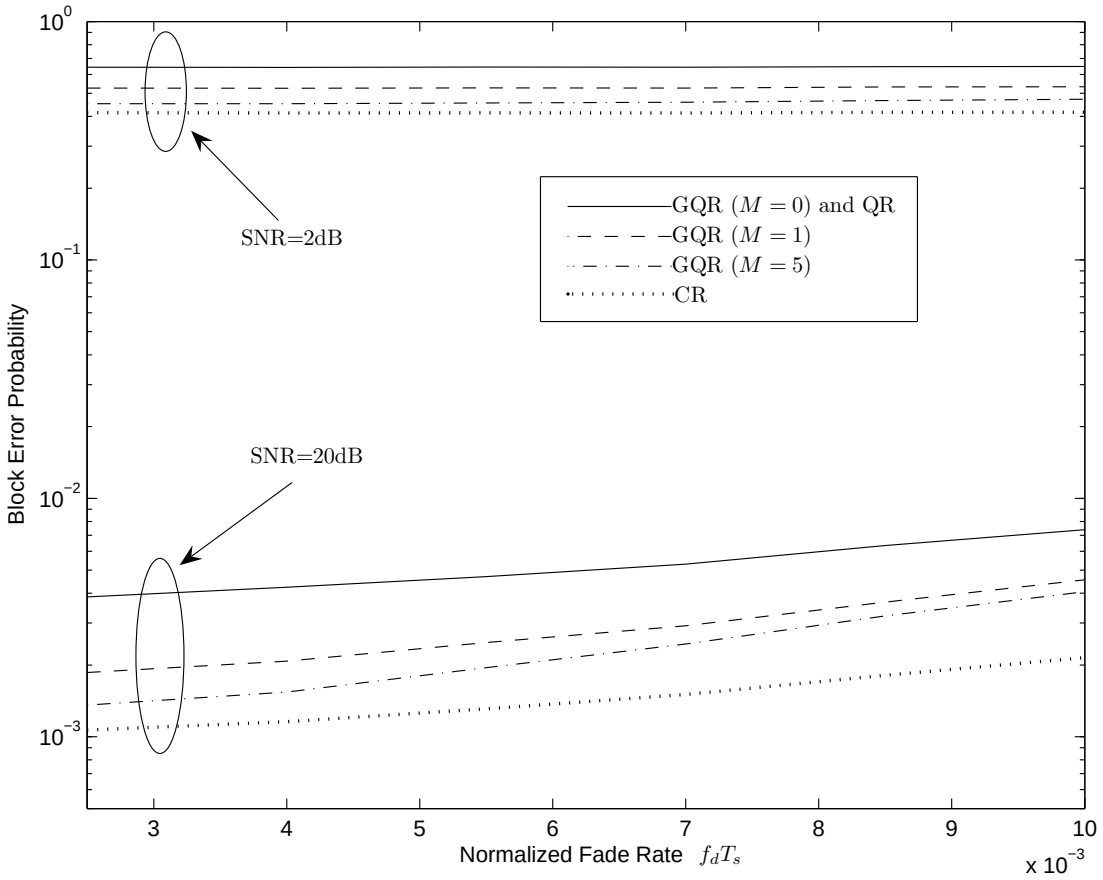

Fig. 3.10: BEPs of the QR, the CR and the GQR for the USTC-OD in [67] with $N_T = 2$ and $L = 16$ versus the normalized fade rate f_dT_s for $N_R = 1$. The channel memory span is $M_1 = M_2 = M = 0, 1, 5$.

the results for the NOUSTC with block-circulant structure of size $L = 17$ with $N_T = 2$ in [54, Table II]. This constellation is generated by using the construction in (2.40) with $\mathbf{u}' = [12\ 11\ 9\ 14\ 6\ 10\ 0]$. The normalized fade rate is set to be $f_dT_s = 0.0025$ and 0.01. For this constellation, we only can employ Method 2 to estimate the channel. We can see that for this case, the GQR in (3.88) also provides large performance improvements in both slow and fast fading environments.

We did not consider the optimum order in which the signal matrices $\mathbf{\Psi}_l$ and $\mathbf{\Psi}_j$ are chosen from the signal matrix set $\{\mathbf{\Psi}_1, \mathbf{\Psi}_2, \cdots, \mathbf{\Psi}_L\}$ for comparison in the GQRs given in (3.62) and (3.88). Our simulations have shown that the BEP of the GQRs does not show any significant difference between the different orders.

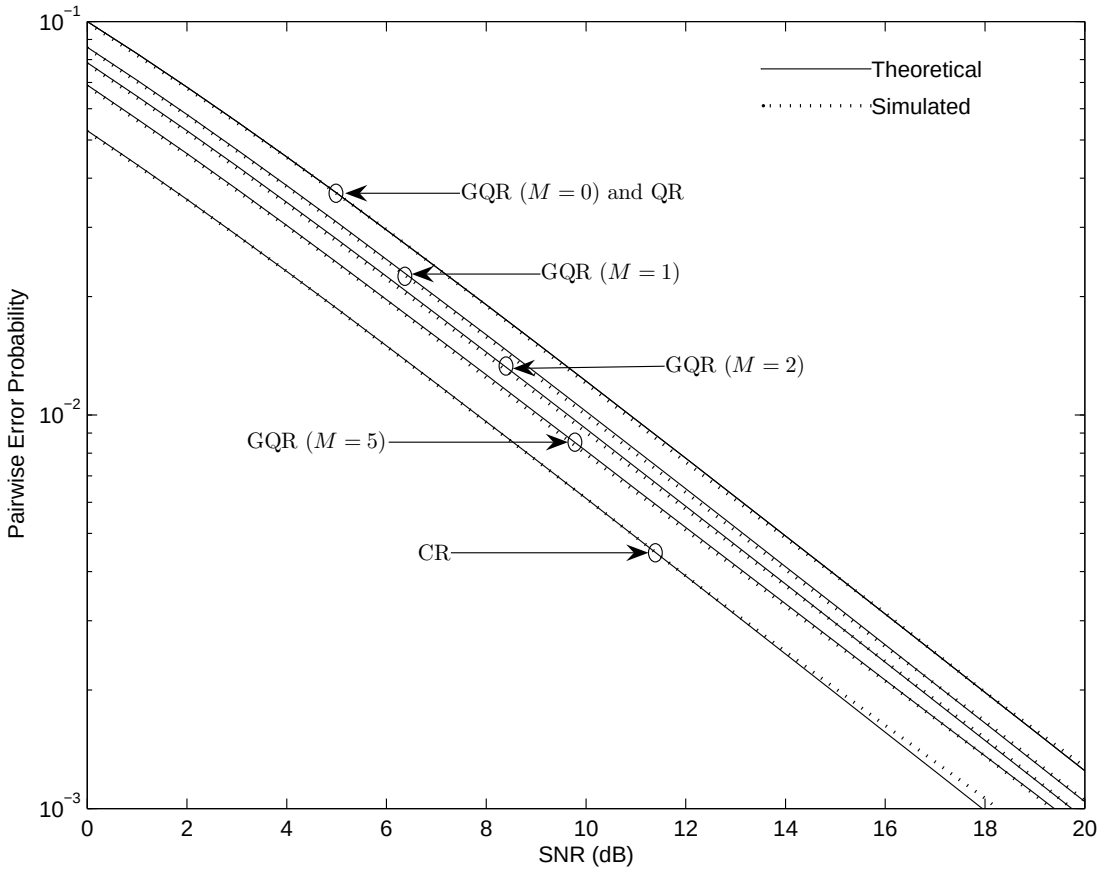

Fig. 3.11: PEPs of the QR, the CR and the GQR for the OUSTC in [54] with $N_T = 1$, $L = 8$, $N_R = 1$, $d = 0$, $\delta = 1.4142$, and $f_d T_s = 0.0025$. The channel memory span is $M_1 = M_2 = M = 0, 1, 2, 5$.

The important point that we want to demonstrate is that as the channel memory span exploited in channel estimation increases, the BEP of the GQRs converges to that of the CR, and we have achieved this.

3.4 Summary

In this chapter, we have reviewed the idea of the GQR proposed for binary orthogonal signals over the flat Rayleigh fading channel in SIMO systems. This GQR improves the error performance over the QR by exploiting the channel memory and acquiring CSI inherent in the received data signals themselves. Furthermore, we have extended this concept to the USTM scheme. Although USTM is effec-

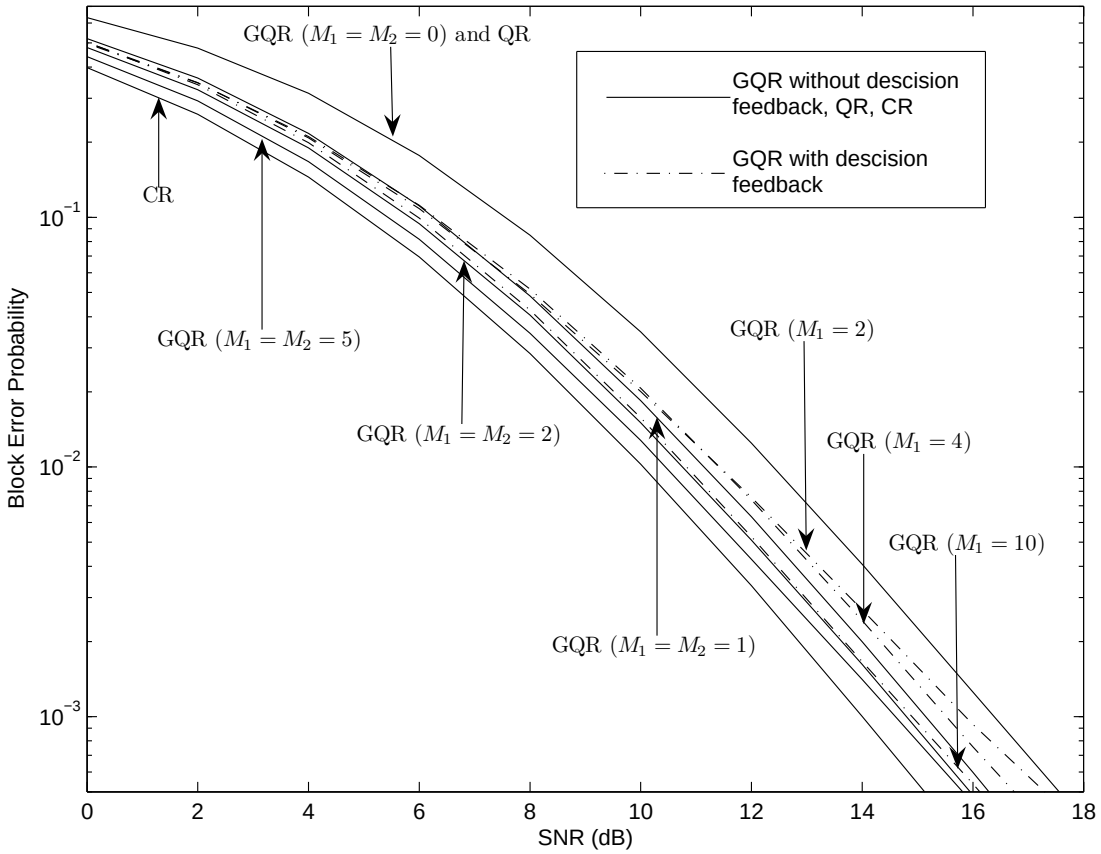

Fig. 3.12: BEPs of the QR, the CR and the GQR for the NOUSTC in [67] with $N_T = 3$, $L = 27$, $N_R = 1$ and $f_d T_s = 0.0025$. Two methods are used to estimate the channel. For Method 1 which does not employ decision feedback, the channel memory span is $M_1 = M_2 = 0, 1, 2, 5$, while for Method 2 which employs decision feedback, the channel memory span is $M_2 = 0$ and $M_1 = 0, 2, 4, 10$.

tive in data detections without CSI at the receiver, perfect knowledge of CSI at the receiver can bring about a 2–4 dB gain in SNR. To realize this large performance improvement potential and at the same time conserve bandwidth resources, we have proposed the GQRs for the USTC-OD, OUSTC and general NOUSTC, which estimate the channel gains without requiring additional training signals to be sent, and which exploit the channel memory to improve the channel estimation accuracy. Closed-form expressions of the PEP have been derived for the GQR designed for the USTC-OD with two or four transmit antennas, and for the GQR designed for OUSTC. Our analytical and simulation results have shown that the error probabilities of these GQRs reduce from that of the QR to that of the CR as

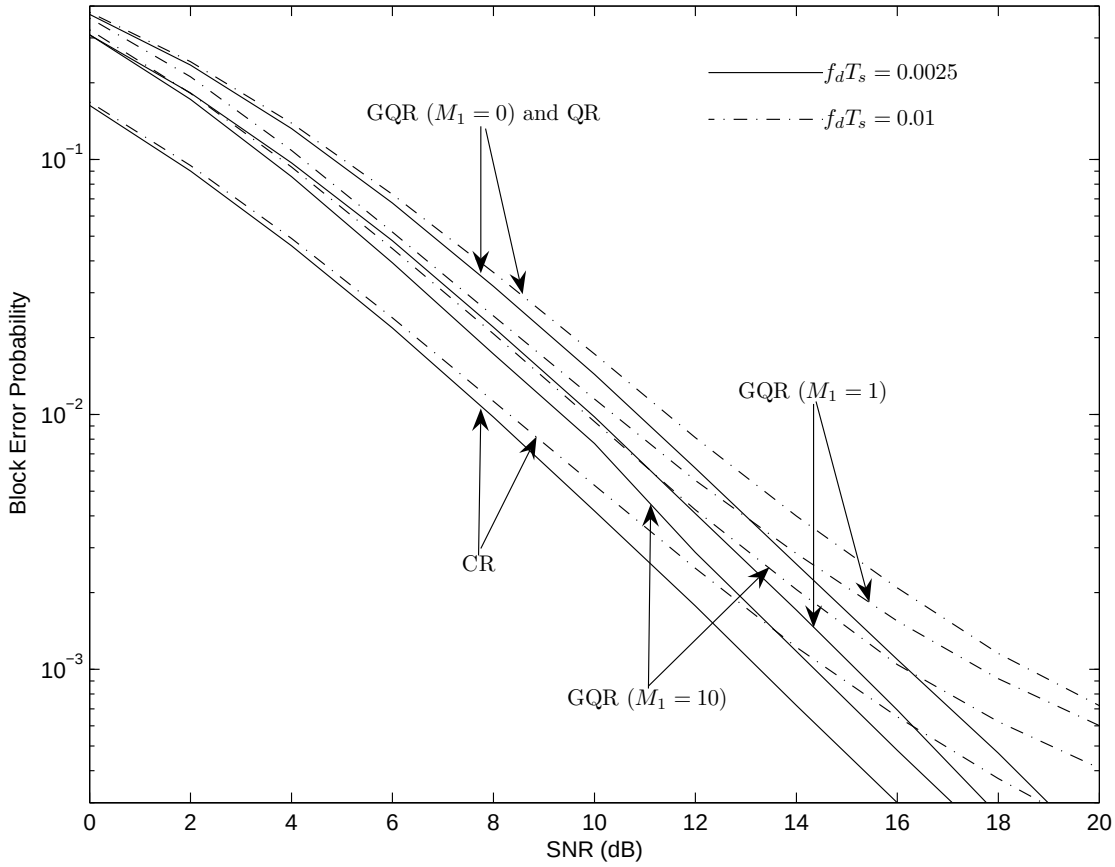

Fig. 3.13: BEPs of the QR, the CR and the GQR for the NOUSTC in [54] with $N_T = 2$, $L = 17$, $N_R = 1$ and $f_dT_s = 0.0025, 0.01$. The decision-feedback method is employed to estimate the channel. The channel memory span is $M_2 = 0$ and $M_1 = 0, 1, 10$.

the channel memory span exploited in channel estimation increases. The GQRs have been shown to work well even in fast fading environments, although they provide more improvements in slow fading environments. In addition, the GQR for the USTC-OD with two or four transmit antennas have been simplified. The complexity of this simplified GQR for large-sized constellations can be much less than that of the QR and even that of the simplified form of the QR, provided that the channel memory span exploited in channel estimation is small enough.

Besides using the existing USTC designed in the literature for the QR, it is also desirable to obtain some new unitary constellations for the GQRs. Since the error probabilities of the GQRs are upper bounded by that of the QR and lower bounded by that of the CR, we can first obtain the constellations optimal for

the QR. This step can minimize the upper bound on the PEP of the GQRs, and ensure a good performance when the GQRs only use the received signals in the current time-block to estimate the channel. Then from the constellations optimal for the QR, we should choose those having the best performance for the CR. This step can minimize the lower bound on the PEP of the GQRs, and thus allow a larger improvement potential in the use of the GQRs.

Chapter 4

Computing and Bounding the First-Order Marcum Q-Function

In this chapter and the subsequent two chapters, we extend our work to the performance analysis of QFRs in general. As reviewed in Chapter 1, the first-order Marcum Q-function and the generalized Marcum Q-function are often involved in the error performance analysis of QFRs. Thus, studying these Marcum Q-functions can facilitate our research on QFRs. We present our results on the first-order Marcum Q-function in this chapter, and the results on the generalized Marcum Q-function in Chapter 5. Applications to the performance analysis of QFRs will be given in Chapter 6.

The first-order Marcum Q-function, $Q(a, b)$, can be given a geometric interpretation which explains $Q(a, b)$ as the probability that a complex, Gaussian random variable with real, nonnegative mean a, takes on values outside of a disk $\mathbb{B}_{O,b}$ of radius b centered at the origin O. This interpretation engenders a fruitful approach for deriving new representations and tight, upper and lower bounds on $Q(a, b)$. The new representations obtained involve finite-range integrals whose integrands are given in terms of either purely exponential functions, or a product of an exponential function and a complementary error function, i.e, $\mathrm{erfc}(\cdot)$. These representations are shown to be simpler than their counterparts in the lit-

erature. The new bounds obtained include the generic exponential bounds and simple exponential bounds, generic erfc bounds and simple erfc bounds, generic single-integral bounds and simple single-integral bounds. Here, the generic bounds involve an arbitrarily large number of terms, and the simple bounds involve just a few terms. The new generic bounds approach the exact value of $Q(a,b)$ as the number of terms involved increases. The new simple bounds are tighter than the existing exponential bounds in most cases, especially when the arguments a and b are large. Thus, in many applications requiring further analytical manipulations of $Q(a,b)$, these new bounds can lead to some closed-form results which are better than the results available so far.

4.1 Introduction

The first-order Marcum Q-function, $Q(\cdot,\cdot)$, was first introduced in [103, 104], and utilized extensively to deal with problems in radar and communications [1]. It is the tail probability of a normalized Rician random variable, defined by

$$Q(a,b)=\int_b^\infty x\exp\left(-\frac{x^2+a^2}{2}\right)I_0(ax)dx,\ a\geq 0,\ b\geq 0. \tag{4.1}$$

Here, $I_0(\cdot)$ is the modified Bessel function of the first kind of order zero, given by [124, eq. (8.431 3)]

$$I_0(x)=\frac{1}{\pi}\int_0^\pi e^{x\cos\theta}d\theta. \tag{4.2}$$

In recent years, the importance of this Q-function increases since it appears frequently in the performance analyses of digital communications, especially in evaluating the error performance of QFRs for a variety of partially coherent, differentially coherent, and quadratic detections [1, 5]. A lot of work has been done for the numerical computation of $Q(a,b)$ [105–112], and there has been a built-in function in MATLAB to compute numerical values of $Q(a,b)$ easily. However, it is also often desirable to have a further analytical handle on $Q(a,b)$, for instance, in

optimization of system performance with respect to system parameters. In problems involving transmission over fading channels especially, one often would also need to do statistical averaging over the arguments a and/or b of the function. In these scenarios, the form in (4.1) is not easy to use, since it requires one to compute an infinite integral with an integrand involving $I_0(\cdot)$ over an argument-dependent range. Some alternative representations of $Q(a,b)$ were developed in [113–115], which involve only a finite integral over one or two exponential integrands. These alternative representations can help to solve some problems arising from further manipulating $Q(a,b)$, such as in [5, 31, 117], and may even lead to closed-form results in the error performance analysis of some communication problems, such as in [118]. However, they cannot solve all the problems encountered, and cannot give closed-form results for all the error performance analysis problems of interest. Bounding $Q(a,b)$ using simple functions such as the exponential function and the erfc function, is, therefore, a promising approach to facilitating analytical work involving $Q(a,b)$. Some exponential bounds have been derived in [23, 114, 120, 121] by using mathematical approaches, but unfortunately, these bounds are not sufficiently tight, particularly when the arguments a and b are large.

Here, we present a novel approach for computing and bounding the first-order Marcum Q-function that is based purely on simple geometric arguments. This geometric view was first presented briefly in [129], and is fully developed here. In this geometric view, $Q(a,b)$ is the probability that a complex, Gaussian random variable z with real, nonnegative mean a, takes on values outside of the region $\mathbb{B}_{O,b}$ bounded by a circle of radius b centered at the origin O. By evaluating this probability in polar coordinates, we immediately obtain a pair of new representations of $Q(a,b)$ that involve only a single finite integral with purely exponential integrands, and that are valid for either $a \geq b$ or $b \geq a$. These new representations are shown to be simpler and more convenient to use than those in [113–115]. By evaluating this probability in rectangular coordinates, we also obtain a new rep-

resentation of $Q(a, b)$, which involves a single finite integral whose integrand is a product of an exponential function and an erfc function. This new representation is valid for all the values of a and b concerned. Although this representation is not as simple as those obtained by using polar coordinates, upper bounding the erfc function in the integrand of this representation can lead to a very tight upper bound on $Q(a, b)$. Besides, the integrand of this representation is also simpler than the representation in [116] which also involves a finite integral with integrand involving the erfc function.

In addition to these new representations, the geometric view of the Q-function turns out to lead to a very fruitful approach to bounding the function. By computing the probability of z lying outside of various geometrical shapes whose boundaries tightly enclose, or are tightly enclosed by the boundary of $\mathbb{B}_{O,b}$ mentioned above, a lot of new, upper and lower bounds on $Q(a, b)$ can be derived. We first derive some generic exponential bounds, which involve only the exponential function, by choosing variations of the circular region such as sectors[1], or angular sectors of annuli[2] to be the bounding geometrical shapes. These generic exponential bounds involve an arbitrarily large number of exponential terms, and approach the exact value of $Q(a, b)$ as the number of exponential terms involved increases. Some special cases of these generic bounds with only two exponential terms are given as new simple exponential bounds which are shown to be much tighter than the existing exponential bounds in [114, 120], and tighter than the exponential bounds in [121] for most cases.

Then we turn to the derivation of erfc bounds on $Q(a, b)$. Here, an erfc bound is a bound involving only the erfc function, or involving both the erfc and exponential functions. To the best of the authors' knowledge, there are no such erfc bounds available in the literature. We first develop some generic erfc

[1]A sector is the portion of a circular region bounded by two radii and the arc in between them.

[2]An annulus, as defined in complex function theory [130], is the region between two concentric circles. An angular sector of an annulus is the segment of the annulus bounded by two radii and the two arcs in between them.

bounds by using a set of rectangular regions as bounding shapes. Then we derive a simple, tight, upper erfc bound on $Q(a, b)$ by upper bounding the integrand of the new representation which involves the erfc function, as mentioned above. A simple, tight, lower erfc bound is also given as a special case of our generic lower erfc bound. In a wide range of values of the arguments a and b, these simple erfc bounds are much tighter than the exponential bounds involving only several exponential functions. They are also simple enough to lead to closed-form results in many theoretical analyses involving $Q(a, b)$.

After deriving these closed-form bounds, we also investigate the possibility to derive some tighter bounds which involve single finite integrals but sill can lead to some closed-form results in some applications. We give some new upper and lower single-integral bounds which involve only single integrals with simple, purely exponential integrands. These single-integral bounds are obtained by using polygons as the bounding shapes. Some generic single-integral bounds are first derived, whose bounding shapes are arbitrary bounding polygons with an arbitrarily large number of equal or nonequal sides. Then some simple single-integral bounds are given, which involve three or four single integrals. These simple single-integral bounds are the special cases of the generic bounds, obtained by using simple equilateral hexagons as the bounding shapes. The advantage of these single-integral bounds is that the single integrals involved are similar to those involved in the error probability expression of the general two-dimensional signal constellations [60]. Therefore, all the computational techniques exploited to compute this error probability can be used to compute our single-integral bounds straightforwardly. This property may be helpful in some applications of our single-integral bounds.

Besides the exponential bounds, there are also some I_0-bounds, which involve the use of $I_0(\cdot)$, available in the literature [116, 121, 122]. The I_0-bounds in [122] are the tightest in most cases, but they involve the product of $I_0(\cdot)$ and $\mathrm{erfc}(\cdot)$, or even more complicated functions of $I_0(\cdot)$, and thus, are not easy to use in the further analytical manipulations of $Q(a, b)$. Compared to these I_0-bounds, our

bounds are easier to handle in theoretical analyses, and thus are more desirable. We will include these I_0-bounds in our numerical results just as a reference of tightness of our bounds.

In Section 4.2, we present the geometric view of $Q(a, b)$. In Section 4.3, we give the new finite-integral representations. In Sections 4.4 and 4.5, we propose generic and simple exponential bounds, respectively. In Sections 4.6 and 4.7, we develop generic and simple erfc bounds, respectively. In Sections 4.8 and 4.9, we give generic and simple single-integral bounds, respectively. Section 4.10 presents the numerical results and comparisons to show the tightness of our bounds.

4.2 The Geometric View of $Q(a, b)$

Since the Marcum Q-function is the tail probability of a Rician random variable, and this variable arises from the magnitude of a complex Gaussian random variable, we therefore start with considering the random variable z given by

$$z = a + y = (a + y_1) + \jmath y_2 = z_1 + \jmath z_2. \tag{4.3}$$

Here, $a \geq 0$ is the mean value that can be assumed to be a known, real constant, and y is a circularly symmetric, zero-mean, complex, Gaussian random variable with $\mathcal{CN}(0, 2\sigma_y^2)$ distribution. The real and imaginary parts of y, i.e., y_1 and y_2, respectively, are i.i.d. real Gaussian random variables with mean zero and variance σ_y^2. The real and imaginary parts of z, i.e., z_1 and z_2, respectively, are given by

$$\begin{cases} z_1 = a + y_1, & \text{(4.4a)} \\ z_2 = y_2. & \text{(4.4b)} \end{cases}$$

The envelope R of z, where

$$R = |z| = \sqrt{(a + y_1)^2 + y_2^2}, \tag{4.5}$$

is Rician distributed with PDF given by [1, Chap. 2, eq. (2.1–141)]

$$p_R(R) = \frac{R}{\sigma_y^2} e^{-(R^2+a^2)/2\sigma_y^2} I_0\left(\frac{Ra}{\sigma_y^2}\right),\ R \geq 0. \tag{4.6}$$

The probability of R being greater than a real constant $b \geq 0$ is then given by

$$\Pr(R > b) = \int_b^\infty \frac{R}{\sigma_y^2} e^{-(R^2+a^2)/2\sigma_y^2} I_0\left(\frac{Ra}{\sigma_y^2}\right) dR = Q\left(\frac{a}{\sigma_y}, \frac{b}{\sigma_y}\right). \tag{4.7}$$

For simplicity, in the following discussions, we normalize a and b by σ_y, or, equivalently, set $\sigma_y^2 = 1$. Thus, evaluating $Q(a, b)$ in (4.1) is the same as computing the probability $\Pr(R > b)$. From Fig. 4.1, we can see that $Q(a, b)$ or $\Pr(R > b)$ is the probability that the point z lies outside of the disk $\mathbb{B}_{O,b}$ of radius b and centered at the origin O of the z_1z_2-coordinate system. Since the probability $\Pr(R > b) = \Pr(\sqrt{z_1^2 + z_2^2} > b)$ can also be written as $\Pr(\sqrt{(a + y_1)^2 + y_2^2} > b)$, it is clear that $Q(a, b)$ is also equal to the probability that in the y_1y_2-coordinate system, centered at the point A, i.e., $(z_1 = a, z_2 = 0)$, the complex random variable y lies outside of $\mathbb{B}_{O,b}$. Thus, we have

$$Q(a, b) = 1 - \Pr(z \in \mathbb{B}_{O,b}) = 1 - \Pr(y \in \mathbb{B}_{O,b}). \tag{4.8}$$

4.3 New Finite-Integral Representations for $Q(a, b)$

Based on the geometric view of $Q(a, b)$ given above, we derive some new finite-integral representations for $Q(a, b)$. In Section 4.3.1, by evaluating the probabilities in (4.8) using polar coordinates, we obtain a pair of representations whose integrands only involve the exponential function. In Section 4.3.2, by evaluating the probabilities in (4.8) using rectangular coordinates, we obtain one representation whose integrand only involves the erfc-function as well as the exponential function.

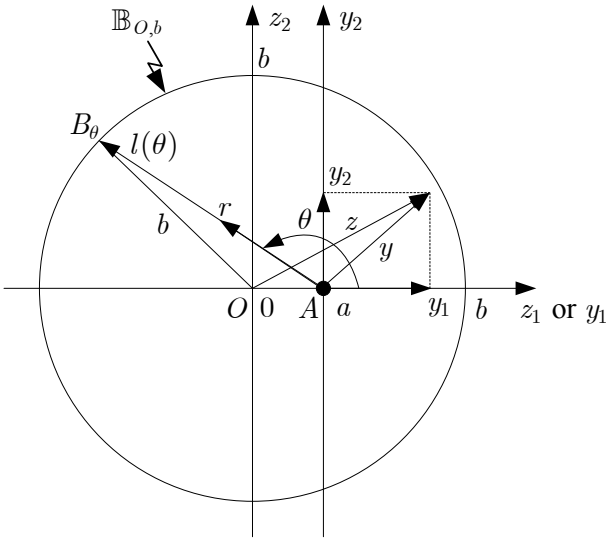

(a) $b > a$

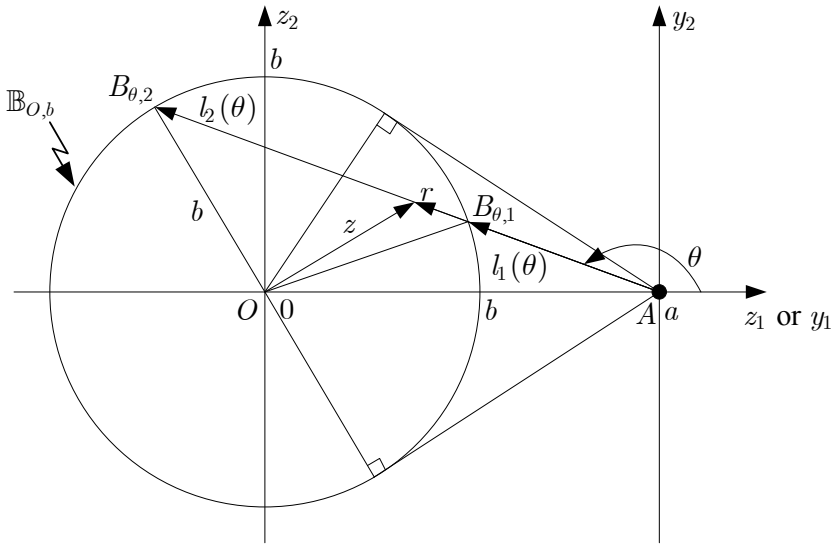

(b) $a > b$

Fig. 4.1: Geometric view of $Q(a, b)$.

4.3.1 Representations with Integrands Involving the Exponential Function

In the polar coordinate system centered at the point A, the PDF of y is given by

$$p_y(r, \theta) = \frac{r}{2\pi} e^{-r^2/2},\ r \geq 0. \tag{4.9}$$

We can see that the PDF of y in (4.9) is isotropic, i.e., independent of θ.

4.3.1.1 New Representation for the Case of $b \geq a \geq 0$

For the case of $b \geq a \geq 0$, as shown in Fig. 4.1(a), we use $l(\theta)$ to denote the length of the line segment AB_θ, where B_θ is a point on the boundary of $\mathbb{B}_{O,b}$ such that the angle from the positive y_1-axis to AB_θ is θ. Using the law of cosines, we get

$$b^2 = a^2 + l^2(\theta) - 2al(\theta)\cos(\pi - \theta) = a^2 + l^2(\theta) + 2al(\theta)\cos\theta,$$

from which we can solve for the value of $l(\theta)$. Choosing the positive root, we have

$$l(\theta) = -a\cos\theta + \sqrt{b^2 - a^2\sin^2\theta}. \tag{4.10}$$

Then evaluating the probability $\Pr(y \in \mathbb{B}_{O,b})$ in (4.8) using (4.9) gives the new representation of $Q(a, b)$, namely

$$\begin{aligned} Q(a,b) &= 1 - \int_{\theta=-\pi}^{\pi}\int_{r=0}^{l(\theta)} \frac{r}{2\pi} e^{-r^2/2} dr d\theta \\ &= \frac{1}{\pi}\int_0^{\pi} \exp\left[-\frac{1}{2}\left(-a\cos\theta + \sqrt{b^2 - a^2\sin^2\theta}\right)^2\right] d\theta,\ b \geq a \geq 0. \end{aligned} \tag{4.11}$$

This representation only involves one finite integral, and its integrand is a pure exponential function. By defining $0 \leq \zeta = a/b \leq 1$, we can rewrite (4.11) in the form

$$Q(b\zeta, b) = \frac{1}{\pi}\int_0^{\pi} \exp\left[-\frac{b^2}{2}\left(-\zeta\cos\theta + \sqrt{1 - \zeta^2\sin^2\theta}\right)^2\right] d\theta,\ 0 \leq \zeta \leq 1. \tag{4.12}$$

4.3.1.2 New Representation for the Case of $a \geq b \geq 0$ and $a \neq 0$

For the case of $a \geq b \geq 0$ and $a \neq 0$, as shown in Fig. 4.1(b), we have two line segments, $AB_{\theta,1}$ and $AB_{\theta,2}$, where $B_{\theta,1}$ and $B_{\theta,2}$ are the two points on the

boundary of $\mathbb{B}_{O,b}$, forming the same angle of θ with the positive y_1-axis. Their lengths are denoted as $l_1(\theta)$ for $AB_{\theta,1}$, and as $l_2(\theta)$ for $AB_{\theta,2}$, given, respectively, by

$$\begin{cases} l_1(\theta) = -a\cos\theta - \sqrt{b^2 - a^2\sin^2\theta}, & \text{(4.13a)} \\ l_2(\theta) = -a\cos\theta + \sqrt{b^2 - a^2\sin^2\theta}. & \text{(4.13b)} \end{cases}$$

Thus, we obtain the new representation of $Q(a,b)$ as

$$\begin{aligned} Q(a,b) &= 1 - \int_{\theta=\pi-\arcsin(b/a)}^{\pi+\arcsin(b/a)} \int_{r=l_1(\theta)}^{l_2(\theta)} \frac{r}{2\pi} e^{-r^2/2} dr d\theta \\ &= 1 - \frac{1}{\pi}\int_{\pi-\arcsin(b/a)}^{\pi} \left\{ \exp\left[-\frac{1}{2}\left(-a\cos\theta - \sqrt{b^2 - a^2\sin^2\theta}\right)^2\right] \right. \\ &\quad \left. - \exp\left[-\frac{1}{2}\left(-a\cos\theta + \sqrt{b^2 - a^2\sin^2\theta}\right)^2\right] \right\} d\theta, a \geq b \geq 0, a \neq 0. \end{aligned} \quad \text{(4.14)}$$

This new representation also only involves one finite integral, and its integrand is a difference of two pure exponential functions. The lower limit of the integral in (4.14) is only dependent on the ratio b/a, which can be regarded as a constant when averaging over fading in many communication problems [120]. By defining $0 \leq \zeta = b/a \leq 1$, we can reexpress (4.14) in the following form

$$\begin{aligned} Q(a, a\zeta) = 1 - \frac{1}{\pi}\int_{\pi-\arcsin(\zeta)}^{\pi} &\left\{ \exp\left[-\frac{a^2}{2}\left(-\cos\theta - \sqrt{\zeta^2 - \sin^2\theta}\right)^2\right] \right. \\ &\left. - \exp\left[-\frac{a^2}{2}\left(-\cos\theta + \sqrt{\zeta^2 - \sin^2\theta}\right)^2\right] \right\} d\theta, \quad 0 \leq \zeta \leq 1, \end{aligned} \quad \text{(4.15)}$$

or, equivalently, in the form

$$\begin{aligned} &Q(a, a\zeta) \\ &= 1 - \frac{\exp[-a^2(\zeta^2 - 1)/2]}{\pi}\int_{\pi-\arcsin(\zeta)}^{\pi} \left\{ \exp\left[-a^2\left(\cos^2\theta - \cos\theta\sqrt{\zeta^2 - \sin^2\theta}\right)\right] \right. \\ &\quad \left. - \exp\left[-a^2\left(\cos^2\theta + \cos\theta\sqrt{\zeta^2 - \sin^2\theta}\right)\right] \right\} d\theta, \qquad 0 \leq \zeta \leq 1. \end{aligned} \quad \text{(4.16)}$$

4.3.1.3 Discussions

There are three other pairs of alternative finite-integral representations of $Q(a,b)$, with integrands involving only the exponential function, available in the literature. The first pair was given in [113, eqs. (C-26) and (C-27)], namely

$$Q(a,b) = \frac{1}{2\pi}\int_0^{2\pi} \frac{b^2 - ab\cos\theta}{a^2 - 2ab\cos\theta + b^2} \exp\left(-\frac{b^2 - 2ab\cos\theta + a^2}{2}\right) d\theta, \quad b > a \geq 0, \tag{4.17}$$

and

$$Q(a,b) = 1 + \frac{1}{2\pi}\int_0^{2\pi} \frac{b^2 - ab\cos\theta}{a^2 - 2ab\cos\theta + b^2} \exp\left(-\frac{b^2 - 2ab\cos\theta + a^2}{2}\right) d\theta, \quad a > b \geq 0. \tag{4.18}$$

The second pair representations was developed in [114] and summarized in [5, eqs. (4.43) and (4.44)], given by

$$Q(b\zeta,b) = \frac{1}{\pi}\int_0^{\pi} \frac{1 \pm \zeta\cos\theta}{1 \pm 2\zeta\cos\theta + \zeta^2} \exp\left[-\frac{b^2}{2}\left(1 \pm 2\zeta\cos\theta + \zeta^2\right)\right] d\theta, \quad 0 \leq \zeta = \frac{a}{b} < 1, \tag{4.19}$$

and

$$Q(a,a\zeta) = 1 + \frac{1}{\pi}\int_0^{\pi} \frac{\zeta^2 \pm \zeta\cos\theta}{1 \pm 2\zeta\cos\theta + \zeta^2} \exp\left[-\frac{a^2}{2}\left(1 \pm 2\zeta\cos\theta + \zeta^2\right)\right] d\theta, \quad 0 \leq \zeta = \frac{b}{a} < 1. \tag{4.20}$$

The third pair of representations was proposed in [115] and also summarized in [5, eqs. (4.53) and (4.54)], given by

$$Q(b\zeta,b) = \frac{1}{2\pi}\int_0^{\pi} \left\{ \exp\left[-\frac{b^2}{2}\left(1 \pm 2\zeta\cos\theta + \zeta^2\right)\right] + \exp\left[-\frac{b^2}{2}\left(\frac{(1-\zeta^2)^2}{1 \pm 2\zeta\cos\theta + \zeta^2}\right)\right] \right\} d\theta, \ 0 \leq \zeta = \frac{a}{b} \leq 1, \tag{4.21}$$

and

$$Q(a,a\zeta) = 1 + \frac{1}{2\pi}\int_0^{\pi} \left\{ \exp\left[-\frac{a^2}{2}\left(1 \pm 2\zeta\cos\theta + \zeta^2\right)\right] - \exp\left[-\frac{a^2}{2}\left(\frac{(1-\zeta^2)^2}{1 \pm 2\zeta\cos\theta + \zeta^2}\right)\right]\right\} d\theta,\ 0 \le \zeta = \frac{b}{a} \le 1. \quad (4.22)$$

We can see that the pair of representations in (4.19) and (4.20) is equivalent to that in (4.17) and (4.18), just with a halved integration interval. The integrands in (4.17), (4.18), (4.19) and (4.20) are given in terms of one rational function multiplied by one exponential function of trigonometric functions. The integrands in (4.21) and (4.22) consist of two pure exponential functions. For the case of $b \ge a$, we can see that our new representation in (4.11) or (4.12) is simpler than those in (4.17), (4.19), and (4.21), since their integrands involve only one pure exponential function. For the case of $a \ge b$, our new representation in (4.14) or (4.15) is similar to that in (4.22) with two pure exponential integrands. However, the integration interval in (4.15) is less than or equal to half of that in (4.22), i.e., not greater than $\pi/2$. Besides, in our forms, the integrands are always determinate, since the parameters a, b and θ only appear in the numerators. Thus, our forms are more robust than the existing forms mentioned above, which may be unstable for some combinations of the arguments. Furthermore, similar to those in (4.21) and (4.22), both our results in (4.11) and (4.14) are valid for the case of $b = a$, i.e., they give the same result as [5, eq. (4.40)]

$$Q(a,a) = \frac{1}{2}\left[1 + \exp\left(-a^2\right) I_0\left(a^2\right)\right]. \quad (4.23)$$

In this aspect, our representations are also better than the pair in (4.17) and (4.18) and the pair in (4.19) and (4.20), since the latter two pairs do not hold for this special case.

4.3.2 Representations with Integrands Involving the Erfc Function

We now derive another new representation for $Q(a, b)$, whose integrand involves the erfc function as well as the exponential function. As shown in Fig. 4.1, for both the cases of $b \geq a$ and $a \geq b$, in the y_1y_2-rectangular coordinate system, the probability of the point z lying inside of $\mathbb{B}_{O,b}$ is given by

$$\begin{aligned}\Pr(z \in \mathbb{B}_{O,b}) &= \frac{1}{2\pi}\int_{y_1=-(b+a)}^{b-a} e^{-y_1^2/2}\int_{y_2=-\sqrt{b^2-(a+y_1)^2}}^{\sqrt{b^2-(a+y_1)^2}} e^{-y_2^2/2}dy_2dy_1 \\ &= \frac{1}{2}\text{erfc}\left(-\frac{b+a}{\sqrt{2}}\right) - \frac{1}{2}\text{erfc}\left(\frac{b-a}{\sqrt{2}}\right) \\ &\quad - \frac{1}{\sqrt{2\pi}}\int_{-(b+a)}^{b-a} e^{-y_1^2/2}\text{erfc}\left(\sqrt{\frac{b^2-(a+y_1)^2}{2}}\right)dy_1. \quad (4.24)\end{aligned}$$

Thus, the first-order Marcum Q-function can be written as

$$\begin{aligned}Q(a, b) = &\frac{1}{2}\text{erfc}\left(\frac{b+a}{\sqrt{2}}\right) + \frac{1}{2}\text{erfc}\left(\frac{b-a}{\sqrt{2}}\right) \\ &+ \frac{1}{\sqrt{2\pi}}\int_{-(b+a)}^{b-a} e^{-y_1^2/2}\text{erfc}\left(\sqrt{\frac{b^2-(a+y_1)^2}{2}}\right)dy_1, \ a \geq 0, b \geq 0. \quad (4.25)\end{aligned}$$

Compared to the new representations in (4.11) and (4.14) derived using the polar coordinate system, the new representation in (4.25) is valid for the entire ranges of a and b. The shortcoming of the representation in (4.25) is that its integrand involves the erfc function, and its integration limits are dependent on the values of the arguments a and b. Thus, it is not as simple as the representations in (4.11) and (4.14). However, this representation leads to a very tight upper erfc bound, which will be shown in Section 4.7.

There is an alternative representation for $Q(a, b)$ with integrand involving the

erfc function available in [116, eq. (3)], namely

$$Q(a,b) = \exp\left(-\frac{b^2+a^2}{2}\right) I_0(ab) + \frac{a}{\sqrt{2\pi}} \int_0^{\pi} \cos\theta \exp\left(-\frac{a^2}{2}\sin^2\theta\right) \operatorname{erfc}\left(\frac{b-a\cos\theta}{\sqrt{2}}\right) d\theta, \quad a \geq 0, b \geq 0. \tag{4.26}$$

This representation requires a finite integration over a fixed interval, and it is also valid over the entire ranges of a and b. Our new representation in (4.25) is simpler than that in (4.26) in the sense that the integrand in (4.25) is simpler.

4.4 New Generic Exponential Bounds

In addition to the new representations shown above, the geometric view of $Q(a,b)$ can also lead to some tight bounds. The exponential function is the most desirable functional form to use when we have to average the bounds on $Q(a,b)$ over a fading distribution. By using our geometric approach, i.e., computing the probability of z lying outside of sectors or angular sectors of annuli that completely cover or are completely covered by the disk $\mathbb{B}_{O,b}$, we can easily obtain bounds in which only the exponential function is involved. Here, we present some generic upper and lower exponential bounds, which involve an arbitrarily large number of exponential terms. Some special cases of these bounds will be given in Section 4.5 to illustrate the use of these generic bounds.

4.4.1 Bounds for the Case of $b \geq a \geq 0$

As shown by the solid lines inside $\mathbb{B}_{O,b}$ in Fig. 4.2, upper exponential bounds can be obtained by using a set of contiguous, concentric sectors, centered at the point A, to fill $\mathbb{B}_{O,b}$. The sectors are chosen to be symmetrical about the z_1-axis. Since the PDF of y, centered at the point A, in (4.9) is isotropic, the probability of z, centered at the origin O, lying inside the union of all the sectors is equal

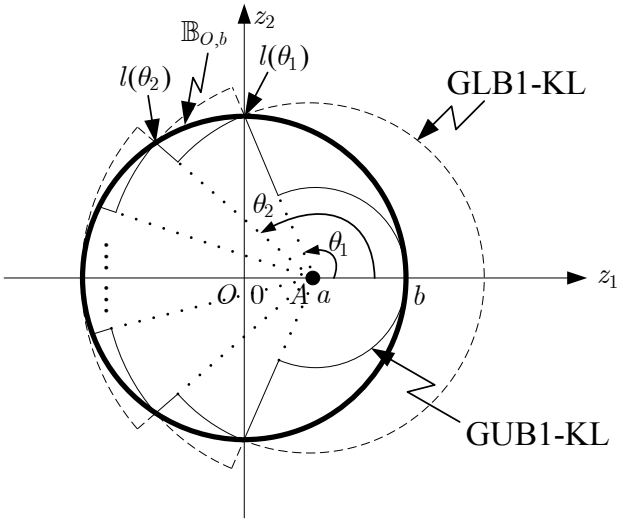

Fig. 4.2: Diagram of the derivation of the new generic exponential bounds GUB1-KL and GLB1-KL on $Q(a,b)$ for the case of $b > a$.

to twice the probability of z, or equivalently y, lying inside the union of the N sectors in the upper half plane. Then in the upper half plane, the $(N+1)$ angles, i.e., $0 = \theta_0 < \theta_1 < \cdots < \theta_N = \pi$, are first defined, and the ith sector, denoted as $\mathbb{B}_{A,l(\theta_{i-1}),\theta_{i-1},\theta_i}$, is set to be centered at the point A with the radius $l(\theta_{i-1})$, covering the angle from θ_{i-1} to θ_i. Thus, the probability of z lying inside $\mathbb{B}_{A,l(\theta_{i-1}),\theta_{i-1},\theta_i}$ is given by

$$\begin{aligned}\Pr(z \in \mathbb{B}_{A,l(\theta_{i-1}),\theta_{i-1},\theta_i}) &= \int_{\theta=\theta_{i-1}}^{\theta_i} \int_{r=0}^{l(\theta_{i-1})} \frac{r}{2\pi} e^{-r^2/2} dr d\theta \\ &= \frac{\theta_i - \theta_{i-1}}{2\pi} \left\{ 1 - \exp\left[-\frac{l^2(\theta_{i-1})}{2} \right] \right\}. \end{aligned} \tag{4.27}$$

Our first generic, upper, exponential bound on $Q(a,b)$, denoted as GUB1-KL (after the authors), is, therefore, given by

$$\begin{aligned} Q(a,b) &\leq Q_{GUB1\text{-}KL}(a,b) \\ &= 1 - 2\sum_{i=1}^{N} \Pr(z \in \mathbb{B}_{A,l(\theta_{i-1}),\theta_{i-1},\theta_i}) \\ &= \frac{1}{\pi} \sum_{i=1}^{N} (\theta_i - \theta_{i-1}) \exp\left[-\frac{1}{2} \left(-a\cos\theta_{i-1} + \sqrt{b^2 - a^2 \sin^2\theta_{i-1}} \right)^2 \right], \\ & \qquad\qquad b \geq a \geq 0, \end{aligned} \tag{4.28}$$

were we have $0 = \theta_0 < \theta_1 < \cdots < \theta_N = \pi$, and N is the number of sectors in the upper (or lower) half plane.

Similarly, by using a set of contiguous, concentric sectors to form a region whose boundary circumscribes the boundary of $\mathbb{B}_{O,b}$, as shown by the dashed lines outside $\mathbb{B}_{O,b}$ in Fig. 4.2, we can obtain our first generic, lower, exponential bound, denoted as GLB1-KL, on $Q(a,b)$. For this case, the ith sector has a radius of $l(\theta_i)$, and is denoted by $\mathbb{B}_{A,l(\theta_i),\theta_{i-1},\theta_i}$. Thus, GLB1-KL is given by

$$\begin{aligned} Q(a,b) &\geq Q_{GLB1\text{-}KL}(a,b) \\ &= 1 - 2\sum_{i=1}^{N} \Pr(z \in \mathbb{B}_{A,l(\theta_i),\theta_{i-1},\theta_i}) \\ &= \frac{1}{\pi}\sum_{i=1}^{N} (\theta_i - \theta_{i-1}) \exp\left[-\frac{1}{2}\Big(-a\cos\theta_i + \sqrt{b^2 - a^2\sin^2\theta_i}\Big)^2\right], \\ & \qquad\qquad b \geq a \geq 0, \end{aligned} \tag{4.29}$$

where we also have $0 = \theta_0 < \theta_1 < \cdots < \theta_N = \pi$.

In both (4.28) and (4.29), as N approaches infinity, the area covered by the union of the bounding sectors approaches that covered by $\mathbb{B}_{O,b}$, and thus, GUB1-KL and GLB1-KL approach the exact value of $Q(a,b)$.

Incidentally, we can also obtain our generic exponential bounds GUB1-KL in (4.28) and GLB1-KL in (4.29) by applying the rectangular numerical integration rule [130] to the new representation for $Q(a,b)$ in (4.11). Since the integrand in (4.11) is a monotonic, non-increasing function of θ for $0 \leq \theta \leq \pi$, we can partition the interval $[0,\pi]$ into N uniform or nonuniform subintervals, i.e., choose $N-1$ arbitrary values θ_1, θ_2, ..., θ_{N-1} of θ such that $0 = \theta_0 < \theta_1 < \cdots < \theta_N = \pi$, and rewrite (4.11) as

$$Q(a,b) = \frac{1}{\pi}\sum_{i=1}^{N} \int_{\theta_{i-1}}^{\theta_i} \exp\left[-\frac{1}{2}\Big(-a\cos\theta + \sqrt{b^2 - a^2\sin^2\theta}\Big)^2\right] d\theta. \tag{4.30}$$

The integral in (4.30) for each value of i can be upper bounded by the product of $(\theta_i - \theta_{i-1})$ and the value of the integrand evaluated at $\theta = \theta_{i-1}$. This gives

GUB1-KL in (4.28). GLB1-KL in (4.29) is also easy to obtain from (4.30) by replacing the integral over $[\theta_{i-1}, \theta_i)$ by the product of $(\theta_i - \theta_{i-1})$ and the value of the integrand evaluated at $\theta = \theta_i$. This procedure is similar to that used in [131] to obtain the improved upper bound for the erfc function.

4.4.2 Bounds for the Case of $a \geq b \geq 0$ and $a \neq 0$

For this case, since the point A is outside of $\mathbb{B}_{O,b}$, we need to use angular sectors of annuli, instead of sectors, to bound the disk $\mathbb{B}_{O,b}$. As shown by the solid lines inside $\mathbb{B}_{O,b}$ in Fig. 4.3(a), a generic, upper, exponential bound can be obtained by using a set of contiguous angular sectors of concentric annuli to fill $\mathbb{B}_{O,b}$. The ith angular sector of the annulus in the upper half plane, denoted as $\mathbb{B}_{A,l_1(\theta_i),l_2(\theta_i),\theta_i,\theta_{i+1}}$, is centered at A with an inner radius of $l_1(\theta_i)$ and an outer radius of $l_2(\theta_i)$, and covers the angle from θ_i to θ_{i+1}. The probability of z lying inside this ith angular sector of the annulus is given by

$$\begin{aligned}\Pr(z \in \mathbb{B}_{A,l_1(\theta_i),l_2(\theta_i),\theta_i,\theta_{i+1}}) &= \int_{\theta=\theta_i}^{\theta_{i+1}} \int_{r=l_1(\theta_i)}^{l_2(\theta_i)} \frac{r}{2\pi} e^{-r^2/2} dr d\theta \\ &= \frac{\theta_{i+1} - \theta_i}{2\pi} \left\{ \exp\left[-\frac{l_1^2(\theta_i)}{2}\right] - \exp\left[-\frac{l_2^2(\theta_i)}{2}\right] \right\}. \quad (4.31)\end{aligned}$$

Thus, we obtain our second generic upper exponential bound, denoted as GUB2-KL, namely

$$\begin{aligned}Q(a,b) &\leq Q_{GUB2\text{-}KL}(a,b) \\ &= 1 - 2\sum_{i=1}^{N-1} \Pr(z \in \mathbb{B}_{A,l_1(\theta_i),l_2(\theta_i),\theta_i,\theta_{i+1}}) \\ &= 1 - \frac{1}{\pi}\sum_{i=1}^{N-1} (\theta_{i+1} - \theta_i) \left\{ \exp\left[-\frac{1}{2}\Big(-a\cos\theta_i - \sqrt{b^2 - a^2\sin^2\theta_i}\Big)^2\right] \right. \\ &\quad \left. - \exp\left[-\frac{1}{2}\Big(-a\cos\theta_i + \sqrt{b^2 - a^2\sin^2\theta_i}\Big)^2\right] \right\}, \; a \geq b \geq 0, \; a \neq 0. \quad (4.32)\end{aligned}$$

Here, we have $\pi - \arcsin(b/a) = \theta_0 < \theta_1 < \cdots < \theta_N = \pi$, and there are only $(N-1)$ angular sectors of annuli used in the upper (or lower) half plane.

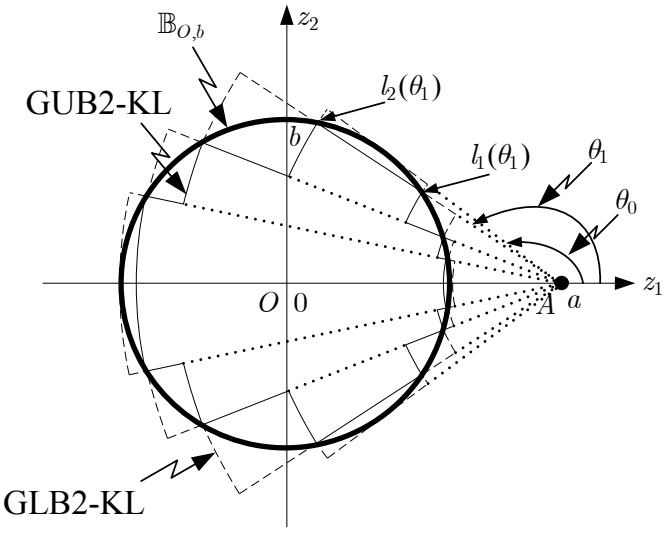

(a) Simpler case

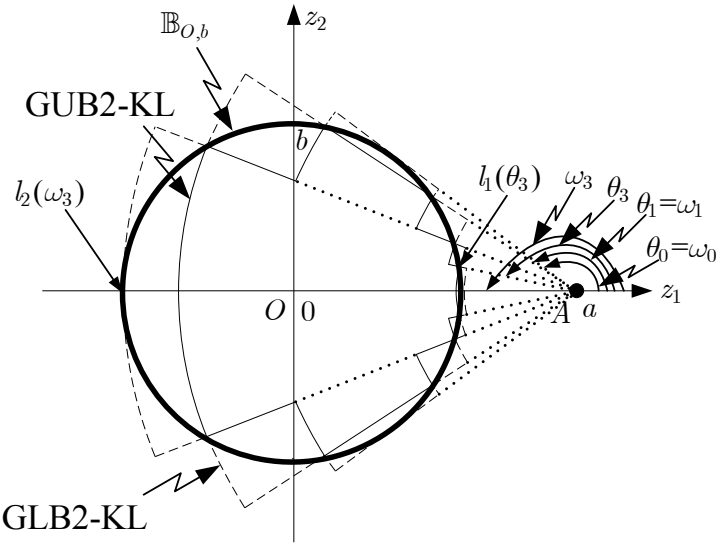

(b) General case

Fig. 4.3: Diagram of the derivation of the new generic exponential bounds GUB2-KL and GLB2-KL on $Q(a, b)$ for the case of $a > b$.

From Fig. 4.3(b), it is also easy to understand that instead of setting both the inner and outer radii of the $(i + 1)$th angular sector to be different from those of the ith angular sector, i.e., setting the $(i + 1)$th angular sector as $\mathbb{B}_{A,l_1(\theta_{i+1}),l_2(\theta_{i+1}),\theta_{i+1},\theta_{i+2}}$, we can also leave either the inner radius or the outer radius of the $(i+1)$th angular sector unchanged, i.e., set the $(i+1)$th angular sector as $\mathbb{B}_{A,l_1(\theta_i),l_2(\theta_{i+1}),\theta_{i+1},\theta_{i+2}}$ or $\mathbb{B}_{A,l_1(\theta_{i+1}),l_2(\theta_i),\theta_{i+1},\theta_{i+2}}$. For this more general case,

our upper bound GUB2-KL becomes

$$\begin{aligned} Q(a,b) &\le Q_{GUB2\text{-}KL}(a,b) \\ &= 1 - \frac{1}{\pi}\left\{\sum_{i=1}^{N-1}(\theta_{i+1}-\theta_i)\exp\left[-\frac{1}{2}\left(-a\cos\theta_i - \sqrt{b^2-a^2\sin^2\theta_i}\right)^2\right]\right. \\ &\quad \left. - \sum_{j=1}^{M-1}(\omega_{j+1}-\omega_j)\exp\left[-\frac{1}{2}\left(-a\cos\omega_j + \sqrt{b^2-a^2\sin^2\omega_j}\right)^2\right]\right\}, \\ &\qquad\qquad a \ge b \ge 0,\ a \ne 0. \quad (4.33) \end{aligned}$$

Here, we have $\pi - \arcsin(b/a) = \theta_0 < \theta_1 < \cdots < \theta_N = \pi$, $\pi - \arcsin(b/a) = \omega_0 < \omega_1 < \cdots < \omega_M = \pi$, and $\theta_1 = \omega_1$.

A generic lower exponential bound can be obtained similarly by using a set of contiguous angular sectors of concentric annuli to form a region whose boundary circumscribes that of $\mathbb{B}_{O,b}$, as shown by the dashed lines outside of $\mathbb{B}_{O,b}$ in Fig. 4.3(a). For this case, the ith angular sector of the annulus in the upper half plane is denoted by $\mathbb{B}_{A,l_1(\theta_i),l_2(\theta_i),\theta_{i-1},\theta_i}$, which is centered at A and covers the angle from θ_{i-1} to θ_i with the inner radius of $l_1(\theta_i)$ and the outer radius of $l_2(\theta_i)$. The probability of z lying inside $\mathbb{B}_{A,l_1(\theta_i),l_2(\theta_i),\theta_{i-1},\theta_i}$ is then given by

$$\Pr(z \in \mathbb{B}_{A,l_1(\theta_i),l_2(\theta_i),\theta_{i-1},\theta_i}) = \frac{\theta_i - \theta_{i-1}}{2\pi}\left\{\exp\left[-\frac{l_1^2(\theta_i)}{2}\right] - \exp\left[-\frac{l_2^2(\theta_i)}{2}\right]\right\}.$$

Thus, our second generic lower exponential bound, denoted as GLB2-KL, is given by

$$\begin{aligned} Q(a,b) &\ge Q_{GLB2\text{-}KL}(a,b) \\ &= 1 - 2\sum_{i=1}^{N}\Pr(z \in \mathbb{B}_{A,l_1(\theta_i),l_2(\theta_i),\theta_{i-1},\theta_i}) \\ &= 1 - \frac{1}{\pi}\sum_{i=1}^{N}(\theta_i - \theta_{i-1})\left\{\exp\left[-\frac{1}{2}\left(-a\cos\theta_i - \sqrt{b^2-a^2\sin^2\theta_i}\right)^2\right]\right. \\ &\quad \left. - \exp\left[-\frac{1}{2}\left(-a\cos\theta_i + \sqrt{b^2-a^2\sin^2\theta_i}\right)^2\right]\right\},\ a \ge b \ge 0,\ a \ne 0. \quad (4.34) \end{aligned}$$

Here, we have $\pi - \arcsin(b/a) = \theta_0 < \theta_1 < \cdots < \theta_N = \pi$, and there are N angular

sectors of annuli used in the upper (or lower) half plane.

For this lower bound, we can also choose either the inner or the outer radius to be the same for two adjacent angular sectors of annuli, as shown in Fig. 4.3(b), and this leads to a more general expression for our lower bound, GLB2-KL, i.e.,

$$\begin{aligned} Q(a,b) &\geq Q_{GLB2\text{-}KL}(a,b) \\ &= 1 - \frac{1}{\pi}\left\{\sum_{i=1}^{N}(\theta_i - \theta_{i-1})\exp\left[-\frac{1}{2}\left(-a\cos\theta_i - \sqrt{b^2 - a^2\sin^2\theta_i}\right)^2\right]\right. \\ &\quad \left. - \sum_{j=1}^{M}(\omega_j - \omega_{j-1})\exp\left[-\frac{1}{2}\left(-a\cos\omega_j + \sqrt{b^2 - a^2\sin^2\omega_j}\right)^2\right]\right\}, \\ &\qquad\qquad a \geq b \geq 0,\ a \neq 0, \quad (4.35) \end{aligned}$$

where we have $\pi - \arcsin(b/a) = \theta_0 < \theta_1 < \cdots < \theta_N = \pi$ and $\pi - \arcsin(b/a) = \omega_0 < \omega_1 < \cdots < \omega_M = \pi$.

Similar to the case of $b \geq a$, GUB2-KL in (4.33) and GLB2-KL in (4.35) can also be obtained by applying the rectangular numerical integration rule [130] to the new form of $Q(a,b)$ in (4.14), making use of the non-decreasing property of the first integrand and the non-increasing property of the second integrand. Compared to this mathematical interpretation, our geometric derivation shows more clearly the geometric meaning of the generic bounds, which enables one to judge the tightness of the bounds geometrically.

4.5 New Simple Exponential Bounds

Here, we illustrate some special cases of the above generic exponential bounds with only two exponential terms.

We first consider the case of $b \geq a \geq 0$. For the upper bound GUB1-KL in (4.28) and the lower bound GLB1-KL in (4.29) with $N = 2$, the value of the angle θ_1 will affect greatly the tightness of the bounds. We use θ_1^{opt} to denote such a value of θ_1 that GUB1-KL or GLB1-KL with this θ_1^{opt} is the tightest over the

entire range of a and b among GUB1-KL or GLB1-KL with all possible values of $\theta_1 \in (0, \pi)$. It is easy to see that θ_1^{opt} should be a function of a and b. However, it is difficult to obtain θ_1^{opt} analytically from (4.28) or (4.29). We have also tried the numerical method, i.e., to find a functional form for θ_1^{opt} which gives a best fit to some numerical values of θ_1^{opt} as a function of a and b. We find that for GUB1-KL, θ_1^{opt} can be approximately expressed as a negative exponential function for a given value of a, and as a positive exponential function for a given value of b. However, it is difficult to find a functional form which gives a good approximation to θ_1^{opt} as a function of both a and b, and the result obtained thus far cannot provide a much better performance than that obtained by simply setting θ_1 as a constant. Thus, by comparing the performance of the bounds with different constant values of θ_1, we recommend here $\theta_1 = \pi/2$ for GUB1-KL and $\theta_1 = \pi/3$ for GLB1-KL. This gives our first new simple upper bound, denoted as UB1-KL, namely

$$\begin{aligned} Q(a,b) &\le Q_{UB1\text{-}KL}(a,b) \\ &= \frac{1}{2}\left\{\exp\left(-\frac{b^2-a^2}{2}\right) + \exp\left[-\frac{(b-a)^2}{2}\right]\right\}, \quad b \ge a \ge 0, \end{aligned} \tag{4.36}$$

and our first new simple lower bound, denoted as LB1-KL, namely

$$\begin{aligned} Q(a,b) &\ge Q_{LB1\text{-}KL}(a,b) \\ &= \frac{1}{3}\exp\left[-\frac{\left(-a+\sqrt{4b^2-3a^2}\right)^2}{8}\right] + \frac{2}{3}\exp\left[-\frac{(b+a)^2}{2}\right], \\ & \qquad\qquad b \ge a \ge 0. \end{aligned} \tag{4.37}$$

These two bounds are not the tightest for all the possible values of a and b which satisfy $b \ge a \ge 0$, but they are simple with reasonable tightness for all a and b over this range.

Next, we consider the case of $a \ge b \ge 0$ and $a \ne 0$. For the upper bound GUB2-KL in (4.33) with $N = M = 2$, the value of $\theta_1 = \omega_1$ has to be dependent on the ratio b/a, since we have $\theta_0 = \omega_0 = \pi - \arcsin(b/a)$. From our numerical

results, we find that setting

$$\theta_1 = \omega_1 = \pi - \frac{17}{24}\arcsin\frac{b}{a}$$

gives a bound reasonably tight over the ranges of a and b with $a \geq b$. This leads to our second simple upper bound, UB2-KL, i.e.,

$$\begin{aligned} & Q(a,b) \\ & \leq Q_{UB2\text{-}KL}(a,b) \\ & = 1 - \frac{17\arcsin\frac{b}{a}}{24\pi}\left\{\exp\left[-\frac{l_1^2\left(\pi - \frac{17}{24}\arcsin\frac{b}{a}\right)}{2}\right] - \exp\left[-\frac{l_2^2\left(\pi - \frac{17}{24}\arcsin\frac{b}{a}\right)}{2}\right]\right\}, \\ & \qquad\qquad a \geq b \geq 0,\ a \neq 0. \end{aligned} \quad (4.38)$$

For the lower bound GLB2-KL in (4.35), the only special case with two exponential terms is given by setting $N = M = 1$ in (4.35). This leads to our second simple lower bound LB2-KL, i.e.,

$$\begin{aligned} Q(a,b) & \geq Q_{LB2\text{-}KL}(a,b) \\ & = 1 - \frac{\arcsin(b/a)}{\pi}\left\{\exp\left[-\frac{(b-a)^2}{2}\right] - \exp\left[-\frac{(b+a)^2}{2}\right]\right\}, \\ & \qquad\qquad a \geq b \geq 0,\ a \neq 0. \end{aligned} \quad (4.39)$$

A point to note is that the simple bounds shown above are just the bounds that are generally tight over the entire ranges of a and b concerned, instead of the tightest bounds. For a subrange of a and b of interest, one can obtain some simple bounds tighter than those shown here by choosing better values for the parameters in our generic bounds.

4.6 New Generic Erfc Bounds

In addition to the generic exponential bounds in Section 4.4, we can also derive some generic erfc bounds, which involve only the erfc function, by evaluating in

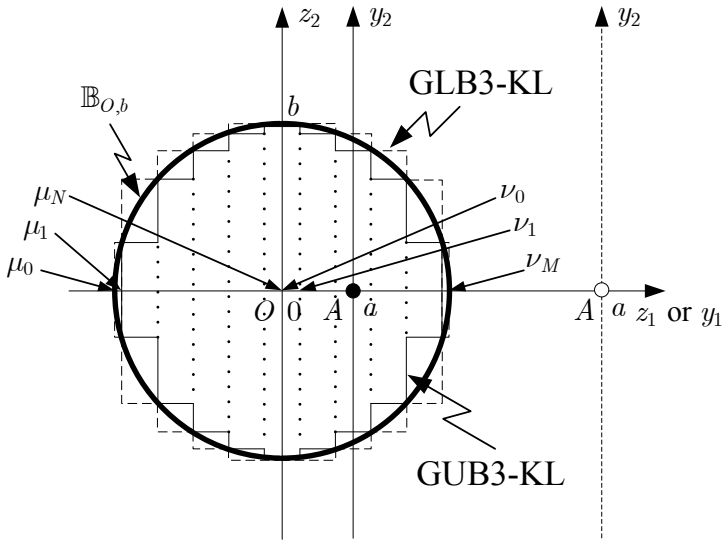

Fig. 4.4: Diagram of the derivation of the new generic erfc bounds GUB3-KL and GLB3-KL on $Q(a, b)$.

rectangular coordinates the probability of z lying outside of the union of a set of rectangular regions. Although these generic erfc bounds are not as simple as the generic exponential bounds, they may be tighter than the latter for some cases. The generic upper erfc bounds can be obtained by using a set of contiguous rectangular regions to fill the disk $\mathbb{B}_{O,b}$, as shown by the solid lines inside $\mathbb{B}_{O,b}$ in Fig. 4.4. Thus we obtain the generic upper erfc bound, denoted as GUB3-KL, namely

$$\begin{aligned}
Q(a,b) &\le Q_{GUB3\text{-}KL}(a,b) \\
&= 1 - \frac{1}{2\pi}\sum_{i=1}^{N-1}\int_{y_1=\mu_i}^{\mu_{i+1}}\int_{y_2=-\sqrt{b^2-(a+\mu_i)^2}}^{\sqrt{b^2-(a+\mu_i)^2}} e^{-\left(y_1^2+y_2^2\right)/2}dy_2dy_1 \\
&\quad -\frac{1}{2\pi}\sum_{j=1}^{M-1}\int_{y_1=\nu_{j-1}}^{\nu_j}\int_{y_2=-\sqrt{b^2-(a+\nu_j)^2}}^{\sqrt{b^2-(a+\nu_j)^2}} e^{-\left(y_1^2+y_2^2\right)/2}dy_2dy_1 \\
&= 1 - \frac{1}{2}\sum_{i=1}^{N-1}\left[\mathrm{erfc}\left(\frac{\mu_i}{\sqrt{2}}\right) - \mathrm{erfc}\left(\frac{\mu_{i+1}}{\sqrt{2}}\right)\right]\left[1-\mathrm{erfc}\left(\sqrt{\frac{b^2-(a+\mu_i)^2}{2}}\right)\right] \\
&\quad - \frac{1}{2}\sum_{j=1}^{M-1}\left[\mathrm{erfc}\left(\frac{\nu_{j-1}}{\sqrt{2}}\right) - \mathrm{erfc}\left(\frac{\nu_j}{\sqrt{2}}\right)\right]\left[1-\mathrm{erfc}\left(\sqrt{\frac{b^2-(a+\nu_j)^2}{2}}\right)\right], \\
&\qquad\qquad a \ge 0, b \ge 0, \quad (4.40)
\end{aligned}$$

where we have $-b-a=\mu_0<\mu_1<\cdots<\mu_N=-a$ and $-a=\nu_0<\nu_1<\cdots<\nu_M=b-a$.

The generic lower erfc bound, denoted as GLB3-KL, can be obtained by using a set of contiguous rectangular regions to cover $\mathbb{B}_{O,b}$, as shown by the dashed lines outside $\mathbb{B}_{O,b}$ in Fig. 4.4, namely

$$\begin{aligned}
Q(a,b) &\geq Q_{GLB3\text{-}KL}(a,b) \\
&= 1-\frac{1}{2\pi}\sum_{i=1}^{N}\int_{y_1=\mu_{i-1}}^{\mu_i}\int_{y_2=-\sqrt{b^2-(a+\mu_i)^2}}^{\sqrt{b^2-(a+\mu_i)^2}} e^{-\left(y_1^2+y_2^2\right)/2}dy_2dy_1 \\
&\quad -\frac{1}{2\pi}\sum_{j=1}^{M}\int_{y_1=\nu_{j-1}}^{\nu_j}\int_{y_2=-\sqrt{b^2-(a+\nu_{j-1})^2}}^{\sqrt{b^2-(a+\nu_{j-1})^2}} e^{-\left(y_1^2+y_2^2\right)/2}dy_2dy_1 \\
&= 1-\frac{1}{2}\sum_{i=1}^{N}\left[\operatorname{erfc}\left(\frac{\mu_{i-1}}{\sqrt{2}}\right)-\operatorname{erfc}\left(\frac{\mu_i}{\sqrt{2}}\right)\right]\left[1-\operatorname{erfc}\left(\sqrt{\frac{b^2-(a+\mu_i)^2}{2}}\right)\right] \\
&\quad -\frac{1}{2}\sum_{j=1}^{M}\left[\operatorname{erfc}\left(\frac{\nu_{j-1}}{\sqrt{2}}\right)-\operatorname{erfc}\left(\frac{\nu_j}{\sqrt{2}}\right)\right]\left[1-\operatorname{erfc}\left(\sqrt{\frac{b^2-(a+\nu_{j-1})^2}{2}}\right)\right], \\
&\qquad\qquad a\geq 0, b\geq 0. \quad (4.41)
\end{aligned}$$

Here, we have $-b-a=\mu_0<\mu_1<\cdots<\mu_N=-a$ and $-a=\nu_0<\nu_1<\cdots<\nu_M=b-a$. From Fig. 4.4, it is clear that GUB3-KL and GLB3-KL are valid for both the cases of $b\geq a\geq 0$ and $a\geq b\geq 0$, and approach the exact value of $Q(a,b)$ as the values of N and M increase.

As in the case of the generic exponential bounds in Section 4.4, the generic erfc bounds in (4.40) and (4.41) can also be obtained by applying the rectangular integration rule [130] to the equation in the first line of (4.24) to evaluate $Q(a,b)$ in the rectangular coordinate system.

4.7 New Simple Erfc Bounds

We now give some simple erfc bounds which only involve a few terms. According to our numerical results, we find that the generic erfc bound GUB3-KL in (4.40) evaluated with a small number of terms is not tight. Thus, we give here

another tight simple erfc bound which is derived from the new representation in (4.25) for $Q(a,b)$. As shown in Section 4.3.2, for both the cases of $b \geq a$ and $a \geq b$, the new representation (4.25) for $Q(a,b)$ is valid. Since $\mathrm{erfc}(x)$ is well known to be bounded by an exponential function, i.e.,

$$\mathrm{erfc}(x) \leq e^{-x^2}, \qquad x \geq 0, \tag{4.42}$$

we can obtain our third new simple upper bound, referred to as UB3-KL, by using (4.42) in the integral in (4.25), namely

$$\begin{aligned} Q(a,b) &\leq Q_{UB3\text{-}KL}(a,b) \\ &= \frac{1}{2}\mathrm{erfc}\left(\frac{b+a}{\sqrt{2}}\right) + \frac{1}{2}\mathrm{erfc}\left(\frac{b-a}{\sqrt{2}}\right) + \frac{1}{\sqrt{2\pi}}\int_{-(b+a)}^{b-a} e^{-y_1^2/2} e^{-[b^2-(a+y_1)^2]/2} dy_1 \\ &= \frac{1}{2}\mathrm{erfc}\left(\frac{b+a}{\sqrt{2}}\right) + \frac{1}{2}\mathrm{erfc}\left(\frac{b-a}{\sqrt{2}}\right) \\ &\quad + \frac{1}{a\sqrt{2\pi}}\left\{\exp\left[-\frac{(b-a)^2}{2}\right] - \exp\left[-\frac{(b+a)^2}{2}\right]\right\}, \; a > 0, \; b \geq 0. \end{aligned} \tag{4.43}$$

This new bound, UB3-KL, only involves the erfc and exponential functions, and is easy to handle, both analytically and numerically. For example, in a fading scenario, the average of the erfc function over a fading distribution can be calculated in closed form for the Rayleigh [5, eq. (5.6)], Nakagami-m [5, eq. (5.18)], and Rician [132, eq. (19)] fading channels. Therefore, evaluating the average of UB3-KL over these fading channels in closed form will not pose any problem. As will be shown in Section 4.10, this bound is very tight for large values of a and b.

Other simple upper erfc bounds can also be obtained by using a few rectangular regions, or together with some sectors, to fill the disk $\mathbb{B}_{O,b}$. While many such bounds can be obtained, most are not as tight and simple as UB3-KL in (4.43). For instance, the bounds obtained by using a single inscribed square region and the bound obtained by using a combination of a rectangular region and a right semicircular region have been shown to be loose in [133] and [134], respectively.

A tight, simple, lower erfc bound on $Q(a,b)$ can be obtained by setting $N =$

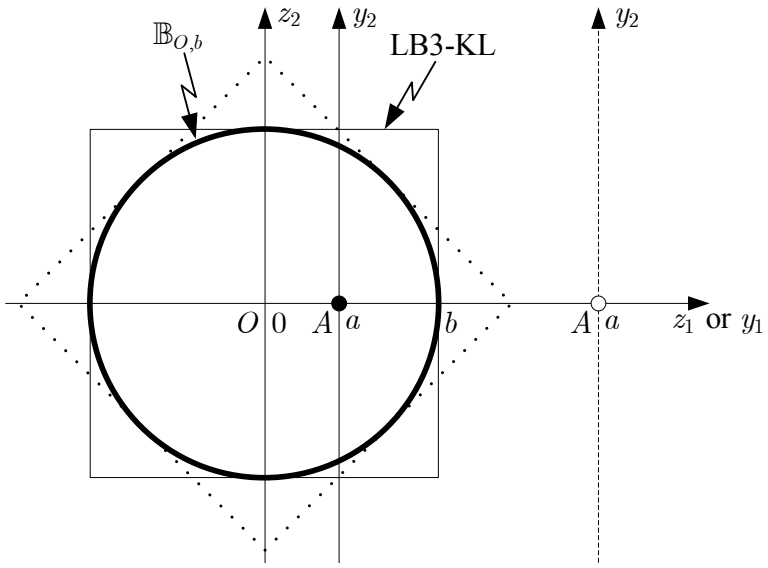

Fig. 4.5: Diagram of the derivation of the simple lower erfc bound LB3-KL on $Q(a,b)$.

$M = 1$ in GLB3-KL (4.41). This corresponds to using a square region centered at the origin O as the bounding shape, whose sides are $2b$ in length, parallel to either the z_1-axis or the z_2-axis, as shown by the solid lines outside of $\mathbb{B}_{O,b}$ in Fig. 4.5. This gives our third, new, simple lower bound, abbreviated as LB3-KL, namely

$$\begin{aligned} Q(a,b) &\geq Q_{LB3\text{-}KL}(a,b) \\ &= \frac{1}{2}\left[\operatorname{erfc}\left(\frac{b+a}{\sqrt{2}}\right) + \operatorname{erfc}\left(\frac{b-a}{\sqrt{2}}\right)\right]\left[1 - \operatorname{erfc}\left(\frac{b}{\sqrt{2}}\right)\right] + \operatorname{erfc}\left(\frac{b}{\sqrt{2}}\right), \\ &\qquad a \geq 0, b \geq 0. \end{aligned} \quad (4.44)$$

This bound turns out to be very tight for large values of a and b, and is valid for both the cases of $b \geq a$ and $a \geq b$. It involves the product of two different erfc functions. The integral involved in averaging the product of two different erfc functions over a fading distribution has been solved for Rayleigh fading in [135], and will be solved for Nakagami-m fading and given a pair of upper and lower bounds for Rician fading in Chapter 6. Thus, it is easy to evaluate or bound the average of our erfc bound LB3-KL over these fading channels in closed form.

Another simple, lower erfc bound on $Q(a,b)$ can be derived by computing the probability of z lying outside of a square region which is obtained by rotating the

square region used in the derivation of LB3-KL 45°, as shown by the dotted lines outside of $\mathbb{B}_{O,b}$ in Fig. 4.5. However, the results in [134] show that this bound is not as tight as LB3-KL in (4.44).

4.8 New Generic Single-Integral Bounds

In Section 4.4, we have derived the generic exponential bounds which are obtained by using variations of circular regions as bounding shapes. In Section 4.6, we have derived the generic erfc bounds which are obtained by using variations of rectangular regions as bounding shapes. Both of these two types of bounds are closed-form bounds. In this section, we derive some generic single-integral bounds which involve single finite integrals and which are obtained by using polygons as bounding shapes. The bounding polygons considered here involve an arbitrarily large number of sides, and can be equilateral or inequilateral. Thus, the generic bounds obtained involve an arbitrarily large number of single integrals.

4.8.1 Upper Bounds

We first derive generic upper single-integral bounds on $Q(a, b)$ by computing the probability of z lying outside of the polygon $\mathbb{P}_{U,N}$ which has N sides, and which is inscribed within $\mathbb{B}_{O,b}$, as shown in Fig. 4.6. To construct $\mathbb{P}_{U,N}$, we first choose N points (B_i, $i = 1, \cdots, N$) on the boundary of $\mathbb{B}_{O,b}$ such that N angles ψ_i's between the positive z_1-axis and the segment OB_i are formed and given by $0 = \psi_1 < \ldots < \psi_N < \psi_{N+1} = 2\pi$, and then we connect adjacent points using straight line segments. The length of the line segment AB_i, denoted as $l(\psi_i)$, is given by

$$l(\psi_i) = \sqrt{b^2 + a^2 - 2ab\cos(\psi_i)}. \tag{4.45}$$

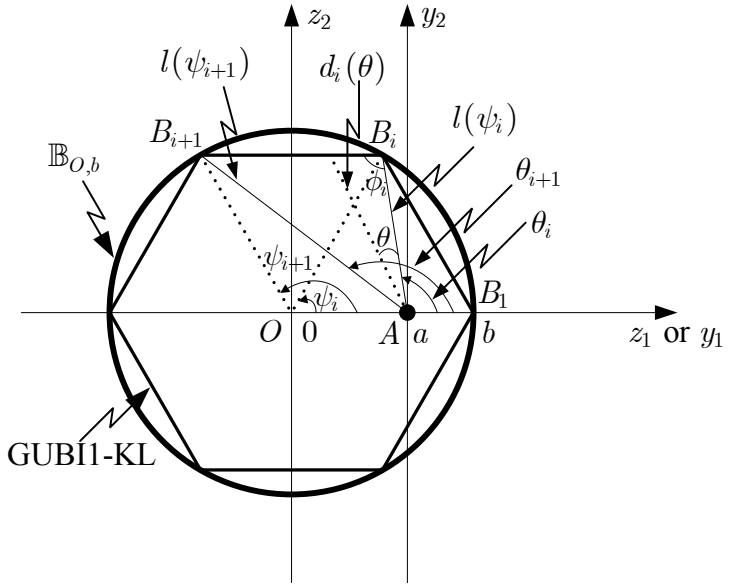

(a) GUBI1-KL for the case of $b > a$

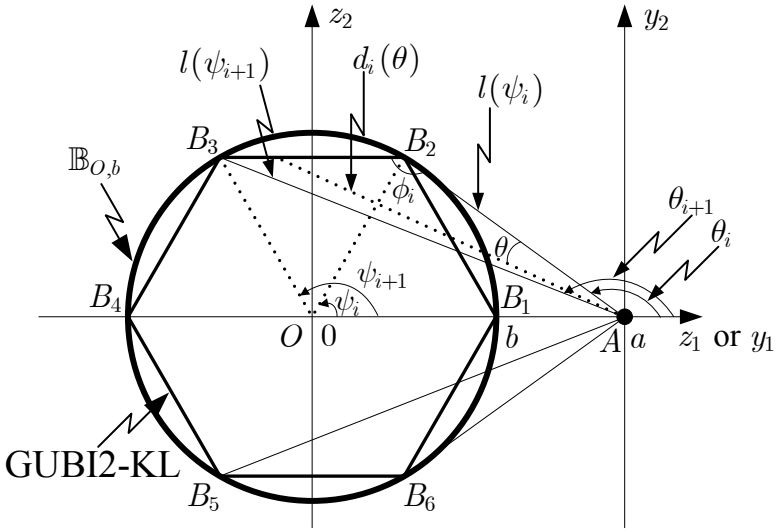

(b) GUBI2-KL for the case of $a > b$

Fig. 4.6: Diagram of the derivation of the new generic upper single-integral bounds GUBI1-KL and GUBI2-KL on $Q(a, b)$.

The angle from the positive y_1-axis to AB_i, denoted as θ_i, is given by

$$\begin{aligned}\theta_i &= \begin{cases} \arccos[(b\cos(\psi_i) - a)/l(\psi_i)], & \text{if } \psi_i \leq \pi \\ 2\pi - \arccos[(b\cos(\psi_i) - a)/l(\psi_i)], & \text{if } \psi_i > \pi \end{cases} \\ &= \text{sign}(\pi - \psi_i)(\arccos[(b\cos(\psi_i) - a)/l(\psi_i)] - \pi) + \pi, \end{aligned} \tag{4.46}$$

where sign$(\cdot)$ is the three-valued sign function, given by

$$\text{sign}(x) = \begin{cases} 1, & \text{if } x > 0, \\ 0, & \text{if } x = 0, \\ -1, & \text{if } x < 0. \end{cases} \tag{4.47}$$

The angle between the line segments AB_i and B_iB_{i+1}, denoted as ϕ_i, is given by

$$\phi_i = \arccos\left[\frac{l^2(\psi_i) - l^2(\psi_{i+1}) + 2b^2[1 - \cos(\psi_{i+1} - \psi_i)]}{4b\sin[(\psi_{i+1} - \psi_i)/2]l(\psi_i)}\right]. \tag{4.48}$$

We first consider the case of $b > a$, as shown in Fig. 4.6(a). The probability of z lying inside the triangular region $\triangle AB_iB_{i+1}$ is given by

$$\begin{aligned} \Pr\left(z \in \triangle AB_iB_{i+1}\right) &= \int_{\theta=0}^{\theta_{i+1}-\theta_i} \int_{r=0}^{d_i(\theta)} \frac{r}{2\pi} e^{-r^2/2} dr d\theta \\ &= \frac{\theta_{i+1} - \theta_i}{2\pi} - \frac{1}{2\pi} \int_{\theta=0}^{\theta_{i+1}-\theta_i} \exp\left[-\frac{d_i^2(\theta)}{2}\right] d\theta, \end{aligned} \tag{4.49}$$

where $d_i(\theta)$ is given by

$$\begin{aligned} d_i(\theta) &= \frac{l(\psi_i)\sin(\phi_i)}{\sin(\pi - \phi_i - \theta)} \\ &= \frac{l(\psi_i)\sin(\phi_i)}{\sin(\phi_i + \theta)}. \end{aligned} \tag{4.50}$$

Substituting (4.50) into (4.49) gives

$$\Pr(z \in \triangle AB_iB_{i+1}) = \frac{\theta_{i+1} - \theta_i}{2\pi} - \frac{1}{2\pi} \int_{\theta=0}^{\theta_{i+1}-\theta_i} \exp\left[-\frac{l^2(\psi_i)\sin^2(\phi_i)}{2\sin^2(\phi_i + \theta)}\right] d\theta. \tag{4.51}$$

The probability of z lying inside the entire polygon $\mathbb{P}_{U,N}$ is, therefore, given by

$$\Pr(z \in \mathbb{P}_{U,N}) = \sum_{i=1}^{N} \Pr(z \in \triangle AB_iB_{(i+1) \text{ modulo } N}). \tag{4.52}$$

This gives our first generic upper bound involving single integrals, abbreviated as

GUBI1-KL, namely

$$\begin{aligned} Q(a,b) &\leq Q_{GUBI1\text{-}KL}(a,b) \\ &= 1 - \Pr(z \in \mathbb{P}_{U,N}) \\ &= \frac{1}{2\pi} \sum_{i=1}^{N} \int_{\theta=0}^{\theta_{i+1}-\theta_i} \exp\left[-\frac{l^2(\psi_i)\sin^2(\phi_i)}{2\sin^2(\phi_i+\theta)}\right] d\theta, \qquad b > a \geq 0, \end{aligned} \tag{4.53}$$

where $\{\theta_i, i = 1, \ldots, N+1\}$ are defined by (4.46), and we have $0 = \theta_1 < \ldots < \theta_N < \theta_{N+1} = 2\pi$.

If the points $\{B_i\}_{i=1}^{N}$ are chosen to be symmetrical about the z_1-axis, and we have $\psi_{N/2+1} = \pi$, then (4.53) reduces to

$$Q_{GUBI1\text{-}KL}(a,b) = \frac{1}{\pi} \sum_{i=1}^{N/2} \int_{\theta=0}^{\theta_{i+1}-\theta_i} \exp\left[-\frac{l^2(\psi_i)\sin^2(\phi_i)}{2\sin^2(\phi_i+\theta)}\right] d\theta, \qquad b > a \geq 0. \tag{4.54}$$

This generic bound involves $N/2$ single integrals.

We also note that the region covered by one acute-angled (obtuse-angled) triangle can be seen as the addition (subtraction) of the regions covered by two right-angled triangles which have a common leg. For example, for the case of using an equilateral hexagon as the bounding shape, as shown in Fig. 4.7, we have

$$\begin{aligned} \triangle AB_1B_2 &= \triangle AE_1B_1 + \triangle AE_1B_2, \\ \triangle AB_2B_3 &= \triangle AE_2B_3 - \triangle AE_2B_2, \quad \text{for } a > b/2 \\ \triangle AB_2B_3 &= \triangle AE_2B_3 + \triangle AE_2B_2, \quad \text{for } a < b/2 \\ \triangle AB_3B_4 &= \triangle AE_3B_3 + \triangle AE_3B_4. \end{aligned}$$

Thus, the probability of z lying inside each acute-angled or obtuse-angled triangle is also equal to the sum of the probabilities of z lying inside the two right-angled triangles. This means that we can split each integral in (4.51) into two simpler

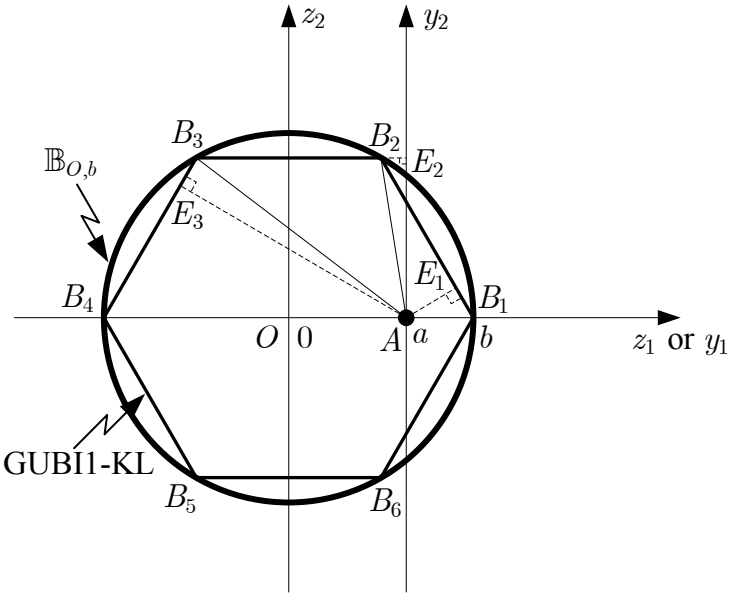

Fig. 4.7: Diagram of the split of the triangles in the derivation of the generic single-integral bounds on $Q(a, b)$.

integrals, namely, we have

$$\Pr(z \in \triangle AB_iB_{i+1}) = \frac{\theta_{i+1} - \theta_i}{2\pi} - \frac{1}{2\pi}\int_{\theta=0}^{\frac{\pi}{2}-\phi_i} \exp\left[-\frac{l^2(\psi_i)\sin^2(\phi_i)}{2\cos^2(\theta)}\right] d\theta$$
$$- \frac{1}{2\pi}\int_{\theta=0}^{\theta_{i+1}-\theta_i-(\frac{\pi}{2}-\phi_i)} \exp\left[-\frac{l^2(\psi_i)\sin^2(\phi_i)}{2\cos^2(\theta)}\right] d\theta. \quad (4.55)$$

Here, $l(\psi_i)\sin(\phi_i)$ is the length of the common leg, and $(\frac{\pi}{2} - \phi_i)$ is positive when ϕ_i is an acute angle, and is negative when ϕ_i is an obtuse angle. The alternative expression for the bound GUBI1-KL in (4.54) is, therefore, given by

$$\begin{aligned} Q(a,b) &\le Q_{GUBI1a\text{-}KL}(a,b) \\ &= \frac{1}{\pi}\sum_{i=1}^{N/2}\left\{\int_{\theta=0}^{\frac{\pi}{2}-\phi_i} \exp\left[-\frac{l^2(\psi_i)\sin^2(\phi_i)}{2\cos^2(\theta)}\right] d\theta \right. \\ &\quad \left. + \int_{\theta=0}^{\theta_{i+1}-\theta_i-(\frac{\pi}{2}-\phi_i)} \exp\left[-\frac{l^2(\psi_i)\sin^2(\phi_i)}{2\cos^2(\theta)}\right] d\theta\right\}, \\ &\qquad\qquad b > a \ge 0. \end{aligned} \quad (4.56)$$

This alternative expression involves N simpler single integrals.

We now turn to the case of $b < a$, as shown in Fig. 4.6(b). For this case, (4.50)

still holds, but (4.49) and (4.52) are not accurate anymore. This is because when we have $b < a$, θ_i's do not monotonically increase as i increases, i.e., $(\theta_{i+1} - \theta_i)$ may be negative. As the point B_i moves counterclockwise along the boundary of $\mathbb{B}_{O,b}$, ψ_i increases from 0 to 2π. The corresponding θ_i will first decrease from π to its minimum value of $\pi - \arcsin(b/a)$, and then increase to its maximum value of $\pi + \arcsin(b/a)$, and finally return to π. Here, the minimum and maximum values of θ_i correspond, respectively, to the upper and lower tangential points on which AB_i is tangential to the boundary of $\mathbb{B}_{O,b}$. Therefore, (4.49) should be modified to

$$\begin{aligned}\Pr(z \in \triangle AB_iB_{i+1}) &= \int_{\theta=0}^{|\theta_{i+1}-\theta_i|} \int_{r=0}^{d_i(\theta)} \frac{r}{2\pi} e^{-r^2/2} dr d\theta \\ &= \frac{|\theta_{i+1} - \theta_i|}{2\pi} - \frac{1}{2\pi} \int_{\theta=0}^{|\theta_{i+1}-\theta_i|} \exp\left[-\frac{d_i^2(\theta)}{2}\right] d\theta. \quad (4.57)\end{aligned}$$

The second point to note is that when we combine the probabilities of z lying inside all the triangular regions, we will not simply add these probabilities up, as we did in (4.52). Actually, we need to add $\Pr(z \in \triangle AB_iB_{i+1})$ when $(\theta_{i+1} - \theta_i)$ is positive, and subtract $\Pr(z \in \triangle AB_iB_{i+1})$ when $(\theta_{i+1} - \theta_i)$ is negative. After considering all these modifications, we obtain the second new generic upper bound, abbreviated as GUBI2-KL, namely

$$\begin{aligned}&Q(a,b) \\ &\leq Q_{GUBI2\text{-}KL}(a,b) \\ &= 1 - \Pr(z \in \mathbb{P}_{U,N}) \\ &= 1 + \frac{1}{2\pi} \sum_{i=1}^{N} \text{sign}[\theta_{(i+1) \text{ modulo } N} - \theta_i] \int_{\theta=0}^{|\theta_{(i+1) \text{ modulo } N} - \theta_i|} \exp\left[-\frac{l^2(\psi_i)\sin^2(\phi_i)}{2\sin^2(\phi_i + \theta)}\right] d\theta, \\ &\qquad\qquad a > b > 0. \quad (4.58)\end{aligned}$$

We find that in (4.58), the effect of the signs before the integrals can be reflected by setting the upper integral limit as $(\theta_{i+1} - \theta_i)$ and the angle variable in the integrand as $|\theta|$. Thus, we obtain an alternative expression for our new upper

bound GUBI2-KL in (4.58), namely

$$Q_{GUBI2\text{-}KL}(a,b) = 1 + \frac{1}{2\pi}\sum_{i=1}^{N}\int_{\theta=0}^{\theta_{(i+1) \text{ modulo } N}-\theta_i} \exp\left[-\frac{l^2(\psi_i)\sin^2(\phi_i)}{2\sin^2(\phi_i+|\theta|)}\right] d\theta, \quad a > b > 0. \tag{4.59}$$

Although this expression is more compact than that in (4.58), the existence of $|\theta|$ in the integrand makes it difficult to compute (4.59) numerically by using Mathematica. Thus, we will still use (4.58) as the expression of the bound GUBI2-KL in the subsequent discussion.

If we choose the points $\{B_i\}_{i=1}^{N}$ symmetrically about the z_1-axis, and set $\theta_{N/2+1} = \pi$, GUBI2-KL in (4.58) can be reduced to

$$\begin{aligned} Q(a,b) &\le Q_{GUBI2\text{-}KL}(a,b) \\ &= 1 + \frac{1}{\pi}\sum_{i=1}^{N/2}\text{sign}(\theta_{i+1}-\theta_i)\int_{\theta=0}^{|\theta_{i+1}-\theta_i|}\exp\left[-\frac{l^2(\psi_i)\sin^2(\phi_i)}{2\sin^2(\phi_i+\theta)}\right]d\theta, \ a > b > 0. \end{aligned} \tag{4.60}$$

Similar to the case of $b > a$, each integral in (4.60) can be split into two parts, and the alternative expression is given by

$$\begin{aligned} Q_{GUBI2a\text{-}KL}(a,b) = 1 + \frac{1}{\pi}\sum_{i=1}^{N/2}\text{sign}(\theta_{i+1}-\theta_i)\Bigg\{&\int_{\theta=0}^{\frac{\pi}{2}-\phi_i}\exp\left[-\frac{l^2(\psi_i)\sin^2(\phi_i)}{2\cos^2(\theta)}\right]d\theta \\ &+ \int_{\theta=0}^{|\theta_{i+1}-\theta_i|-(\frac{\pi}{2}-\phi_i)}\exp\left[-\frac{l^2(\psi_i)\sin^2(\phi_i)}{2\cos^2(\theta)}\right]d\theta\Bigg\}, \ a > b > 0. \end{aligned} \tag{4.61}$$

4.8.2 Lower Bounds

Generic lower single-integral bounds for $Q(a,b)$ can be obtained by computing the probability of z lying outside the polygon $\mathbb{P}_{L,N}$ whose boundary circumscribes $\mathbb{B}_{O,b}$, as shown in Fig. 4.8. Here, $\mathbb{P}_{L,N}$ is formed by two steps. We first choose N points (B_i, $i = 1, \cdots, N$) on the boundary of $\mathbb{B}_{O,b}$ such that N angles ψ_i's

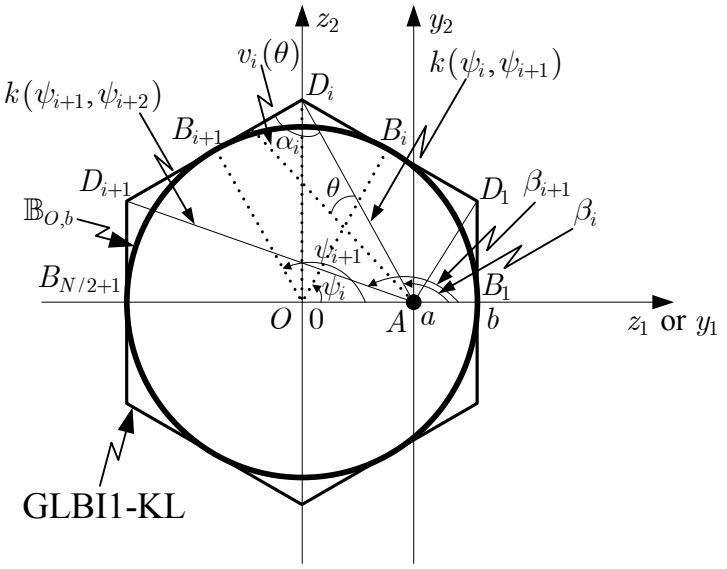

(a) GLBI1-KL for the case of $b > a$

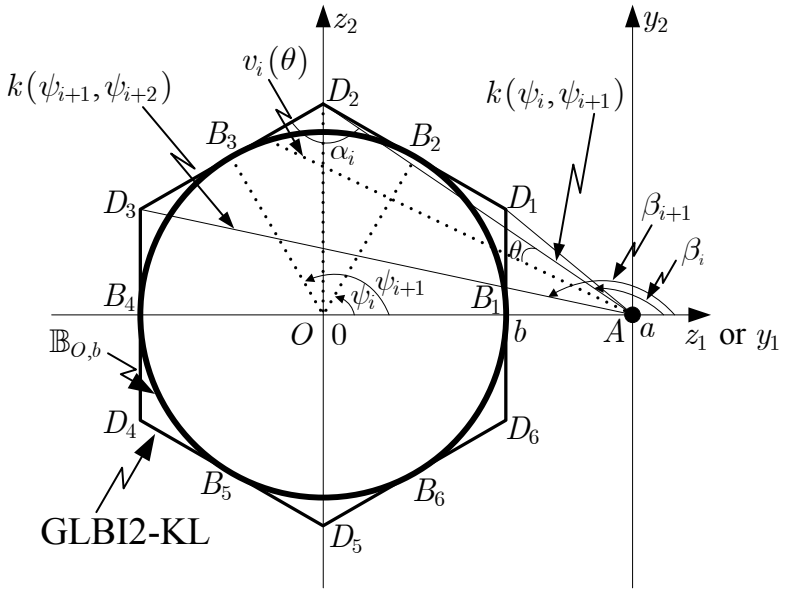

(b) GLBI2-KL for the case of $a > b$

Fig. 4.8: Diagram of the derivation of the new generic lower single-integral bounds GLBI1-KL and GLBI2-KL on $Q(a, b)$.

between the positive z_1-axis and OB_i are formed and given by $0 = \psi_1 < \ldots < \psi_N < \psi_{N+1} = 2\pi$. Then at each point B_i, we draw a line tangential to the boundary of $\mathbb{B}_{O,b}$. The point of intersection of the tangential lines at B_i and B_{i+1} is the vertex D_i of $\mathbb{P}_{L,N}$. We only discuss the case that the points $\{B_i\}_{i=1}^N$ are

chosen to be symmetrical about the z_1-axis. The length of the line segment OD_i, denoted as $q_{i,i+1}$, is given by

$$q_{i,i+1} = \frac{b}{\cos\left[(\psi_{i+1} - \psi_i)/2\right]}. \tag{4.62}$$

The length of the line segment AD_i, denoted as $k(\psi_i, \psi_{i+1})$, is thus given by

$$k(\psi_i, \psi_{i+1}) = \sqrt{a^2 + q_{i,i+1}^2 - 2aq_{i,i+1}\cos\left(\frac{\psi_i + \psi_{i+1}}{2}\right)}. \tag{4.63}$$

The angle from the positive y_1-axis to the line segment AD_i, denoted as β_i, is given by

$$\begin{aligned}\beta_i &= \begin{cases} \arccos\left[\frac{q_{i,i+1}\cos[(\psi_i+\psi_{i+1})/2]-a}{k(\psi_i,\psi_{i+1})}\right], & \text{if } \psi_i < \pi \\ 2\pi - \arccos\left[\frac{q_{i,i+1}\cos[(\psi_i+\psi_{i+1})/2]-a}{k(\psi_i,\psi_{i+1})}\right], & \text{if } \psi_i \geq \pi \end{cases} \\ &= \text{sign}\left[\text{sign}(\pi - \psi_i) - 0.5\right]\left\{\arccos\left[\frac{q_{i,i+1}\cos\left[(\psi_i + \psi_{i+1})/2\right] - a}{k(\psi_i, \psi_{i+1})}\right] - \pi\right\} + \pi. \end{aligned} \tag{4.64}$$

The angle between the line segments AD_i and D_iD_{i+1}, denoted as α_i, is given by

$$\begin{aligned}\alpha_i = \frac{\pi}{2} - \frac{\psi_{i+1} - \psi_i}{2} &+ \text{sign}\left[\text{sign}(\pi - \psi_i) - 0.5\right] \\ &\cdot \arccos\left[\frac{q_{i,i+1} - a\cos\left[(\psi_i + \psi_{i+1})/2\right]}{k(\psi_i, \psi_{i+1})}\right]. \end{aligned} \tag{4.65}$$

We first consider the case of $b > a$, as shown in Fig. 4.8(a). The probability of z lying inside the triangular region $\triangle AD_iD_{i+1}$ is given by

$$\Pr(z \in \triangle AD_iD_{i+1}) = \int_{\theta=0}^{\beta_{i+1}-\beta_i}\int_{r=0}^{v_i(\theta)} \frac{r}{2\pi}e^{-r^2/2}drd\theta. \tag{4.66}$$

Here, $v_i(\theta)$ is given by

$$v_i(\theta) = \frac{k(\psi_i, \psi_{i+1})\sin(\alpha_i)}{\sin(\alpha_i + \theta)}. \tag{4.67}$$

Substituting (4.67) into (4.66) gives

$$\Pr(z \in \triangle AD_iD_{i+1}) = \frac{\beta_{i+1}-\beta_i}{2\pi} - \frac{1}{2\pi}\int_{\theta=0}^{\beta_{i+1}-\beta_i} \exp\left[-\frac{k^2(\psi_i,\psi_{i+1})\sin^2(\alpha_i)}{2\sin^2(\alpha_i+\theta)}\right] d\theta. \tag{4.68}$$

The probability of z lying inside the entire polygon $\mathbb{P}_{L,N}$ is, therefore, given by

$$\Pr(z \in \mathbb{P}_{L,N}) = \sum_{i=1}^{N} \Pr(z \in \triangle AD_iD_{(i+1) \text{ modulo } N}). \tag{4.69}$$

Here, "modulo" denotes the modulo operation with $n \text{ modulo } n = n$. Thus, our first generic single-integral lower bound, denoted as GLBI1-KL, is given by

$$\begin{aligned} Q(a,b) &\geq Q_{GLBI1\text{-}KL}(a,b) \\ &= 1 - \Pr(z \in \mathbb{P}_{L,N}) \\ &= \frac{1}{2\pi}\sum_{i=1}^{N}\int_{\theta=0}^{\beta_{i+1}-\beta_i} \exp\left[-\frac{k^2(\psi_i,\psi_{i+1})\sin^2(\alpha_i)}{2\sin^2(\alpha_i+\theta)}\right] d\theta, \ b \geq a \geq 0, \end{aligned} \tag{4.70}$$

where $(\beta_i, i = 1, \ldots, N)$ are defined in (4.64), and we have $0 < \beta_1 < \ldots < \beta_N < 2\pi$ and $\beta_{N+1} = \beta_1 + 2\pi$. Since the points $\{B_i\}_{i=1}^N$ are chosen to be symmetrical about the z_1-axis here, the probability $\Pr(z \in \mathbb{P}_{L,N})$ is twice the probability of z lying inside the upper half of the polygon $\mathbb{P}_{L,N}$. Thus, if we set $\psi_{N/2+1} = \pi$, the bound GLBI1-KL can be reduced to

$$\begin{aligned} Q(a,b) &\geq Q_{GLBI1\text{-}KL}(a,b) \\ &= \frac{1}{\pi}\int_{\theta=0}^{\beta_1} \exp\left[-\frac{(b-a)^2}{2\cos^2(\theta)}\right] d\theta \\ &\quad + \frac{1}{\pi}\sum_{i=1}^{\frac{N}{2}-1}\int_{\theta=0}^{\beta_{i+1}-\beta_i} \exp\left[-\frac{k^2(\psi_i,\psi_{i+1})\sin^2(\alpha_i)}{2\sin^2(\alpha_i+\theta)}\right] d\theta \\ &\quad + \frac{1}{\pi}\int_{\theta=0}^{\pi-\beta_{N/2}} \exp\left[-\frac{(b+a)^2}{2\cos^2(\theta)}\right] d\theta, \quad b \geq a \geq 0. \end{aligned} \tag{4.71}$$

This bound involves $(N/2+1)$ single integrals, and its alternative expression is

given by

$$Q_{GLBI1a\text{-}KL}(a,b) = \frac{1}{\pi}\int_{\theta=0}^{\beta_1} \exp\left[-\frac{(b-a)^2}{2\cos^2\beta}\right] d\theta + \frac{1}{\pi}\sum_{i=1}^{N/2-1}\left\{\int_{\theta=0}^{\frac{\pi}{2}-\alpha_i} \exp\left[-\frac{k^2(\psi_i,\psi_{i+1})\sin^2(\alpha_i)}{2\cos^2(\theta)}\right] d\theta + \int_{\theta=0}^{\beta_{i+1}-\beta_i-(\frac{\pi}{2}-\alpha_i)} \exp\left[-\frac{k^2(\psi_i,\psi_{i+1})\sin^2(\alpha_i)}{2\cos^2(\theta)}\right] d\theta\right\} + \frac{1}{\pi}\int_{\theta=0}^{\pi-\beta_{N/2}} \exp\left[-\frac{(b+a)^2}{2\cos^2\beta}\right] d\theta, \qquad b \geq a \geq 0, \quad (4.72)$$

which involves N simpler single integrals.

Similar to the case of the upper bound, the lower bound for $a > b$, as shown in Fig. 4.8(b), can be obtained by making some small modifications in the derivation of GLBI1-KL in (4.70). We first compute the probabilities of z lying inside the triangles $\triangle AD_iD_{(i+1) \text{ modulo } N}, i = 1,\ldots,N$, taking into account the fact that $(\beta_{i+1}-\beta_i)$ may be negative, and then use the sign of the upper integral limit $(\beta_{i+1}-\beta_i)$ to determine the sign before the ith probability $\Pr(z \in \triangle AD_iD_{(i+1) \text{ modulo } N})$ in the sum of the total probability $\Pr(z \in \mathbb{P}_{L,N})$. In addition, for this case, the angle α_i computed by using (4.65) is not always positive. Since we need the absolute value of this angle, we replace α_i in the integrand with $|\alpha_i|$. After considering all these modifications, we have the second generic lower bound, GLBI2-KL, namely

$$\begin{aligned} Q(a,b) &\geq Q_{GLBI2\text{-}KL}(a,b) \\ &= 1 - \Pr(z \in \mathbb{P}_{L,N}) \\ &= 1 + \frac{1}{2\pi}\sum_{i=1}^{N} \text{sign}[\beta_{(i+1) \text{ modulo } N} - \beta_i] \\ &\quad \cdot \int_{\theta=0}^{|\beta_{(i+1) \text{ modulo } N}-\beta_i|} \exp\left[-\frac{k^2(\psi_i,\psi_{i+1})\sin^2(\alpha_i)}{2\sin^2(|\alpha_i|+\theta)}\right] d\theta, a \geq b > 0, \quad (4.73) \end{aligned}$$

where $\{\beta_i\}_{i=1}^N$ are defined in (4.64). Considering the symmetric positions of

$\{B_i\}_{i=1}^{N}$, and $\psi_{N/2+1} = \pi$, the bound GLBI2-KL in (4.73) can be reduced to

$$\begin{aligned} Q(a,b) &\geq Q_{GLBI2\text{-}KL}(a,b) \\ &= 1 + \frac{1}{\pi}\int_{\theta=0}^{\beta_1-\pi} \exp\left[-\frac{(a-b)^2}{2\cos^2(\theta)}\right] d\theta + \frac{1}{\pi}\sum_{i=1}^{\frac{N}{2}-1} \operatorname{sign}(\beta_{i+1}-\beta_i) \\ &\quad \cdot \int_{\theta=0}^{|\beta_{i+1}-\beta_i|} \exp\left[-\frac{k^2(\psi_i,\psi_{i+1})\sin^2(\alpha_i)}{2\sin^2(|\alpha_i|+\theta)}\right] d\theta \\ &\quad + \frac{1}{\pi}\int_{\theta=0}^{\pi-\beta_{N/2}} \exp\left[-\frac{(b+a)^2}{2\cos^2(\theta)}\right] d\theta, \qquad a \geq b > 0. \end{aligned} \tag{4.74}$$

An alternative expression for (4.74) is given by

$$\begin{aligned} Q_{GLBI2a\text{-}KL}(a,b) &= 1 + \frac{1}{\pi}\int_{\theta=0}^{\beta_1-\pi} \exp\left[-\frac{(a-b)^2}{2\cos^2\beta}\right] d\theta + \frac{1}{\pi}\sum_{i=1}^{\frac{N}{2}-1} \operatorname{sign}(\beta_{i+1}-\beta_i) \\ &\quad \cdot \left\{ \int_{\theta=0}^{\frac{\pi}{2}-\alpha_i} \exp\left[-\frac{k^2(\psi_i,\psi_{i+1})\sin^2(\alpha_i)}{2\cos^2(\theta)}\right] d\theta \right. \\ &\quad \left. + \int_{\theta=0}^{|\beta_{i+1}-\beta_i|-(\frac{\pi}{2}-\alpha_i)} \exp\left[-\frac{k^2(\psi_i,\psi_{i+1})\sin^2(\alpha_i)}{2\cos^2(\theta)}\right] d\theta \right\} \\ &\quad + \frac{1}{\pi}\int_{\theta=0}^{\pi-\beta_{N/2}} \exp\left[-\frac{(b+a)^2}{2\cos^2\beta}\right] d\theta, \qquad a \geq b > 0. \end{aligned} \tag{4.75}$$

From the geometric approach, it is clear that the generic upper and lower single-integral bounds derived in this section approach the exact value of $Q(a,b)$ as N, the number of sides of the bounding polygons, increases, since the area covered by the bounding polygons grows closer to $\mathbb{B}_{O,b}$. Although these bounds involve single integrals, one advantage of these bounds is that the integrals involved have a form similar to that in the error probability expression of the general two-dimensional signal constellations [60]. Thus, we can apply all the techniques exploited for the computations of this error probability to our bounds. For instance, when the ratio a/b is independent of the instantaneous SNR, like in the expression for the conditional error probability of a variety of single-channel, partially coherent, differentially coherent, and quadratic detections [114, eq. (14)], the integral limits and angles in our single-integral bounds are all fixed values,

independent of the instantaneous SNR. Then the closed form results for averaging these bounds over Rayleigh and Nakagami-m fading channels can be obtained easily by using the results in [5, Sections 5.4.2 and 5A.1 5].

4.9 New Simple Single-Integral Bounds

We now derive some simple single-integral bounds which involve only a few single integrals. These bounds are special cases of the generic single-integral bounds derived in Section 4.8, and are obtained by using an equilateral hexagon to bound $\mathbb{B}_{O,b}$, as shown in Figs. 4.6 and 4.8. Thus, the ψ_i's in GUBI1-KL in (4.54), GUBI2-KL in (4.60), GLBI1-KL in (4.71), and GLBI2-KL in (4.74) are given by $\psi_i = (i-1)\pi/3$, $i = 1, \cdots, 6$.

4.9.1 Upper Bounds

We first show the upper bound on $Q(a,b)$ for the case of $b > a$. This upper bound is obtained by computing the probability of z lying outside the equilateral hexagon $\mathbb{P}_{U,6}$ which is inscribed within $\mathbb{B}_{O,b}$, as shown in Fig. 4.6(a). Since $\mathbb{P}_{U,6}$ is symmetrical about the z_1-axis, and the PDF of y in (4.9) is isotropic, the probability $\Pr(z \in \mathbb{P}_{U,6})$ is twice the probability of z lying inside the upper half of the hexagon $\mathbb{P}_{U,6}$, i.e., we have

$$\Pr(z \in \mathbb{P}_{U,6}) = 2\left[\Pr(z \in \triangle AB_1B_2) + \Pr(z \in \triangle AB_2B_3) + \Pr(z \in \triangle AB_3B_4)\right]. \tag{4.76}$$

Now, we compute the probabilities of z lying inside the three triangles in (4.76) one by one according to (4.45), (4.46), (4.48), and (4.51). In the triangle $\triangle AB_1B_2$, the sides and angles are given by

$$l(\psi_1) = b - a,$$
$$l(\psi_2) = \sqrt{b^2 + a^2 - ab},$$

$$\begin{aligned}\theta_1 &= 0,\\ \theta_2 &= \arccos\left[\frac{b-2a}{2\sqrt{b^2+a^2-ab}}\right],\\ \phi_1 &= \frac{\pi}{3}.\end{aligned}$$

Thus, the probability of z lying inside the triangle $\triangle AB_1B_2$ is given by

$$\begin{aligned}&\Pr(z\in\triangle AB_1B_2)\\ &=\frac{1}{2\pi}\arccos\left[\frac{b-2a}{2\sqrt{b^2+a^2-ab}}\right]-\frac{1}{2\pi}\int_{\theta=0}^{\arccos\left[\frac{b-2a}{2\sqrt{b^2+a^2-ab}}\right]}\exp\left[-\frac{3(b-a)^2}{8\sin^2(\pi/3+\theta)}\right]d\theta.\end{aligned}\tag{4.77}$$

Similarly, in the triangle $\triangle AB_2B_3$, the sides and angles are given by

$$\begin{aligned}l(\psi_3) &= \sqrt{b^2+a^2+ab},\\ \theta_3-\theta_2 &= \arccos\left[\frac{b^2+2a^2}{2\sqrt{b^4+a^4+a^2b^2}}\right],\\ \phi_2 &= \arccos\left[\frac{b-2a}{2\sqrt{b^2+a^2-ab}}\right],\end{aligned}$$

and thus, the probability $\Pr(z\in\triangle AB_2B_3)$ is given by

$$\begin{aligned}&\Pr(z\in\triangle AB_2B_3)\\ &=\frac{1}{2\pi}\arccos\left[\frac{b^2+2a^2}{2\sqrt{b^4+a^4+a^2b^2}}\right]-\frac{1}{2\pi}\\ &\cdot\int_{\theta=0}^{\arccos\left[\frac{b^2+2a^2}{2\sqrt{b^4+a^4+a^2b^2}}\right]}\exp\left[-\frac{3b^2}{8\sin^2(\arccos[(b-2a)/(2\sqrt{b^2+a^2-ab})]+\theta)}\right]d\theta.\end{aligned}\tag{4.78}$$

Finally, in the triangle $\triangle AB_3B_4$, the sides and angles are given by

$$\begin{aligned}l(\psi_4) &= b+a,\\ \theta_4-\theta_3 &= \arccos\left[\frac{b+2a}{2\sqrt{b^2+a^2+ab}}\right],\\ \theta_4 &= \pi,\end{aligned}$$

$$\phi_3 = \arccos\left[\frac{b-a}{2\sqrt{b^2+a^2+ab}}\right],$$

and the probability $\Pr(z \in \triangle AB_3B_4)$ is given by

$$\begin{aligned}
&\Pr(z \in \triangle AB_3B_4) \\
&= \frac{1}{2\pi}\arccos\left[\frac{b+2a}{2\sqrt{b^2+a^2+ab}}\right] \\
&\quad - \frac{1}{2\pi}\int_{\theta=0}^{\arccos\left[\frac{b+2a}{2\sqrt{b^2+a^2+ab}}\right]} \exp\left[-\frac{3(b+a)^2}{8\sin^2(\arccos[(b-a)/(2\sqrt{b^2+a^2+ab})]+\theta)}\right] d\theta.
\end{aligned} \tag{4.79}$$

Substituting (4.77), (4.78), and (4.79) into (4.76), and also noting that we have the sum of the angles

$$(\theta_2-\theta_1)+(\theta_3-\theta_2)+(\theta_4-\theta_3) = \theta_4-\theta_1 = \pi,$$

we obtain our first simple upper bound involving single integrals, abbreviated as UBI1-KL, namely

$$\begin{aligned}
&Q(a,b) \\
&< Q_{UBI1\text{-}KL}(a,b) \\
&= 1-\Pr(z \in \mathbb{P}_{U,6}) \\
&= \frac{1}{\pi}\Bigg\{ \int_{\theta=0}^{\arccos\left[\frac{b-2a}{2\sqrt{b^2+a^2-ab}}\right]} \exp\left[-\frac{3(b-a)^2}{8\sin^2(\pi/3+\theta)}\right] d\theta \\
&\quad + \int_{\theta=0}^{\arccos\left[\frac{b^2+2a^2}{2\sqrt{b^4+a^4+a^2b^2}}\right]} \exp\left[-\frac{3b^2}{8\sin^2(\arccos[(b-2a)/(2\sqrt{b^2+a^2-ab})]+\theta)}\right] d\theta \\
&\quad + \int_{\theta=0}^{\arccos\left[\frac{b+2a}{2\sqrt{b^2+a^2+ab}}\right]} \exp\left[-\frac{3(b+a)^2}{8\sin^2(\arccos[(b-a)/(2\sqrt{b^2+a^2+ab})]+\theta)}\right] d\theta \Bigg\}, \\
&\qquad\qquad b > a > 0.
\end{aligned} \tag{4.80}$$

This upper bound involves three finite single integrals. As mentioned in Section 4.8.1 and shown in Fig. 4.7, the probability of z lying inside each acute-

angled or obtuse-angled triangle is also equal to the sum of the probabilities of z lying inside the two right-angled triangles. For example, by using the equality $\angle E_1AB_1 + \angle E_1AB_2 = \angle B_1AB_2$, i.e.,

$$\frac{\pi}{6} + \arctan\left[\frac{b+a}{\sqrt{3}(b-a)}\right] = \arccos\left[\frac{b-2a}{2\sqrt{b^2+a^2-ab}}\right], \tag{4.81}$$

the probability $\Pr(z \in \triangle AB_1B_2)$ in (4.77) can be given alternatively by

$$\begin{aligned}
&\Pr(z \in \triangle AB_1B_2) \\
&= \int_{\theta=0}^{\frac{\pi}{6}} \int_{r=0}^{\frac{\sqrt{3}(b-a)}{2\cos(\theta)}} \frac{r}{2\pi} e^{-r^2/2} dr + \int_{\theta=0}^{\arctan\left[\frac{b+a}{\sqrt{3}(b-a)}\right]} \int_{r=0}^{\frac{\sqrt{3}(b-a)}{2\cos(\theta)}} \frac{r}{2\pi} e^{-r^2/2} dr d\theta \\
&= \frac{1}{2\pi} \arccos\left[\frac{b-2a}{2\sqrt{b^2+a^2-ab}}\right] - \frac{1}{2\pi} \int_{\theta=0}^{\frac{\pi}{6}} \exp\left[-\frac{3(b-a)^2}{8\cos^2(\theta)}\right] d\theta \\
&\quad - \frac{1}{2\pi} \int_{\theta=0}^{\arctan\left[\frac{b+a}{\sqrt{3}(b-a)}\right]} \exp\left[-\frac{3(b-a)^2}{8\cos^2(\theta)}\right] d\theta.
\end{aligned} \tag{4.82}$$

As a result, each integral in (4.80) can be split into two simpler integrals, and this gives the alternative form

$$\begin{aligned}
&Q(a,b) \\
&< Q_{UBI1a\text{-}KL}(a,b) \\
&= 1 - 2[\Pr(z \in \triangle AB_1E_1) + \Pr(z \in \triangle AE_1B_2) + \Pr(z \in \triangle AE_2B_3) \\
&\quad - \Pr(z \in \triangle AE_2B_2) + \Pr(z \in \triangle AB_3E_3) + \Pr(z \in \triangle AE_3B_4)] \\
&= \frac{1}{\pi} \int_{\theta=0}^{\frac{\pi}{6}} \left\{ \exp\left[-\frac{3(b-a)^2}{8\cos^2(\theta)}\right] + \exp\left[-\frac{3(b+a)^2}{8\cos^2(\theta)}\right] \right\} d\theta \\
&\quad + \frac{1}{\pi} \int_{\theta=0}^{\arctan\left[\frac{b+a}{\sqrt{3}(b-a)}\right]} \exp\left[-\frac{3(b-a)^2}{8\cos^2(\theta)}\right] d\theta + \frac{1}{\pi} \int_{\theta=0}^{\arctan\left[\frac{b+2a}{\sqrt{3}b}\right]} \exp\left[-\frac{3b^2}{8\cos^2(\theta)}\right] d\theta \\
&\quad + \frac{1}{\pi} \int_{\theta=0}^{\arctan\left[\frac{b-2a}{\sqrt{3}b}\right]} \exp\left[-\frac{3b^2}{8\cos^2(\theta)}\right] d\theta + \frac{1}{\pi} \int_{\theta=0}^{\arctan\left[\frac{b-a}{\sqrt{3}(b+a)}\right]} \exp\left[-\frac{3(b+a)^2}{8\cos^2(\theta)}\right] d\theta, \\
&\qquad\qquad\qquad\qquad\qquad\qquad\qquad\qquad\qquad\qquad\qquad\qquad\qquad\qquad b > a > 0.
\end{aligned} \tag{4.83}$$

In the first equality in (4.83), the probability $\Pr(z \in \triangle AE_2B_2)$ is deducted from the total probability, because we consider here the case of $a > b/2$. However,

the final result in (4.83) holds for either $a > b/2$ or $a < b/2$. This is because the sign before the probability $\Pr(z \in \triangle AE_2B_2)$ can be reflected by the sign of the upper integral limit $\arctan\left[(b-2a)/(\sqrt{3}b)\right]$. If we have $a > b/2$, then $\arctan\left[(b-2a)/(\sqrt{3}b)\right]$ will be negative, and thus the integral

$$\int_{\theta=0}^{\arctan\left[\frac{b-2a}{\sqrt{3}b}\right]} \exp\left[-\frac{3b^2}{8\cos^2(\theta)}\right] d\theta = -\int_{\theta=0}^{\arctan\left[\frac{2a-b}{\sqrt{3}b}\right]} \exp\left[-\frac{3b^2}{8\cos^2(\theta)}\right] d\theta \tag{4.84}$$

will be negative; while if we have $a < b/2$, then the integral limit $\arctan\left[(b-2a)/(\sqrt{3}b)\right]$ will be positive, and thus the integral in (4.84) will be positive.

We now turn to the case of $b < a$, as shown in Fig. 4.6(b). According to (4.57), the probability of z lying inside the triangle $\triangle AB_1B_2$ is given by

$$\begin{aligned}\Pr(z \in \triangle AB_1B_2) = &\frac{1}{2\pi}\arccos\left[\frac{2a-b}{2\sqrt{b^2+a^2-ab}}\right] \\ &- \frac{1}{2\pi}\int_{\theta=0}^{\arccos\left[\frac{2a-b}{2\sqrt{b^2+a^2-ab}}\right]} \exp\left[-\frac{3(a-b)^2}{8\sin^2(2\pi/3+\theta)}\right] d\theta, \end{aligned} \tag{4.85}$$

while the probabilities of z lying inside the triangles $\triangle AB_2B_3$ and $\triangle AB_3B_4$ are still given by (4.78) and (4.79), respectively. The probability $\Pr(z \in \mathbb{P}_{U,6})$ is not given by (4.76) anymore for this case, and it becomes

$$\Pr(z \in \mathbb{P}_{U,6}) = 2\left[-\Pr(z \in \triangle AB_1B_2) + \Pr(z \in \triangle AB_2B_3) + \Pr(z \in \triangle AB_3B_4)\right]. \tag{4.86}$$

Since we have

$$\theta_1 = \theta_4 = \pi,$$

$$(\theta_2 - \theta_1) + (\theta_3 - \theta_2) + (\theta_4 - \theta_3) = \theta_4 - \theta_1 = 0,$$

our second simple upper bound involving single integrals, abbreviated as UBI2-KL, is given by

$$\begin{aligned}
&Q(a,b)\\
&< Q_{UBI2\text{-}KL}(a,b)\\
&= 1-\Pr(z\in\mathbb{P}_{U,6})\\
&= 1-\frac{1}{\pi}\int_{\theta=0}^{\arccos\left[\frac{2a-b}{2\sqrt{b^2+a^2-ab}}\right]}\exp\left[-\frac{3(b-a)^2}{8\sin^2(2\pi/3+\theta)}\right]d\theta\\
&\quad+\frac{1}{\pi}\int_{\theta=0}^{\arccos\left[\frac{b^2+2a^2}{2\sqrt{b^4+a^4+a^2b^2}}\right]}\exp\left[-\frac{3b^2}{8\sin^2(\arccos[(b-2a)/(2\sqrt{b^2+a^2-ab})]+\theta)}\right]d\theta\\
&\quad+\frac{1}{\pi}\int_{\theta=0}^{\arccos\left[\frac{b+2a}{2\sqrt{b^2+a^2+ab}}\right]}\exp\left[-\frac{3(b+a)^2}{8\sin^2(\arccos[(b-a)/(2\sqrt{b^2+a^2+ab})]+\theta)}\right]d\theta,\\
&\qquad\qquad a>b>0. \qquad (4.87)
\end{aligned}$$

This upper bound also involves three finite single-integrals. Similar to the case of $b>a$, each integral in (4.87) can be split into two parts, and the alternative expression is given by

$$\begin{aligned}
&Q(a,b)\\
&< Q_{UBI2a\text{-}KL}(a,b)\\
&= 1+\frac{1}{\pi}\int_{\theta=0}^{\frac{\pi}{6}}\left\{\exp\left[-\frac{3(b-a)^2}{8\cos^2(\theta)}\right]+\exp\left[-\frac{3(b+a)^2}{8\cos^2(\theta)}\right]\right\}d\theta\\
&\quad+\frac{1}{\pi}\int_{\theta=0}^{\arctan\left[\frac{b+a}{\sqrt{3}(b-a)}\right]}\exp\left[-\frac{3(b-a)^2}{8\cos^2(\theta)}\right]d\theta+\frac{1}{\pi}\int_{\theta=0}^{\arctan\left[\frac{b+2a}{\sqrt{3}b}\right]}\exp\left[-\frac{3b^2}{8\cos^2(\theta)}\right]d\theta\\
&\quad+\frac{1}{\pi}\int_{\theta=0}^{\arctan\left[\frac{b-2a}{\sqrt{3}b}\right]}\exp\left[-\frac{3b^2}{8\cos^2(\theta)}\right]d\theta+\frac{1}{\pi}\int_{\theta=0}^{\arctan\left[\frac{b-a}{\sqrt{3}(b+a)}\right]}\exp\left[-\frac{3(b+a)^2}{8\cos^2(\theta)}\right]d\theta,\\
&\qquad\qquad a>b>0. \qquad (4.88)
\end{aligned}$$

Comparing (4.88) with (4.83), we can see that the only difference between the expression for UBI2a-KL and the expression for UBI1a-KL is the constant term 1.

4.9.2 Lower Bounds

Now, we derive simple lower bounds for $Q(a,b)$ by computing the probability of z lying outside the equilateral hexagon $\mathbb{P}_{L,6}$ whose boundary circumscribes that of $\mathbb{B}_{O,b}$, as shown in Fig. 4.8.

We first consider the case of $b > a$. As shown in Fig. 4.8(a), the probability $\Pr(z \in \mathbb{P}_{L,6})$ is given by

$$\begin{aligned}\Pr(z \in \mathbb{P}_{L,6}) = 2[&\Pr(z \in \triangle AB_1D_1) + \Pr(z \in \triangle AD_1D_2) + \Pr(z \in \triangle AD_2D_3) \\ &+ \Pr(z \in \triangle AD_3B_4)],\end{aligned} \tag{4.89}$$

where $\triangle AB_1D_1$ and $\triangle AD_3B_4$ are right-angled triangles. According to (4.62), (4.63), (4.64), (4.65), (4.68), (4.69), and (4.71), we obtain our first simple single-integral lower bound, abbreviated as LBI1-KL, namely

$$\begin{aligned}
&Q(a,b) \\
&> Q_{LBI1\text{-}KL}(a,b) \\
&= 1 - \Pr(z \in \mathbb{P}_{L,6}) \\
&= \frac{1}{\pi}\Bigg\{ \int_{\theta=0}^{\arctan\left[\frac{b}{\sqrt{3}(b-a)}\right]} \exp\left[-\frac{(b-a)^2}{2\cos^2(\theta)}\right] d\theta \\
&\quad + \int_{\theta=0}^{\arccos\left[\frac{a^2-ab+2b^2/3}{\sqrt{(a^2+4b^2/3-2ab)(a^2+4b^2/3)}}\right]} \exp\left[-\frac{(b-a/2)^2}{2\sin^2\left(\arccos\left(\frac{2b-3a}{2\sqrt{3a^2+4b^2-6ab}}\right)+\theta\right)}\right] d\theta \\
&\quad + \int_{\theta=0}^{\arccos\left[\frac{a^2+ab+2b^2/3}{\sqrt{(a^2+4b^2/3+2ab)(a^2+4b^2/3)}}\right]} \exp\left[-\frac{(b+a/2)^2}{2\sin^2\left(\arccos\left(\frac{2b-3a}{2\sqrt{3a^2+4b^2}}\right)+\theta\right)}\right] d\theta \\
&\quad + \int_{\theta=0}^{\arctan\left[\frac{b}{\sqrt{3}(b+a)}\right]} \exp\left[-\frac{(b+a)^2}{2\cos^2(\theta)}\right] d\theta \Bigg\}, \qquad b > a > 0.
\end{aligned} \tag{4.90}$$

This lower bound involves four finite single-integrals.

Similarly, for the case of $b < a$, as shown in Fig. 4.8(b), the probability

$\Pr(z \in \mathbb{P}_{L,6})$ is given by

$$\begin{aligned}\Pr(z \in \mathbb{P}_{L,6}) = 2[&-\Pr(z \in \triangle AB_1D_1) + \Pr(z \in \triangle AD_1D_2) + \Pr(z \in \triangle AD_2D_3) \\ &+ \Pr(z \in \triangle AD_3B_4)].\end{aligned} \tag{4.91}$$

According to (4.62), (4.63), (4.64), (4.65), (4.68), (4.69), and (4.74), our second simple single-integral lower bound, denoted as LBI2-KL, is thus given by

$$\begin{aligned}
&Q(a,b) \\
&> Q_{LBI2\text{-}KL}(a,b) \\
&= 1 - \Pr(z \in \mathbb{P}_{L,6}) \\
&= 1 + \frac{1}{\pi}\Bigg\{ \int_{\theta=0}^{\arctan\left[\frac{b}{\sqrt{3}(b-a)}\right]} \exp\left[-\frac{(b-a)^2}{2\cos^2(\theta)}\right] d\theta \\
&\quad + \int_{\theta=0}^{\arccos\left[\frac{a^2-ab+2b^2/3}{\sqrt{(a^2+4b^2/3-2ab)(a^2+4b^2/3)}}\right]} \exp\left[-\frac{(b-a/2)^2}{2\sin^2\left(\arccos\left(\frac{2b-3a}{2\sqrt{3a^2+4b^2-6ab}}\right)+\theta\right)}\right] d\theta \\
&\quad + \int_{\theta=0}^{\arccos\left[\frac{a^2+ab+2b^2/3}{\sqrt{(a^2+4b^2/3+2ab)(a^2+4b^2/3)}}\right]} \exp\left[-\frac{(b+a/2)^2}{2\sin^2\left(\arccos\left(\frac{2b-3a}{2\sqrt{3a^2+4b^2}}\right)+\theta\right)}\right] d\theta \\
&\quad + \int_{\theta=0}^{\arctan\left[\frac{b}{\sqrt{3}(b+a)}\right]} \exp\left[-\frac{(b+a)^2}{2\cos^2(\theta)}\right] d\theta \Bigg\}, \qquad a > b > 0.
\end{aligned} \tag{4.92}$$

This expression also only differs from the expression for LBI1-KL in (4.90) in the constant term 1.

4.10 Comparison and Numerical Results

In this section, we study the tightness of our new upper and lower bounds on $Q(a,b)$ derived in Sections 4.4, 4.5, 4.6, 4.7, 4.8, and 4.9, and compare their tightness with the existing bounds in the literature. We first discuss the closed-form bounds in 4.4, 4.5, 4.6, 4.7. Then we show the performance of the single-integral bounds in 4.8 and 4.9.

4.10.1 Performance of the Closed-Form Bounds

In the literature, there are two types of bounds available, i.e., exponential bounds which involve only the exponential function, and I_0-bounds which involve the I_0 function, i.e., involve the use of $I_0(\cdot)$, $I_0(\cdot)\text{erfc}(\cdot)$, $\sqrt{I_0(\cdot)}$, or even more complicated functions of $I_0(\cdot)$. In general, I_0-bounds are not convenient to use in theoretical analyses, and thus are not as useful as our exponential bounds and erfc bounds in this sense. In the following discussions, we focus on the comparison between our exponential/erfc bounds and the existing exponential bounds. We will also compare our bounds with the existing I_0-bounds, but only for a reference purpose.

4.10.1.1 Upper Bounds for the Case of $b \geq a \geq 0$

For this case, we have derived one generic exponential bound, i.e, GUB1-KL in (4.28), which converges to the exact value of $Q(a,b)$ as N, the number of exponential terms involved, increases. We have also shown one of its special cases, i.e., UB1-KL in (4.36), by defining $N = 2$ and $\theta_1 = \pi/2$. The existing exponential bound UB1-SA given in [23, eq. (44)] and [120, eq. (3)], i.e.,

$$Q(a,b) \leq Q_{UB1\text{-}SA}(a,b) = \exp\left[-\frac{(b-a)^2}{2}\right], \ b \geq a \geq 0, \tag{4.93}$$

is also a special case of GUB1-KL with $N = 1$. That means UB1-SA can be obtained by using the disk $\mathbb{B}_{A,b-a}$ of radius $(b-a)$ centered at A as the bounding shape. Thus, all the bounds obtained by setting N to a value larger than one in GUB1-KL, such as UB1-KL in (4.36), are tighter than UB1-SA in (4.93). Besides the exponential bounds, we have also derived one generic erfc bound, i.e, GUB3-KL in (4.40), and one simple erfc bound, i.e, UB3-KL in (4.43). According to our numerical results, the generic erfc bound GUB3-KL is looser than the generic exponential bound GUB1-KL when evaluated with a similar number of terms, although the former is more complicated than the latter. Thus, we skip the

numerical results for GUB3-KL here.

The other existing exponential bounds in the literature include UB1-S in [114, eq. (12)], given by

$$Q(a,b) \leq Q_{UB1\text{-}S}(a,b) = \frac{b}{b-a}\exp\left[-\frac{(b-a)^2}{2}\right], \ b > a \geq 0, \tag{4.94}$$

and UB1-AT in [121, eq. (17)], given by

$$\begin{aligned} Q(a,b) &\leq Q_{UB1\text{-}AT}(a,b) \\ &= \frac{1}{2}\sqrt{\frac{1}{2}\left[1+\frac{1}{1-(a/b)^2}\right]}\left\{\exp\left[-\frac{(b-a)^2}{2}\right]+\exp\left[-\frac{(b+a)^2}{2}\right]\right\}, \\ & \qquad\qquad b > a \geq 0. \end{aligned} \tag{4.95}$$

It has been shown in [120] that UB1-SA in (4.93) is always tighter than UB1-S in (4.94). Thus, our bound UB1-KL in (4.36) is also tighter than UB1-S.

The I_0-bounds available in the literature include the bound UB1-C in [116, eq. (5)], given by

$$\begin{aligned} Q(a,b) &\leq Q_{UB1\text{-}C}(a,b) \\ &= \exp\left(-\frac{a^2+b^2}{2}\right) I_0(ab) + a\sqrt{\frac{\pi}{8}}\text{erfc}\left(\frac{b-a}{\sqrt{2}}\right), \quad b \geq a \geq 0, \end{aligned} \tag{4.96}$$

the bound UB2-AT in [121, eq. (12)], given by

$$\begin{aligned} Q(a,b) &\leq Q_{UB2\text{-}AT}(a,b) \\ &= \sqrt{\frac{1}{2}\left[1+\frac{1}{1-(a/b)^2}\right]}\exp\left(-\frac{b^2+a^2}{2}\right)\sqrt{I_0\left(2ab\right)}, \ b > a \geq 0, \end{aligned} \tag{4.97}$$

and the bound UB1-CF in [122, eq. (7)], given by

$$\begin{aligned} Q(a,b) &\leq Q_{UB1\text{-}CF}(a,b) \\ &= \frac{I_0(ab)}{e^{ab}}\left\{\exp\left[-\frac{(b-a)^2}{2}\right]+a\sqrt{\frac{\pi}{2}}\text{erfc}\left(\frac{b-a}{\sqrt{2}}\right)\right\}, b \geq a \geq 0. \end{aligned} \tag{4.98}$$

The bound UB1-CF can be reexpressed as

$$\begin{aligned} Q(a,b) &\le Q_{UB1\text{-}CF}(a,b) \\ &= \exp\left(-\frac{a^2+b^2}{2}\right) I_0(ab) + a\sqrt{\frac{\pi}{8}}\mathrm{erfc}\left(\frac{b-a}{\sqrt{2}}\right)\frac{2I_0(ab)}{\exp(ab)},\ b \ge a \ge 0. \end{aligned} \tag{4.99}$$

Thus, if we have $2I_0(ab)/\exp(ab) < 1$, i.e., $ab > 0.877$, UB1-CF is tighter than UB1-C. Among these I_0-bounds, UB1-C is simpler, but it is not tight in most cases, especially when the value of ab is large. The other two I_0-bounds, UB2-AT and UB1-CF, are more complicated than our exponential bounds, and even are harder to handle than our simple erfc bounds when analytical manipulations are concerned, since they involve $\sqrt{I_0(\cdot)}$ or the product $I_0(\cdot)\mathrm{erfc}(\cdot)$.

Figs. 4.9, 4.10, and 4.11 shows, respectively, the results for the cases of $b > a = 0.5, 1, 5$. The exact value and our new bounds are shown by the solid lines. The existing exponential bounds and I_0-bounds in the literature are shown by the dashed lines and dotted lines, respectively. Some markers are used when two lines are too close to tell them apart. For simplicity, we just choose equispaced points for θ_i, i.e., $\theta_i = i\pi/N$, in GUB1-KL. We use a subscript, say, $N = n$, on a generic bound to denote the value of the bound evaluated with $N = n$ and equispaced $\{\theta_i\}_{i=0}^N$. In Figs. 4.9 and 4.10, we ignore the results for the I_0-bounds to make other results presented clearly. We can see that our simple exponential bound UB1-KL is tighter than the existing bounds UB1-S and UB1-SA in all the cases shown, as expected. It is also tighter than UB1-AT when a is large, say $a = 5$. Although our simple erfc bound UB3-KL is looser than the other bounds when a is close to zero, say $a = 0.1$, it can be tighter than UB1-S and UB1-SA when a is a little larger, as in the case of $a = 0.5$. It grows even tighter as a increases, and becomes the tightest simple bound when a is large, say $a = 5$. The existing exponential bound UB1-AT is tight when a is small, but it loses its tightness and becomes looser than our simple bounds UB1-KL and UB3-KL when a is large. Actually, it is looser than UB1-KL and UB3-KL even in the case of $a = 1$ when b

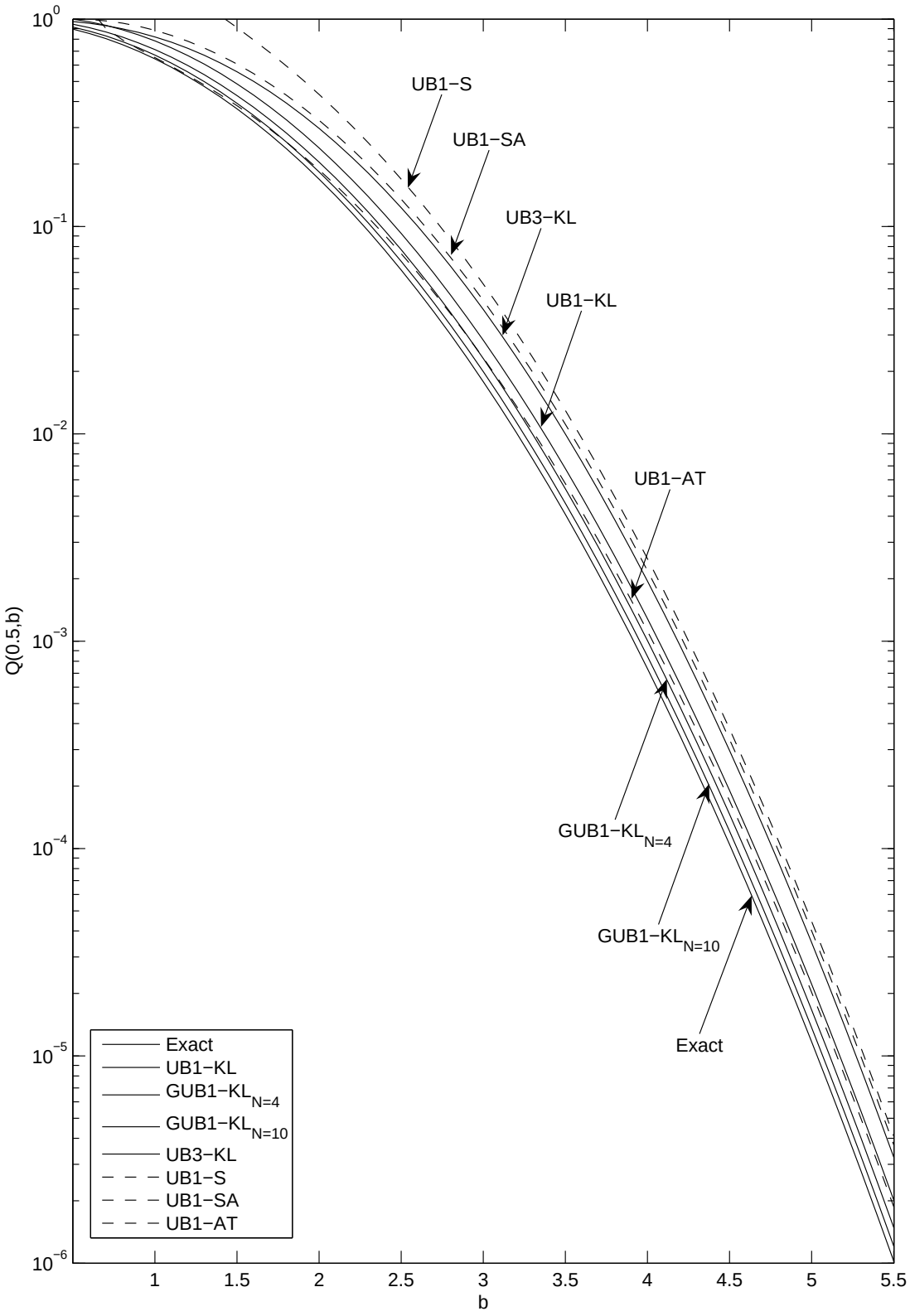

Fig. 4.9: The first-order Marcum Q-function $Q(a, b)$ and its upper bounds versus b for the case of $b \geq a = 0.5$.

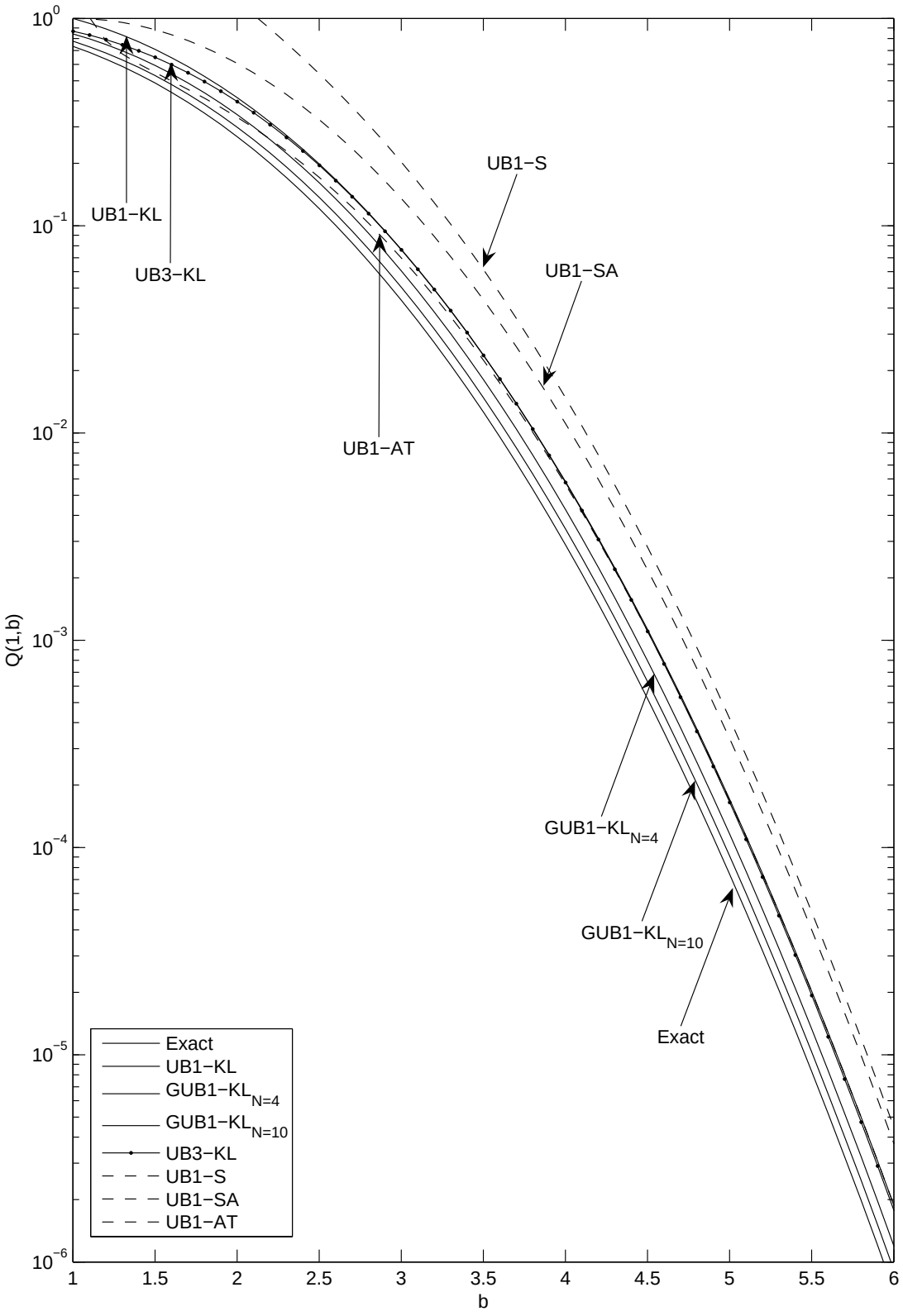

Fig. 4.10: The first-order Marcum Q-function $Q(a, b)$ and its upper bounds versus b for the case of $b \geq a = 1$.

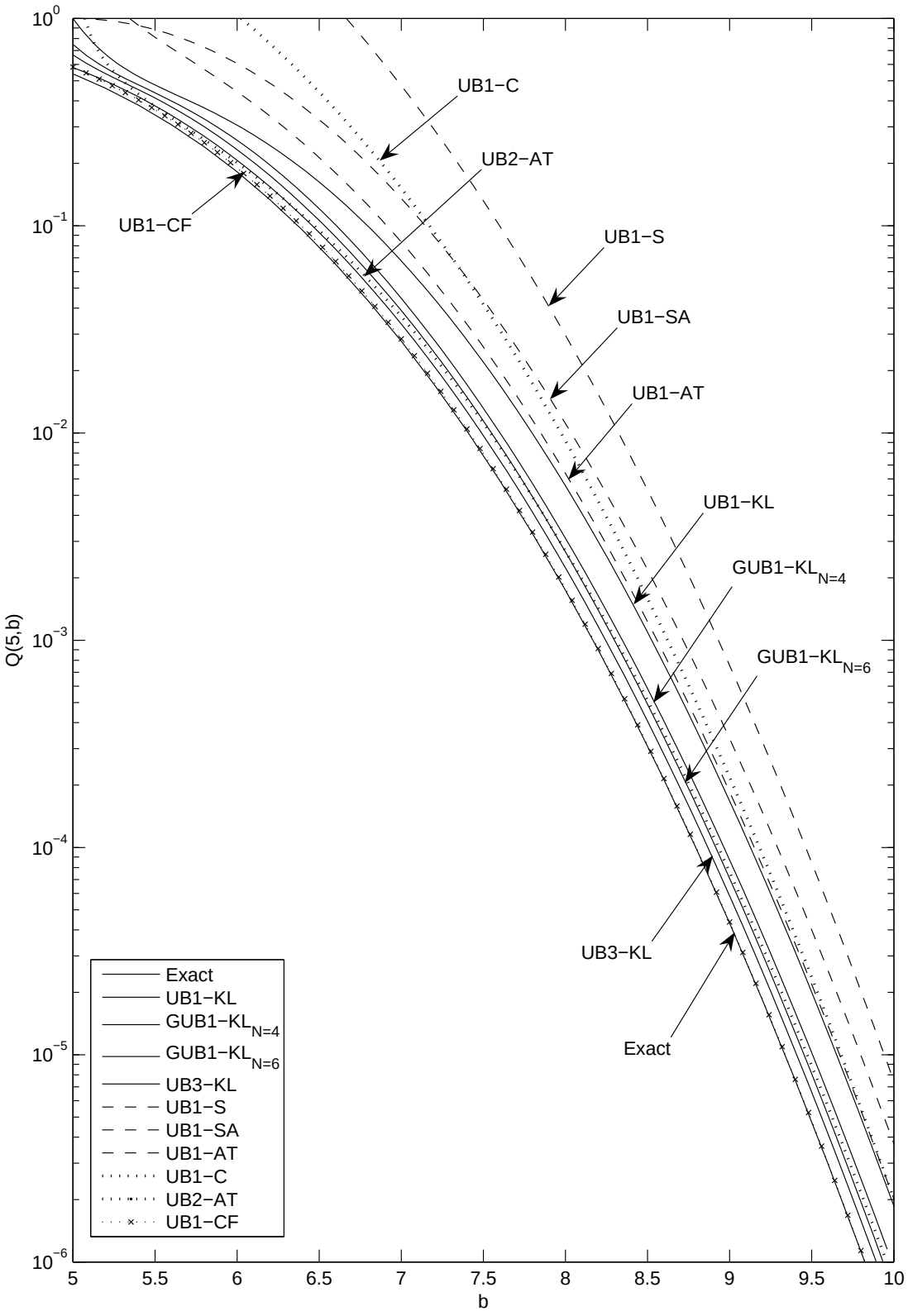

Fig. 4.11: The first-order Marcum Q-function $Q(a, b)$ and its upper bounds versus b for the case of $b \geq a = 5$.

is either close to a or much larger than a. Our generic exponential bound GUB1-KL evaluated with a few terms is already very tight. We can see that for the case of $a = 5$, GUB1-KL evaluated with $N = 2, 4, 6$ terms is tighter than the existing exponential bounds UB1-S, UB1-SA, and UB1-AT. The tightness of the generic bound GUB1-KL increases with N, but the incremental improvement decreases as N increases further.

4.10.1.2 Upper Bounds for the Case of $a \geq b \geq 0$

Thus far, for the case of $a > b$, the only upper bound reported in the literature is the bound UB2-CF in [122, eq. (12)], given by

$$\begin{aligned} Q(a,b) &\leq Q_{UB2\text{-}CF}(a,b) \\ &= 1 - \frac{I_0(ab)}{\exp(ab)} \Bigg\{ \exp\left(-\frac{a^2}{2}\right) - \exp\left[-\frac{(b-a)^2}{2}\right] \\ &\quad + a\sqrt{\frac{\pi}{2}} \left[\operatorname{erfc}\left(-\frac{a}{\sqrt{2}}\right) - \operatorname{erfc}\left(\frac{b-a}{\sqrt{2}}\right)\right] \Bigg\}, \end{aligned} \tag{4.100}$$

which is an I_0-bound. Our new closed-form bounds for this case include one generic exponential bound, i.e., GUB2-KL in (4.33), its special case with $N = M = 2$ and $\theta_1 = \omega_1 = \pi - \frac{17}{24} \arcsin \frac{b}{a}$, i.e., UB2-KL in (4.38), one generic erfc bound, i.e., GUB3-KL in (4.40), and one simple erfc bound, i.e., UB3-KL in (4.43). Thus, our work here not only provides some exponential upper bounds for the case of $a > b$ for the first time, it also provides a systematic approach to generating such simple and tight bounds. Since GUB3-KL is not as good as GUB2-KL, it is not discussed here further.

Fig. 4.12 shows the results for the case of $b < a = 5$. Here, we also choose equispaced points for θ_i and ω_i in GUB2-KL, i.e., $M = N$ and $\theta_i = \omega_i = \pi - \arcsin(b/a) + i \arcsin(b/a)/N$. We can see that our simple erfc bound UB3-KL is very tight for a large a, and is close to the I_0-bound UB2-CF. The tightness of UB3-KL grows as a increases. The generic bound GUB2-KL with ten terms, i.e.,

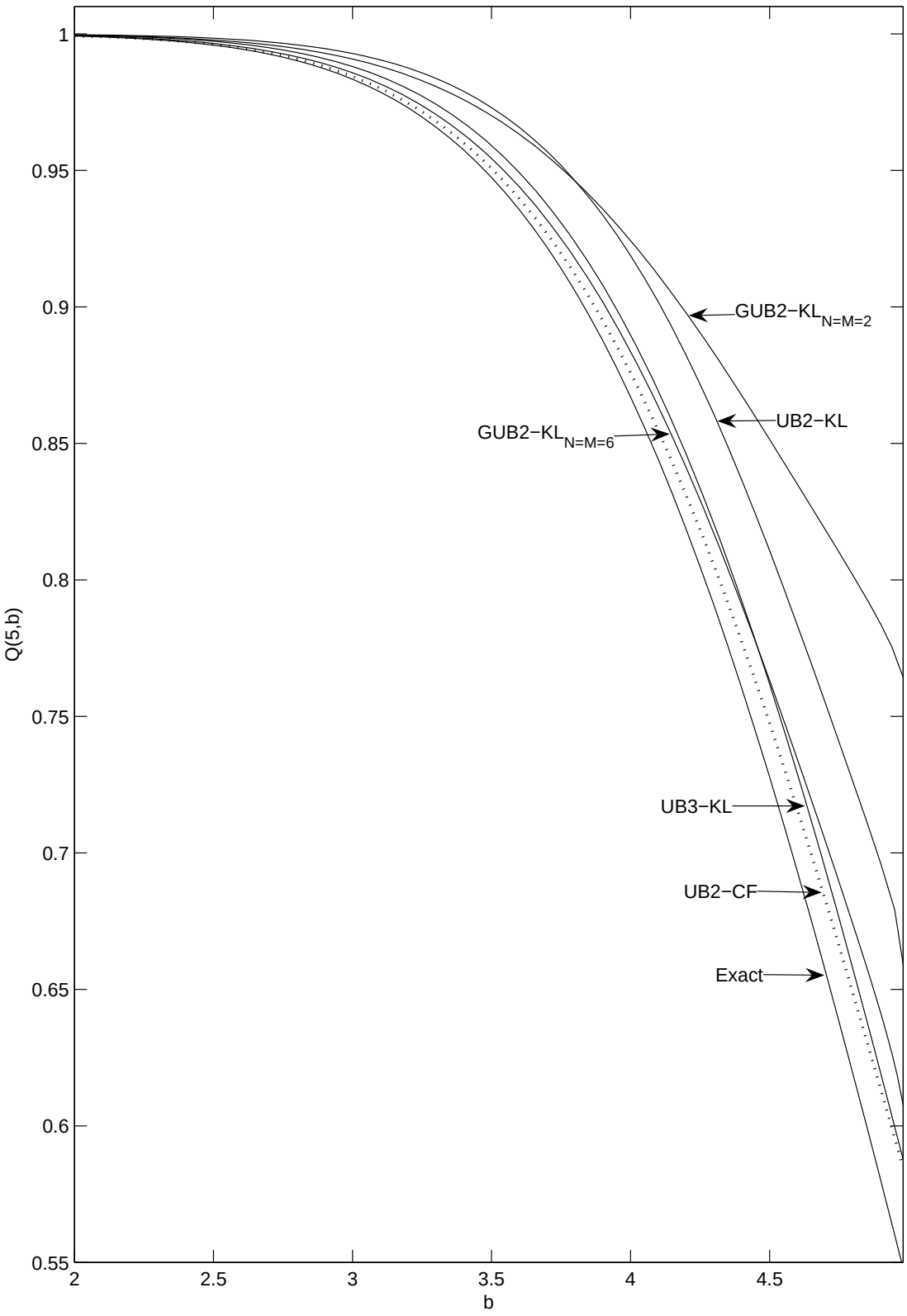

Fig. 4.12: The first-order Marcum Q-function $Q(a, b)$ and its upper bounds versus b for the case of $b \leq a = 5$.

$N = M = 6$, is already tight and close to the tight erfc bound, UB3-KL, and the I_0-bound, UB2-CF. The bounds UB2-KL and GUB2-KL$_{N=M=2}$ are two special cases of GUB2-KL with two exponential terms, one with $\theta_1 = \omega_1 = \pi - \frac{17}{24}\arcsin\frac{b}{a}$ and the other with $\theta_1 = \omega_1 = \pi - \frac{1}{2}\arcsin\frac{b}{a}$. They have shown different tightness. UB2-KL is a little looser than GUB2-KL$_{N=M=2}$ when b is much smaller than a, but is much tighter than GUB2-KL$_{N=M=2}$ when b is close to a. This shows that in addition to increasing the values of N and M, properly choosing the values of θ_i and ω_j can also improve the tightness of the generic bound.

4.10.1.3 Lower Bounds for the Case of $b \geq a \geq 0$

For this case, we have derived one generic exponential bound, i.e., GLB1-KL in (4.29), its special case with $N = 2$ and $\theta_1 = \pi/3$, i.e., LB1-KL in (4.37), one generic erfc bound, i.e., GLB3-KL in (4.41), and its special case with $N = M = 1$, i.e., LB3-KL in (4.44). The existing exponential bound LB1-SA in [120, eq. (3)], i.e.,

$$Q(a,b) \geq Q_{LB1\text{-}SA}(a,b) = \exp\left[-\frac{(b+a)^2}{2}\right], \quad b \geq a \geq 0 \tag{4.101}$$

is a special case of GLB1-KL with $N = 1$. From our geometric approach, it is clear that GLB1-KL with $N > 1$ is tighter than LB1-SA. The other two existing exponential bounds are LB1-S in [114, eq. (12)], given by

$$Q(a,b) \geq Q_{LB1\text{-}S}(a,b) = \frac{b}{b+a}\exp\left[-\frac{(b+a)^2}{2}\right], \quad b \geq a \geq 0, \tag{4.102}$$

and LB1-AT in [121, eq. (18)], given by

$$Q(a,b) \geq Q_{LB1\text{-}AT}(a,b) = \exp\left(-\frac{b^2}{2}\right), \qquad a \geq 0, b \geq 0. \tag{4.103}$$

From [120], LB1-SA is always tighter than LB1-S. It is also clear that LB1-KL and LB1-AT are always tighter than LB1-SA. The I_0-bounds in the literature include

the bound LB1-C in [116, eq. (4)] given by

$$Q(a,b) \geq Q_{LB1\text{-}C}(a,b) = \exp\left(-\frac{a^2+b^2}{2}\right) I_0(ab), \quad b \geq a \geq 0, \quad (4.104)$$

and the bound LB1-CF in [122, eq. (9)] given by

$$Q(a,b) \geq Q_{LB1\text{-}CF}(a,b) = \frac{I_0(ab)b}{\exp(ab)}\sqrt{\frac{\pi}{2}}\text{erfc}\left(\frac{b-a}{\sqrt{2}}\right), \quad b \geq a \geq 0. \quad (4.105)$$

Figs. 4.13 and 4.14 show the lower bounds for the case of $b > a = 1, 5$, respectively. We set $\theta_i = i\pi/N$ for GLB1-KL, and $\mu_i = -b - a + bi/N$ and $\nu_j = -a + bj/M$ for GLB3-KL. We can see that although GLB1-KL$_{N=2}$, LB1-S, LB1-SA, and LB1-AT are very tight at a small value of a, say $a = 0.1$, they are loose for a larger value of a. In Fig. 4.14, LB1-SA, LB1-S and LB1-AT are not shown, since they are much looser than the other bounds for this case. Both LB1-KL and GLB1-KL$_{N=2}$ are the special cases of GLB1-KL with two exponential terms, one with $\theta_1 = \pi/3$ and the other with $\theta_1 = \pi/2$. The results show that when a is not close to zero, setting $\theta_1 = \pi/3$ instead of $\theta_1 = \pi/2$ in GLB1-KL with $N = 2$ can bring about a lot of gains. We also can see that when a is not too small, the erfc bound LB3-KL is the tightest simple bound, and increasing the values of N and M in GLB3-KL will not bring much incremental improvement.

4.10.1.4 Lower Bounds for the Case of $a \geq b \geq 0$

The new generic erfc bound GLB3-KL in (4.41) and its special case LB3-KL in (4.44) are still valid for this case. We have also derived one generic exponential bound, i.e., GLB2-KL in (4.35). Our simple exponential bound LB2-KL in (4.39) is a special case of GLB2-KL with $N = M = 1$. There are four existing exponential bounds in the literature, including the bound LB2-S in [114, eq. (13)], given by

$$Q(a,b) \geq Q_{LB2\text{-}S}(a,b) = 1 - \frac{a}{a-b}\exp\left[-\frac{(a-b)^2}{2}\right], \quad a > b \geq 0, \quad (4.106)$$

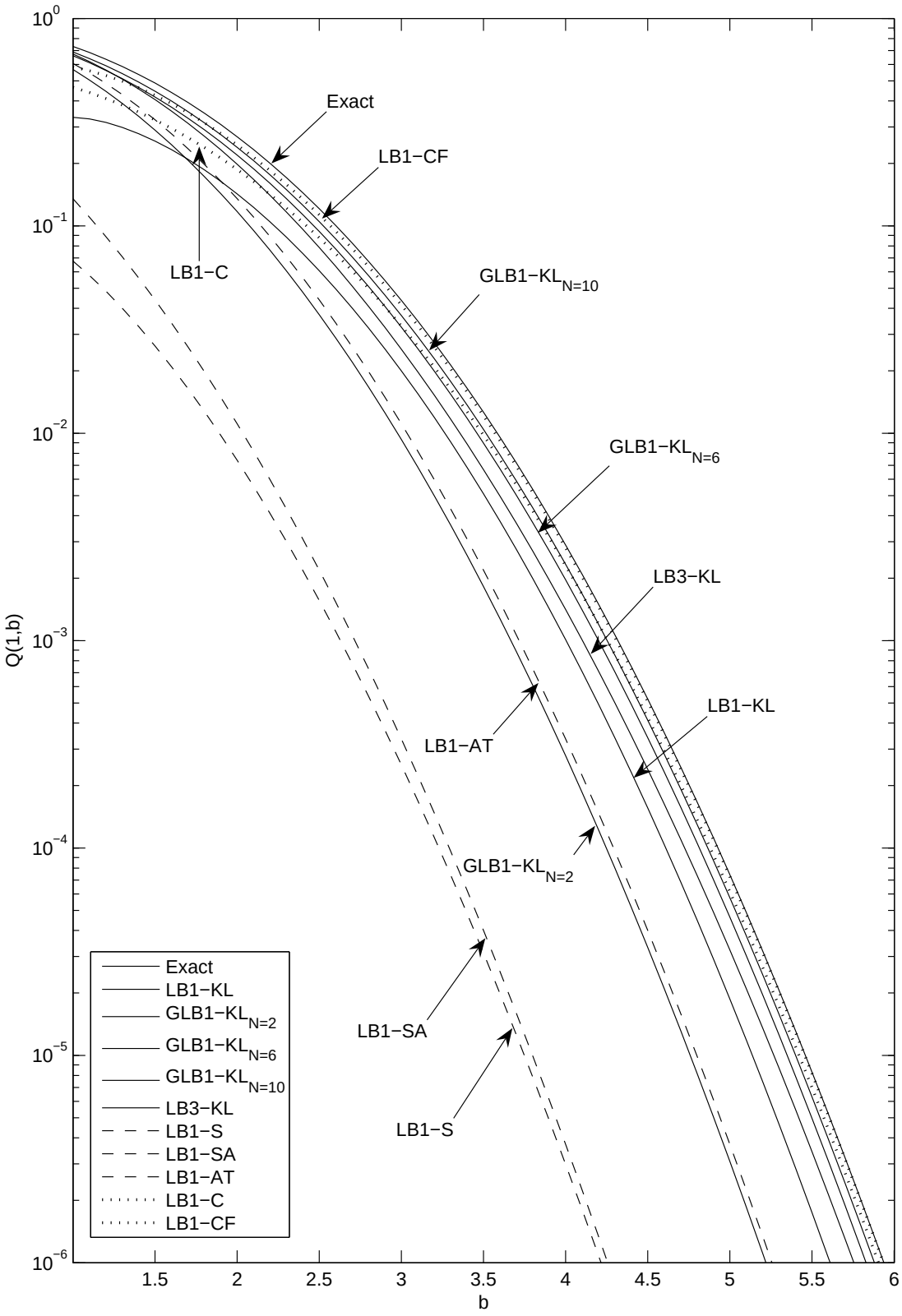

Fig. 4.13: The first-order Marcum Q-function $Q(a, b)$ and its lower bounds versus b for the case of $b \geq a = 1$.

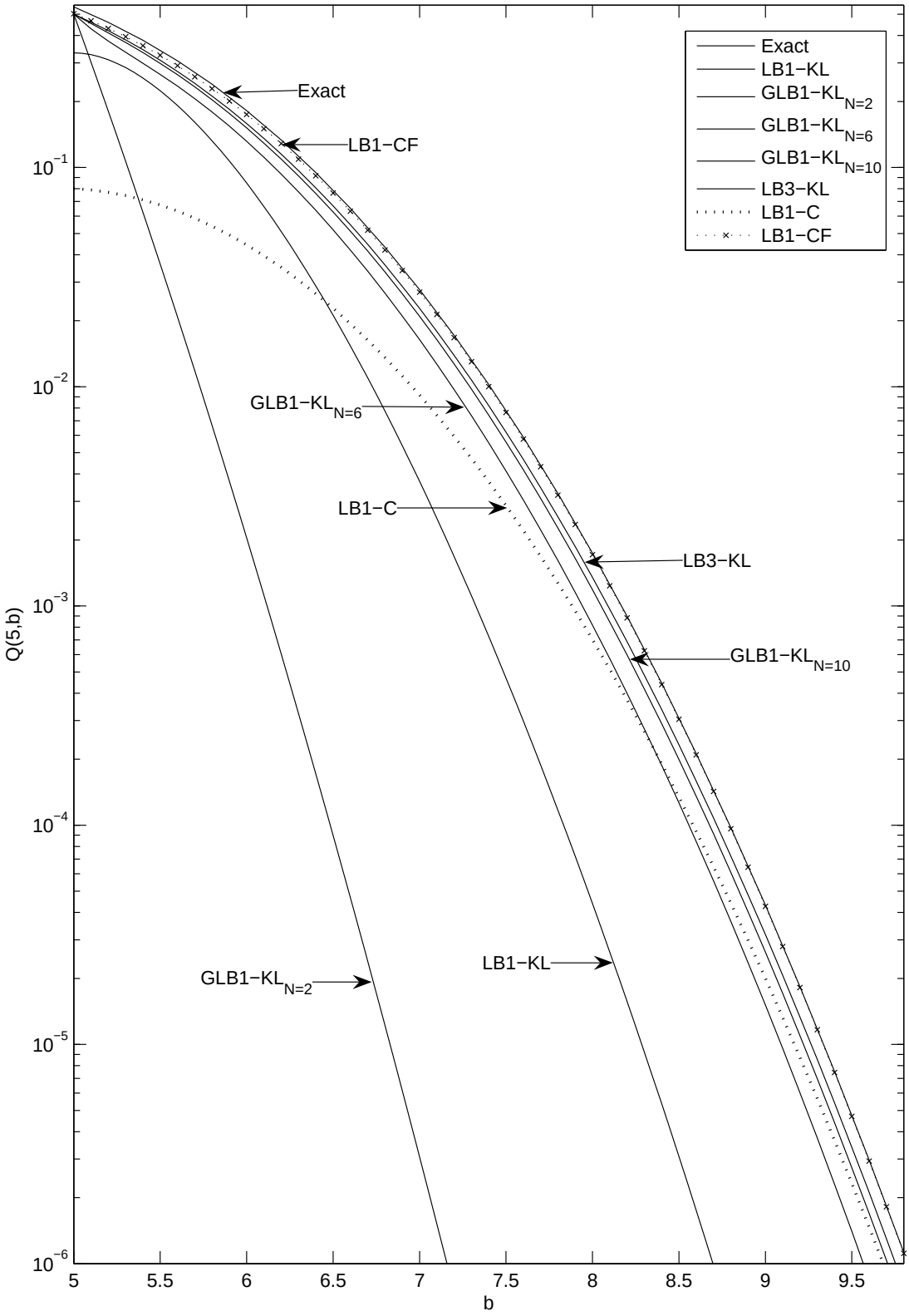

Fig. 4.14: The first-order Marcum Q-function $Q(a, b)$ and its lower bounds versus b for the case of $b \geq a = 5$.

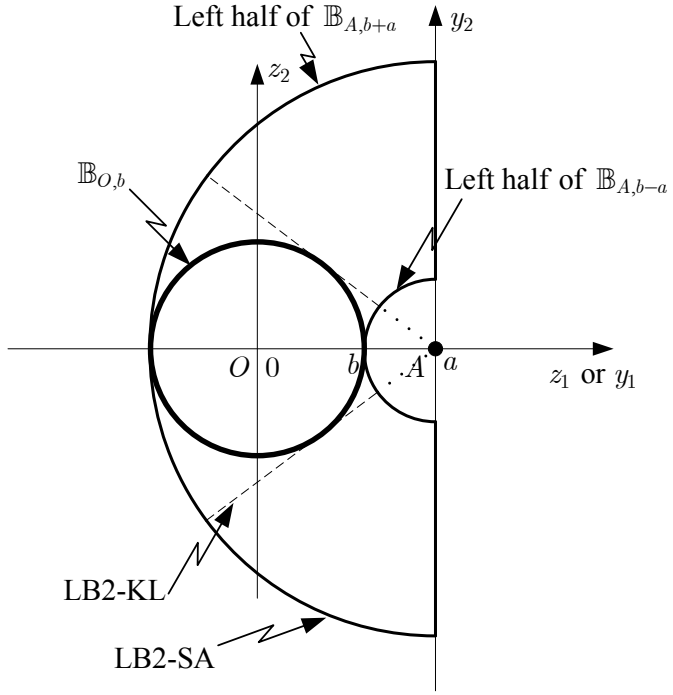

Fig. 4.15: Diagram of the derivation of the lower exponential bounds LB2-KL and LB2-SA for the case of $a > b$.

the bound LB2-SA in [120, eq. (4)], give by

$$Q(a,b) \geq Q_{LB2\text{-}SA}(a,b) = 1 - \frac{1}{2}\left\{\exp\left[-\frac{(b-a)^2}{2}\right] - \exp\left[-\frac{(b+a)^2}{2}\right]\right\},\ a \geq b \geq 0, \quad (4.107)$$

the bound LB1-AT in [121, eq. (18)] or in (4.103), and the bound LB2-AT in [121, eq. (21)], given by

$$Q(a,b) \geq Q_{LB2\text{-}AT}(a,b) = 1 - \frac{1}{2}\sqrt{\frac{(b/a)^2}{2\left[1-(b/a)^2\right]}}\left\{\exp\left[-\frac{(b-a)^2}{2}\right] + \exp\left[-\frac{(b+a)^2}{2}\right]\right\}, \quad a > b \geq 0. \quad (4.108)$$

From [120], LB2-SA is always tighter than LB2-S. It is also easy to see that LB2-KL is always tighter than LB2-SA, since the factor $\arcsin(b/a)/\pi$ preceding the braces in (4.39) is less than the factor $1/2$ preceding the braces in (4.107). Actually,

LB2-SA can also be obtained by using our geometric approach. As shown in Fig. 4.15, when we use the left half of the annulus between the boundaries of the disks $\mathbb{B}_{A,b+a}$ and $\mathbb{B}_{A,b-a}$ as the bounding shape, we can obtain the lower bound LB2-SA. The bounding shape for LB2-KL is just a part of that for LB2-SA, i.e., the part between the dashed lines. Thus, using this geometric approach, it is also easy to prove that LB2-KL is tighter than LB2-SA. The existing I_0-bound LB1-C in [116, eq. (4)] or in (4.104) is also valid for this case. The other two I_0-bounds in the literature include the bound LB3-AT in [121, eq. (20)], given by

$$\begin{aligned} Q(a,b) &\geq Q_{LB3\text{-}AT}(a,b) \\ &= 1 - \sqrt{\frac{(b/a)^2}{2\left(1-(b/a)^2\right)}} \exp\left[-\frac{b^2+a^2}{2}\right] \sqrt{I_0\left(2ab\right)}, a > b \geq 0, \quad (4.109) \end{aligned}$$

and LB2-CF in [122, eq. (14)], given by

$$\begin{aligned} Q(a,b) &\geq Q_{LB2\text{-}CF}(a,b) \\ &= 1 - \exp\left(-\frac{a^2-c^2}{2}\right)\left\{\exp\left(-\frac{c^2}{2}\right) - \exp\left[-\frac{(b-c)^2}{2}\right]\right. \\ &\quad \left. + c\sqrt{\frac{\pi}{2}}\left[\operatorname{erfc}\left(-\frac{c}{\sqrt{2}}\right) - \operatorname{erfc}\left(\frac{b-c}{\sqrt{2}}\right)\right]\right\}, \ a \geq b \geq 0, \quad (4.110) \end{aligned}$$

where $c = [\log I_0(ab)]/b$. We can see that LB2-CF is very complicated because of the factor c.

In our numerical results in Figs. 4.16 and 4.17, we set $\theta_i = \pi - \arcsin(b/a) + i\arcsin(b/a)/N$ and $\omega_j = \pi - \arcsin(b/a) + j\arcsin(b/a)/M$ for GLB2-KL, and $\mu_i = -b - a + bi/N$ and $\nu_j = -a + bj/M$ for GLB3-KL. Fig. 4.16 shows the results for the case of $b < a = 1$. In this case, for GLB2-KL, increasing the value of M is more useful than increasing the value of N, so we just set $N = 1$. GLB2-KL$_{N=1,M=3}$ is just a little looser than GLB3-KL$_{N=1,M=3}$ when b is close to a, but it is much simpler than the latter. GLB2-KL$_{N=1,M=9}$ is close to the tightest I_0-bound LB2-CF. Our simple exponential bound LB2-KL is much tighter than those existing exponential bounds, i.e., LB2-S, LB2-SA, LB1-AT, and LB2-AT.

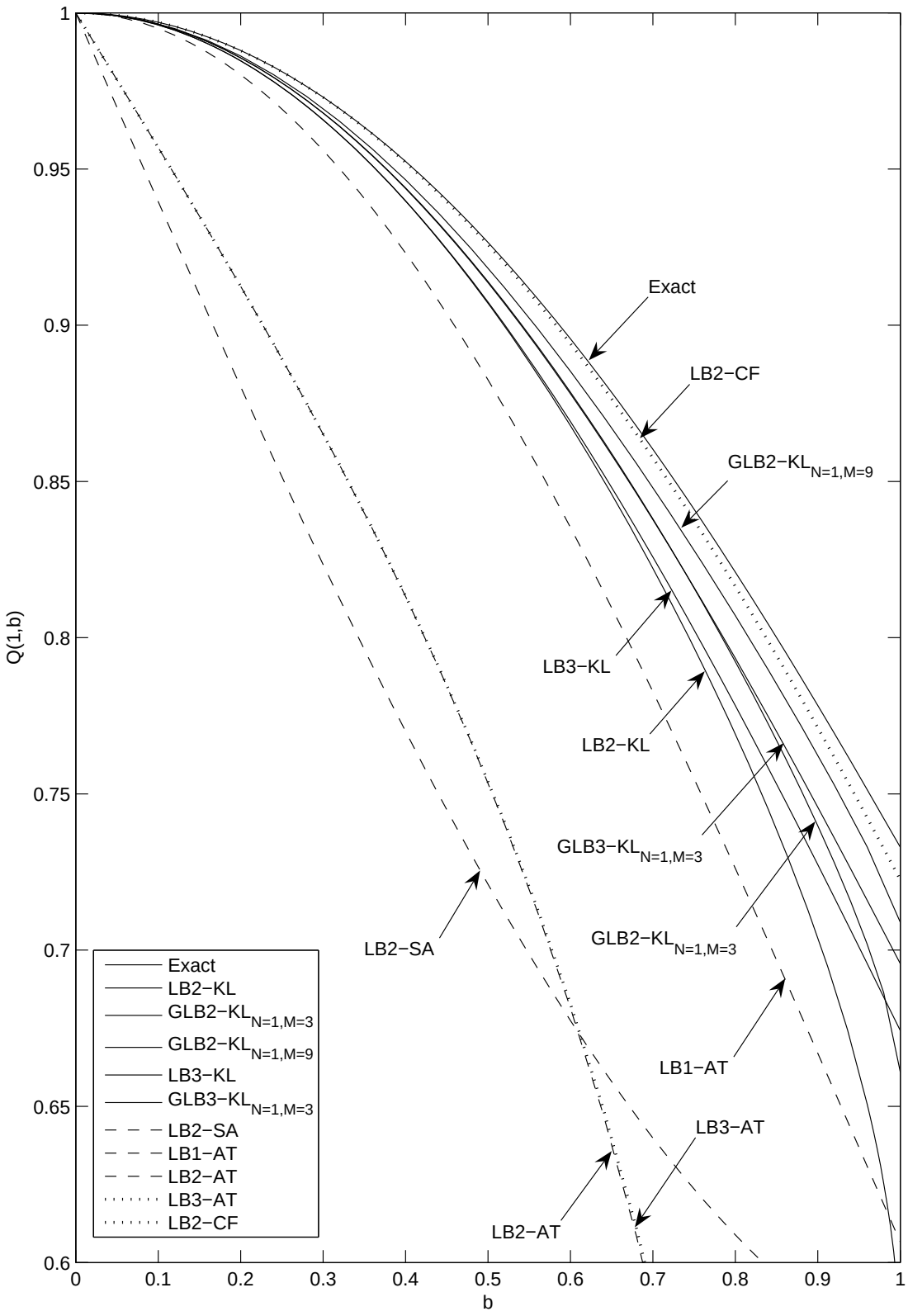

Fig. 4.16: The first-order Marcum Q-function $Q(a, b)$ and its lower bounds versus b for the case of $b \leq a = 1$.

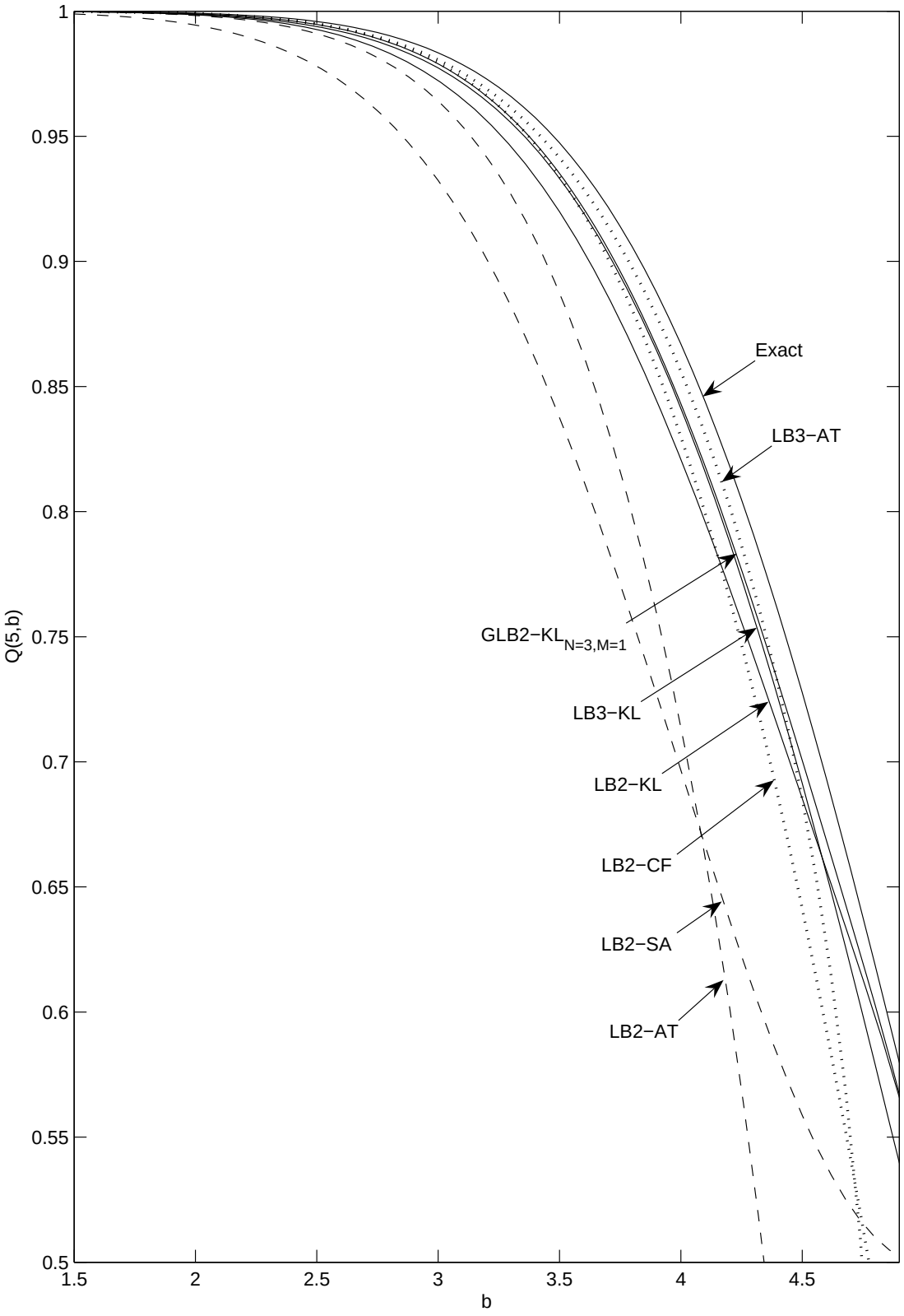

Fig. 4.17: The first-order Marcum Q-function $Q(a, b)$ and its lower bounds versus b for the case of $b \leq a = 5$.

Fig. 4.17 shows the results for the case of $b < a = 5$. Unlike the case of $a = 1$, for GLB2-KL, increasing the value of N is now more useful than increasing the value of M. We can see that LB3-KL, GLB2-KL$_{N=3,M=1}$ and LB2-KL are very close to one another, and are even tighter than LB2-CF and LB3-AT when b is close to a. There are some bounds which are not shown here, such as LB1-C and LB2-S, since they are much looser than the others.

4.10.2 Performance of the Single-Integral Bounds

In this section, we give some numerical results to show the tightness of our new single-integral bounds on $Q(a, b)$ derived in Sections 4.8 and 4.9. We have shown in Section 4.10.1 that our simple erfc bounds, i.e., UB3-KL in (4.43) and LB3-KL in (4.44), are the tightest simple bounds over a wide range of values of a and b, especially in the cases that a and b are large. Our generic erfc bounds, i.e., GUB3-KL in (4.40) and GLB3-KL in (4.41), will provide just a little improvement over these simple erfc bounds, but with a large increase in the complexity of the bounds. Thus here, we mainly compare our new single-integral bounds with these simple erfc bounds, and only show the results for the cases of small a where our single-integral bounds can provide further improvements over these simple erfc bounds. In Section 4.5, the lower erfc bound LB3-KL was obtained by using the square region, whose sides are of length $2b$ and are parallel to either of the axes, to cover $\mathbb{B}_{O,b}$, as shown by the solid lines outside of $\mathbb{B}_{O,b}$ in Fig. 4.5. It is clear that LB3-KL can also be given alternatively by setting $N = 4$ and $\psi_i = (i-1)2\pi/N$ in our generic single-integral lower bounds, i.e., GLBI1-KL in (4.71) for $b > a$ and GLBI2-KL in (4.74) for $a > b$. In our numerical results, we choose equispaced points for ψ_i in our generic single-integral bounds for simplicity, i.e., $\psi_i = (i-1)2\pi/N, i = 1, \cdots, N$. Thus, LB3-KL is equal to GLBI1-KL$_{N=4}$ for $b > a$, and equal to GLBI2-KL$_{N=4}$ for $a > b$. Our simple single-integral bounds in Section 4.9 are also presented as the special cases of the generic bounds with $N = 6$.

Fig. 4.18 shows the numerical results for the case of $b \geq a = 1$. The bound GUBI1-KL in (4.54) is shown with $N = 6, 8, 10$, and the bound GLBI1-KL in (4.71) is shown with $N = 4, 6, 8$. We can see that the tightness of both these two generic bounds increases with the value of N. For this small value of $a = 1$, GUBI1-KL$_{N=10}$, which involves five single integrals, and GLBI1-KL$_{N=6}$, which involves four single integrals, are tighter than UB3-KL and LB3-KL, respectively. These results show that GUBI1-KL and GLBI1-KL evaluated with just a few integrals can be tighter than the simple erfc bounds. Fig. 4.19 shows the numerical results for the case of $b \leq a = 2$. Since for this case, our simple exponential bounds UB2-KL in (4.38) and LB2-KL in (4.39) are tighter than the erfc bounds UB3-KL in (4.43) and LB3-KL in (4.44), respectively, we also include them for comparison. We can see that GUBI2-KL and GLBI2-KL evaluated with a few integrals can be tighter than the simple exponential bounds and erfc bounds.

Now, we compare our generic single-integral bounds with the generic exponential bounds derived in Section 4.4. The exponential bounds involve only exponential functions, and thus, are the most desirable form when one has to integrate the bounds on $Q(a, b)$ over a fading distribution. However, in some applications, bounds which are tighter than the exponential bounds but are not very complicated may be needed. Our generic single-integral bounds may provide a way to obtain such bounds. Here, we only illustrate the comparisons between GUBI1-KL in (4.54) and GUB1-KL in (4.28), and between GLBI1-KL in (4.71) and GLB1-KL in (4.29) for the case of $b > a$. As shown in Fig. 4.20, we set the two types of bounds to involve the same number of terms and cover the same angular ranges. Using the same definitions of the arguments as those in (4.54) and (4.71), we rewrite GUB1-KL in (4.28) and GLB1-KL in (4.29), respectively, as

$$\begin{aligned} Q(a,b) &\leq Q_{GUB1\text{-}KL}(a,b) \\ &= \frac{1}{\pi}\sum_{i=1}^{N/2}(\theta_{i+1}-\theta_i)\exp\left[-\frac{1}{2}\Big(-a\cos\theta_i+\sqrt{b^2-a^2\sin^2\theta_i}\Big)^2\right],\ b\geq a\geq 0, \end{aligned} \tag{4.111}$$

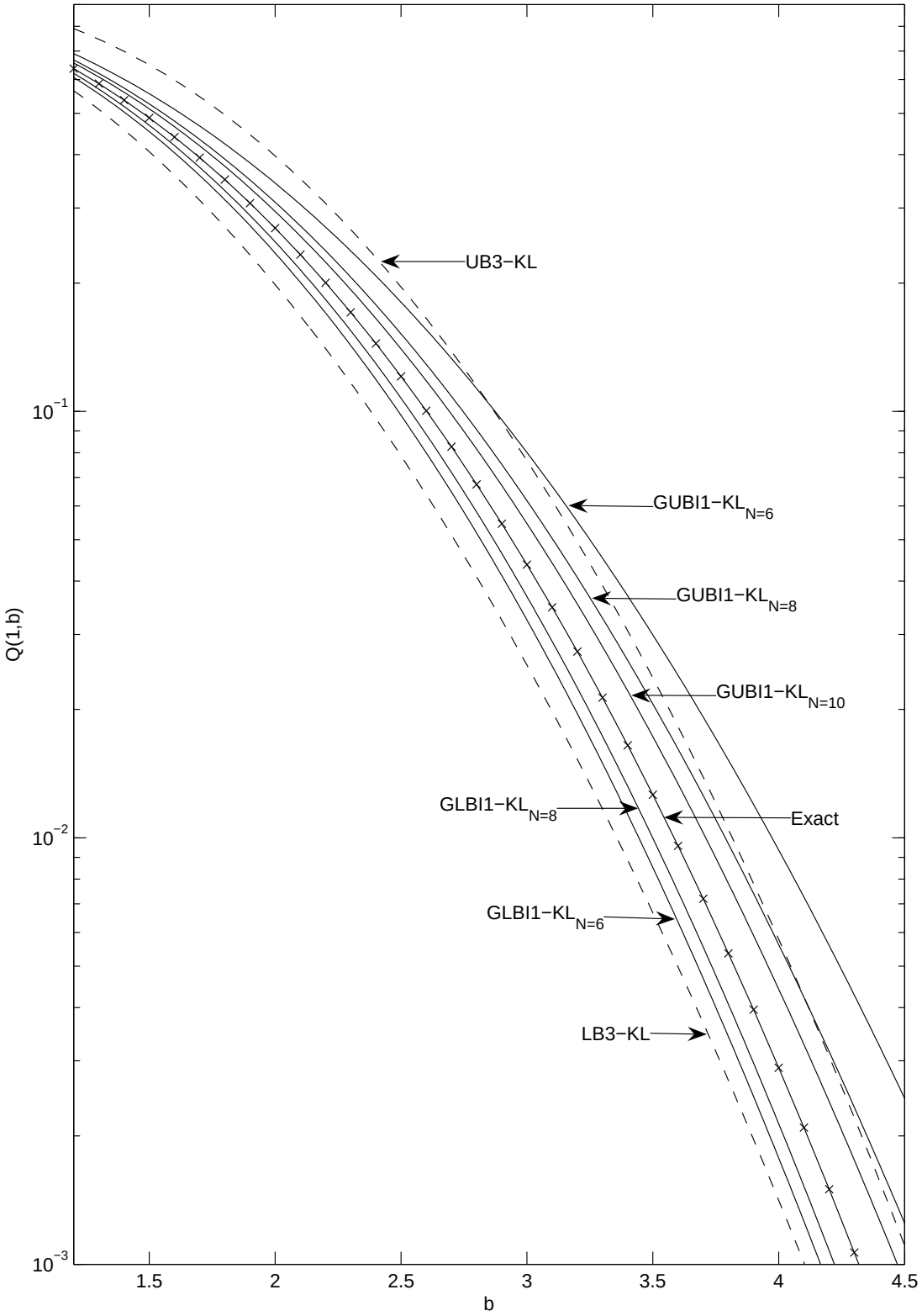

Fig. 4.18: The first-order Marcum Q-function $Q(a, b)$ and its upper and lower bounds versus b for the case of $b \geq a = 1$.

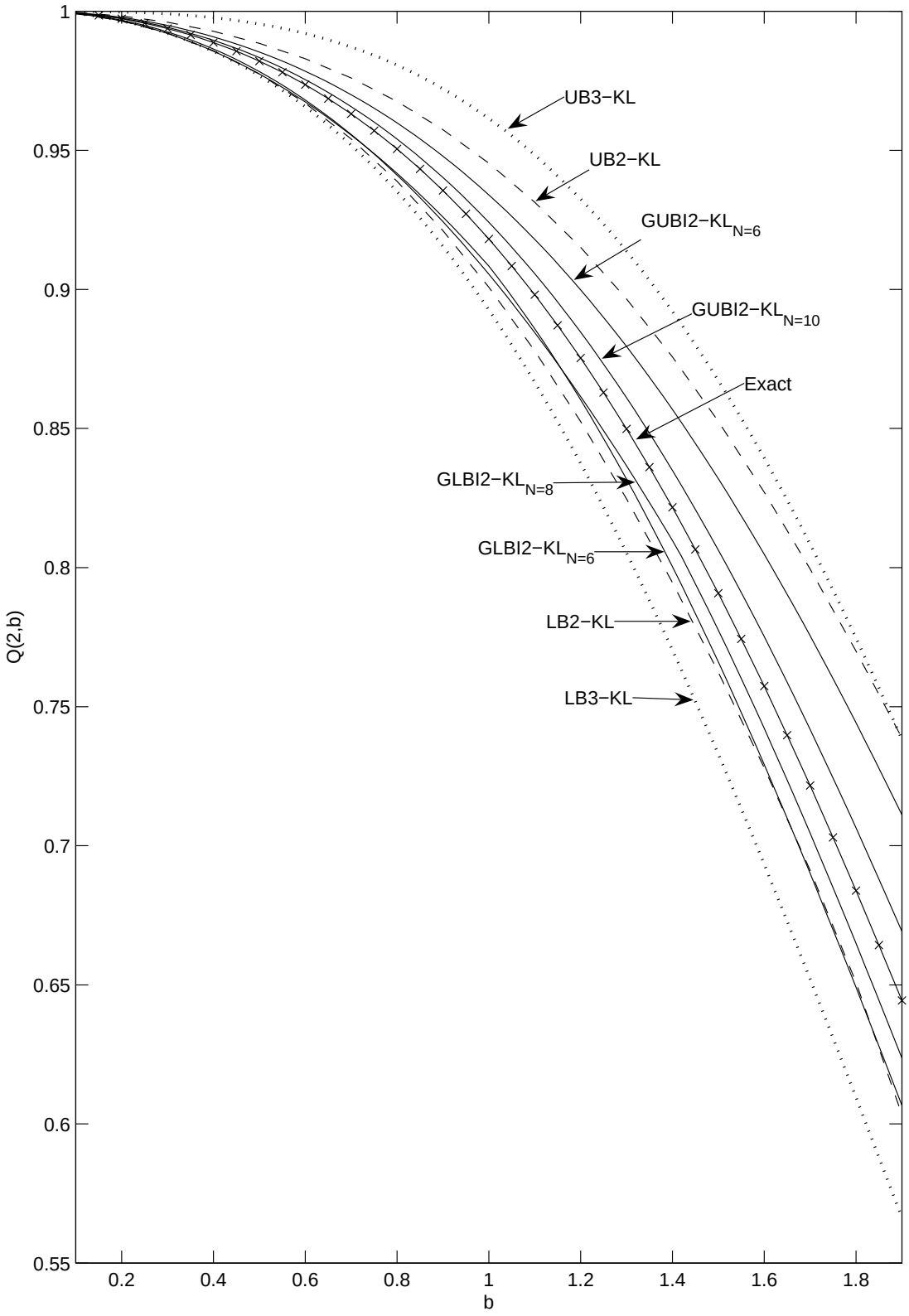

Fig. 4.19: The first-order Marcum Q-function $Q(a, b)$ and its upper and lower bounds versus b for the case of $b \leq a = 2$.

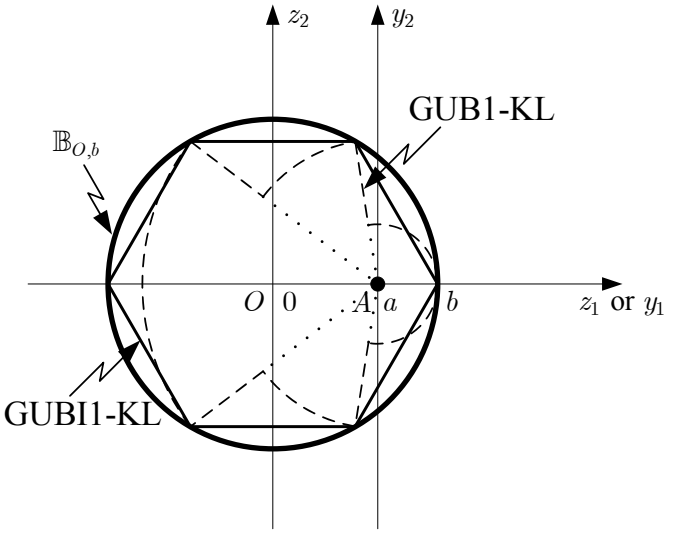

(a) GUBI1-KL and GUB1-KL for the case of $b > a$

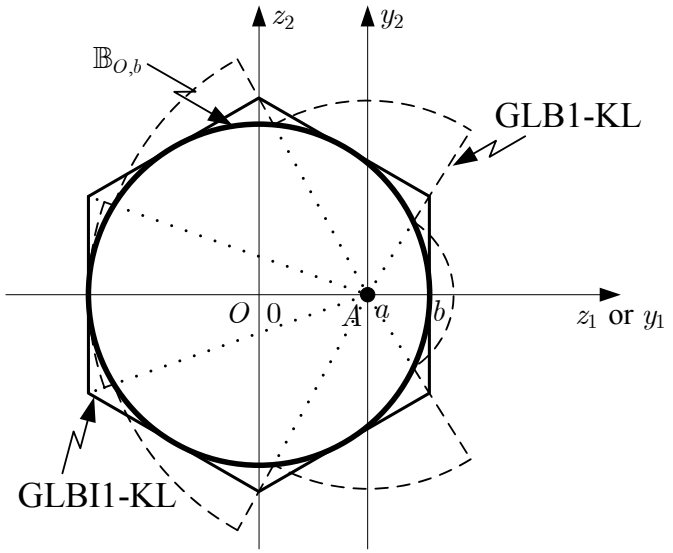

(b) GLBI1-KL and GLB1-KL for the case of $b > a$

Fig. 4.20: Comparisons between the generic single-integral bounds and generic exponential bounds.

$$
\begin{aligned}
Q(a,b) &\geq Q_{GLB1\text{-}KL}(a,b) \\
&= \frac{\beta_1}{\pi}\exp\left[-\frac{1}{2}\left(-a\cos\beta_1+\sqrt{b^2-a^2\sin^2\beta_1}\right)^2\right] \\
&\quad+\frac{1}{\pi}\sum_{i=1}^{N/2-1}(\beta_{i+1}-\beta_i)\exp\left[-\frac{1}{2}\left(-a\cos\beta_{i+1}+\sqrt{b^2-a^2\sin^2\beta_{i+1}}\right)^2\right] \\
&\quad+\frac{\pi-\beta_{N/2}}{\pi}\exp\left[-\frac{(b+a)^2}{2}\right], \qquad b\geq a\geq 0. \qquad (4.112)
\end{aligned}
$$

Fig. 4.21 shows the comparison between the generic exponential bounds and the generic single-integral bounds. We can see that for the case of $a = 1$, when the settings for N and θ_i or β_i are the same for the two types of bounds, GUBI1-KL can only provide some improvements over GUB1-KL when b is not much larger than a, but GLBI1-KL can provide more improvements over GLB1-KL.

4.11 Summary

By taking a geometric view of the first-order Marcum Q-function, $Q(a, b)$, a very general and powerful approach for computing and bounding the Q-function has been presented that leads to many new results. New finite-integral representations of $Q(a, b)$ have been derived, which are simpler than their counterparts in the literature. New closed-form bounds have also been derived, including the generic and simple exponential bounds and the generic and simple erfc bounds. The generic bounds have been shown to approach the exact value of $Q(a, b)$ as the number of terms involved increases, and the simple bounds have been shown to be tighter than the existing exponential bounds in most cases, especially when the arguments a and b are large. In addition to the closed-form bounds, new bounds involving single finite integrals have also been developed, including the generic and simple single-integral bounds.

Among these bounds, the exponential bounds are the easiest to handle in theoretical analyses. If the tightness of the exponential bounds does not satisfy the need, we can use the erfc bounds. The new, simple erfc bounds, UB3-KL and LB3-KL, turn out to be close to the tightest existing I_0-bounds when the arguments a and b are not too small, and they are given in a form simpler than the latter. Thus, although our simple erfc bounds are not the tightest closed-form bounds with just a few terms, they are the ones that can lead to the tightest closed-form results in many theoretical analyses involving $Q(a, b)$. Bounds which are tighter than these simple erfc bounds may be obtained by using the generic

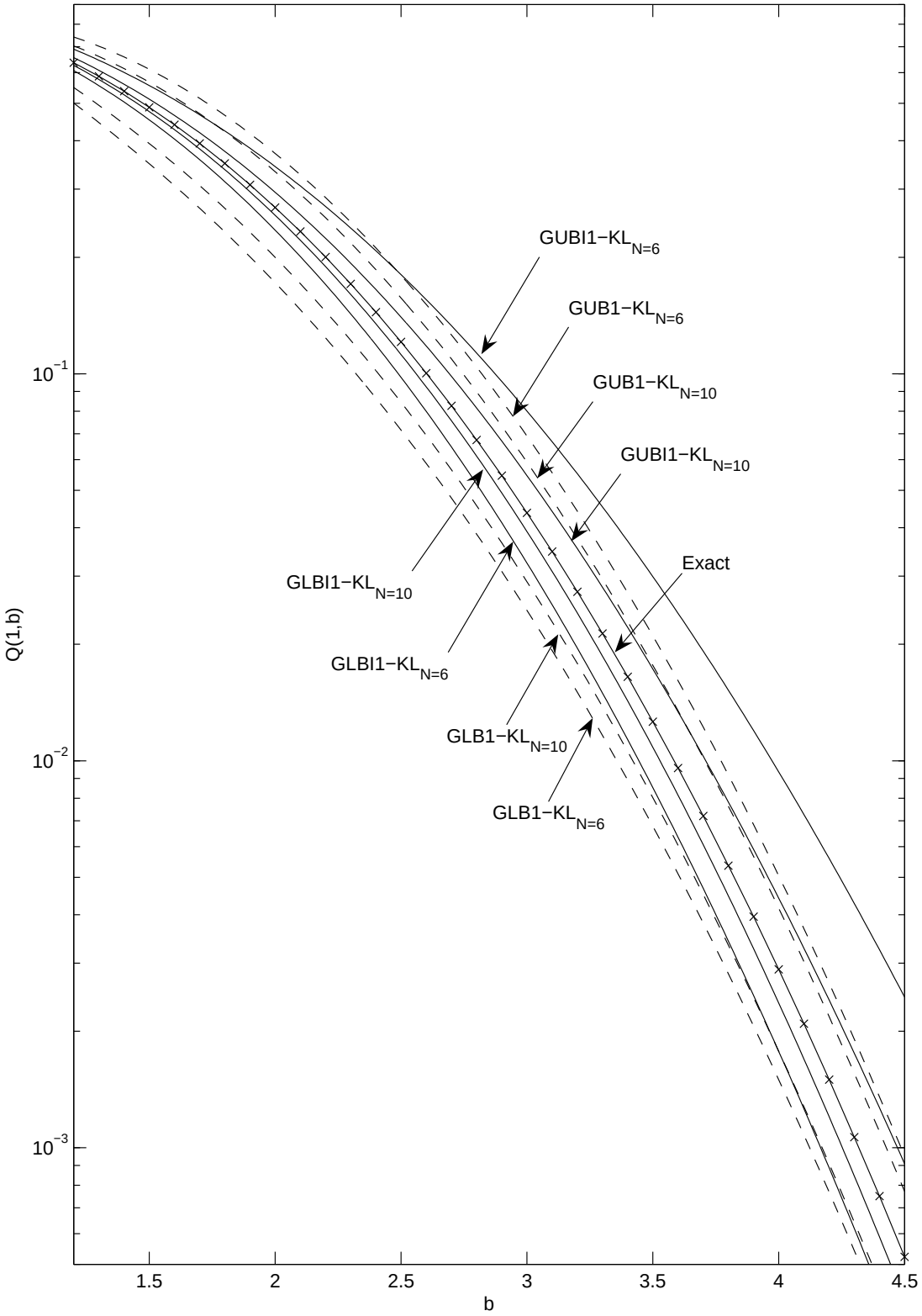

Fig. 4.21: The first-order Marcum Q-function $Q(a, b)$ and its upper and lower bounds versus b for the case of $b \geq a = 1$.

erfc bounds, or the generic and simple single-integral bounds, but at a cost of involving more complicated terms.

Chapter 5

Computing and Bounding the Generalized Marcum Q-Function

In this chapter, we extend the geometric approach to the generalized Marcum Q-function. The generalized Marcum Q-function of order m, $Q_m(a,b)$, is interpreted geometrically as the probability of a $2m$-dimensional, real, Gaussian random vector $\mathbf{z}_{2m}$, whose mean vector has a Frobenius norm of a, lying outside of a hyperball $\mathbb{B}_{O,b}^{2m}$ of $2m$ dimensions, with radius b, and centered at the origin O. Based on this new geometric interpretation, some new representations and closed-form bounds are derived for $Q_m(a,b)$. For the case where m is an odd multiple of 0.5, a new closed-form representation is proposed, which involves only exponential and erfc functions, and thus is easy to handle in computations. For the case where m is an integer, a pair of new finite-integral representations for $Q_m(a,b)$ is proposed. In addition to the new representations, some generic exponential bounds and generic erfc bounds on $Q_m(a,b)$ of integer order m are also derived by computing the probability of $\mathbf{z}_{2m}$ lying outside of various bounding geometrical shapes whose surfaces tightly enclose, or are tightly enclosed by the surface of $\mathbb{B}_{O,b}^{2m}$. These bounding shapes consist of an arbitrarily large number of parts. As their closeness of fit with $\mathbb{B}_{O,b}^{2m}$ improves, our generic bounds approach the exact value of $Q_m(a,b)$. Besides, the functions, $Q_{m+0.5}(a,b)$ and $Q_{m-0.5}(a,b)$, which

can be evaluated using our new closed-form representation mentioned above, are also shown to be tight upper and lower bounds, respectively, on $Q_m(a,b)$. Their average is a good approximation to $Q_m(a,b)$.

5.1 Introduction

In Chapter 4, we have shown a geometric view of the first-order Marcum Q-function, $Q(a,b)$, and based on this geometric view, we have developed some new representations and bounds for $Q(a,b)$. In this chapter, we extend this geometric approach to the case of the generalized Marcum Q-function, $Q_m(a,b)$. The generalized Marcum Q-function is defined as [1, eq. (2.1–122)]

$$Q_m(a,b) = \int_b^\infty x \left(\frac{x}{a}\right)^{m-1} \exp\left(-\frac{x^2+a^2}{2}\right) I_{m-1}(ax)dx,\ a>0,\ b\geq 0, \quad (5.1)$$

where $I_m(\cdot)$ is the mth-order modified Bessel function of the first kind, and is given by [124, eq. (8.431 3)]

$$I_m(x) = \frac{\left(\frac{x}{2}\right)^m}{\Gamma\left(m+\frac{1}{2}\right)\Gamma\left(\frac{1}{2}\right)} \int_0^\pi e^{\pm x\cos\theta} \sin^{2m}(\theta)d\theta. \quad (5.2)$$

Here, the order m can be an integer or a non-integer [5]. It is clear that when we have $m=1$, $Q_m(a,b)$ in (5.1) reduces to $Q(a,b)$ in (4.1). This generalized Marcum Q-function is often involved in the error performance analysis of multi-channel detections in wireless communication systems [1, 5]. The infinite-integral representation of $Q_m(a,b)$ in (5.1), involving $I_{m-1}(\cdot)$ in the integrand and the argument b in the lower integral limit, may pose problems for theoretical analyses and numerical computations in some applications. Therefore, for $Q_m(a,b)$ of integer order m, some alternative finite-integral representations have been derived in [113, Appendix C] and [114]. To further simplify analytical results or to facilitate analytical manipulations of $Q_m(a,b)$, some simple exponential bounds,

which involve only the exponential function, have been given in [120, 121]. Some I_k-bounds, which involve $I_0(\cdot)$ or $\{I_k(\cdot)\}_{k=0}^{m-1}$, have also been given in [121, 122], but these I_k-bounds are too complicated to use in some further analytical manipulations of $Q_m(a,b)$, such as in averaging $Q_m(a,b)$ over a fading distribution. All these existing results were obtained by using a mathematical approach, usually resorting to alternative expressions or bounds of the functions involved in defining the Q-function. Thus far, closed-form representations of $Q_m(a,b)$ for integer or non-integer m are not available in the literature.

In this chapter, we use a novel geometric approach to derive some new representations and bounds for $Q_m(a,b)$. We introduce a new geometric interpretation of $Q_m(a,b)$ as the probability of a real, Gaussian random vector $\mathbf{z}_n$ of $n = 2m$ dimensions, with a mean vector of Frobenius norm a, lying outside of the region enclosed by a hypersphere $\mathbb{S}_{O,b}^n$ of n dimensions[1], with radius b, and centered at the origin O. Based on this new interpretation, we first propose a new, closed-form representation of $Q_m(a,b)$ for the case of odd n. This new representation only involves the exponential function and the erfc function, and thus, is easy to use in both numerical and analytical work. It is valid for the entire ranges of $a > 0$ and $b \geq 0$. For the special case of $a = 0$, we also propose a new, closed-form representation of $Q_m(0,b)$, which can be used in evaluating the tail probability of a central chi-square random variable with an odd number n of degrees of freedom. For the case of even n, i.e., integer m, we also give a new pair of finite-integral representations of $Q_m(a,b)$, one for $b \geq a$ and the other for $a \geq b$, whose integrands involve only the exponential function. This pair of new forms is more robust than the forms in [113, Appendix C] and [114]. Since so far, we are not able to obtain a closed-form representation of $Q_m(a,b)$ for integer m, we develop

[1]A hypersphere of n dimensions may have different definitions in different contexts. Here, a hypersphere of n dimensions, also known as an n-sphere, is defined as the set of points $(z_1, z_2, \ldots, z_n)$ such that we have $\sum_{i=1}^{n}(z_i - c_i)^2 = b^2$, where the point $(c_1, c_2, \ldots, c_n)$ is the center of the hypersphere, and b is the radius of the hypersphere [136, Chap. 1]. This definition is different from that given in [137, eq. (10.1)] where the equation $\sum_{i=1}^{n}(z_i - c_i)^2 = b^2$ defines an $(n-1)$-sphere, but is used in the discussions in [137, Chap. VIII 13–14] and [138].

some closed-form bounds for $Q_m(a,b)$ by computing the probability of $\mathbf{z}_n$ lying outside of various geometrical bounding shapes whose surfaces tightly enclose, or are tightly enclosed by the n-sphere $\mathbb{S}^n_{O,b}$. We first derive some generic exponential bounds which involve only the exponential function, and then derive some generic erfc bounds which involve only the exponential function and the erfc function. The geometrical bounding shapes used in the derivations of these generic bounds consist of an arbitrarily large number of components. As these bounding shapes converge to the hyperball[2] $\mathbb{B}^{2m}_{O,b}$ which is the region enclosed by the n-sphere $\mathbb{S}^{2m}_{O,b}$, our generic bounds approach the exact value of $Q_m(a,b)$. In addition to these generic bounds, we also prove that $Q_{m+0.5}(a,b)$ is a tight upper bound on $Q_m(a,b)$, irrespective of whether n is even or odd. Thus, for the case of even n, $Q_{m+0.5}(a,b)$ and $Q_{m-0.5}(a,b)$ can be used, respectively, as tight upper and lower bounds on $Q_m(a,b)$, and they can be evaluated using our new closed-form representation for odd n. Our numerical results show that $Q_{m+0.5}(a,b)$ and $Q_{m-0.5}(a,b)$ are very tight, close to or tighter than the tightest closed-form bounds available in the literature. The average of these two bounds also approximates $Q_m(a,b)$ very well.

Section 5.2 gives the new geometric view of $Q_m(a,b)$. Section 5.3 derives the new representations of $Q_m(a,b)$. Section 5.4 presents the new, generic, exponential bounds on $Q_m(a,b)$ of integer order m. Section 5.5 gives the new erfc bounds on $Q_m(a,b)$ of integer order m, including the justification of using $Q_{m+0.5}(a,b)$ and $Q_{m-0.5}(a,b)$ as bounds on $Q_m(a,b)$, and the derivation of the new, generic, erfc bounds. Section 5.6 presents numerical results and comparisons with existing bounds in the literature.

[2]A hyperball of n dimensions, also known as an n-ball, is the region inside an n-sphere [139, 140]. Here, our results hold irrespective of whether or not the n-ball includes the points on the n-sphere.

5.2 The Geometric View of $Q_m(a,b)$

For the case where the order of the Marcum Q-function, m, satisfies $m = 0.5n$ and $n \in \mathbb{N}$, where $\mathbb{N}$ is the positive integer set, $Q_m(a,b)$ can be shown to be the tail probability of a normalized noncentral chi-square random variable with n degrees of freedom. It is clear that this chi-square random variable can be obtained from the norm square of an n-dimensional, real, Gaussian random vector $\mathbf{z}_n$, namely,

$$\mathbf{z}_n = (z_1 \; z_2 \; \cdots \; z_n)^\top = \mathbf{p}_n + \mathbf{y}_n. \tag{5.3}$$

Here, $\mathbf{p}_n = (p_1 \; p_2 \; \cdots \; p_n)^\top$ is a real, constant mean vector with the Frobenius norm a, i.e., $\|\mathbf{p}_n\| = \sqrt{\sum_{i=1}^n p_i^2} = a$, and $\mathbf{y}_n = (y_1 \; y_2 \; \cdots \; y_n)^\top$ is a real, Gaussian noise vector, whose entries are independent Gaussian random variables, each with zero mean and identical variance σ_y^2. Thus, the Frobenius norm square of $\mathbf{z}_n$, i.e.,

$$R_1 = \|\mathbf{z}_n\|^2 = \sum_{i=1}^n z_i^2, \tag{5.4}$$

has a noncentral chi-square distribution with n degrees of freedom and noncentrality parameter $a^2 = \|\mathbf{p}_n\|^2 = \sum_{i=1}^n p_i^2$. Its PDF is given by [1, eq. (2.1–118)]

$$p_{R_1}(R_1) = \frac{1}{2\sigma_y^2}\left(\frac{R_1}{a^2}\right)^{(n-2)/4} e^{-(R_1+a^2)/2\sigma_y^2} I_{\frac{n}{2}-1}\left(\frac{\sqrt{R_1}a}{\sigma_y^2}\right), \qquad R_1 \geq 0.$$

The probability of R_1 being greater than a real constant b^2, where $b \geq 0$, or, equivalently, $R = \sqrt{R_1}$ being greater than b, is then given by [1, eq. (2.1–124)]

$$\Pr(R > b) = \int_{b^2}^{\infty} p_{R_1}(R_1) dR_1 = Q_m\left(\frac{a}{\sigma_y}, \frac{b}{\sigma_y}\right). \tag{5.5}$$

In the following discussions, we simply set $\sigma_y^2 = 1$, and thus, $Q_m(a,b)$ is the tail probability of R or R_1. This means that evaluating $Q_m(a,b)$ in (5.1) is the same as computing the probability $\Pr(R > b)$. This probability can be interpreted geometrically as the probability of the vector $\mathbf{z}_n$ lying outside of the hyperball $\mathbb{B}_{O,b}^n$ which is centered at the origin O, i.e., $(z_1 = \cdots = z_n = 0)$, and has a radius

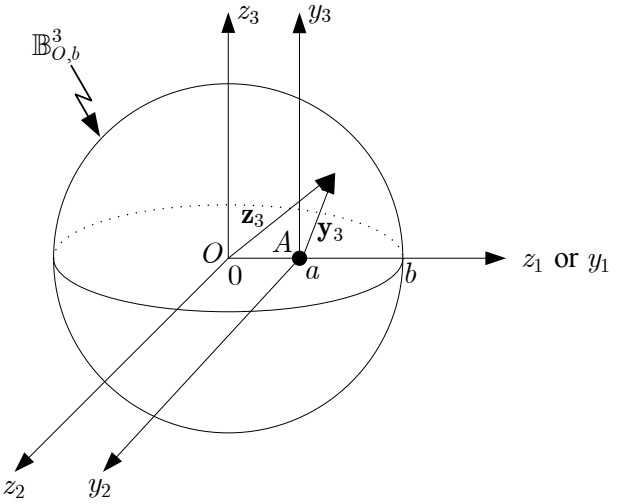

Fig. 5.1: Geometric view of $Q_m(a,b)$ for the case of $n=3$ and $m=1.5$.

of b. Since this geometric interpretation holds for any mean vector $\mathbf{p}_n$ of norm a, we can, without loss of generality, treat the mean vector as $\mathbf{p}_n = (a \;\; 0 \;\; \cdots \;\; 0)^\top$ hereafter, and this leads to $z_1 = a + y_1$, and $z_i = y_i$, $i = 2, \cdots, n$. Fig. 5.1 shows the case of $n = 3$ and $m = 1.5$, where the noise vector $\mathbf{y}_n$ is centered at the point A, i.e., ($z_1 = a$, $z_2 = \cdots = z_n = 0$). Since we have $\Pr(R > b) = \Pr(\sqrt{(a+y_1)^2 + \sum_{i=2}^n y_i^2} > b)$, it is easy to see that $Q_m(a,b)$ is also equal to the probability of $\mathbf{y}_n$ lying outside of $\mathbb{B}^n_{O,b}$. Thus, we have

$$Q_m(a,b) = 1 - \Pr\left(\mathbf{z}_n \in \mathbb{B}^n_{O,b}\right) = 1 - \Pr\left(\mathbf{y}_n \in \mathbb{B}^n_{O,b}\right). \tag{5.6}$$

In the next section, we will evaluate the probability in (5.6) first for the case of odd n, i.e., m being an odd multiple of 0.5, and then for the case of even n, i.e., m being an integer.

5.3 New Representations of $Q_m(a,b)$

To compute the probability of the vector $\mathbf{z}_n$ lying inside of $\mathbb{B}^n_{O,b}$ in (5.6), we can slice up $\mathbb{B}^n_{O,b}$ using a set of parallel $(n-1)$-flats[3] which are perpendicular to the z_1-

[3]In n-dimensional space, a p-flat has p dimensions, and is defined by $(n-p)$ independent linear equations [136, 137]. Thus, in 3-dimensional space, a p-flat specializes to a 2-dimensional

axis and defined by the equations $z_1 = a+y_1$ for each value of $y_1 \in [-(a+b),\, b-a]$. Each of these flats intersects $\mathbb{B}^n_{O,b}$ in an $(n-1)$-ball $\mathbb{B}^{n-1}_{Z_1,b'}$ which is enclosed by the $(n-1)$-dimensional hypersphere of radius $b' = \sqrt{b^2 - z_1^2}$ centered at the point Z_1, i.e., $(z_1 = a+y_1,\, z_2 = \cdots = z_n = 0)$. Since the two $(n-1)$-dimensional subvectors $\mathbf{z}'_{n-1} = (z_2\ z_3\ \cdots\ z_n)^\top$ and $\mathbf{y}'_{n-1} = (y_2\ y_3\ \cdots\ y_n)^\top$ are identical, the norm square $R'_1 = \left\|\mathbf{z}'_{n-1}\right\|^2 = \sum_{i=2}^n y_i^2$ has a central chi-square distribution with $(n-1)$ degrees of freedom with PDF [1, eq. (2.1–110)]

$$p_{R'_1}(R'_1) = \frac{1}{2^{(n-1)/2}\Gamma\left(\frac{n-1}{2}\right)} {R'_1}^{(n-3)/2} e^{-R'_1/2}, \qquad R'_1 \geq 0. \tag{5.7}$$

The conditional probability of $\mathbf{z}'_{n-1}$ lying inside $\mathbb{B}^{n-1}_{Z_1,b'}$ is given by

$$\begin{aligned}\Pr\left(\mathbf{z}'_{n-1} \in \mathbb{B}^{n-1}_{Z_1,b'} \,|z_1 = a+y_1\right) &= \Pr\left(R'_1 \leq b'^2 \,|z_1 = a+y_1\right) \\ &= \frac{1}{2^{(n-1)/2}\Gamma\left(\frac{n-1}{2}\right)} \int_0^{b^2-(a+y_1)^2} {R'_1}^{(n-3)/2} e^{-R'_1/2} dR'_1.\end{aligned} \tag{5.8}$$

The probability of $\mathbf{z}_n$ lying inside $\mathbb{B}^n_{O,b}$ is, therefore, given by

$$\Pr(\mathbf{z}_n \in \mathbb{B}^n_{O,b}) = \int_{y_1=-(a+b)}^{b-a} \left[\Pr(\mathbf{z}'_{n-1} \in \mathbb{B}^{n-1}_{Z_1,b'} \,|z_1 = a+y_1)\right] \frac{e^{-y_1^2/2}}{\sqrt{2\pi}} dy_1. \tag{5.9}$$

Substituting (5.8) into (5.9) gives

$$\begin{aligned}&\Pr(\mathbf{z}_n \in \mathbb{B}^n_{O,b}) \\ &= \frac{1}{2^{n/2}\sqrt{\pi}\Gamma\left(\frac{n-1}{2}\right)} \int_{y_1=-(a+b)}^{b-a} e^{-y_1^2/2} \int_{R'_1=0}^{b^2-(a+y_1)^2} {R'_1}^{(n-3)/2} e^{-R'_1/2} dR'_1 dy_1.\end{aligned} \tag{5.10}$$

According to (5.6), the conditional probability in (5.8) can also be written as

$$\Pr\left(\mathbf{z}'_{n-1} \in \mathbb{B}^{n-1}_{Z_1,b'} \,|z_1 = a+y_1\right) = 1 - Q_{m-0.5}\left(0, \sqrt{b^2-(a+y_1)^2}\right). \tag{5.11}$$

plane for $p = 2$, or a straight line for $p = 1$.

Using (5.6) and (5.11) in (5.9), we can obtain

$$1-Q_m(a,b)=\int_{y_1=-(a+b)}^{b-a}\left[1-Q_{m-0.5}\left(0,\sqrt{b^2-(a+y_1)^2}\right)\right]\frac{e^{-y_1^2/2}}{\sqrt{2\pi}}dy_1. \quad (5.12)$$

5.3.1 Representations for the Case of Odd n

When n is odd and thus m is an odd multiple of 0.5, $Q_{m-0.5}\left(0,\sqrt{b^2-(a+y_1)^2}\right)$ in (5.12) has a closed-form expression, given by [5, eq. (4.73)]

$$Q_{m-0.5}\left(0,\sqrt{b^2-(a+y_1)^2}\right)=\exp\left[-\frac{b^2-(a+y_1)^2}{2}\right]\sum_{k=0}^{m-1.5}\frac{1}{k!}\left[\frac{b^2-(a+y_1)^2}{2}\right]^k, \quad n=2m \text{ is odd.} \quad (5.13)$$

The mth-order Marcum Q-function is therefore given by

$$\begin{aligned}
&Q_m(a,b)\\
&=1-\int_{-(a+b)}^{b-a}\left\{1-\exp\left[-\frac{b^2-(a+y_1)^2}{2}\right]\sum_{k=0}^{m-1.5}\frac{1}{k!}\left[\frac{b^2-(a+y_1)^2}{2}\right]^k\right\}\frac{e^{-y_1^2/2}}{\sqrt{2\pi}}dy_1\\
&=\frac{1}{2}\mathrm{erfc}\left(\frac{a+b}{\sqrt{2}}\right)+\frac{1}{2}\mathrm{erfc}\left(\frac{b-a}{\sqrt{2}}\right)+\frac{1}{\sqrt{2\pi}}\exp\left(-\frac{b^2-a^2}{2}\right)\sum_{k=0}^{m-1.5}\frac{1}{2^k k!}\\
&\quad\cdot\int_{-(a+b)}^{b-a}\exp(ay_1)\left[b^2-(a+y_1)^2\right]^k dy_1, \qquad n=2m \text{ is odd.}
\end{aligned} \quad (5.14)$$

By defining $y_1'=a+y_1$ and performing some manipulations, we obtain

$$\begin{aligned}
&\int_{-(a+b)}^{b-a}\exp(ay_1)\left[b^2-(a+y_1)^2\right]^k dy_1\\
&=\exp\left(-a^2\right)\sum_{q=0}^{k}(-1)^q\binom{k}{q}b^{2(k-q)}\int_{-b}^{b}\exp(ay_1')y_1'^{2q}dy_1'\\
&=\exp\left(-a^2\right)\sum_{q=0}^{k}(-1)^q\binom{k}{q}\frac{b^{2(k-q)}(2q)!}{a^{2q+1}}\sum_{i=0}^{2q}\frac{(-ab)^i\exp(ab)-(ab)^i\exp(-ab)}{i!}.
\end{aligned} \quad (5.15)$$

In the last step of (5.15), we have used the following formula [124, eq. (2.321 2)]

$$\int e^{ax}x^n dx = e^{ax}\sum_{i=0}^{n}\frac{(-1)^{n-i}\,n!x^i}{i!a^{n-i+1}}. \tag{5.16}$$

Substituting (5.15) into (5.14) gives

$$Q_m(a,b) = \frac{1}{2}\mathrm{erfc}\left(\frac{a+b}{\sqrt{2}}\right) + \frac{1}{2}\mathrm{erfc}\left(\frac{b-a}{\sqrt{2}}\right) + \frac{1}{a\sqrt{2\pi}}\sum_{k=0}^{m-1.5}\frac{b^{2k}}{2^k}\sum_{q=0}^{k}\frac{(-1)^q\,(2q)!}{(k-q)!q!}$$
$$\cdot\left\{\sum_{i=0}^{2q}\frac{1}{(ab)^{2q-i}\,i!}\left[(-1)^i\exp\left(-\frac{(b-a)^2}{2}\right) - \exp\left(-\frac{(b+a)^2}{2}\right)\right]\right\},$$
$$a>0,\ b\geq 0,\ n=2m \text{ is odd.} \tag{5.17}$$

This new closed-form representation involves only simple exponential functions and erfc functions, and is easy to evaluate both numerically and analytically. We can see that (5.17) is valid for the entire ranges of $a>0$ and $b\geq 0$.

For the special case of $a=0$, it is easy to obtain from (5.14)

$$Q_m(0,b) = \mathrm{erfc}\left(\frac{b}{\sqrt{2}}\right) + \frac{1}{\sqrt{2\pi}}\exp\left(-\frac{b^2}{2}\right)\sum_{k=0}^{m-1.5}\frac{b^{2k+1}}{2^{k-1}}\sum_{q=0}^{k}\frac{(-1)^q}{(k-q)!q!(2q+1)},$$
$$b\geq 0,\ n=2m \text{ is odd.} \tag{5.18}$$

By using Mathematica, we obtain the following equalities

$$\sum_{q=0}^{k}\frac{(-1)^q}{(k-q)!q!(2q+1)} = \frac{\sqrt{\pi}}{2\Gamma(k+3/2)} = \frac{2^k}{(2k+1)!!}, \tag{5.19}$$

where $x!! = x(x-2)(x-4)\times\cdots$. Using these equalities in (5.18), we can reduce the expression for $Q_m(0,b)$ to

$$Q_m(0,b) = \mathrm{erfc}\left(\frac{b}{\sqrt{2}}\right) + \frac{1}{\sqrt{2}}\exp\left(-\frac{b^2}{2}\right)\sum_{k=0}^{m-1.5}\frac{b^{2k+1}}{2^k\Gamma(k+3/2)}$$
$$= \mathrm{erfc}\left(\frac{b}{\sqrt{2}}\right) + \sqrt{\frac{2}{\pi}}\exp\left(-\frac{b^2}{2}\right)\sum_{k=0}^{m-1.5}\frac{b^{2k+1}}{(2k+1)!!},$$
$$b\geq 0,\ n=2m \text{ is odd.} \tag{5.20}$$

To the best of our knowledge, this is a new closed-form result for the tail probability of a central chi-square random variable with an odd number n of degrees of freedom.

The new representation for $Q_m(a,b)$ in (5.17) can also be expressed in terms of the complementary incomplete gamma function which is defined as

$$\Gamma(s,x) = \int_x^\infty t^{s-1}e^{-t}dt. \tag{5.21}$$

This function has a closed-form expression when its first argument s is equal to a positive integer l, namely [124, eq. (8.352 2)]

$$\Gamma(l,x) = \int_x^\infty t^{l-1}e^{-t}dt = e^{-x}\sum_{k=0}^{l-1}\frac{(l-1)!}{k!}x^k. \tag{5.22}$$

Thus, (5.17) can be rewritten as

$$Q_m(a,b) = \frac{1}{2}\mathrm{erfc}\left(\frac{a+b}{\sqrt{2}}\right) + \frac{1}{2}\mathrm{erfc}\left(\frac{b-a}{\sqrt{2}}\right) + \frac{1}{a\sqrt{2\pi}}\exp\left(-\frac{b^2+a^2}{2}\right)\sum_{k=0}^{m-1.5}\frac{b^{2k}}{2^k}$$
$$\cdot\sum_{q=0}^{k}\frac{(-1)^q\left[\Gamma(2q+1,-ab)-\Gamma(2q+1,ab)\right]}{(k-q)!q!\,(ab)^{2q}},$$
$$a>0,\ b\geq 0,\ n=2m \text{ is odd.} \tag{5.23}$$

By using Mathematica, we find that $Q_m(0,b)$ in (5.20) can also be written in terms of the Gamma functions as

$$Q_m(0,b) = \frac{\Gamma(m,b^2/2)}{\Gamma(m)}. \tag{5.24}$$

This expression is the same as those in [118, eq. (10)] and [5, eq. (4.71)], and has been shown in [118] to be valid for any order m. Thus, (5.24) has two alternative closed-form expressions, one in (5.20) for m being an odd multiple of 0.5, and one in [5, eq. (4.73)], i.e.,

$$Q_m(0,b) = \sum_{i=0}^{m-1}\exp\left(-\frac{b^2}{2}\right)\frac{(b^2/2)^i}{i!}, \tag{5.25}$$

for integer m.

From (5.17) or (5.23), it is easy to see that for odd n, the generalized Marcum Q-function satisfies the recursion relation

$$Q_{m+1}(a,b) = Q_m(a,b) + \frac{b^{2m-1}}{2^m a\sqrt{\pi}} \sum_{q=0}^{m-0.5} \frac{(-1)^q (2q)!}{(m-0.5-q)!q!} \left\{ \sum_{i=0}^{2q} \frac{1}{(ab)^{2q-i} i!} \cdot \left[(-1)^i \exp\left(-\frac{(b-a)^2}{2}\right) - \exp\left(-\frac{(b+a)^2}{2}\right) \right] \right\}, \quad a>0,\ b\geq 0,\ n=2m \text{ is odd}, \tag{5.26}$$

or equivalently

$$Q_{m+1}(a,b) = Q_m(a,b) + \frac{b^{2m-1}}{2^m a\sqrt{\pi}} \exp\left(-\frac{b^2+a^2}{2}\right) \cdot \sum_{q=0}^{m-0.5} \frac{(-1)^q \left[\Gamma\left(2q+1,-ab\right) - \Gamma\left(2q+1,ab\right)\right]}{(m-0.5-q)!q!\,(ab)^{2q}}, \quad a>0,\ b\geq 0,\ n=2m \text{ is odd}. \tag{5.27}$$

In [5, eq. (4.61)], a recursion relation has been given for any order m, i.e.,

$$Q_{m+1}(a,b) = Q_m(a,b) + \left(\frac{b}{a}\right)^m \exp\left[-\left(\frac{b^2+a^2}{2}\right)\right] I_m(ab),\ a>0,\ b\geq 0. \tag{5.28}$$

Thus, the relations in (5.26) and (5.27) are the two new alternative forms of (5.28) for the case that m is an odd multiple of 0.5.

5.3.2 Representations for the Case of Even n

For the case of even n, according to (5.20), $Q_{m-0.5}\left(0, \sqrt{b^2-(a+y_1)^2}\right)$ in (5.12) can also be given a closed-form expression. Substituting this closed-form expression into (5.12) and performing some manipulations will lead to the same expression for $Q_m(a,b)$ as that in [1, eq. (2.1–122)], i.e.,

$$Q_m(a,b) = Q(a,b) + \exp\left(-\frac{b^2+a^2}{2}\right) \sum_{k=1}^{m-1} \left(\frac{b}{a}\right)^k I_k(ab). \tag{5.29}$$

Here, we use another approach, i.e., using the probability in (5.10), to derive a pair of new representations of $Q_m(a,b)$ involving only finite-range integrals. By defining $R' = \sqrt{R'_1}$, we can rewrite (5.10) as

$$\begin{aligned}&\Pr(\mathbf{z}_n \in \mathbb{B}^n_{O,b})\\ &= \frac{1}{2^{m-1}\sqrt{\pi}\Gamma\left(m-\frac{1}{2}\right)} \int_{y_1=-(a+b)}^{b-a} \int_{R'=0}^{\sqrt{b^2-(a+y_1)^2}} {R'}^{2(m-1)} \exp\left(-\frac{y_1^2+{R'}^2}{2}\right) dR' dy_1.\end{aligned} \tag{5.30}$$

In the polar coordinate system, we define $r = \sqrt{y_1^2 + {R'}^2}$ and $\theta = \arctan\left(R'/y_1\right)$. Thus, (5.30) can be rewritten as

$$\Pr(\mathbf{z}_n \in \mathbb{B}^n_{O,b}) = \frac{1}{2^{m-1}\sqrt{\pi}\Gamma\left(m-\frac{1}{2}\right)} \int_{\theta=\theta_1}^{\theta_2} \int_{r=l_1(\theta)}^{l_2(\theta)} \left(r\sin\theta\right)^{2(m-1)} \exp\left(-\frac{r^2}{2}\right) r dr d\theta. \tag{5.31}$$

Here, for the case of $b \geq a$, we have $\theta_1 = 0$, $\theta_2 = \pi$, and

$$\begin{cases} l_1(\theta) = 0, \\ l_2(\theta) = -a\cos\theta + \sqrt{b^2 - a^2\sin^2\theta}. \end{cases} \tag{5.32}$$

For the case of $a \geq b$, we have $\theta_1 = \pi - \arcsin(b/a)$, $\theta_2 = \pi$, and

$$\begin{cases} l_1(\theta) = -a\cos\theta - \sqrt{b^2 - a^2\sin^2\theta}, \\ l_2(\theta) = -a\cos\theta + \sqrt{b^2 - a^2\sin^2\theta}. \end{cases} \tag{5.33}$$

By defining $r' = r^2/2$ and using (5.16), (5.31) can be reduced as

$$\begin{aligned}\Pr(\mathbf{z}_n \in \mathbb{B}^n_{O,b}) &= \frac{1}{\sqrt{\pi}\Gamma\left(m-\frac{1}{2}\right)} \int_{\theta=\theta_1}^{\theta_2} \sin^{2(m-1)}\theta \int_{r'=l_1^2(\theta)/2}^{l_2^2(\theta)/2} r'^{(m-1)} \exp\left(-r'\right) dr' d\theta \\ &= \frac{\Gamma(m)}{\sqrt{\pi}\Gamma\left(m-\frac{1}{2}\right)} \int_{\theta=\theta_1}^{\theta_2} \sin^{2(m-1)}\theta \left\{ \exp\left[-\frac{l_1^2(\theta)}{2}\right] \sum_{k=0}^{m-1} \frac{1}{k!} \left[\frac{l_1^2(\theta)}{2}\right]^k \right. \\ &\quad \left. - \exp\left[-\frac{l_2^2(\theta)}{2}\right] \sum_{k=0}^{m-1} \frac{1}{k!} \left[\frac{l_2^2(\theta)}{2}\right]^k \right\} d\theta.\end{aligned} \tag{5.34}$$

Thus, for the case of $b \geq a \geq 0$, the new representation of $Q_m(a,b)$ is given by

$$\begin{aligned} & Q_m(a,b) \\ &= 1 - \frac{\Gamma(m)}{\sqrt{\pi}\Gamma\left(m-\frac{1}{2}\right)} \int_{\theta=0}^{\pi} \sin^{2(m-1)}\theta \left\{ 1 - \exp\left[-\frac{l_2^2(\theta)}{2}\right] \sum_{k=0}^{m-1} \frac{1}{k!} \left[\frac{l_2^2(\theta)}{2}\right]^k \right\} d\theta \\ &= \frac{\Gamma(m)}{\sqrt{\pi}\Gamma\left(m-\frac{1}{2}\right)} \int_{\theta=0}^{\pi} \sin^{2(m-1)}\theta \exp\left[-\frac{l_2^2(\theta)}{2}\right] \sum_{k=0}^{m-1} \frac{1}{k!} \left[\frac{l_2^2(\theta)}{2}\right]^k d\theta, \\ & \qquad\qquad b \geq a \geq 0, \text{ integer } m. \end{aligned} \tag{5.35}$$

Here, we have used the formulas in [124, eqs. (3.621 3) and (2.513 1)], i.e.,

$$\int_{\theta=0}^{\pi/2} \sin^{2n}\theta d\theta = \frac{(2n-1)!!\pi}{(2n)!!2} = \frac{\pi}{2^{2n+1}} \binom{2n}{n} = \frac{\sqrt{\pi}\Gamma(n+\frac{1}{2})}{2\Gamma(n+1)}. \tag{5.36}$$

For the case of $a \geq b \geq 0$, the new representation of $Q_m(a,b)$ is given by

$$\begin{aligned} & Q_m(a,b) \\ &= 1 - \frac{\Gamma(m)}{\sqrt{\pi}\Gamma\left(m-\frac{1}{2}\right)} \int_{\theta=\pi-\arcsin(b/a)}^{\pi} \sin^{2(m-1)}\theta \left\{ \exp\left[-\frac{l_1^2(\theta)}{2}\right] \sum_{k=0}^{m-1} \frac{1}{k!} \left[\frac{l_1^2(\theta)}{2}\right]^k \right. \\ & \quad \left. - \exp\left[-\frac{l_2^2(\theta)}{2}\right] \sum_{k=0}^{m-1} \frac{1}{k!} \left[\frac{l_2^2(\theta)}{2}\right]^k \right\} d\theta, \qquad a \geq b \geq 0, \text{ integer } m. \end{aligned} \tag{5.37}$$

There are another two pairs of alternative finite-integral representations available in the literature. The first pair was given in [113, eq. (C-26)], i.e.,

$$Q_m(a,b) = \frac{a}{2\pi}\left(\frac{b}{a}\right)^m \int_0^{2\pi} \frac{b\cos(m-1)\theta - a\cos m\theta}{a^2 - 2ab\cos\theta + b^2} \exp\left[-\frac{b^2 - 2ab\cos\theta + a^2}{2}\right] d\theta, \quad b > a > 0, \tag{5.38}$$

and in [113, eq. (C-27)], i.e.,

$$\begin{aligned} & Q_m(a,b) \\ &= 1 + \frac{a}{2\pi}\left(\frac{b}{a}\right)^m \int_0^{2\pi} \frac{b\cos(m-1)\theta - a\cos m\theta}{a^2 - 2ab\cos\theta + b^2} \exp\left[-\frac{b^2 - 2ab\cos\theta + a^2}{2}\right] d\theta, \\ & \qquad\qquad a > b \geq 0. \end{aligned} \tag{5.39}$$

The second pair was given in [114, eq. (7)] or equivalently in [5, eq. (4.69)], i.e.,

$$Q_m(b\zeta, b) = \frac{1}{2\pi}\int_{-\pi}^{\pi} \frac{\zeta^{-(m-1)}\left\{\cos\left[(m-1)\left(\theta+\frac{\pi}{2}\right)\right] - \zeta\cos\left[m\left(\theta+\frac{\pi}{2}\right)\right]\right\}}{1+2\zeta\sin\theta+\zeta^2} \cdot \exp\left[-\frac{b^2}{2}\left(1+2\zeta\sin\theta+\zeta^2\right)\right] d\theta, \qquad 0^+ \le \zeta = \frac{a}{b} < 1, \quad (5.40)$$

and in [114, eq. (10)] or equivalently in [5, eq. (4.77)], i.e.,

$$Q_m(a, a\zeta) = 1 - \frac{1}{2\pi}\int_{-\pi}^{\pi} \frac{\zeta^{m}\left\{\cos\left[m\left(\theta+\frac{\pi}{2}\right)\right] - \zeta\cos\left[(m-1)\left(\theta+\frac{\pi}{2}\right)\right]\right\}}{1+2\zeta\sin\theta+\zeta^2} \cdot \exp\left[-\frac{a^2}{2}\left(1+2\zeta\sin\theta+\zeta^2\right)\right] d\theta, \qquad 0 \le \zeta = \frac{b}{a} < 1. \quad (5.41)$$

The integration interval in (5.37) is not greater than $\pi/2$, and thus, is less than that in (5.39) and (5.41). Besides, in the new representations in (5.35) and (5.37), the integrands are always determinate, since the arguments a, b, and θ appear only in the numerators. By contrast, in the existing representations given in (5.38) through (5.41), the denominators of the integrands may be close to zero for some combinations of the arguments. Thus, our new representations are more robust than these existing representations.

Thus far, $Q_m(a, b)$ of integer order m cannot be given a closed-form representation which only involves some elementary functions, such as the exponential and erfc functions. The representations available are not simple to use in obtaining closed-form analytical results in some further manipulations of $Q_m(a, b)$. In Sections 5.4 and 5.5, we derive some closed-form bounds for $Q_m(a, b)$ of integer order m, which may facilitate some theoretical analyses involving $Q_m(a, b)$.

5.4 New Exponential Bounds for $Q_m(a, b)$ of Integer Order m

In this section, we derive new, generic, exponential bounds for $Q_m(a, b)$, which involve only exponential functions and have an arbitrarily large number of terms.

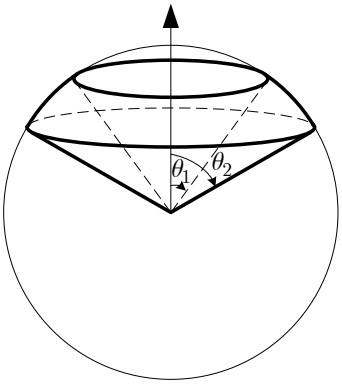

Fig. 5.2: Diagram of a spherical sector.

5.4.1 Bounds for the Case of $b \geq a \geq 0$

A generic, upper, exponential bound on $Q_m(a, b)$ can be obtained by using a set of contiguous, hyperspherical sectors[4] to fill the hyperball $\mathbb{B}^n_{O,b}$, as shown by the solid lines inside $\mathbb{B}^n_{O,b}$ in Fig. 5.3(a). The axes of these hyperspherical sectors all lie on the z_1-axis, or, equivalently, the y_1-axis, and their vertices all lie on the point A, i.e., $(z_1 = a, z_2 = \cdots = z_n = 0)$ or $(y_1 = y_2 = \cdots = y_n = 0)$. Each of them covers one of N angular ranges defined by $0 = \theta_0 < \theta_1 < \cdots < \theta_N = \pi$. We use $\mathbb{B}^n_{A,l_2(\theta),\theta_1,\theta_2}$ to denote a hyperspherical sector which covers the angular range $[\theta_1, \theta_2]$ of the n-ball $\mathbb{B}^n_{A,l_2(\theta)}$ centered at the point A and with the radius $l_2(\theta)$ defined in (5.32). Thus, for the generic upper exponential bound, the ith hyperspherical sector in the bounding shape is denoted as $\mathbb{B}^n_{A,l_2(\theta_{i-1}),\theta_{i-1},\theta_i}$. The probability of $\mathbf{z}_n$ lying inside $\mathbb{B}^n_{A,l_2(\theta_{i-1}),\theta_{i-1},\theta_i}$ is given by the probability $\Pr(\mathbf{z}_n \in \mathbb{B}^n_{A,l_2(\theta_{i-1})}) = [1 - Q_m(0, l_2(\theta_{i-1}))]$ times the ratio of the surface content of the region on the surface of $\mathbb{B}^n_{A,l(\theta_{i-1})}$ which is demarcated by $\mathbb{B}^n_{A,l(\theta_{i-1}),\theta_{i-1},\theta_i}$ to the surface content

[4]In 3-dimensional Euclidean space, a spherical sector is a part of a ball, and is a solid of revolution with the same axis as the ball [141], as shown in Fig. 5.2. Its intersection with the half-plane starting from its axis is a sector bounded by two radii of the ball and the arc in between them. If the angles between the positive axis of the ball and the two radii are denoted as θ_1 and θ_2, then they satisfy $0 \leq \theta_1, \theta_2 \leq \pi$ and $0 \leq \theta_2 - \theta_1 \leq \pi$. We say that this spherical sector covers the angular range $[\theta_1, \theta_2]$ of the ball. If we have $\theta_1 = 0$ and $\theta_2 = \pi$, the spherical sector covers the whole ball. This concept can be extended straightforwardly to n-dimensional Euclidean space. A hyperspherical sector is the part of an n-ball between the two hypersurfaces formed by rotating two radii around the axis. If the angles between the positive axis of the n-ball and the two radii are θ_1 and θ_2, we say that this hyperspherical sector covers the angular range $[\theta_1, \theta_2]$ of the n-ball.

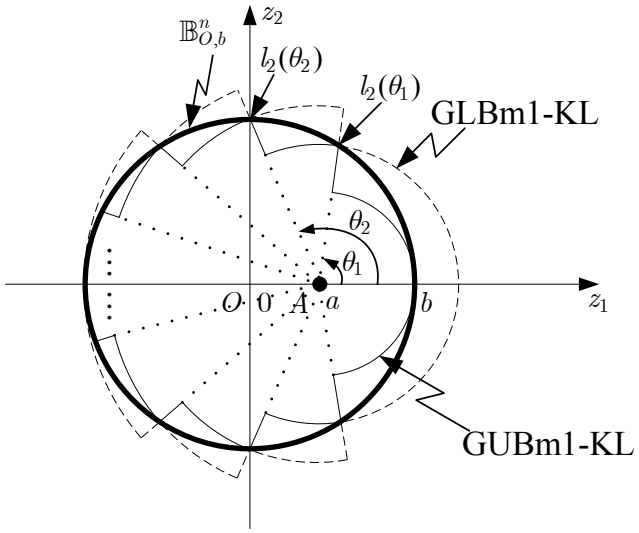

(a) GUBm1-KL and GLBm1-KL for the case of $b > a$

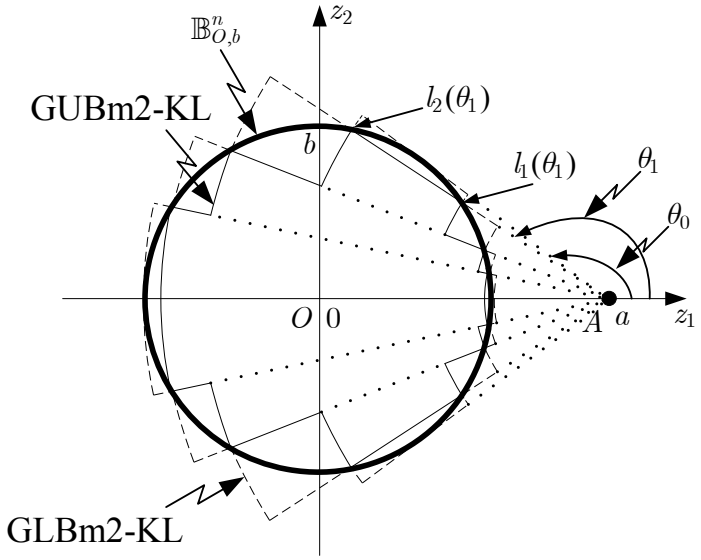

(b) GUBm2-KL and GLBm2-KL for the case of $a > b$

Fig. 5.3: Diagram of the derivation of the new generic exponential bounds on $Q_m(a, b)$.

of the entire n-ball $\mathbb{B}^n_{A,l_2(\theta_{i-1})}$ [138, eq. (4.1)]. As we have mentioned in Section 5.3.1, the expression for $Q_m(0, b)$ is given in closed form in (5.20) for odd n and in (5.25) for even n. Here, n is even, and thus, we have

$$\begin{aligned}&\Pr(\mathbf{z}_n \in \mathbb{B}^n_{A,l_2(\theta_{i-1}),\theta_{i-1},\theta_i}) \\ &= \frac{\int_{\theta_{i-1}}^{\theta_i} S_{n-1}(\sin\theta)d\theta}{S_n(1)} \left\{1 - \exp\left[-\frac{l_2^2\left(\theta_{i-1}\right)}{2}\right] \sum_{k=0}^{m-1} \frac{1}{k!} \left[\frac{l_2^2\left(\theta_{i-1}\right)}{2}\right]^k\right\}, \quad (5.42)\end{aligned}$$

where $S_n(c)$ is the surface content of an n-sphere with radius c, i.e., [137, pg. 136]

$$S_n(c) = \frac{2\pi^{n/2}c^{n-1}}{\Gamma\left(\frac{n}{2}\right)}. \tag{5.43}$$

Using (5.43) in (5.42), we obtain

$$\begin{aligned}
&\Pr(\mathbf{z}_n \in \mathbb{B}^n_{A,l_2(\theta_{i-1}),\theta_{i-1},\theta_i}) \\
&= \frac{\Gamma(m)\int_{\theta_{i-1}}^{\theta_i}\sin^{2(m-1)}\theta d\theta}{\sqrt{\pi}\Gamma\left(m-\frac{1}{2}\right)}\left\{1-\exp\left[-\frac{l_2^2\left(\theta_{i-1}\right)}{2}\right]\sum_{k=0}^{m-1}\frac{1}{k!}\left[\frac{l_2^2\left(\theta_{i-1}\right)}{2}\right]^k\right\}.
\end{aligned} \tag{5.44}$$

The integral in (5.44) can be solved by using [124, eq. 2.513 1]

$$\int \sin^{2n}\theta d\theta = \frac{\theta}{2^{2n}}\binom{2n}{n} + \frac{(-1)^n}{2^{2n-1}}\sum_{i=0}^{n-1}(-1)^i\binom{2n}{i}\frac{\sin[(2n-2i)\theta]}{2n-2i}. \tag{5.45}$$

Thus, we obtain our first generic upper bound on $Q_m(a,b)$, denoted as GUBm1-KL, namely

$$\begin{aligned}
Q_m(a,b) &\leq Q_{GUBm1\text{-}KL}(a,b) \\
&= 1-\sum_{i=1}^{N}\Pr(\mathbf{z}_n \in \mathbb{B}^n_{A,l_2(\theta_{i-1}),\theta_{i-1},\theta_i}) \\
&= \sum_{i=1}^{N}\frac{\Gamma(m)\int_{\theta_{i-1}}^{\theta_i}\sin^{2(m-1)}\theta d\theta}{\sqrt{\pi}\Gamma\left(m-\frac{1}{2}\right)}\left\{\exp\left[-\frac{l_2^2\left(\theta_{i-1}\right)}{2}\right]\sum_{k=0}^{m-1}\frac{1}{k!}\left[\frac{l_2^2\left(\theta_{i-1}\right)}{2}\right]^k\right\} \\
&= \sum_{i=1}^{N}\left\{\frac{\theta_i-\theta_{i-1}}{\pi}+\sum_{j=0}^{m-2}\frac{(-1)^{m-1-j}\binom{2m-2}{j}}{\pi\binom{2m-2}{m-1}}\right. \\
&\quad \left.\cdot\frac{\sin[2(m-1-j)\theta_i]-\sin[2(m-1-j)\theta_{i-1}]}{m-1-j}\right\} \\
&\quad \cdot\left\{\exp\left[-\frac{l_2^2\left(\theta_{i-1}\right)}{2}\right]\sum_{k=0}^{m-1}\frac{1}{k!}\left[\frac{l_2^2\left(\theta_{i-1}\right)}{2}\right]^k\right\}, b\geq a\geq 0,\ m \text{ integer.}
\end{aligned} \tag{5.46}$$

Here, we have $0=\theta_0<\theta_1<\cdots<\theta_N=\pi$. The bound GUBm1-KL in (5.46) on $Q_m(a,b)$ reduces to the bound GUB1-KL in (4.28) on $Q(a,b)$ when $m=1$.

When we set $N=1$ in (5.46), the generic upper bound GUBm1-KL reduces

to

$$Q_m(a,b) \leq \exp\left[-\frac{(b-a)^2}{2}\right] \sum_{k=0}^{m-1} \frac{1}{k!} \left[\frac{(b-a)^2}{2}\right]^k, \qquad b \geq a \geq 0,\ m \text{ integer.} \tag{5.47}$$

This upper bound uses the n-ball $\mathbb{B}^n_{A,b-a}$ as the bounding shape.

When we set $N = 2$ and $\theta_1 = \pi/2$ in (5.46), GUBm1-KL reduces to

$$\begin{aligned} Q_m(a,b) \leq \frac{1}{2} \Bigg\{ & \exp\left[-\frac{(b-a)^2}{2}\right] \sum_{k=0}^{m-1} \frac{1}{k!} \left[\frac{(b-a)^2}{2}\right]^k \\ & + \exp\left[-\frac{b^2-a^2}{2}\right] \sum_{k=0}^{m-1} \frac{1}{k!} \left[\frac{b^2-a^2}{2}\right]^k \Bigg\}, \qquad b \geq a \geq 0,\ m \text{ integer.} \end{aligned} \tag{5.48}$$

This upper bound uses the combination of two semi-hyperballs, $\mathbb{B}^n_{A,b-a}$ and $\mathbb{B}^n_{A,\sqrt{b^2-a^2}}$, as the bounding shape.

Similarly, a generic, lower, exponential bound can be obtained by using a set of contiguous hyperspherical sectors to cover the hyperball $\mathbb{B}^n_{O,b}$, as shown by the dashed lines outside $\mathbb{B}^n_{O,b}$ in Fig. 5.3(a). Here, the ith hyperspherical sector is denoted as $\mathbb{B}^n_{A,l_2(\theta_i),\theta_{i-1},\theta_i}$ which covers the angular range $[\theta_{i-1}, \theta_i]$ of the n-ball $\mathbb{B}^n_{A,l_2(\theta_i)}$. The probability of $\mathbf{z}_n$ lying inside $\mathbb{B}^n_{A,l_2(\theta_i),\theta_{i-1},\theta_i}$ is given by

$$\begin{aligned} & \Pr(\mathbf{z}_n \in \mathbb{B}^n_{A,l_2(\theta_i),\theta_{i-1},\theta_i}) \\ &= \frac{\int_{\theta_{i-1}}^{\theta_i} S_{n-1}(\sin\theta) d\theta}{S_n(1)} \left\{1 - \exp\left[-\frac{l_2^2(\theta_i)}{2}\right] \sum_{k=0}^{m-1} \frac{1}{k!} \left[\frac{l_2^2(\theta_i)}{2}\right]^k \right\} \\ &= \frac{\Gamma(m) \int_{\theta_{i-1}}^{\theta_i} \sin^{2(m-1)}\theta d\theta}{\sqrt{\pi}\Gamma\left(m-\frac{1}{2}\right)} \left\{1 - \exp\left[-\frac{l_2^2(\theta_i)}{2}\right] \sum_{k=0}^{m-1} \frac{1}{k!} \left[\frac{l_2^2(\theta_i)}{2}\right]^k \right\}. \end{aligned} \tag{5.49}$$

Then our first generic lower bound on $Q_m(a,b)$, denoted as GLBm1-KL, is given

by

$$
\begin{aligned}
Q_m(a,b) &\geq Q_{GLBm1\text{-}KL}(a,b) \\
&= 1 - \sum_{i=1}^{N} \Pr(\mathbf{z}_n \in \mathbb{B}^n_{A,l_2(\theta_i),\theta_{i-1},\theta_i}) \\
&= \sum_{i=1}^{N} \frac{\Gamma(m) \int_{\theta_{i-1}}^{\theta_i} \sin^{2(m-1)} \theta d\theta}{\sqrt{\pi}\Gamma\left(m-\frac{1}{2}\right)} \left\{ \exp\left[-\frac{l_2^2(\theta_i)}{2}\right] \sum_{k=0}^{m-1} \frac{1}{k!} \left[\frac{l_2^2(\theta_i)}{2}\right]^k \right\} \\
&= \sum_{i=1}^{N} \left\{ \frac{\theta_i - \theta_{i-1}}{\pi} + \sum_{j=0}^{m-2} \frac{(-1)^{m-1-j}\binom{2m-2}{j}}{\pi\binom{2m-2}{m-1}} \right. \\
&\quad \left. \cdot \frac{\sin[2(m-1-j)\theta_i] - \sin[2(m-1-j)\theta_{i-1}]}{m-1-j} \right\} \\
&\quad \cdot \left\{ \exp\left[-\frac{l_2^2(\theta_i)}{2}\right] \sum_{k=0}^{m-1} \frac{1}{k!} \left[\frac{l_2^2(\theta_i)}{2}\right]^k \right\}, b \geq a \geq 0,\ m \text{ integer.} \quad (5.50)
\end{aligned}
$$

Here, we also have $0 = \theta_0 < \theta_1 < \cdots < \theta_N = \pi$. The bound GLBm1-KL in (5.50) on $Q_m(a,b)$ reduces to the bound GLB1-KL in (4.29) on $Q(a,b)$ when $m = 1$.

When we set $N = 1$ in (5.50), the generic lower bound GLBm1-KL reduces to

$$
Q_m(a,b) \geq \exp\left[-\frac{(b+a)^2}{2}\right] \sum_{k=0}^{m-1} \frac{1}{k!} \left[\frac{(b+a)^2}{2}\right]^k, \qquad b \geq a \geq 0,\ m \text{ integer.} \quad (5.51)
$$

This lower bound uses the hyperball $\mathbb{B}^n_{A,b+a}$ as the bounding shape.

When we set $N = 2$ and $\theta_1 = \pi/2$ in (5.50), GLBm1-KL reduces to

$$
\begin{aligned}
&Q_m(a,b) \\
&\geq \frac{1}{2} \left\{ \exp\left[-\frac{b^2-a^2}{2}\right] \sum_{k=0}^{m-1} \frac{1}{k!} \left[\frac{b^2-a^2}{2}\right]^k + \exp\left[-\frac{(b+a)^2}{2}\right] \sum_{k=0}^{m-1} \frac{1}{k!} \left[\frac{(b+a)^2}{2}\right]^k \right\}, \\
&\qquad\qquad b \geq a \geq 0,\ m \text{ integer.} \quad (5.52)
\end{aligned}
$$

This lower bound uses the combination of two semi-hyperballs, $\mathbb{B}^n_{A,\sqrt{b^2-a^2}}$ and $\mathbb{B}^n_{A,b+a}$, as the bounding shape.

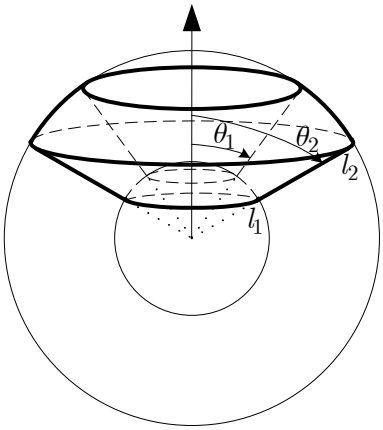

Fig. 5.4: Diagram of a spherical annulus.

5.4.2 Bounds for the Case of $a \geq b \geq 0$ and $a \neq 0$

For this case, since the point A is outside of $\mathbb{B}^n_{O,b}$, we have to use a set of contiguous, hyperspherical annuli[5], instead of hyperspherical sectors, to construct a bounding shape. We use $\mathbb{B}^n_{A,l_1(\theta),l_2(\theta),\theta_1,\theta_2}$ to denote a hyperspherical annulus which covers the angular range $[\theta_1, \theta_2]$ of the n-dimensional hollow ball $\mathbb{B}^n_{A,l_1(\theta),l_2(\theta)}$ which is centered at the point A and has inner radius $l_1(\theta)$ and outer radius $l_2(\theta)$ defined in (5.33). We first define $\pi - \arcsin(b/a) = \theta_0 < \theta_1 < \cdots < \theta_N = \pi$, and derive the upper generic exponential bound. As shown by the solid lines inside $\mathbb{B}^n_{O,b}$ in Fig. 5.3(b), the ith hyperspherical annulus can be denoted as $\mathbb{B}^n_{A,l_1(\theta_i),l_2(\theta_i),\theta_i,\theta_{i+1}}$.

[5]In 3-dimensional Euclidean space, a spherical shell is the region between two concentric spheres of different radii [142]. We define a spherical annulus as an angular sector of a spherical shell with inner radius l_1 and outer radius l_2, as shown in Fig. 5.4, which is a solid of revolution with the same axis as the spherical shell. The intersection of this spherical annulus with the half-plane starting from its axis is an angular sector of an annulus bounded by two radii of the shell and the two arcs in between them. If the angles between the positive axis of the spherical annulus and the two radii are denoted as θ_1 and θ_2, then we say that this spherical annulus covers the angular range $[\theta_1, \theta_2]$ of the spherical shell. This concept can be extended straightforwardly to n-dimensional Euclidean space. A hyperspherical annulus is defined as the part of an n-dimensional hollow ball, with inner radius l_1 and outer radius l_2, between the two hypersurfaces formed by rotating two radii around the axis. If the angles between the positive axis of the hyperspherical annulus and the two radii are θ_1 and θ_2, we say that this hyperspherical annulus covers the angular range $[\theta_1, \theta_2]$ of the n-dimensional hollow ball.

Similar to (5.42), the probability of $\mathbf{z}_n$ lying inside $\mathbb{B}^n_{A,l_1(\theta_i),l_2(\theta_i),\theta_i,\theta_{i+1}}$ is given by

$$\begin{aligned}
&\Pr(\mathbf{z}_n \in \mathbb{B}^n_{A,l_1(\theta_i),l_2(\theta_i),\theta_i,\theta_{i+1}}) \\
&= \frac{\int_{\theta_i}^{\theta_{i+1}} S_{n-1}(\sin\theta)d\theta}{S_n(1)} \left\{ \exp\left[-\frac{l_1^2(\theta_i)}{2}\right] \sum_{k=0}^{m-1} \frac{1}{k!} \left[\frac{l_1^2(\theta_i)}{2}\right]^k \right. \\
&\quad \left. - \exp\left[-\frac{l_2^2(\theta_i)}{2}\right] \sum_{k=0}^{m-1} \frac{1}{k!} \left[\frac{l_2^2(\theta_i)}{2}\right]^k \right\}. \qquad (5.53)
\end{aligned}$$

Thus, we obtain our second generic upper bound on $Q_m(a,b)$, denoted as GUBm2-KL, namely

$$\begin{aligned}
&Q_m(a,b) \\
&\le Q_{GUBm2\text{-}KL}(a,b) \\
&= 1 - \sum_{i=1}^{N-1} \Pr(\mathbf{z}_n \in \mathbb{B}^n_{A,l_1(\theta_i),l_2(\theta_i),\theta_i,\theta_{i+1}}) \\
&= 1 - \sum_{i=1}^{N-1} \frac{\int_{\theta_i}^{\theta_{i+1}} S_{n-1}(\sin\theta)d\theta}{S_n(1)} \left\{ \exp\left[-\frac{l_1^2(\theta_i)}{2}\right] \sum_{k=0}^{m-1} \frac{1}{k!} \left[\frac{l_1^2(\theta_i)}{2}\right]^k \right. \\
&\quad \left. - \exp\left[-\frac{l_2^2(\theta_i)}{2}\right] \sum_{k=0}^{m-1} \frac{1}{k!} \left[\frac{l_2^2(\theta_i)}{2}\right]^k \right\} \\
&= 1 - \sum_{i=1}^{N-1} \left\{ \frac{\theta_{i+1}-\theta_i}{\pi} + \sum_{j=0}^{m-2} \frac{(-1)^{m-1-j}\binom{2m-2}{j}}{\pi\binom{2m-2}{m-1}} \right. \\
&\quad \left. \cdot \frac{\sin[2(m-1-j)\theta_{i+1}] - \sin[2(m-1-j)\theta_i]}{m-1-j} \right\} \\
&\quad \cdot \left\{ \exp\left[-\frac{l_1^2(\theta_i)}{2}\right] \sum_{k=0}^{m-1} \frac{1}{k!} \left[\frac{l_1^2(\theta_i)}{2}\right]^k - \exp\left[-\frac{l_2^2(\theta_i)}{2}\right] \sum_{k=0}^{m-1} \frac{1}{k!} \left[\frac{l_2^2(\theta_i)}{2}\right]^k \right\}, \\
&\qquad\qquad a \ge b \ge 0,\ a \ne 0,\ m \text{ integer}. \qquad (5.54)
\end{aligned}$$

Here, we have $\pi - \arcsin(b/a) = \theta_0 < \theta_1 < \cdots < \theta_N = \pi$. The bound GUBm2-KL in (5.54) on $Q_m(a,b)$ reduces to the bound GUB2-KL in (4.32) on $Q(a,b)$ when $m = 1$.

Similarly, for the lower bound, the ith hyperspherical annulus, denoted as $\mathbb{B}^n_{A,l_1(\theta_i),l_2(\theta_i),\theta_{i-1},\theta_i}$, covers the angular range $[\theta_{i-1},\theta_i]$ of the n-dimensional hollow

ball $\mathbb{B}^n_{A,l_1(\theta_i),l_2(\theta_i)}$, as shown by the dashed lines outside $\mathbb{B}^n_{O,b}$ in Fig. 5.3(b). The probability of $\mathbf{z}_n$ lying inside $\mathbb{B}^n_{A,l_1(\theta_i),l_2(\theta_i),\theta_{i-1},\theta_i}$ is given by

$$\Pr(\mathbf{z}_n \in \mathbb{B}^n_{A,l_1(\theta_i),l_2(\theta_i),\theta_{i-1},\theta_i}) = \frac{\int_{\theta_{i-1}}^{\theta_i} S_{n-1}(\sin\theta)d\theta}{S_n(1)} \Bigg\{ \exp\left[-\frac{l_1^2(\theta_i)}{2}\right] \sum_{k=0}^{m-1} \frac{1}{k!}\left[\frac{l_1^2(\theta_i)}{2}\right]^k - \exp\left[-\frac{l_2^2(\theta_i)}{2}\right] \sum_{k=0}^{m-1} \frac{1}{k!}\left[\frac{l_2^2(\theta_i)}{2}\right]^k \Bigg\}. \tag{5.55}$$

Thus, our second generic lower bound on $Q_m(a,b)$, denoted as GLBm2-KL, is given by

$$\begin{aligned}
&Q_m(a,b) \\
&\geq Q_{GLBm2\text{-}KL}(a,b) \\
&= 1 - \sum_{i=1}^{N} \Pr(\mathbf{z}_n \in \mathbb{B}^n_{A,l_1(\theta_i),l_2(\theta_i),\theta_{i-1},\theta_i}) \\
&= 1 - \sum_{i=1}^{N} \frac{\int_{\theta_{i-1}}^{\theta_i} S_{n-1}(\sin\theta)d\theta}{S_n(1)} \Bigg\{ \exp\left[-\frac{l_1^2(\theta_i)}{2}\right] \sum_{k=0}^{m-1} \frac{1}{k!}\left[\frac{l_1^2(\theta_i)}{2}\right]^k \\
&\quad - \exp\left[-\frac{l_2^2(\theta_i)}{2}\right] \sum_{k=0}^{m-1} \frac{1}{k!}\left[\frac{l_2^2(\theta_i)}{2}\right]^k \Bigg\} \\
&= 1 - \sum_{i=1}^{N} \Bigg\{ \frac{\theta_i - \theta_{i-1}}{\pi} + \sum_{j=0}^{m-2} \frac{(-1)^{m-1-j}\binom{2m-2}{j}}{\pi\binom{2m-2}{m-1}} \\
&\quad \cdot \frac{\sin[2(m-1-j)\theta_i] - \sin[2(m-1-j)\theta_{i-1}]}{m-1-j} \Bigg\} \\
&\quad \cdot \Bigg\{ \exp\left[-\frac{l_1^2(\theta_i)}{2}\right] \sum_{k=0}^{m-1} \frac{1}{k!}\left[\frac{l_1^2(\theta_i)}{2}\right]^k - \exp\left[-\frac{l_2^2(\theta_i)}{2}\right] \sum_{k=0}^{m-1} \frac{1}{k!}\left[\frac{l_2^2(\theta_i)}{2}\right]^k \Bigg\}, \\
&\qquad\qquad a \geq b \geq 0,\ a \neq 0,\ m \text{ integer.}
\end{aligned} \tag{5.56}$$

Here, we have $\pi - \arcsin(b/a) = \theta_0 < \theta_1 < \cdots < \theta_N = \pi$. The bound GLBm2-KL in (5.56) on $Q_m(a,b)$ reduces to the bound GLB2-KL in (4.34) on $Q(a,b)$ when $m = 1$.

From the geometrical interpretation of these generic bounds, it is clear that as the number of hyperspherical sectors or hyperspherical annuli used in the bounding

shapes increases, the closeness of fit of the bounding shapes with the hyperball $\mathbb{B}^n_{O,b}$ improves, and thus our generic bounds become tighter and tighter, approaching the exact value of $Q_m(a,b)$.

5.5 New Erfc Bounds for $Q_m(a,b)$ of Integer Order m

In this section, we present some erfc bounds for $Q_m(a,b)$ of integer order m. We give two types of erfc bounds, one from the new representation of $Q_m(a,b)$ for odd n given in Section 5.3.1, and the other from the geometrical bounding shapes.

5.5.1 Bounds from the New Representation of $Q_m(a,b)$ for Odd n

We first prove the inequality

$$Q_m(a,b) < Q_{m+0.5}(a,b), \quad \forall\, m = 0.5n,\ n \in \mathbb{N}. \tag{5.57}$$

This inequality can be proved by using a mathematical approach or a geometric approach. Here, we use a geometric approach, which enables us to discuss the difference between $Q_m(a,b)$ and $Q_{m+0.5}(a,b)$ geometrically.

According to in (5.6), for any $n \in \mathbb{N}$ and $m = 0.5n$, $Q_{m+0.5}(a,b)$ is equal to the probability of the $(n+1)$-dimensional vector $\mathbf{z}_{n+1}$ lying outside of the $(n+1)$-ball $\mathbb{B}^{n+1}_{O,b}$, where O is defined by $(z_1 = z_2 = \cdots = z_{n+1} = 0)$, that is, in $(n+1)$-dimensional space, we have

$$Q_{m+0.5}(a,b) = 1 - \Pr\left(\mathbf{z}_{n+1} \in \mathbb{B}^{n+1}_{O,b}\right). \tag{5.58}$$

Now we consider the geometric interpretation of $Q_m(a,b)$ in $(n+1)$-dimensional space. We define $\mathbb{C}^n_{C,\iota,\mu_1,\mu_2}$ as an n-spherical cylinder[6]. Here, C is the axis of the

[6]A hyperspherical cylinder in n-dimensional space, also known as an n-spherical cylinder, is

n-spherical cylinder, defined by $(n-1)$ linear equations. Thus, C is a straight line in n-dimensional space and a point in $(n-1)$-dimensional space. This n-spherical cylinder intersects the $(n-1)$-flats perpendicular to the axis C in $\mathbb{B}^{n-1}_{C,t}$, and extends from μ_1 to μ_2 along C. Using this definition, $Q_m(a,b)$ can be represented, in $(n+1)$-dimensional space, as the probability of $\mathbf{z}_{n+1}$ lying outside of the hyperspherical cylinder $\mathbb{C}^{n+1}_{O,b,-\infty,\infty}$, where O is defined by $(z_1 = z_2 = \cdots = z_n = 0)$. The $(n+1)$-spherical cylinder $\mathbb{C}^{n+1}_{O,b,-\infty,\infty}$ intersects the n-flats perpendicular to the z_{n+1}-axis in $\mathbb{B}^{n}_{O,b}$, and extends from $-\infty$ to ∞ along the z_{n+1}-axis. Then we have

$$Q_m(a,b) = 1 - \Pr\left(\mathbf{z}_{n+1} \in \mathbb{C}^{n+1}_{O,b,-\infty,\infty}\right). \tag{5.59}$$

From the geometric point of view, it is easy to see that the $(n+1)$-ball $\mathbb{B}^{n+1}_{O,b}$ is contained in the $(n+1)$-spherical cylinder $\mathbb{C}^{n+1}_{O,b,-\infty,\infty}$. From the mathematical point of view, it is also straightforward to prove that $\mathbb{B}^{n+1}_{O,b} \subset \mathbb{C}^{n+1}_{O,b,-\infty,\infty}$, since $\mathbb{C}^{n+1}_{O,b,-\infty,\infty}$ is the set $\{\mathbf{z}_{n+1} | \sum_{i=1}^{n} z_i^2 \leq b^2, -\infty < z_{n+1} < \infty\}$, and $\mathbb{B}^{n+1}_{O,b}$ is the set $\{\mathbf{z}_{n+1} | \sum_{i=1}^{n+1} z_i^2 \leq b^2\} = \{\mathbf{z}_{n+1} | \sum_{i=1}^{n} z_i^2 \leq b^2 - z_{n+1}^2, -b \leq z_{n+1} \leq b\}$. Thus, comparing (5.58) and (5.59) gives the inequality in (5.57). This result means that for integer m, we can use $Q_{m+0.5}(a,b)$ and $Q_{m-0.5}(a,b)$, which can be evaluated easily by (5.17), as upper and lower bounds on $Q_m(a,b)$, respectively.

We next discuss the tightness of the bound in (5.57) from a geometric view. From (5.58) and (5.59), we can see that the difference between $Q_{m+0.5}(a,b)$ and $Q_m(a,b)$ is given by

$$\begin{aligned} Q_{m+0.5}(a,b) - Q_m(a,b) &= \Pr\left(\mathbf{z}_{n+1} \in \mathbb{C}^{n+1}_{O,b,-\infty,\infty}\right) - \Pr\left(\mathbf{z}_{n+1} \in \mathbb{B}^{n+1}_{O,b}\right) \\ &= \Pr\left(\mathbf{z}_{n+1} \in \left[\mathbb{C}^{n+1}_{O,b,-\infty,\infty} - \mathbb{B}^{n+1}_{O,b}\right]\right) \\ &= \Pr\left(\mathbf{z}_{n+1} \in \mathbb{D}^{n+1}_{O,b,-\infty,\infty}\right), \forall\, m = 0.5n,\ n \in \mathbb{N}. \end{aligned} \tag{5.60}$$

Here, $\mathbb{D}^{n+1}_{O,b,-\infty,\infty} = \left[\mathbb{C}^{n+1}_{O,b,-\infty,\infty} - \mathbb{B}^{n+1}_{O,b}\right]$ is the region inside $\mathbb{C}^{n+1}_{O,b,-\infty,\infty}$ but outside

a region such that its intersections with the $(n-1)$-flats perpendicular to the axis of the cylinder are $(n-1)$-balls with the same radius, and the centers of these $(n-1)$-balls all lie on the axis of the cylinder [138].

$\mathbb{B}^{n+1}_{O,b}$, i.e., the remaining part of the infinite $(n+1)$-spherical cylinder $\mathbb{C}^{n+1}_{O,b,-\infty,\infty}$ after the removal of the $(n+1)$-ball $\mathbb{B}^{n+1}_{O,b}$ from its center. Now we can see that the tightness of the bound in (5.57) is determined by the probability $\Pr\big(\mathbf{z}_{n+1} \in \mathbb{D}^{n+1}_{O,b,-\infty,\infty}\big)$. We first consider the case that the center of the Gaussian distribution lies at a given point of the positive z_1-axis, i.e., a is fixed, and the radius b of $\mathbb{B}^{n+1}_{O,b}$ and $\mathbb{B}^{n}_{O,b}$ increases from 0 to ∞. We find that $\Pr\big(\mathbf{z}_{n+1} \in \mathbb{D}^{n+1}_{O,b,-\infty,\infty}\big)$ will start with a very small value, and increase to its maximum value when b increases to a value around a or a little larger than a, and then decrease and approach zero as b increases further. The small values of this probability at the two ends result from the fact that $\mathbf{z}_{n+1}$ is most likely to lie outside $\mathbb{C}^{n+1}_{O,b,-\infty,\infty}$ when $b \ll a$, and to lie inside $\mathbb{B}^{n+1}_{O,b}$ when $b \gg a$. The maximum value of this probability will be smaller for larger a and b, since the probability of $\mathbf{z}_{n+1}$ lying inside $\mathbb{B}^{n+1}_{O,b}$ will be larger for a larger radius b. For the case that the radius b is fixed, we can find a similar trend when a increases from 0 to ∞, that is, $P\big(\mathbf{z}_{n+1} \in \mathbb{D}^{n+1}_{O,b,-\infty,\infty}\big)$ will first increase from a small value, and attain its peak when a increases to a value less than b, and then decrease and approach zero as a increases further.

5.5.2 Bounds from the Geometrical Bounding Shapes

We now derive some generic erfc bounds, which involve erfc functions and exponential functions and have an arbitrarily large number of terms, by using the geometrical bounding shapes.

We consider the use of a set of contiguous, hyperspherical cylinders to bound the hyperball $\mathbb{B}^{n}_{O,b}$. The axes of these hyperspherical cylinders all lie on the y_1-axis. As shown in Fig. 5.5, we divide the area $y_1 \in [-b-a, -a]$ on the y_1-axis into N parts by defining $-b-a = \mu_0 < \mu_1 < \cdots < \mu_N = -a$, and divide the area $y_1 \in [-a, b-a]$ on the y_1-axis into M parts by defining $-a = \nu_0 < \nu_1 < \cdots < \nu_M = b-a$. Each of these parts is covered by a hyperspherical cylinder. For one of these hyperspherical cylinders, say $\mathbb{C}^{n}_{O',\iota_i,\mu_i,\mu_{i+1}}$ where O' is defined by

$(z_2 = z_3 = \cdots = z_n = 0)$, the probability of $\mathbf{z}_n$ lying inside $\mathbb{C}^n_{O',\iota_i,\mu_i,\mu_{i+1}}$ is given by

$$\Pr\left(\mathbf{z}_n \in \mathbb{C}^n_{O',\iota_i,\mu_i,\mu_{i+1}}\right) = \left[1 - Q_{m-0.5}\left(0, \iota_i\right)\right] \int_{y_1=\mu_i}^{\mu_{i+1}} \frac{e^{-y_1^2/2}}{\sqrt{2\pi}} dy_1. \tag{5.61}$$

Here, $Q_{m-0.5}(0, b)$ is given by (5.20) for integer m. Thus, as shown by the solid lines inside $\mathbb{B}^n_{O,b}$ in Fig. 5.5, our third generic upper bound on $Q_m(a, b)$, denoted as GUBm3-KL, is given by

$$\begin{aligned}
&Q_m(a,b) \\
&\leq Q_{GUBm3\text{-}KL}(a,b) \\
&= 1 - \sum_{i=1}^{N-1} \Pr\left(\mathbf{z}_n \in \mathbb{C}^n_{O',\sqrt{b^2-(a+\mu_i)^2},\mu_i,\mu_{i+1}}\right) \\
&\quad - \sum_{j=1}^{M-1} \Pr\left(\mathbf{z}_n \in \mathbb{C}^n_{O',\sqrt{b^2-(a+\nu_j)^2},\nu_{j-1},\nu_j}\right) \\
&= 1 - \sum_{i=1}^{N-1} \left[1 - Q_{m-0.5}\left(0, \sqrt{b^2-(a+\mu_i)^2}\right)\right] \int_{y_1=\mu_i}^{\mu_{i+1}} \frac{e^{-\frac{y_1^2}{2}}}{\sqrt{2\pi}} dy_1 \\
&\quad - \sum_{j=1}^{M-1} \left[1 - Q_{m-0.5}\left(0, \sqrt{b^2-(a+\nu_j)^2}\right)\right] \int_{y_1=\nu_{j-1}}^{\nu_j} \frac{e^{-\frac{y_1^2}{2}}}{\sqrt{2\pi}} dy_1 \\
&= 1 - \frac{1}{2} \sum_{i=1}^{N-1} \left[1 - \mathrm{erfc}\left(\sqrt{\frac{b^2-(a+\mu_i)^2}{2}}\right) - \sqrt{\frac{2}{\pi}} \exp\left(-\frac{b^2-(a+\mu_i)^2}{2}\right)\right. \\
&\quad \left. \cdot \sum_{k=0}^{m-2} \frac{\left(b^2-(a+\mu_i)^2\right)^{k+1/2}}{(2k+1)!!}\right] \left[\mathrm{erfc}\left(\frac{\mu_i}{\sqrt{2}}\right) - \mathrm{erfc}\left(\frac{\mu_{i+1}}{\sqrt{2}}\right)\right] \\
&\quad - \frac{1}{2} \sum_{j=1}^{M-1} \left[1 - \mathrm{erfc}\left(\sqrt{\frac{b^2-(a+\nu_j)^2}{2}}\right) - \sqrt{\frac{2}{\pi}} \exp\left(-\frac{b^2-(a+\nu_j)^2}{2}\right)\right. \\
&\quad \left. \cdot \sum_{k=0}^{m-2} \frac{\left(b^2-(a+\nu_j)^2\right)^{k+1/2}}{(2k+1)!!}\right] \left[\mathrm{erfc}\left(\frac{\nu_{j-1}}{\sqrt{2}}\right) - \mathrm{erfc}\left(\frac{\nu_j}{\sqrt{2}}\right)\right], \\
&\qquad\qquad a \geq 0,\ b \geq 0,\ m \text{ integer.}
\end{aligned} \tag{5.62}$$

Here, we have $-b - a = \mu_0 < \mu_1 < \cdots < \mu_N = -a$ and $-a = \nu_0 < \nu_1 < \cdots < \nu_M = b - a$. The bound GUBm3-KL in (5.62) on $Q_m(a, b)$ reduces to the bound GUB3-KL in (4.40) on $Q(a, b)$ when $m = 1$.

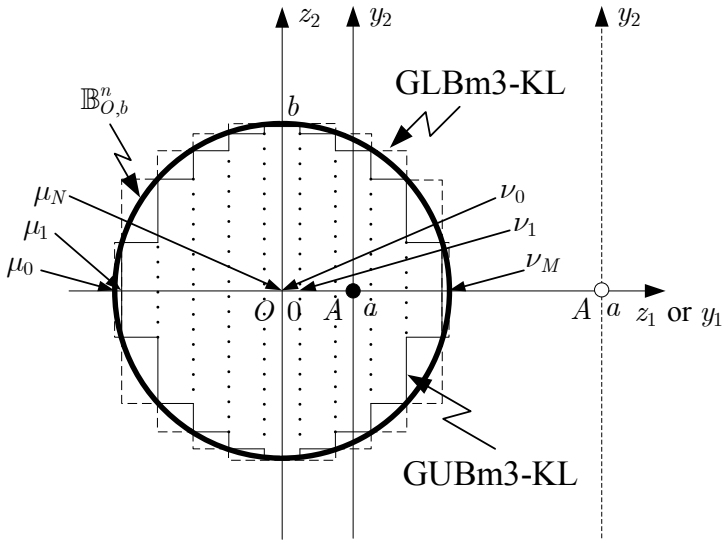

Fig. 5.5: Diagram of the derivation of the new generic erfc bounds GUBm3-KL and GLBm3-KL on $Q_m(a,b)$.

Similarly, as shown by the dashed lines outside $\mathbb{B}^n_{O,b}$ in Fig. 5.5, our third generic lower bound on $Q_m(a,b)$, denoted as GLBm3-KL, is given by

$$
\begin{aligned}
&Q_m(a,b) \\
&\geq Q_{GLBm3\text{-}KL}(a,b) \\
&= 1 - \sum_{i=1}^{N} \Pr\left(\mathbf{z}_n \in \mathbb{C}^n_{O',\sqrt{b^2-(a+\mu_i)^2},\mu_{i-1},\mu_i}\right) \\
&\quad - \sum_{j=1}^{M} \Pr\left(\mathbf{z}_n \in \mathbb{C}^n_{O',\sqrt{b^2-(a+\nu_{j-1})^2},\nu_{j-1},\nu_j}\right) \\
&= 1 - \frac{1}{2}\sum_{i=1}^{N}\left[1 - \operatorname{erfc}\left(\sqrt{\frac{b^2-(a+\mu_i)^2}{2}}\right) - \sqrt{\frac{2}{\pi}}\exp\left(-\frac{b^2-(a+\mu_i)^2}{2}\right)\right. \\
&\quad \left.\cdot \sum_{k=0}^{m-2}\frac{\left(b^2-(a+\mu_i)^2\right)^{k+1/2}}{(2k+1)!!}\right]\left[\operatorname{erfc}\left(\frac{\mu_{i-1}}{\sqrt{2}}\right) - \operatorname{erfc}\left(\frac{\mu_i}{\sqrt{2}}\right)\right] \\
&\quad - \frac{1}{2}\sum_{j=1}^{M}\left[1 - \operatorname{erfc}\left(\sqrt{\frac{b^2-(a+\nu_{j-1})^2}{2}}\right) - \sqrt{\frac{2}{\pi}}\exp\left(-\frac{b^2-(a+\nu_{j-1})^2}{2}\right)\right. \\
&\quad \left.\cdot \sum_{k=0}^{m-2}\frac{\left(b^2-(a+\nu_{j-1})^2\right)^{k+1/2}}{(2k+1)!!}\right]\left[\operatorname{erfc}\left(\frac{\nu_{j-1}}{\sqrt{2}}\right) - \operatorname{erfc}\left(\frac{\nu_j}{\sqrt{2}}\right)\right], \\
&\qquad\qquad a \geq 0,\ b \geq 0,\ m \text{ integer.} \qquad (5.63)
\end{aligned}
$$

Here, we also have $-b-a=\mu_0<\mu_1<\cdots<\mu_N=-a$ and $-a=\nu_0<\nu_1<\cdots<\nu_M=b-a$. The bound GLBm3-KL in (5.63) on $Q_m(a,b)$ reduces to the bound GLB3-KL in (4.41) on $Q(a,b)$ when $m=1$.

When we set $N=M=1$, GLBm3-KL in (5.63) reduces to

$$Q_m(a,b)\geq 1-\frac{1}{2}\left[1-\operatorname{erfc}\left(\frac{b}{\sqrt{2}}\right)-\sqrt{\frac{2}{\pi}}\exp\left(-\frac{b^2}{2}\right)\sum_{k=0}^{m-2}\frac{b^{2k+1}}{(2k+1)!!}\right] \cdot\left[\operatorname{erfc}\left(\frac{-b-a}{\sqrt{2}}\right)-\operatorname{erfc}\left(\frac{b-a}{\sqrt{2}}\right)\right], \qquad a\geq 0,\ b\geq 0,\ m \text{ integer}. \tag{5.64}$$

It is clear that the generic erfc bounds in (5.62) and (5.63) are valid for entire ranges of a and b. They grow tighter as the closeness of fit of the bounding shapes with $\mathbb{B}^n_{O,b}$ improves.

5.6 Comparison and Numerical Results

In this section, we first give some numerical results for $Q_{m+0.5}(a,b)$, $Q_m(a,b)$ and $Q_{m-0.5}(a,b)$ to verify that the generalized Marcum-Q-function is an increasing function of its order. Then we compare the tightness of all the new bounds derived in Sections 5.4 and 5.5 with that of the existing bounds in the literature.

5.6.1 Relationship between $Q_{m\pm0.5}(a,b)$ and $Q_m(a,b)$

We now give some numerical results of $Q_{m+0.5}(a,b)$ and $Q_{m-0.5}(a,b)$ for integer m, and show their relationship with $Q_m(a,b)$. Fig. 5.6 shows the results for different values of a, i.e, $a=1,5,10$. Fig. 5.7 shows the results for different values of m, i.e, $m=5,10,15$. We can see that $Q_{m+0.5}(a,b)$ and $Q_{m-0.5}(a,b)$ are very close to $Q_m(a,b)$, and all of them have a similar shape. Thus, we can use $Q_{m+0.5}(a,b)$ and $Q_{m-0.5}(a,b)$, respectively, as tight upper and lower bounds on $Q_m(a,b)$, just as we have discussed in Section 5.5.1. In Fig. 5.8, the differences $(Q_{m+0.5}(a,b)-Q_m(a,b))$ and $(Q_m(a,b)-Q_{m-0.5}(a,b))$ are shown, which indicate

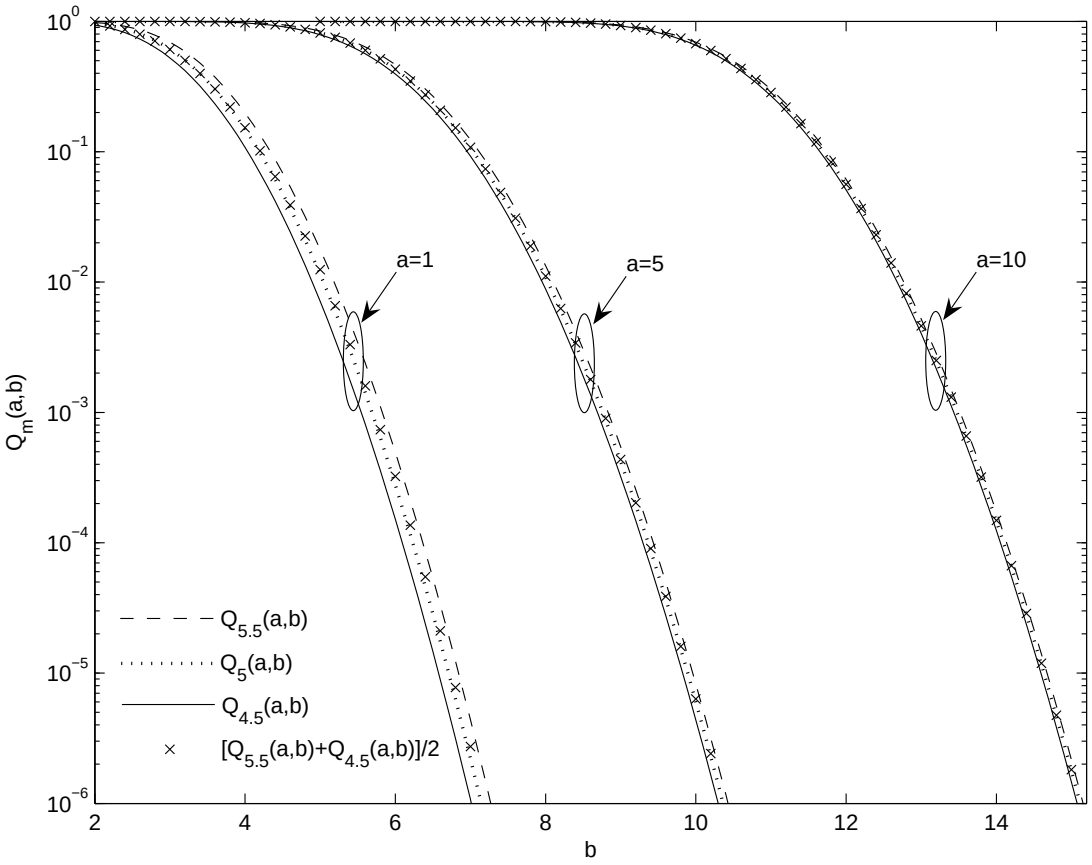

Fig. 5.6: The generalized Marcum Q-function $Q_m(a,b)$, its upper bound $Q_{m+0.5}(a,b)$, its lower bound $Q_{m-0.5}(a,b)$, and its approximation $[Q_{m+0.5}(a,b)+Q_{m-0.5}(a,b)]/2$ versus b for $a=1,5,10$ and $m=5$.

the tightness of the upper bound $Q_{m+0.5}(a,b)$ and the tightness of the lower bound $Q_{m-0.5}(a,b)$, respectively. We can see that for a given a and m, the differences are very small at both the ranges $b \ll a$ and $b \gg a$, and have a peak at a value of b around a or larger than a. We can also see that the peak values of the differences become smaller as a increases. This means that the upper and lower bounds grow tighter as a increases. These results are consistent with our predictions in Section 5.5.1. In addition, we also find that although $[Q_{m+0.5}(a,b) - Q_m(a,b)]$ is not the same as $[Q_m(a,b) - Q_{m-0.5}(a,b)]$, their difference is very small for large a or b. Since $Q_{m+0.5}(a,b)$ and $Q_{m-0.5}(a,b)$ have a similar shape to that of $Q_m(a,b)$, and have a similar tightness as bounds on $Q_m(a,b)$, we can use their average as a good

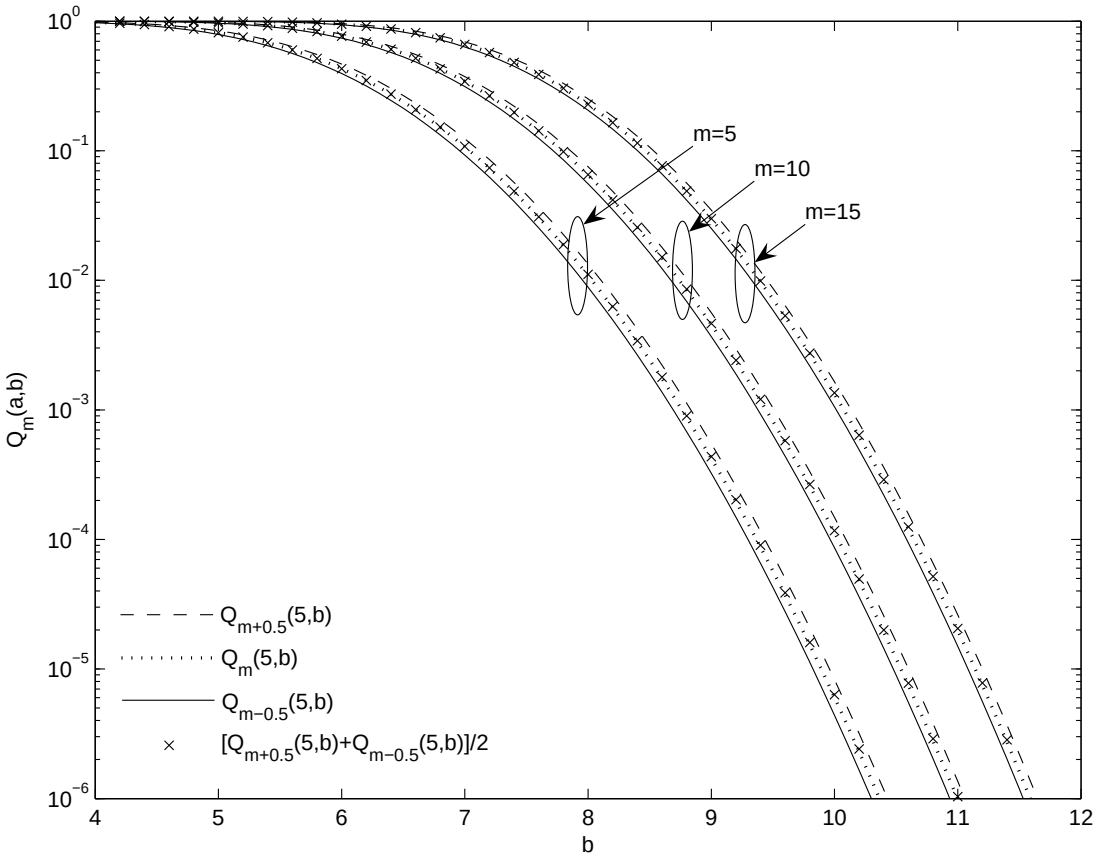

Fig. 5.7: The generalized Marcum Q-function $Q_m(a,b)$, its upper bound $Q_{m+0.5}(a,b)$, its lower bound $Q_{m-0.5}(a,b)$, and its approximation $[Q_{m+0.5}(a,b)+Q_{m-0.5}(a,b)]/2$ versus b for $m=5,10,15$ and $a=5$.

approximation to $Q_m(a,b)$. Their average can be obtained from (5.26) as

$$\begin{aligned}&\frac{1}{2}\left[Q_{m+0.5}(a,b)+Q_{m-0.5}(a,b)\right]\\ &=Q_{m-0.5}(a,b)+\frac{b^{2m-2}}{2^{m+0.5}a\sqrt{\pi}}\sum_{q=0}^{m-1}\frac{(-1)^q\,(2q)!}{(m-1-q)!q!}\left\{\sum_{i=0}^{2q}\frac{1}{(ab)^{2q-i}\,i!}\right.\\ &\left.\cdot\left[(-1)^i\exp\left(-\frac{(b-a)^2}{2}\right)-\exp\left(-\frac{(b+a)^2}{2}\right)\right]\right\},\ a>0,b\geq 0,\text{ integer } m.\end{aligned}\tag{5.65}$$

As shown in Figs. 5.6 and 5.7, the average in (5.65) almost coincides with the exact value of $Q_m(a,b)$.

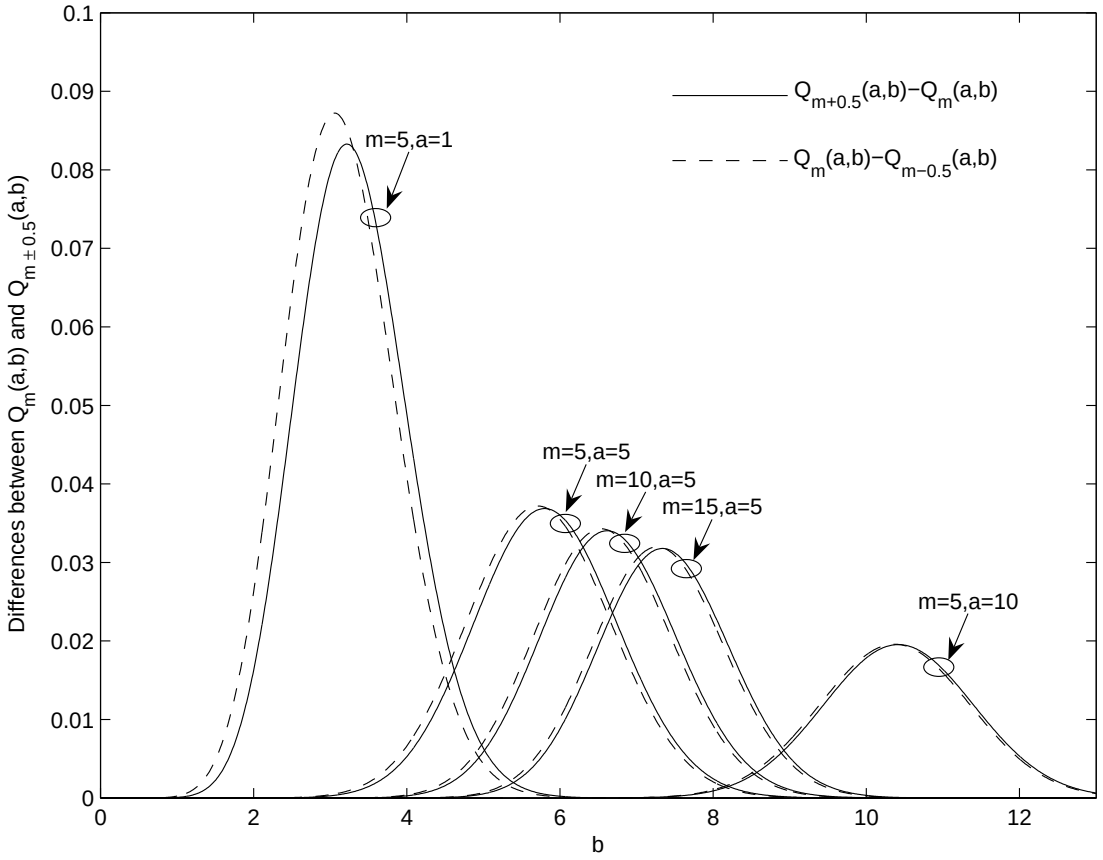

Fig. 5.8: Differences between $Q_m(a,b)$ and its bounds $Q_{m\pm0.5}(a,b)$ versus b for $a = 1, 5, 10$ and $m = 5, 10, 15$.

5.6.2 Performance of the New Bounds

Next, we compare the tightness of our new bounds on $Q_m(a,b)$ in Sections 5.4 and 5.5 with that of the existing bounds on $Q_m(a,b)$ in the literature. There are two types of bounds available in the literature, namely, exponential bounds which involve only the exponential function, and I_k-bounds which involve the function $I_k(\cdot)$. Since most of the existing bounds are valid for only either $b > a$ or $b < a$, we show the comparisons case by case.

5.6.2.1 Bounds for the Case of $b > a$

For the case of $b > a$, the existing upper exponential bounds include UBm1-SA in [120, eq. (8)], given by

$$\begin{aligned} Q_m(a,b) &\le Q_{UBm1\text{-}SA}(a,b) \\ &= \exp\left[-\frac{(b-a)^2}{2}\right] + \frac{1}{\pi}\left\{\exp\left[-\frac{(b-a)^2}{2}\right] - \exp\left[-\frac{(b+a)^2}{2}\right]\right\} \\ &\quad \cdot \left(\frac{b}{a}\right)^{m-1}\left[\frac{1-(a/b)^{m-1}}{1-(a/b)}\right], \qquad b > a > 0, \end{aligned} \tag{5.66}$$

and UBm1-AT in [121, eq. (17)], given by

$$\begin{aligned} Q_m(a,b) &\le Q_{UBm1\text{-}AT}(a,b) \\ &= \frac{1}{2}\sqrt{\frac{2m-1}{2} + \frac{(a/b)^{2(1-m)}}{2[1-(a/b)^2]}}\left\{\exp\left[-\frac{(b-a)^2}{2}\right] + \exp\left[-\frac{(b+a)^2}{2}\right]\right\}, \\ &\qquad\qquad b > a > 0. \end{aligned} \tag{5.67}$$

The existing lower exponential bounds include LBm1-SA in [120, eq. (11)], given by

$$Q_m(a,b) \ge Q_{LBm1\text{-}SA}(a,b) = \exp\left[-\frac{(b+a)^2}{2}\right]\sum_{i=0}^{m-1}\frac{(b^2/2)^i}{i!}, \;\; b > a \ge 0, \tag{5.68}$$

and LBm1-AT in [121, the first line in eq. (18)], given by

$$Q_m(a,b) \ge Q_{LBm1\text{-}AT}(a,b) = \exp\left(-\frac{b^2}{2}\right)\sum_{i=0}^{m-1}\frac{(b^2/2)^i}{i!}, \;\; a \ge 0, b \ge 0. \tag{5.69}$$

There are three existing I_k-bounds available in the literature. The upper bound UBm2-AT in [121, eq. (12)] involves $\sqrt{I_0(\cdot)}$, given by

$$\begin{aligned} Q_m(a,b) &\le Q_{UBm2\text{-}AT}(a,b) \\ &= \sqrt{\frac{2m-1}{2} + \frac{(a/b)^{2(1-m)}}{2[1-(a/b)^2]}}\exp\left(-\frac{b^2+a^2}{2}\right)\sqrt{I_0(2ab)}, \;\; b > a \ge 0. \end{aligned} \tag{5.70}$$

The upper bound UBm1-CF is given by

$$Q_m(a,b) \le Q_{UBm1\text{-}CF}(a,b) = \frac{I_0(ab)}{e^{ab}}\left\{\exp\left[-\frac{(b-a)^2}{2}\right] + a\sqrt{\frac{\pi}{2}}\text{erfc}\left(\frac{b-a}{\sqrt{2}}\right)\right\} + \exp\left(-\frac{a^2+b^2}{2}\right)\sum_{k=1}^{m-1}\left(\frac{b}{a}\right)^k I_k(ab), \quad b \ge a > 0. \tag{5.71}$$

This bound is obtained by using the upper bound UB1-CF in (4.98) to bound $Q(a,b)$ in the series expression of $Q_m(a,b)$ in [122, eq. (2)], i.e,

$$Q_m(a,b) = Q(a,b) + \exp\left(-\frac{a^2+b^2}{2}\right)\sum_{k=1}^{m-1}\left(\frac{b}{a}\right)^k I_k(ab), \ a > 0, b \ge 0. \tag{5.72}$$

Similarly, the lower bound LBm1-CF can be obtained by using the lower bound LB1-CF in (4.105) to bound $Q(a,b)$ in (5.72), and thus, is given by

$$\begin{aligned} Q_m(a,b) &\ge Q_{LBm1\text{-}CF}(a,b) \\ &= \frac{I_0(ab)b}{\exp(ab)}\sqrt{\frac{\pi}{2}}\text{erfc}\left(\frac{b-a}{\sqrt{2}}\right) + \exp\left(-\frac{a^2+b^2}{2}\right)\sum_{k=1}^{m-1}\left(\frac{b}{a}\right)^k I_k(ab), \\ &\qquad b \ge a > 0. \end{aligned} \tag{5.73}$$

These two bounds, UBm1-CF and LBm1-CF, involve $\{I_k(\cdot)\}_{k=0}^{m-1}$. Using a similar method, we can also obtain some new I_k-bounds by using our new bounds on $Q(a,b)$ derived in Chapter 4 to bound $Q(a,b)$ in (5.72). However, these new I_k-bounds, with $\{I_k(\cdot)\}_{k=1}^{m-1}$ being involved, are as complicated as UBm1-CF and LBm1-CF, and thus, are not more desirable than the latter bounds.

For this case, our new bounds derived in this chapter include the generic exponential bounds GUBm1-KL in (5.46) and GLBm1-KL in (5.50), the erfc bounds $Q_{m+0.5}(a,b)$ and $Q_{m-0.5}(a,b)$ in (5.17), and the generic erfc bounds GUBm3-KL in (5.62) and GLBm3-KL in (5.63). We have also given an approximation of $Q_m(a,b)$ in (5.65). For simplicity, we just choose equispaced points for the parameters, i.e., $\theta_i = i\pi/N$ for GUBm1-KL and GLBm1-KL, and $\mu_i = -b - a + bi/N$

and $\nu_j = -a + bj/M$ for GUBm3-KL and GLBm3-KL. Figs. 5.9 and 5.10 show, respectively, the upper and lower bounds on $Q_m(a,b)$ for the case of $b > a = 5$ with $m = 5$. Figs. 5.11 and 5.12 show, respectively, the upper and lower bounds on $Q_m(a,b)$ for the case of $b > a = 5$ with $m = 10$. In our numerical results, the exact value of $Q_m(a,b)$, the erfc bounds $Q_{m+0.5}(a,b)$ and $Q_{m-0.5}(a,b)$, and our generic exponential bounds are shown by the solid lines. Our generic erfc bounds are shown by the dash-dotted lines. The existing exponential bounds and I_k-bounds are shown by the dashed lines and dotted lines, respectively. The approximation of $Q_m(a,b)$ in (5.65) is shown by the marker "×". If the I_k-bounds UBm1-CF and LBm1-CF are too close to the approximation and the exact value of $Q_m(a,b)$ in some cases, they are also marked with "+". We can see that when a and m are large, $Q_{m+0.5}(a,b)$ and $Q_{m-0.5}(a,b)$ outperform most of the other bounds, only a little looser than the pair of UBm1-CF and LBm1-CF. However, the former pair only involves the simple erfc functions and exponential functions, much simpler than the latter pair of I_k-bounds. Our generic upper exponential bound GUBm1-KL and erfc bound GUBm3-KL evaluated with a few terms are much tighter than the existing exponential bounds UBm1-SA and UBm1-AT when b is close to a, but they need to involve more terms to outperform the latter bounds when b is much larger than a. When a is close to zero, say $a = 0.1$, GUBm3-KL is not tight, but GUBm1-KL is still very tight, and can be much tighter than UBm1-SA and UBm1-AT when m is large, say $m = 5$. Our generic lower exponential bound GLBm1-KL and erfc bound GLBm3-KL evaluated with a few terms are much tighter than the existing exponential bounds LBm1-SA and LBm1-AT for a wide range of values of the arguments. The bound LBm1-AT is only tight for small a. The bound LBm1-SA is not shown here, since it is much looser than the others when a is not close to zero.

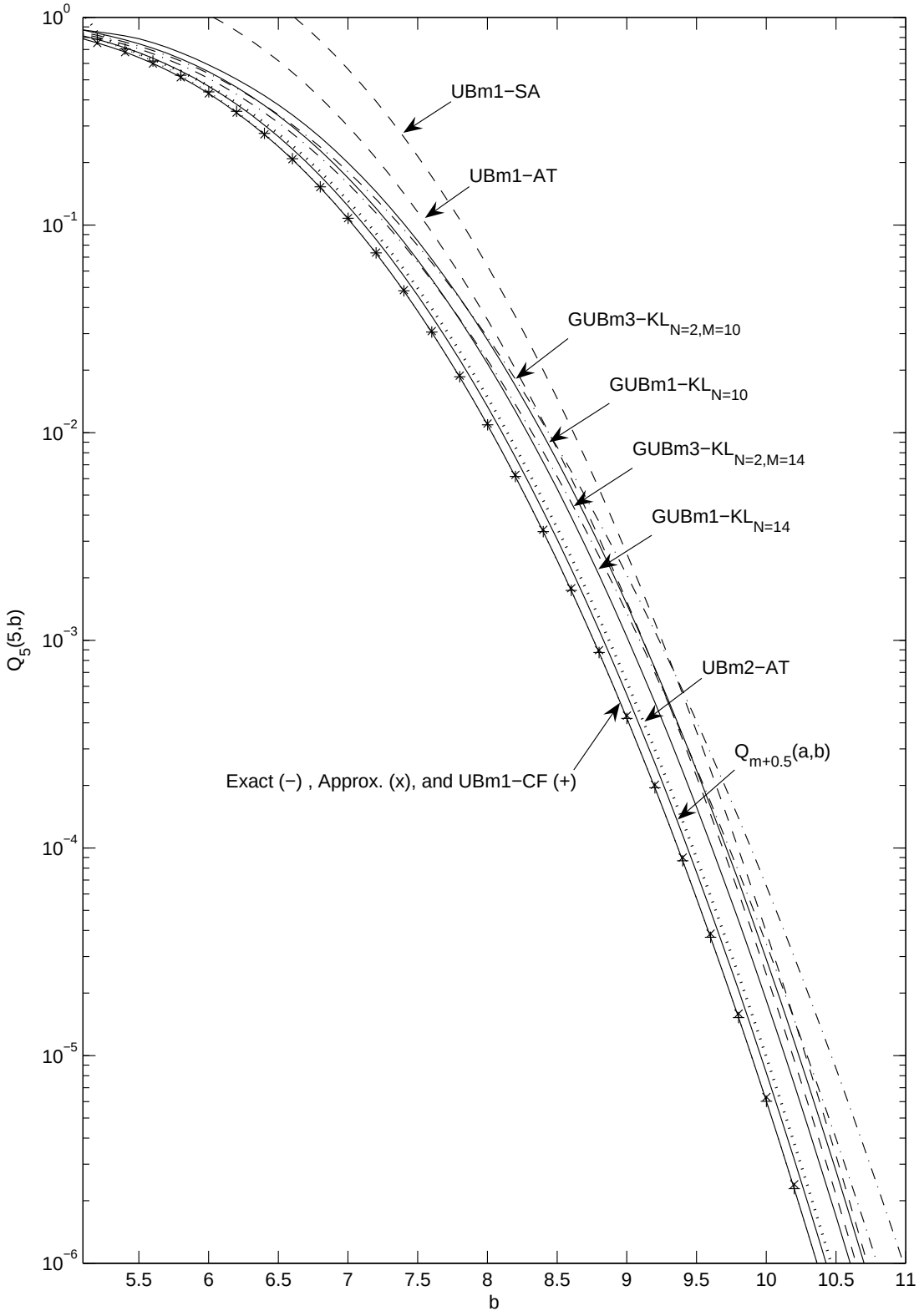

Fig. 5.9: The generalized Marcum Q-function $Q_m(a, b)$ and its upper bounds versus b for the case of $b > a = 5$ and $m = 5$.

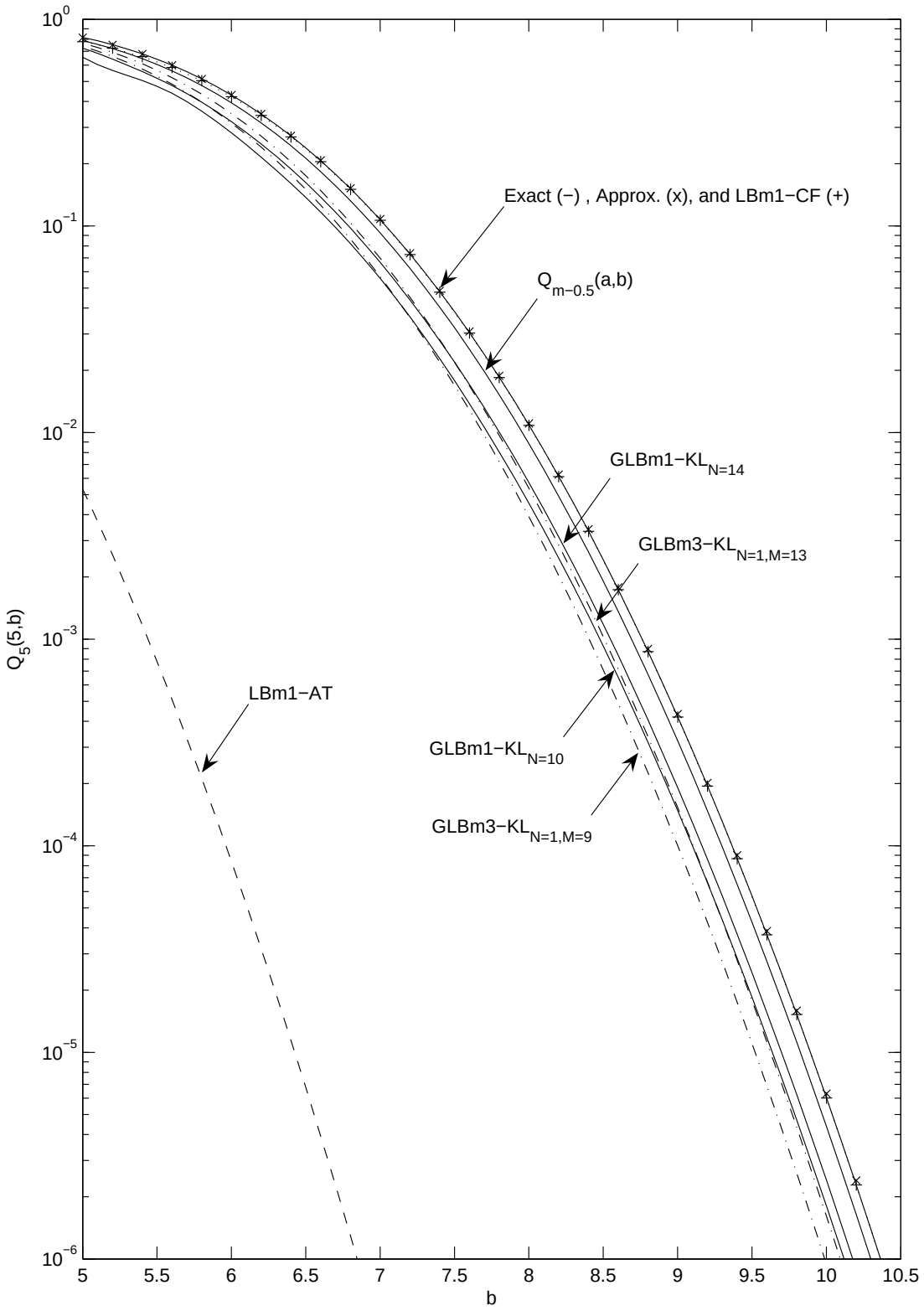

Fig. 5.10: The generalized Marcum Q-function $Q_m(a, b)$ and its lower bounds versus b for the case of $b > a = 5$ and $m = 5$.

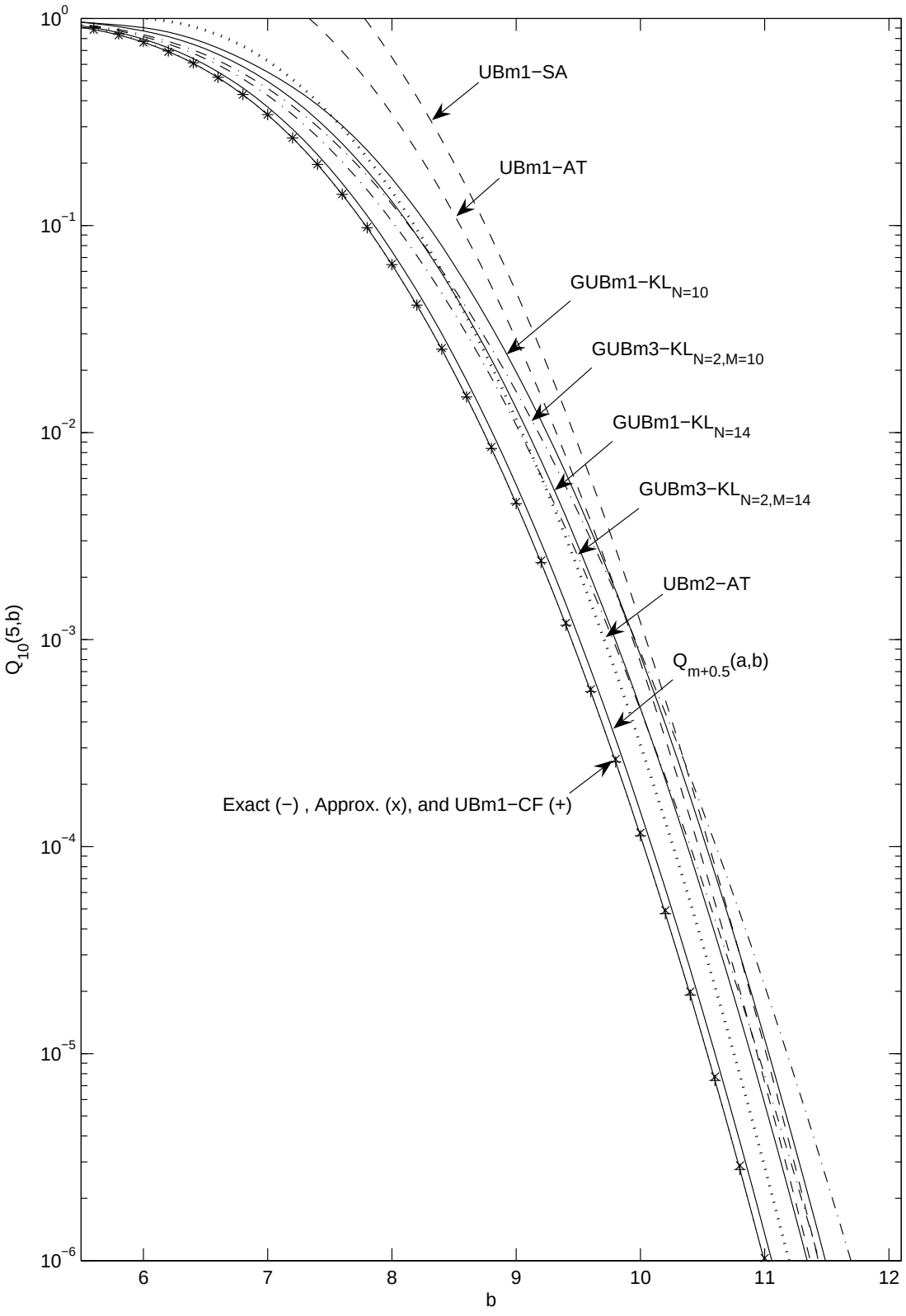

Fig. 5.11: The generalized Marcum Q-function $Q_m(a, b)$ and its upper bounds versus b for the case of $b > a = 5$ and $m = 10$.

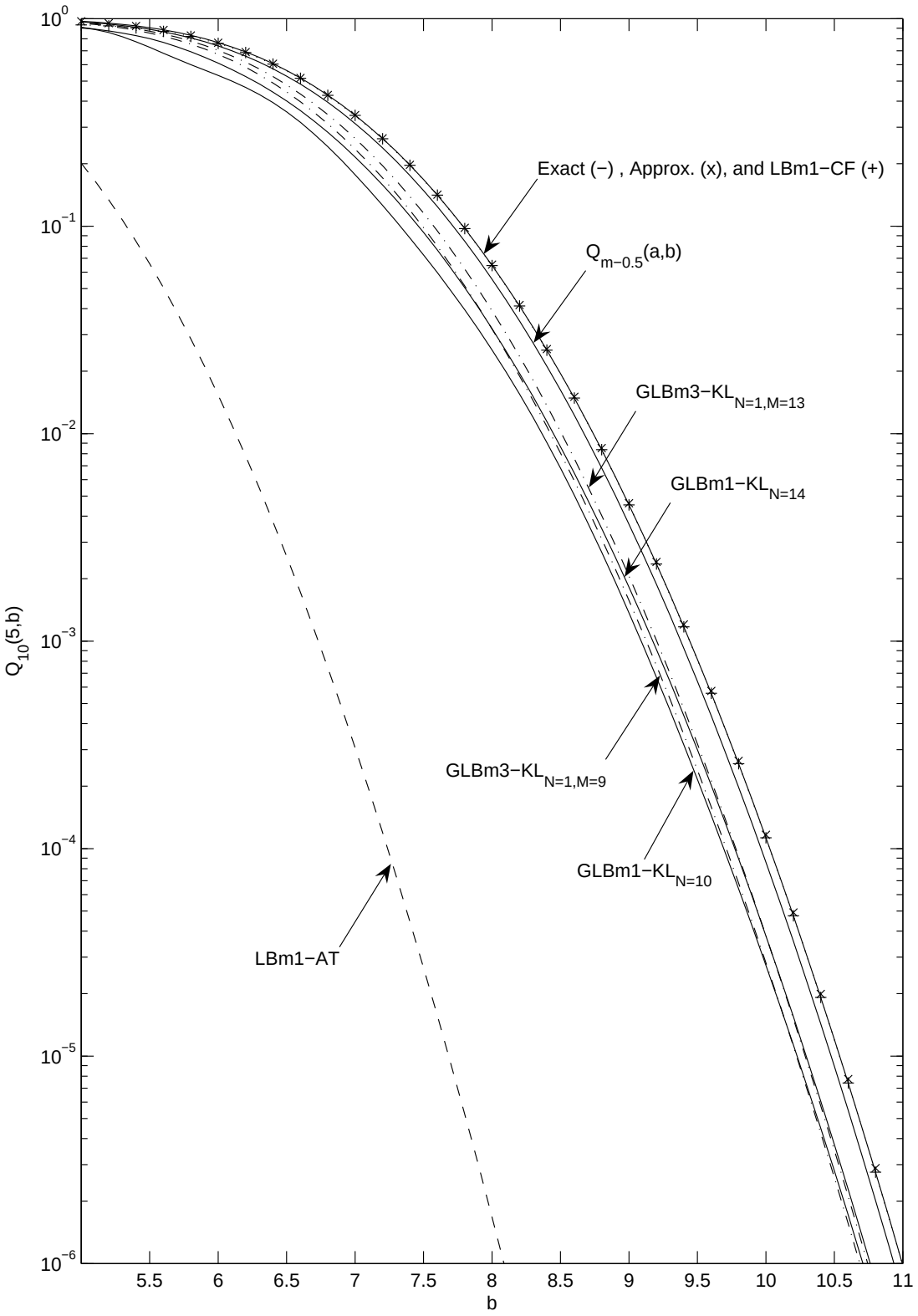

Fig. 5.12: The generalized Marcum Q-function $Q_m(a,b)$ and its lower bounds versus b for the case of $b > a = 5$ and $m = 10$.

5.6.2.2 Bounds for the Case of $a > b$

For the case of $a > b$, the only existing upper bound is the I_k-bound UBm2-CF, which is obtained by using the upper bound UB2-CF in (4.100) to bound $Q(a,b)$ in (5.72), and thus given by

$$\begin{aligned} Q_m(a,b) &\leq Q_{UBm2\text{-}CF}(a,b) \\ &= 1 - \frac{I_0(ab)}{\exp(ab)} \left\{ \exp\left(-\frac{a^2}{2}\right) - \exp\left[-\frac{(b-a)^2}{2}\right] + a\sqrt{\frac{\pi}{2}} \left[\operatorname{erfc}\left(-\frac{a}{\sqrt{2}}\right)\right.\right. \\ &\quad \left.\left. - \operatorname{erfc}\left(\frac{b-a}{\sqrt{2}}\right)\right] \right\} + \exp\left(-\frac{a^2+b^2}{2}\right) \sum_{k=1}^{m-1} \left(\frac{b}{a}\right)^k I_k(ab), a \geq b > 0. \end{aligned} \tag{5.74}$$

The existing lower exponential bounds include the bound LBm2-SA in [120, eq. (12)], given by

$$\begin{aligned} Q_m(a,b) \geq Q_{LBm2\text{-}SA}(a,b) = 1 - \frac{1}{2}\left\{\exp\left[-\frac{(b-a)^2}{2}\right] - \exp\left[-\frac{(b+a)^2}{2}\right]\right\} \\ + \exp\left[-\frac{(b+a)^2}{2}\right] \sum_{i=1}^{m-1} \frac{(b^2/2)^i}{i!}, \ a > b \geq 0, \end{aligned} \tag{5.75}$$

the bound LBm1-AT in [121, eq. (18)], given by (5.69), and the bound LBm2-AT in [121, eq. (21)], given by

$$\begin{aligned} Q_m(a,b) &\geq Q_{LBm2\text{-}AT}(a,b) \\ &= 1 - \frac{1}{2}\sqrt{\frac{(a/b)^{2(1-m)}}{2[(a/b)^2-1]}} \left\{\exp\left[-\frac{(b-a)^2}{2}\right] + \exp\left[-\frac{(b+a)^2}{2}\right]\right\}, \\ &\qquad a > b > 0. \end{aligned} \tag{5.76}$$

The existing lower I_k-bounds include the bound LBm3-AT in [121, eq. (20)], i.e.,

$$\begin{aligned} Q_m(a,b) &\geq Q_{LBm3\text{-}AT}(a,b) \\ &= 1 - \sqrt{\frac{(a/b)^{2(1-m)}}{2[(a/b)^2-1]}} \exp\left(-\frac{b^2+a^2}{2}\right) \sqrt{I_0(2ab)}, \ a > b \geq 0, \end{aligned} \tag{5.77}$$

and the bound LBm2-CF, which is obtained by using the lower bound LB2-CF in (4.110) to bound $Q(a,b)$ in (5.72), and given by

$$\begin{aligned} & Q(a,b) \\ & \geq Q_{LBm2\text{-}CF}(a,b) \\ & = 1-\exp\left(-\frac{a^2-c^2}{2}\right)\left\{\exp\left(-\frac{c^2}{2}\right)-\exp\left[-\frac{(b-c)^2}{2}\right]+c\sqrt{\frac{\pi}{2}}\left[\operatorname{erfc}\left(-\frac{c}{\sqrt{2}}\right)\right.\right. \\ & \quad \left.\left.-\ \operatorname{erfc}\left(\frac{b-c}{\sqrt{2}}\right)\right]\right\}+\exp\left(-\frac{a^2+b^2}{2}\right)\sum_{k=1}^{m-1}\left(\frac{b}{a}\right)^k I_k(ab), \quad a\geq b>0, \end{aligned} \tag{5.78}$$

where $c=[\log I_0(ab)]/b$. The bound LBm3-AT involves $\sqrt{I_0(\cdot)}$, and the bounds UBm2-CF and LBm2-CF involve $\{I_k(\cdot)\}_{k=0}^{m-1}$. Our new bounds include the generic exponential bounds GUBm2-KL in (5.54) and GLBm2-KL in (5.56), the erfc bounds $Q_{m+0.5}(a,b)$ and $Q_{m-0.5}(a,b)$ in (5.17), and the generic erfc bounds GUBm3-KL in (5.62) and GLBm3-KL in (5.63). We also choose equispaced points for θ_i in GUBm2-KL and GLBm2-KL, i.e., we have $\theta_i=\pi-\arcsin(b/a)+i\arcsin(b/a)/N$.

Figs. 5.13 and 5.14 show, respectively, the upper and lower bounds on $Q_m(a,b)$ for the case of $b<a=5$ with $m=5$. Figs. 5.15 and 5.16 show, respectively, the upper and lower bounds on $Q_m(a,b)$ for the case of $b<a=5$ with $m=10$. Since for $a>b$, the value of $Q_m(a,b)$ is close to 1, we show the results on a linear scale. From our numerical results, we can see that $Q_{m+0.5}(a,b)$ is tighter than UBm2-CF when a is not much larger than m. When we have $a\ll m$, as in the case of $a=5$ and $m=10$, UBm2-CF may exceed one and thus become useless. For large a, our generic bounds GUBm2-KL and GUBm3-KL when evaluated with a few terms are not as tight as $Q_{m+0.5}(a,b)$. Our lower bound $Q_{m-0.5}(a,b)$ is tighter than LBm2-CF for a wide range of values of the arguments, and the latter is tighter than the former only when both a and m are small. When evaluated with a few terms, the bounds GLBm2-KL and GLBm3-KL are much tighter than the existing exponential bounds, and even tighter than the I_k-bounds, for a wide

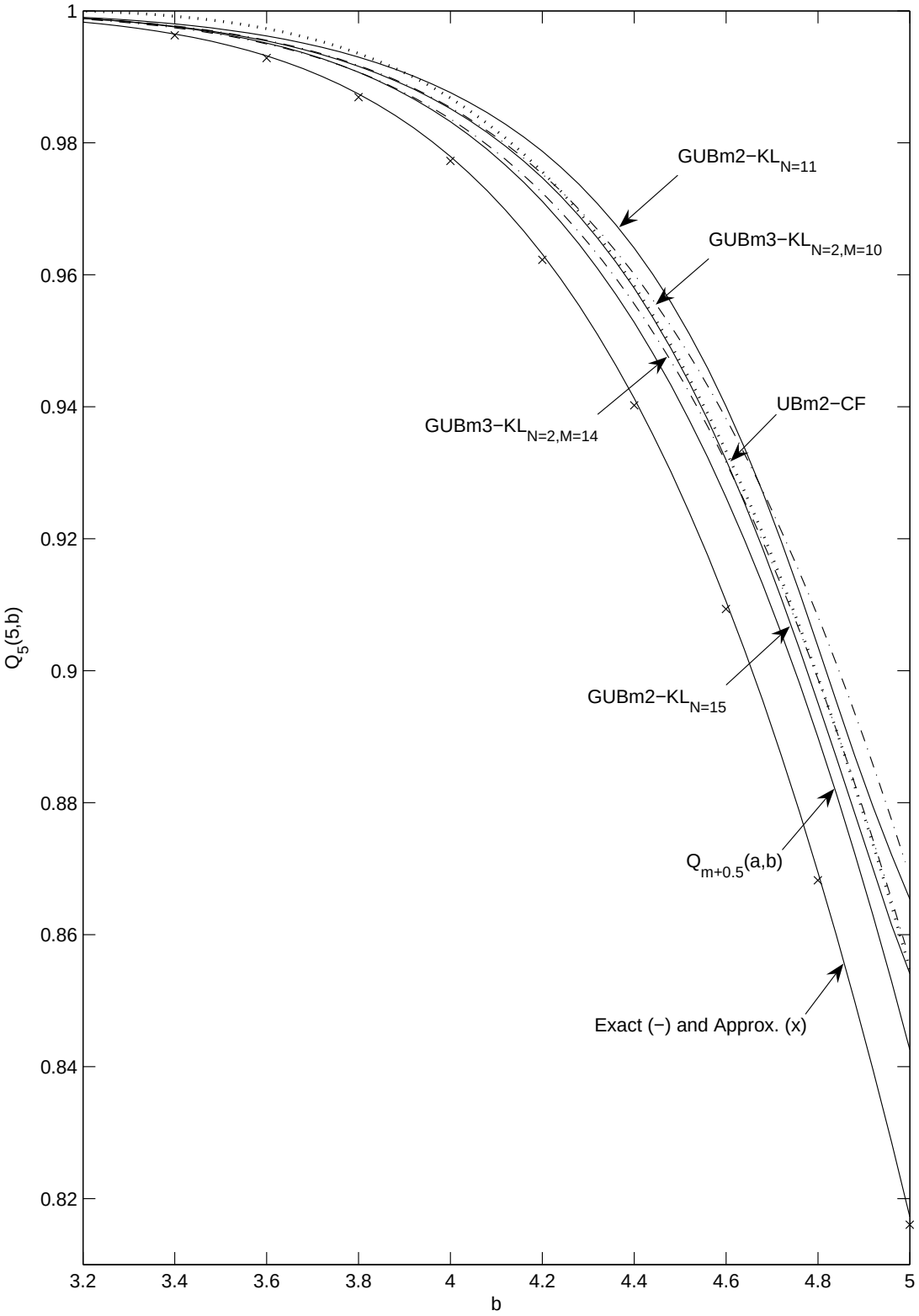

Fig. 5.13: The generalized Marcum Q-function $Q_m(a, b)$ and its upper bounds versus b for the case of $b < a = 5$ and $m = 5$.

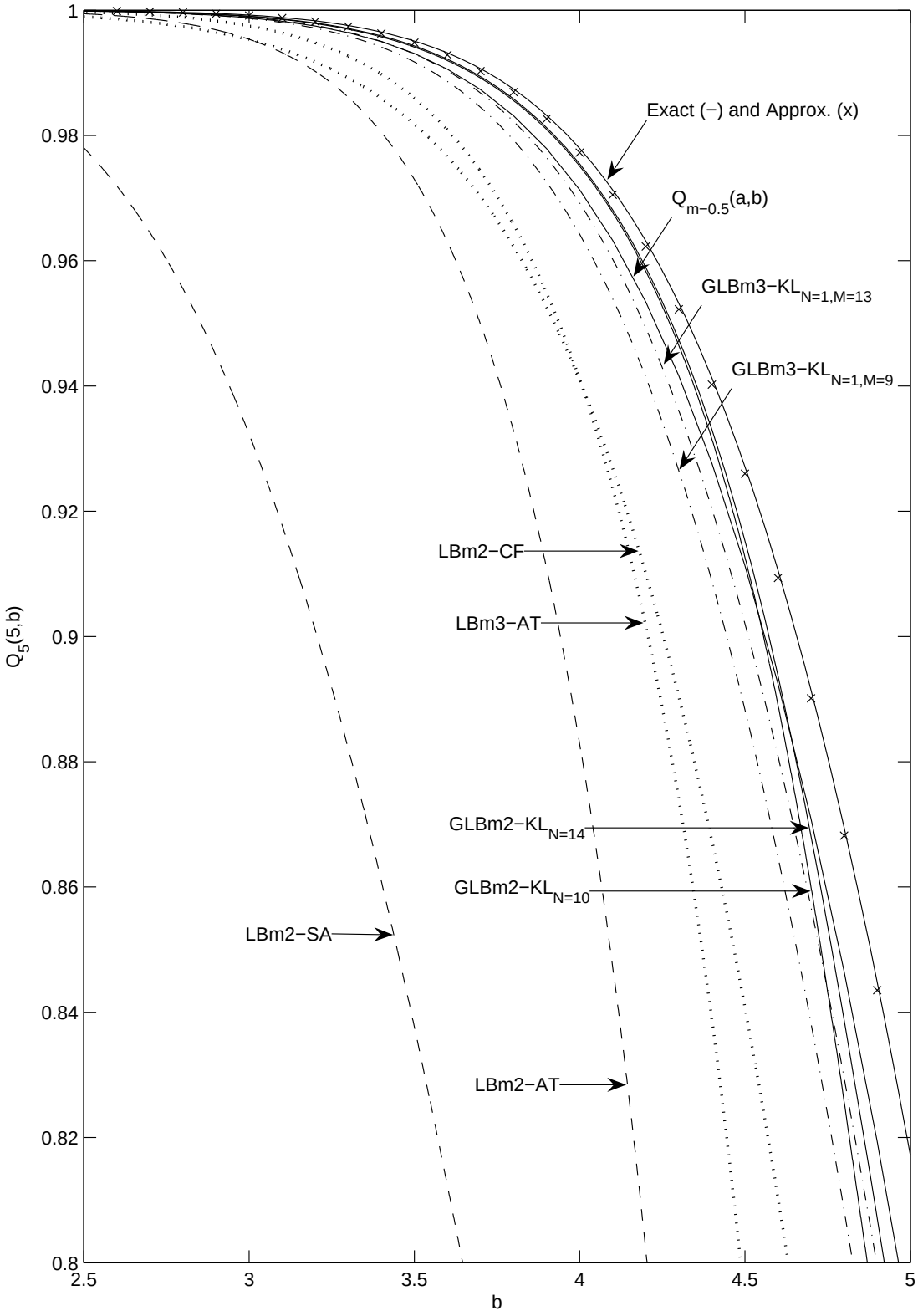

Fig. 5.14: The generalized Marcum Q-function $Q_m(a, b)$ and its lower bounds versus b for the case of $b < a = 5$ and $m = 5$.

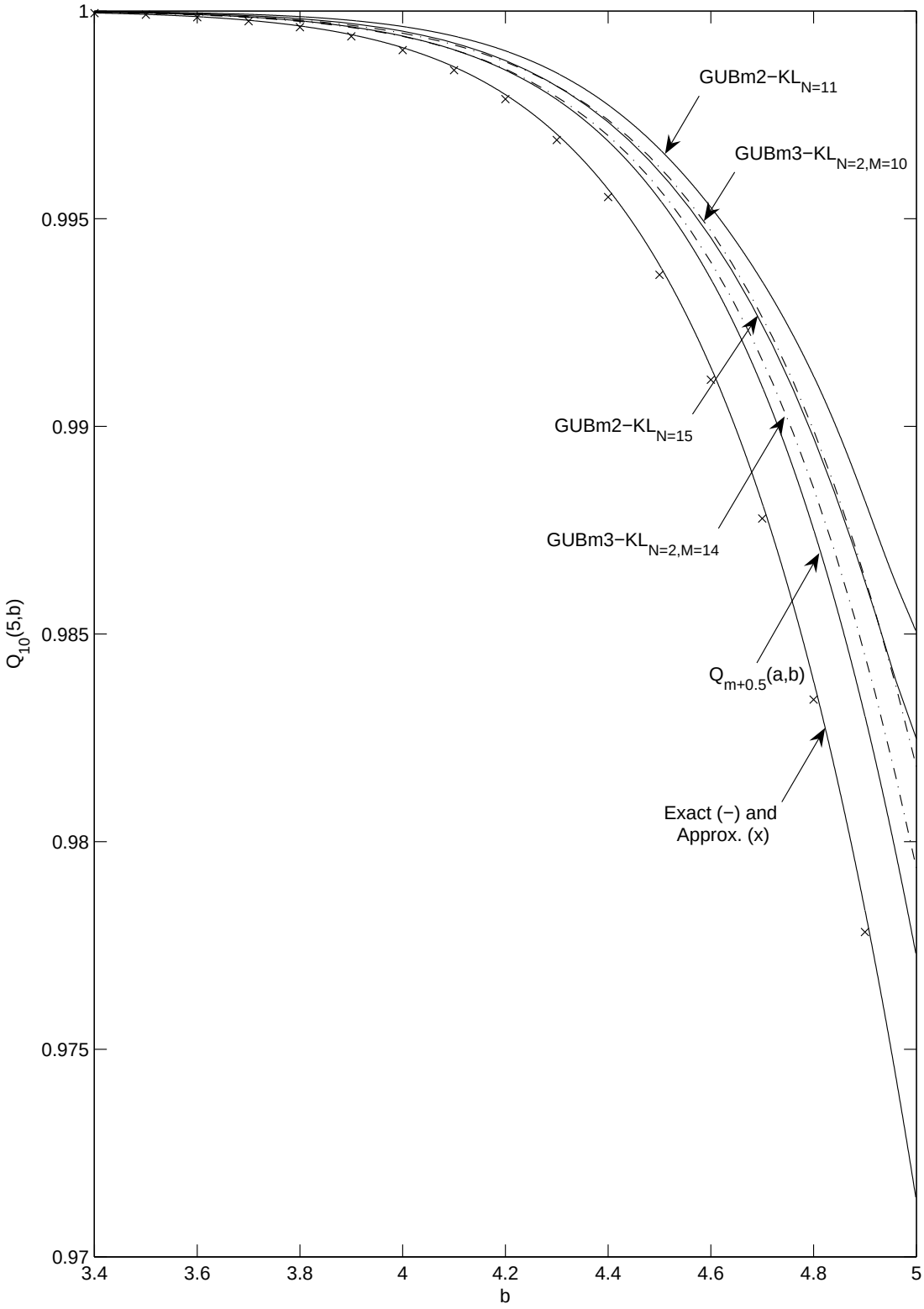

Fig. 5.15: The generalized Marcum Q-function $Q_m(a, b)$ and its upper bounds versus b for the case of $b < a = 5$ and $m = 10$.

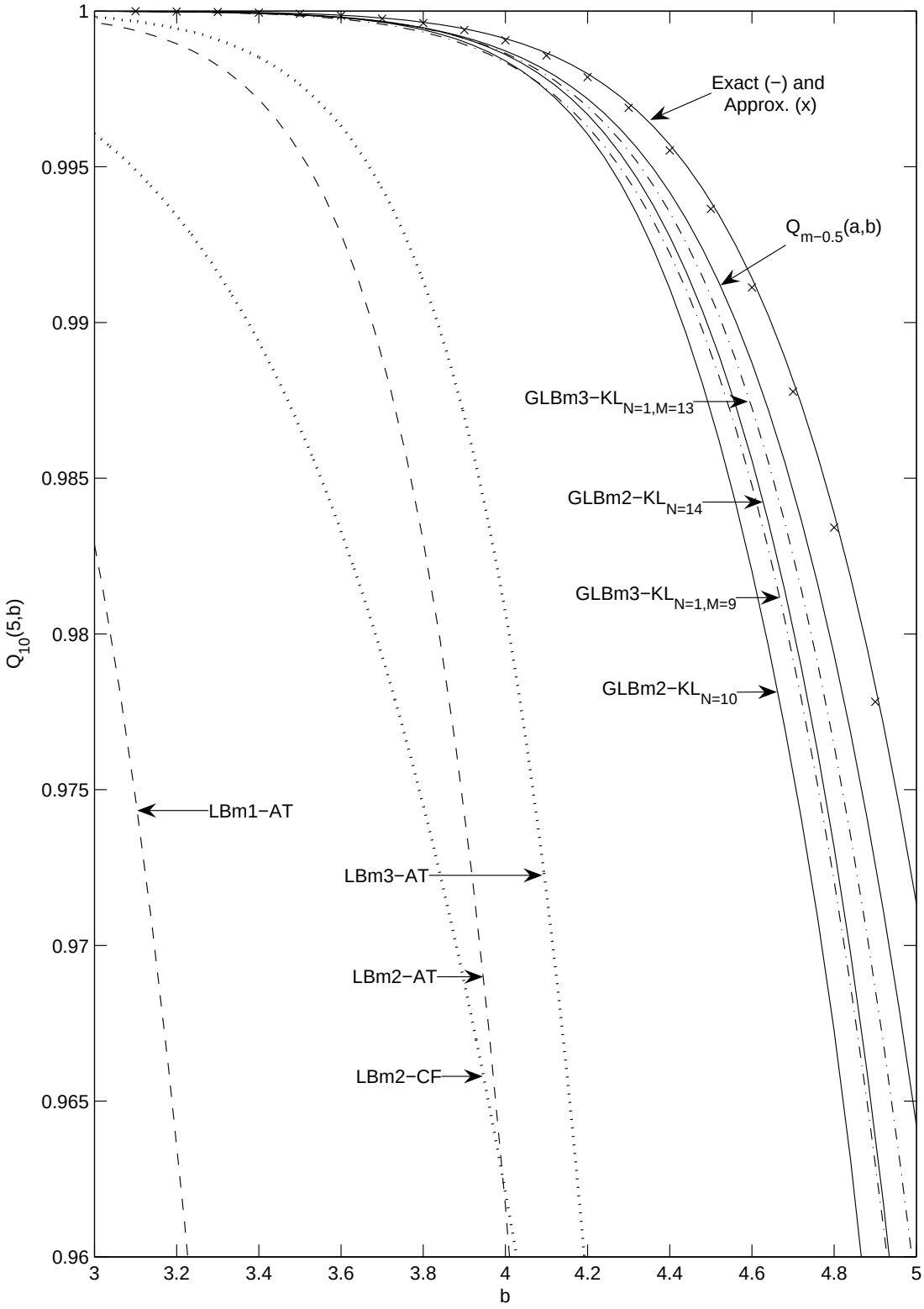

Fig. 5.16: The generalized Marcum Q-function $Q_m(a,b)$ and its lower bounds versus b for the case of $b < a = 5$ and $m = 10$.

range of values of the arguments. The bound LBm1-AT is only tight when a is small. The bounds which are not shown here are much looser than the others for the cases concerned.

5.7 Summary

In this chapter, we have presented a novel geometric view for $Q_m(a, b)$. Based on this geometric view, we have derived a new closed-form representation of $Q_m(a, b)$ for m being an odd multiple of 0.5, which involves only simple exponential functions and erfc functions. We have also derived a pair of new finite-integral representations for $Q_m(a, b)$ of integer order m, which are more robust than their counterparts in the literature.

In addition to these new representations, we have also shown that $Q_{m+0.5}(a, b)$ and $Q_{m-0.5}(a, b)$ are, respectively, tight upper and lower bounds on $Q_m(a, b)$, and their average is a good approximation of $Q_m(a, b)$. Besides, we have developed some generic exponential bounds and erfc bounds on $Q_m(a, b)$ of integer order m. These generic bounds approach the exact value of $Q_m(a, b)$ as the number of terms involved increases. Our upper bounds for $a > b$ are the only upper exponential/erfc bounds available for this case. When evaluated with a few terms, our generic upper bounds for $b > a$ can be tighter than the existing exponential bounds for some values of arguments. Our generic lower bounds for $b > a$ can be tighter than the existing exponential bounds for a wide range of values of the arguments. Our generic lower bounds for $a > b$ can also be tighter than the existing exponential bounds, and even can be tighter than the existing I_k-bounds for a wide range of values of the arguments.

Chapter 6

Performance Analysis of Quadratic-Form Receivers

In this chapter, we show some applications of our new representations, generic exponential bounds and simple erfc bounds, derived in Chapter 4 for the first-order Marcum Q-function, $Q(\cdot,\cdot)$, to the performance analysis of quadratic-form receivers for a variety of single-channel, differentially coherent and quadratic detections. By using our new representations and generic exponential bounds for $Q(\cdot,\cdot)$, we propose an exact, single-finite-integral expression, and a pair of closed-form generic upper and lower bounds for the average bit error probability of quadratic-form receivers over generalized fading channels. To apply our simple erfc bounds on $Q(\cdot,\cdot)$ to bounding the average bit error probability, we first evaluate the integrals involved in averaging the product of two Gaussian Q-functions over fading statistics. For Nakagami-m fading, we obtain an exact closed-form result for the integral involved, and for Rician fading, we obtain a pair of closed-form upper and lower bounds on the integral involved. Then based on these results, we propose two pairs of closed-form upper and lower bounds on the average bit error probability of quadratic-form receivers, one pair for Nakagami-m fading and the other pair for Rician fading, by using our simple erfc bounds on $Q(\cdot,\cdot)$.

6.1 Introduction

In Chapter 1, we have reviewed some research results in the literature for QFRs. We can see that for a variety of coherent, differentially coherent, partially coherent, and quadratic detections with diversity, the decision metric can be expressed as a special case of a general quadratic form in complex Gaussian random variables [1, 24–27]. For this general QFR, the expression of the bit error probability over AWGN channels can be given in terms of the generalized Marcum Q-function, $Q_m(\cdot, \cdot)$, [1, 5, 27, 31]. When a fading environment is considered, we need to average the conditional bit error probability over the distribution of the total instantaneous SNR per bit at the output of the diversity combiner. This requires us to compute the average of the generalized Marcum Q-function over the distribution of the total instantaneous SNR [118, 143]. The computation involved is usually complicated. In [113, 114], the generalized Marcum Q-function has been rewritten into single finite integrals with exponential integrands. Based on these alternative representations, for systems that employ postdetection equal gain combining (EGC) to process signals received from multiple independent channels, the average bit error probability of QFRs for differentially coherent and quadratic detections over generalized fading channels has been given in [31, eq. (76)] and [5, eq. (9.115)] as a single finite integral whose integrand involves the product of the moment generating functions (MGFs) of the subchannel instantaneous SNRs. Integrals involved in the average of the generalized Marcum Q-function over the Rayleigh and Nakagami-m fading distributions have been evaluated in closed form in [118, 143], and used therein to obtain closed-form expressions of the average bit error probability of differentially coherent and quadratic detections for some systems employing postdetection EGC or selection combining (SC). In addition to the exact expressions, some upper bounds on the average bit error probability of differentially coherent and quadratic detections with postdetection EGC over independent generalized fading channels have also been proposed in [120, 121] by using the exponential bounds on the generalized Marcum Q-function derived

therein. Thus far, there is no lower bound on the average bit error probability of the general QFR available in the literature.

Since in this chapter, we mainly want to show some applications of our new representations and bounds derived in Chapter 4 for the first-order Marcum Q-function, $Q(\cdot,\cdot)$, we will focus on the performance analysis of single-channel, differentially coherent and quadratic detections, for which the expression of the bit error probability only involves $Q(\cdot,\cdot)$ with both the arguments being proportional to the square root of the instantaneous SNR. By using our new finite-integral representations of $Q(\cdot,\cdot)$ in Section 4.3.1, we propose a new single-finite-integral expression for the average bit error probability of QFRs over generalized fading channels. By using our generic exponential bounds on $Q(\cdot,\cdot)$ in Section 4.4, we propose a pair of upper and lower generic bounds on the average bit error probability of QFRs over generalized fading channels. Since the generic exponential bounds approach the exact value of $Q(\cdot,\cdot)$ as the number of terms involved increases, our generic performance bounds also approach the exact value of the average bit error probability. Our simple erfc bounds on $Q(a,b)$ in Section 4.7 can also be used to derive bounds on the average bit error probability, but the averages of the product of two Gaussian Q-functions over fading distributions should be solved first. Thus, we first evaluate the integrals involved in the averages of the product of two Gaussian Q-functions over the Nakagami-m and Rician distributions. Then we apply the exact result, or the upper and lower bounds for these integrals to deriving some new upper and lower bounds on the average bit error probability over the Nakagami-m and Rician channels. Our numerical results show that when evaluated with a few terms, our generic upper bounds on the average bit error probability derived from the generic exponential bounds on $Q(a,b)$ are tighter than the existing bounds in [120, 121]. Our upper bounds on the average bit error probability derived from the simple erfc bounds on $Q(a,b)$ are also tighter than the existing bounds in some cases. Our lower bounds are the only lower bounds available, and they are shown to be tight. Thus, our lower bounds together with

our tight upper bounds can give a better approximation to the error performance of QFRs with single-channel reception when the exact, closed-form expression for the average bit error probability is hard to obtain, or is too complicated to use.

In Section 6.2, we review some results in the literature for the bit error probability of QFRs for diversity reception over multiple, independent AWGN channels. In Sections 6.3 and 6.4, we propose a new single-finite-integral expression and a pair of generic upper and lower bounds, respectively, for the average bit error probability of QFRs over generalized fading channels. In Section 6.5, we evaluate the averages of the product of two Gaussian Q-functions over the Nakagami-m and Rician distributions. In Section 6.6, we derive a pair of new, upper and lower bounds on the average bit error probability for each of Nakagami-m fading and Rician fading. In Section 6.7, we show some numerical results for our new exact expression and upper and lower bounds on the average bit error probability, and also compare the tightness of our new upper bounds with that of the existing upper bounds proposed in [120, 121].

6.2 Bit Error Probability of QFRs for Multichannel Detection over AWGN Channels

For a variety of coherent, differentially coherent, partially coherent, and quadratic detections, the decision metric for diversity reception over N independent AWGN channels can be expressed as a special case of the general quadratic form in complex Gaussian random variables given by [1, eq. (B–1)]

$$D = \sum_{k=1}^{N} D_k = \sum_{k=1}^{N} (A|X_k|^2 + B|Y_k|^2 + CX_kY_k^* + C^*X_k^*Y_k). \tag{6.1}$$

Here, A and B are real constants, and C may be a complex constant; $\{X_k\}_{k=1}^N$ are independent complex Gaussian random variables with $\mathcal{CN}(\bar{X}_k, 2\mu_{xx})$ distribution, and $\{Y_k\}_{k=1}^N$ are independent complex Gaussian random variables with

$\mathcal{CN}(\bar{Y}_k, 2\mu_{yy})$ distribution. The pair $\{X_k, Y_k\}$ are correlated with covariance $\mu_{xy} = \frac{1}{2}\mathrm{E}[(X_k - \bar{X}_k)(Y_k - \bar{Y}_k)^*]$, and $\{X_k, Y_i\}$ are independent for $k \neq i$. We need $|C|^2 - AB > 0$, since otherwise D will be always negative or positive, independent of X_k's and Y_k's. If we have $A = 1$, $B = -1$ and $C = 0$, D reduces to the decision metric for quadratic detection in [1, eq. (12.1–5)]. If we have $A = B = 0$ and $C = 1/2$, D reduces to the decision metric for coherent detection in [1, eq. (12.1–7)]. The probability of D being negative is given by [1, eq. (B–21)]

$$\begin{aligned}\Pr(D<0) = Q(a,b) - I_0(ab)\exp\left[-\frac{(a^2+b^2)}{2}\right] + \frac{I_0(ab)\exp\left[-(a^2+b^2)/2\right]}{(1+v_2/v_1)^{2N-1}} \\ \cdot \sum_{k=0}^{N-1}\binom{2N-1}{k}\left(\frac{v_2}{v_1}\right)^k + \frac{\exp\left[-(a^2+b^2)/2\right]}{(1+v_2/v_1)^{2N-1}}\sum_{n=1}^{N-1} I_n(ab) \\ \cdot \sum_{k=0}^{N-1-n}\binom{2N-1}{k}\left[\left(\frac{b}{a}\right)^n\left(\frac{v_2}{v_1}\right)^k - \left(\frac{a}{b}\right)^n\left(\frac{v_2}{v_1}\right)^{2N-1-k}\right]. \quad (6.2)\end{aligned}$$

Here, we have [1, eqs. (B–22), (B–6) and (B–8)]

$$\begin{aligned}
a &= \left[\frac{2v_1^2 v_2(\alpha_1 v_2 - \alpha_2)}{(v_1+v_2)^2}\right]^{1/2}, \\
b &= \left[\frac{2v_1 v_2^2(\alpha_1 v_1 + \alpha_2)}{(v_1+v_2)^2}\right]^{1/2}, \\
v_1 &= \sqrt{w^2 + \frac{1}{4(\mu_{xx}\mu_{yy} - |\mu_{xy}|^2)(|C|^2 - AB)}} - w, \\
v_2 &= \sqrt{w^2 + \frac{1}{4(\mu_{xx}\mu_{yy} - |\mu_{xy}|^2)(|C|^2 - AB)}} + w, \\
w &= \frac{A\mu_{xx} + B\mu_{yy} + C^*\mu_{xy}^* + C\mu_{xy}}{4(\mu_{xx}\mu_{yy} - |\mu_{xy}|^2)(|C|^2 - AB)}, \\
\alpha_1 &= \sum_{k=1}^{N}\alpha_{1k}, \\
\alpha_2 &= \sum_{k=1}^{N}\alpha_{2k}, \\
\alpha_{1k} &= 2(|C|^2 - AB)(|\bar{X}_k|^2\mu_{yy} + |\bar{Y}_k|^2\mu_{xx} - \bar{X}_k^*\bar{Y}_k\mu_{xy} - \bar{X}_k\bar{Y}_k^*\mu_{xy}^*), \\
\alpha_{2k} &= A|\bar{X}_k|^2 + B|\bar{Y}_k|^2 + C^*\bar{X}_k^*\bar{Y}_k + C\bar{X}_k\bar{Y}_k^*. \quad (6.3)
\end{aligned}$$

A point to note is that in the expressions for w and α_{2k} in [1, eq. (B–6)], C should be C^*, and C^* should be C. These errors are corrected in (6.3).

In [31, eq. (60)], the probability in (6.2) has been rewritten in terms of the generalized Marcum Q-function as

$$\begin{aligned}
&\Pr(D<0)\\
&= Q(a,b) - \left[1 - \frac{1}{(1+v_2/v_1)^{2N-1}} \sum_{k=0}^{N-1} \binom{2N-1}{k} \left(\frac{v_2}{v_1}\right)^k\right] I_0(ab) \exp\left[-\frac{(a^2+b^2)}{2}\right]\\
&\quad + \frac{1}{(1+v_2/v_1)^{2N-1}} \left\{\sum_{k=2}^{N} \binom{2N-1}{N-k} \left(\frac{v_2}{v_1}\right)^{N-k} [Q_k(a,b) - Q(a,b)]\right\}\\
&\quad - \frac{1}{(1+v_2/v_1)^{2N-1}} \left\{\sum_{k=2}^{N} \binom{2N-1}{N-k} \left(\frac{v_2}{v_1}\right)^{N-1+k} [Q_k(b,a) - Q(b,a)]\right\}. \qquad (6.4)
\end{aligned}$$

By using the equalities [124, eq. (1.111)]

$$\sum_{k=0}^{N-1} \binom{2N-1}{k} \left(\frac{v_2}{v_1}\right)^k = \sum_{k=1}^{N} \binom{2N-1}{N-k} \left(\frac{v_2}{v_1}\right)^{N-k}, \qquad (6.5)$$

$$\sum_{k=1}^{N} \binom{2N-1}{N-k} \left[\left(\frac{v_2}{v_1}\right)^{N-k} + \left(\frac{v_2}{v_1}\right)^{N+k-1}\right] = \left[1 + \left(\frac{v_2}{v_1}\right)\right]^{2N-1}, \qquad (6.6)$$

and [31, eq. (67)]

$$Q(a,b) - \frac{1}{2} I_0(ab) \exp\left(-\frac{a^2+b^2}{2}\right) = \frac{1}{2}[1 - Q(b,a) + Q(a,b)] \qquad (6.7)$$

in (6.4), we can further simplify (6.4) to

$$\begin{aligned}
&\Pr(D<0)\\
&= \frac{(v_2/v_1)^N}{(1+v_2/v_1)^{2N-1}} \sum_{k=1}^{N} \binom{2N-1}{N-k} \left\{\left(\frac{v_1}{v_2}\right)^k Q_k(a,b) + \left(\frac{v_2}{v_1}\right)^{k-1} [1 - Q_k(b,a)]\right\}. \qquad (6.8)
\end{aligned}$$

For some modulation schemes of interest, we have $v_1 = v_2$. For this special

Table 6.1: Parameters for Four Modulation Schemes with Multichannel Differentially Coherent Detection or Multichannel Quadratic Detection

Modulation	α	β
Binary Orthogonal FSK	0	1
Binary DPSK	0	$\sqrt{2}$
DQPSK with Gray Coding	$\sqrt{2-\sqrt{2}}$	$\sqrt{2+\sqrt{2}}$
Binary Correlated Signals with Correlation Coefficient $0 < \lvert\varsigma\rvert < 1$	$\sqrt{\frac{1-\sqrt{1-\lvert\varsigma\rvert^2}}{2}}$	$\sqrt{\frac{1+\sqrt{1-\lvert\varsigma\rvert^2}}{2}}$

case, from (6.6), we obtain the equality

$$\sum_{k=1}^{N} \binom{2N-1}{N-k} = 2^{2N-2}, \tag{6.9}$$

and (6.8) reduces to [31, eq. (68)]

$$\Pr(D<0) = \frac{1}{2} + \frac{1}{2^{2N-1}} \sum_{k=1}^{N} \binom{2N-1}{N-k} \left[Q_k(a,b) - Q_k(b,a)\right]. \tag{6.10}$$

From (6.10), we can see that for a number of special cases of particular importance, the bit error probability can be given by

$$P_b(\gamma,\alpha,\beta) = \frac{1}{2} + \frac{1}{2^{2N-1}} \sum_{k=1}^{N} \binom{2N-1}{N-k} \left[Q_k(\alpha\sqrt{\gamma},\beta\sqrt{\gamma}) - Q_k(\beta\sqrt{\gamma},\alpha\sqrt{\gamma})\right], \tag{6.11}$$

where γ is the total instantaneous SNR per bit at the output of the combiner, and the values of the arguments α and β are dependent on modulation schemes, and are summarized in Table 6.1 for four different modulation schemes [1, 5, 31, 118].

For the special case of $N = 1$, which corresponds to the case of single-channel

detection, (6.11) reduces to

$$P_b(\gamma, \alpha, \beta) = \frac{1}{2}\left[1 + Q(\alpha\sqrt{\gamma}, \beta\sqrt{\gamma}) - Q(\beta\sqrt{\gamma}, \alpha\sqrt{\gamma})\right]. \tag{6.12}$$

Thus, for quadratic detection of equal energy, equiprobable, correlated binary signals, the bit error probability is given by (6.12) with the arguments [1, eq. (5.4–54)]

$$\begin{cases} \alpha = \sqrt{\dfrac{1 - \sqrt{1 - |\varsigma|^2}}{2}}, & \text{(6.13a)} \\ \beta = \sqrt{\dfrac{1 + \sqrt{1 - |\varsigma|^2}}{2}}, & \text{(6.13b)} \end{cases}$$

where $0 < |\varsigma| < 1$ is the magnitude of the cross-correlation coefficient between the two signals. When we set $\varsigma = 0$ in (6.12) and (6.13), and use the values of the Marcum Q-function for the special cases, i.e.,

$$Q(0, b) = \exp\left(-\frac{b^2}{2}\right), \tag{6.14}$$

$$Q(a, 0) = 1, \tag{6.15}$$

we obtain the well-known result for orthogonal binary FSK with quadratic detection, namely, [1, eq. (5.4–55)]

$$P_b(\gamma, 0, 1) = \frac{1}{2}e^{-\gamma/2}. \tag{6.16}$$

For the case of binary differential PSK (DPSK), we have $\alpha = 0$ and $\beta = \sqrt{2}$, and thus, (6.12) reduces to [1, eq. (5.2–69)]

$$P_b(\gamma, 0, \sqrt{2}) = \frac{1}{2}e^{-\gamma}. \tag{6.17}$$

Finally, for the case of differential quadrature PSK (DQPSK) with Gray coding,

the bit error probability is given by (6.12) with the arguments [1, eq. (5.2–71)]

$$\begin{cases} \alpha = \sqrt{2 - \sqrt{2}}, & \text{(6.18a)} \\ \beta = \sqrt{2 + \sqrt{2}}. & \text{(6.18b)} \end{cases}$$

6.3 Average Bit Error Probability of QFRs for Single-Channel Detection over Fading Channels

From the above section, we can see that the average bit error probability over fading channels for a variety of single-channel, differentially coherent and quadratic detections is given by

$$\begin{aligned} P_b(\alpha, \beta) &= \int_0^\infty p_\gamma(\gamma) P_b(\gamma, \alpha, \beta) d\gamma \\ &= \frac{1}{2} + \frac{1}{2} \int_0^\infty p_\gamma(\gamma) [Q(\alpha\sqrt{\gamma}, \beta\sqrt{\gamma}) - Q(\beta\sqrt{\gamma}, \alpha\sqrt{\gamma})] d\gamma. \end{aligned} \quad (6.19)$$

Here, $p_\gamma(\gamma)$ is the PDF of γ. From Table 6.1, we can see that we usually have $\beta > \alpha \geq 0$.

The closed-form result for $P_b(\alpha, \beta)$ in (6.19) has been given for Rayleigh fading in [31], and for Nakagami-m fading in [118, 143]. However, for the case of Rician fading, the closed-form result for $P_b(\alpha, \beta)$ in (6.19) has only been given in [31] for some simple cases, such as binary orthogonal FSK with quadratic detection and binary DPSK, both of which have $\alpha = 0$. For some more complicated cases, such as DQPSK with Gray coding and binary correlated signals with quadratic detection, only a single-finite-integral result has been given in [31, eqs. (30) and (46)]. This single-finite-integral result was obtained by using the alternative finite-integral representations of $Q(a, b)$ in (4.19) and (4.20) to express the Marcum Q-functions

Table 6.2: PDF and MGF of the SNR per Bit γ for Fading Channels

Fading	**PDF** $p_\gamma(\gamma)$	**MGF** $M_\gamma(s)$
Rayleigh	$\frac{1}{\bar{\gamma}} \exp\left(-\frac{\gamma}{\bar{\gamma}}\right)^\sharp$	$(1 - s\bar{\gamma})^{-1}$
Rician ($K \geq 0^\natural$)	$\frac{(1+K)e^{-K-(1+K)\gamma/\bar{\gamma}}}{\bar{\gamma}} I_0\left(2\sqrt{\frac{K(1+K)\gamma}{\bar{\gamma}}}\right)$	$\frac{1+K}{1+K-s\bar{\gamma}} \exp\left(\frac{Ks\bar{\gamma}}{1+K-s\bar{\gamma}}\right)$
Nakagami-m ($m \geq 1/2$)	$\frac{m^m \gamma^{m-1}}{\bar{\gamma}^m \Gamma(m)} \exp\left(-\frac{m\gamma}{\bar{\gamma}}\right)$	$(1 - s\bar{\gamma}/m)^{-m}$

$^\sharp$ $\bar{\gamma}$ is the average SNR per bit.

$^\natural$ K is the ratio of the power of the line-of-sight component to the average power of the scattered component.

in (6.19) and interchanging the order of integration, namely, [31, eq. (30)]

$$P_b(\alpha, \beta) = \frac{1}{4\pi} \int_{-\pi}^{\pi} \frac{\beta^2 - \alpha^2}{\beta^2 + 2\alpha\beta \sin\theta + \alpha^2} M_\gamma \left[-\frac{1}{2} \left(\beta^2 + 2\alpha\beta \sin\theta + \alpha^2 \right) \right] d\theta, \tag{6.20}$$

where $M_\gamma(s) = \int_0^\infty e^{s\gamma} p_\gamma(\gamma) d\gamma$ is the MGF of γ. The expression of $P_b(\alpha, \beta)$ in (6.20) is a unified form for various fading channels. The PDF and the MGF of γ for the Rayleigh, Rician, Nakagami-m fading channels are summarized in Table 6.2 [5, Table 2.2]. It is clear that the case of Rayleigh fading can be regarded as a special case of Nakagami-m fading with $m = 1$, or as a special case of Rician fading with $K = 0$. Since the MGFs in Table 6.2 for the three fading channels are all given in closed form, the expression of $P_b(\alpha, \beta)$ in (6.20) involves only a single-fold finite-range integral. However, the expression of $P_b(\alpha, \beta)$ in (6.20) may be unstable in some cases, because the denominator $(\beta^2 + 2\alpha\beta \sin\theta + \alpha^2)$ could be small for some parameters combinations.

By using a similar method, we can also obtain a new single-finite-integral result for $P_b(\alpha, \beta)$ in (6.19). We use our new finite-integral representations of $Q(a, b)$ in (4.11) and (4.14) to express $Q(\alpha\sqrt{\gamma}, \beta\sqrt{\gamma})$ and $Q(\beta\sqrt{\gamma}, \alpha\sqrt{\gamma})$, respectively, and

obtain

$$\begin{aligned}
P_b(\alpha,\beta) &= \frac{1}{2} + \frac{1}{2}\int_0^\infty p_\gamma(\gamma)\Bigg\{\frac{1}{\pi}\int_0^\pi \exp\left[-\frac{\gamma}{2}\left(-\alpha\cos\theta + \sqrt{\beta^2-\alpha^2\sin^2\theta}\right)^2\right]d\theta \\
&\quad - 1 + \frac{1}{\pi}\int_{\pi-\arcsin(\alpha/\beta)}^\pi \Bigg\{\exp\left[-\frac{\gamma}{2}\left(-\beta\cos\theta - \sqrt{\alpha^2-\beta^2\sin^2\theta}\right)^2\right] \\
&\quad - \exp\left[-\frac{\gamma}{2}\left(-\beta\cos\theta + \sqrt{\alpha^2-\beta^2\sin^2\theta}\right)^2\right]\Bigg\}d\theta\Bigg\}d\gamma \\
&= \frac{1}{2\pi}\int_0^\pi M_\gamma\left[-\frac{1}{2}\left(-\alpha\cos\theta + \sqrt{\beta^2-\alpha^2\sin^2\theta}\right)^2\right]d\theta \\
&\quad + \frac{1}{2\pi}\int_{\pi-\arcsin(\alpha/\beta)}^\pi \Bigg\{M_\gamma\left[-\frac{1}{2}\left(-\beta\cos\theta - \sqrt{\alpha^2-\beta^2\sin^2\theta}\right)^2\right] \\
&\quad - M_\gamma\left[-\frac{1}{2}\left(-\beta\cos\theta + \sqrt{\alpha^2-\beta^2\sin^2\theta}\right)^2\right]\Bigg\}d\theta. \qquad (6.21)
\end{aligned}$$

We can see that our new expression of $P_b(\alpha,\beta)$ in (6.21) is more robust than that in (6.20), since its integrands are pure MGFs and do not involve denominator terms before the MGFs.

6.4 Bounds on the Average Bit Error Probability Derived from the Generic Exponential Bounds on the First-Order Marcum Q-Function

In addition to the exact expression of the average bit error probability $P_b(\alpha,\beta)$, its upper and lower bounds are also of interest, especially when the closed-form result for $P_b(\alpha,\beta)$ is difficult to obtain or hard to evaluate. Upper bounds on $P_b(\alpha,\beta)$ can be obtained by using an upper bound on $Q(a,b)$ for $b>a$ to bound $Q(\alpha\sqrt{\gamma},\beta\sqrt{\gamma})$ in (6.19) and using a lower bound on $Q(a,b)$ for $a>b$ to bound $Q(\beta\sqrt{\gamma},\alpha\sqrt{\gamma})$ in (6.19). We have derived some exponential bounds and

erfc bounds on $Q(a,b)$ in Chapter 4, and have shown their superiority over the existing exponential bounds in [114, 120, 121] for a wide range of values of the arguments. The I_0-bounds on $Q(a,b)$ proposed in [116, 121, 122] and discussed in Chapter 4 are not suitable for this application. In this section, we focus on the usage of the exponential bounds on $Q(a,b)$ in bounding $P_b(\alpha,\beta)$. In Section 6.6, we will show the usage of the erfc bounds on $Q(a,b)$ in bounding $P_b(\alpha,\beta)$.

In [120], an upper bound on $P_b(\alpha,\beta)$ has been given by using the exponential bound UB1-SA in (4.93) as the upper bound on $Q(a,b)$ for $b>a$ and using the exponential bound LB2-SA in (4.107) as the lower bound on $Q(a,b)$ for $a>b$, namely [120, eq. (18)]

$$\begin{aligned} P_b(\alpha,\beta) &\le P_{b,UB\text{-}SA}(\alpha,\beta) \\ &= \frac{3}{4}M_\gamma\left[-\frac{(\beta-\alpha)^2}{2}\right]-\frac{1}{4}M_\gamma\left[-\frac{(\beta+\alpha)^2}{2}\right]. \end{aligned} \tag{6.22}$$

In [121], another upper bound on $P_b(\alpha,\beta)$ has been given by using the exponential bound UB1-AT in (4.95) as the upper bound on $Q(a,b)$ for $b>a$ and using the exponential bound LB2-AT in (4.108) as the lower bound on $Q(a,b)$ for $a>b$, namely [121, eq. (29)]

$$\begin{aligned} P_b(\alpha,\beta) &\le P_{b,UB\text{-}AT}(\alpha,\beta) \\ &= \frac{1}{4}\left\{\sqrt{\frac{1}{2}\left[1+\frac{1}{1-(a/b)^2}\right]}+\sqrt{\frac{(b/a)^2}{2\left[1-(b/a)^2\right]}}\right\} \\ &\quad\cdot\left\{M_\gamma\left[-\frac{(\beta-\alpha)^2}{2}\right]+M_\gamma\left[-\frac{(\beta+\alpha)^2}{2}\right]\right\}. \end{aligned} \tag{6.23}$$

Similarly, we can also obtain some new upper bounds on $P_b(\alpha,\beta)$ by using our exponential bounds derived in Chapter 4 for $Q(a,b)$. By using the generic upper exponential bound GUB1-KL in (4.28) as the upper bound on $Q(a,b)$ for $b>a$ and using the generic lower exponential bound GLB2-KL in (4.35) as the lower bound on $Q(a,b)$ for $a>b$, we can obtain a generic upper bound on $P_b(\alpha,\beta)$

as

$$\begin{aligned} P_b(\alpha,\beta) &\le P_{b,GUB\text{-}KL}(\alpha,\beta) \\ &= \frac{1}{2} + \frac{1}{2}\int_0^\infty \left[Q_{GUB1\text{-}KL}(\alpha\sqrt{\gamma},\beta\sqrt{\gamma}) - Q_{GLB2\text{-}KL}(\beta\sqrt{\gamma},\alpha\sqrt{\gamma})\right] p_\gamma(\gamma)d\gamma \\ &= \frac{1}{2\pi}\Bigg\{ \sum_{k=1}^{G}(\phi_k - \phi_{k-1}) M_\gamma\left[-\frac{l^2(\phi_{k-1})}{2}\right] + \sum_{i=1}^{H}(\theta_i - \theta_{i-1}) M_\gamma\left[-\frac{l_1^2(\theta_i)}{2}\right] \\ &\quad - \sum_{j=1}^{M}(\omega_j - \omega_{j-1}) M_\gamma\left[-\frac{l_2^2(\omega_j)}{2}\right]\Bigg\}. \end{aligned} \tag{6.24}$$

Here, we have $0 = \phi_0 < \phi_1 < \cdots < \phi_G = \pi$, $\pi - \arcsin(\alpha/\beta) = \theta_0 < \theta_1 < \cdots < \theta_H = \pi$, $\pi - \arcsin(\alpha/\beta) = \omega_0 < \omega_1 < \cdots < \omega_M = \pi$,

$$l(\phi_k) = -\alpha\cos\phi_k + \sqrt{\beta^2 - \alpha^2\sin^2\phi_k}, \tag{6.25}$$

and

$$\begin{cases} l_1(\theta_i) = -\beta\cos\theta_i - \sqrt{\alpha^2 - \beta^2\sin^2\theta_i}, & \text{(6.26a)} \\ l_2(\omega_j) = -\beta\cos\omega_j + \sqrt{\alpha^2 - \beta^2\sin^2\omega_j}. & \text{(6.26b)} \end{cases}$$

Using the MGFs given in Table 6.2, we can see that for Nakagami-m fading, the generic upper bound $P_{b,GUB\text{-}KL}(\alpha,\beta)$ in (6.24) on the average bit error probability becomes

$$\begin{aligned} P_{b,GUB\text{-}KL}(\alpha,\beta) = \frac{1}{2\pi}\Bigg\{ &\sum_{k=1}^{G}(\phi_k - \phi_{k-1})\left[1 + \frac{\bar{\gamma}l^2(\phi_{k-1})}{2m}\right]^{-m} \\ &+ \sum_{i=1}^{H}(\theta_i - \theta_{i-1})\left[1 + \frac{\bar{\gamma}l_1^2(\theta_i)}{2m}\right]^{-m} \\ &- \sum_{j=1}^{M}(\omega_j - \omega_{j-1})\left[1 + \frac{\bar{\gamma}l_2^2(\omega_j)}{2m}\right]^{-m}\Bigg\}. \end{aligned} \tag{6.27}$$

For Rician fading, the generic upper bound $P_{b,GUB\text{-}KL}(\alpha,\beta)$ in (6.24) on the av-

erage bit error probability becomes

$$\begin{aligned}P_{b,GUB\text{-}KL}(\alpha,\beta) = &\sum_{k=1}^{G}\frac{(\phi_k-\phi_{k-1})(1+K)}{\pi[2+2K+\bar{\gamma}l^2(\phi_{k-1})]}\exp\left[-\frac{K\bar{\gamma}l^2(\phi_{k-1})}{2+2K+\bar{\gamma}l^2(\phi_{k-1})}\right]\\ &+\sum_{i=1}^{H}\frac{(\theta_i-\theta_{i-1})(1+K)}{\pi[2+2K+\bar{\gamma}l_1^2(\theta_i)]}\exp\left[-\frac{K\bar{\gamma}l_1^2(\theta_i)}{2+2K+\bar{\gamma}l_1^2(\theta_i)}\right]\\ &-\sum_{j=1}^{M}\frac{(\omega_j-\omega_{j-1})(1+K)}{\pi[2+2K+\bar{\gamma}l_2^2(\omega_j)]}\exp\left[-\frac{K\bar{\gamma}l_2^2(\omega_j)}{2+2K+\bar{\gamma}l_2^2(\omega_j)}\right].\end{aligned} \tag{6.28}$$

In addition to upper bounds, lower bounds on $P_b(\alpha,\beta)$ are also useful. There is no lower bound on $P_b(\alpha,\beta)$ available in the literature. This is because using the mathematical methods in the literature cannot lead to simple upper bounds on $Q(a,b)$ for $a>b$. However, we can obtain some new lower bounds on $P_b(\alpha,\beta)$ here, since we have derived some simple upper bounds on $Q(a,b)$ for $a>b$ in Chapter 4. By using the generic lower exponential bound GLB1-KL in (4.29) as the lower bound on $Q(a,b)$ for $b>a$ and using the generic upper exponential bound GUB2-KL in (4.33) as the upper bound on $Q(a,b)$ for $a>b$, we obtain a generic lower bound on $P_b(\alpha,\beta)$ as

$$\begin{aligned}&P_b(\alpha,\beta)\\ &\geq P_{b,GLB\text{-}KL}(\alpha,\beta)\\ &=\frac{1}{2}+\frac{1}{2}\int_0^{\infty}\left[Q_{GLB1\text{-}KL}(\alpha\sqrt{\gamma},\beta\sqrt{\gamma})-Q_{GUB2\text{-}KL}(\beta\sqrt{\gamma},\alpha\sqrt{\gamma})\right]p_\gamma(\gamma)d\gamma\\ &=\frac{1}{2\pi}\int_0^{\infty}\left\{\sum_{k=1}^{G}(\phi_k-\phi_{k-1})\exp\left[-\frac{l^2(\phi_k)\gamma}{2}\right]+\sum_{i=1}^{H-1}(\theta_{i+1}-\theta_i)\exp\left[-\frac{l_1^2(\theta_i)\gamma}{2}\right]\right.\\ &\quad\left.-\sum_{j=1}^{M-1}(\omega_{j+1}-\omega_j)\exp\left[-\frac{l_2^2(\omega_j)\gamma}{2}\right]\right\}p_\gamma(\gamma)d\gamma\\ &=\frac{1}{2\pi}\left\{\sum_{k=1}^{G}(\phi_k-\phi_{k-1})M_\gamma\left[-\frac{l^2(\phi_k)}{2}\right]+\sum_{i=1}^{H-1}(\theta_{i+1}-\theta_i)M_\gamma\left[-\frac{l_1^2(\theta_i)}{2}\right]\right.\\ &\quad\left.-\sum_{j=1}^{M-1}(\omega_{j+1}-\omega_j)M_\gamma\left[-\frac{l_2^2(\omega_j)}{2}\right]\right\}.\end{aligned} \tag{6.29}$$

Here, the arguments are defined in the same way as those in (6.24), but $\theta_1 = \omega_1$ is required.

It is easy to see that for Nakagami-m fading, the generic lower bound $P_{b,GLB\text{-}KL}(\alpha,\beta)$ in (6.29) for the average bit error probability becomes

$$\begin{aligned} P_{b,GLB\text{-}KL}(\alpha,\beta) = \frac{1}{2\pi}\Bigg\{ & \sum_{k=1}^{G}(\phi_k-\phi_{k-1})\left[1+\frac{\bar{\gamma}l^2(\phi_k)}{2m}\right]^{-m} \\ & + \sum_{i=1}^{H-1}(\theta_{i+1}-\theta_i)\left[1+\frac{\bar{\gamma}l_1^2(\theta_i)}{2m}\right]^{-m} \\ & - \sum_{j=1}^{M-1}(\omega_{j+1}-\omega_j)\left[1+\frac{\bar{\gamma}l_2^2(\omega_j)}{2m}\right]^{-m}\Bigg\}. \end{aligned} \tag{6.30}$$

For Rician fading, the generic lower bound $P_{b,GLB\text{-}KL}(\alpha,\beta)$ in (6.29) for the average bit error probability becomes

$$\begin{aligned} P_{b,GLB\text{-}KL}(\alpha,\beta) = & \sum_{k=1}^{G}\frac{(\phi_k-\phi_{k-1})(1+K)}{\pi[2+2K+\bar{\gamma}l^2(\phi_k)]}\exp\left[-\frac{K\bar{\gamma}l^2(\phi_k)}{2+2K+\bar{\gamma}l^2(\phi_k)}\right] \\ & + \sum_{i=1}^{H-1}\frac{(\theta_{i+1}-\theta_i)(1+K)}{\pi[2+2K+\bar{\gamma}l_1^2(\theta_i)]}\exp\left[-\frac{K\bar{\gamma}l_1^2(\theta_i)}{2+2K+\bar{\gamma}l_1^2(\theta_i)}\right] \\ & - \sum_{j=1}^{M-1}\frac{(\omega_{j+1}-\omega_j)(1+K)}{\pi[2+2K+\bar{\gamma}l_2^2(\omega_j)]}\exp\left[-\frac{K\bar{\gamma}l_2^2(\omega_j)}{2+2K+\bar{\gamma}l_2^2(\omega_j)}\right]. \end{aligned} \tag{6.31}$$

The generic upper bound $P_{b,GUB\text{-}KL}(\alpha,\beta)$ in (6.24) and the generic lower bound $P_{b,GLB\text{-}KL}(\alpha,\beta)$ in (6.29) involve an arbitrarily large number of terms. We have shown in Chapter 4 that our generic exponential bounds on $Q(a,b)$, i.e., GUB1-KL in (4.28), GUB2-KL in (4.33), GLB1-KL in (4.29), and GLB2-KL in (4.35), approach the exact value of $Q(a,b)$ as the number of terms involved increases. Thus, the two error probability bounds, $P_{b,GUB\text{-}KL}(\alpha,\beta)$ and $P_{b,GLB\text{-}KL}(\alpha,\beta)$, which are derived from these generic exponential bounds on $Q(a,b)$, will also approach the exact value of $P_b(\alpha,\beta)$ in (6.21) as the number of terms involved increases.

6.5 Averages of the Product of Two Gaussian Q-Functions over Fading Statistics

In addition to the generic exponential bounds on $Q(a,b)$, we have also derived some erfc bounds on $Q(a,b)$ in Chapter 4. These erfc bounds can also be used to derive bounds on $P_b(\alpha,\beta)$ in (6.19), but averaging the product of two Gaussian Q-functions over the fading statistics will be required. For the case that the two Gaussian Q-functions are identical, the integral involved in the average has been evaluated in closed form for Rayleigh fading [5, eq. (5.29)] and Nakagami-m fading [5, eq. (5.30)]. For the case that the two Gaussian Q-functions are different, the integral involved has only been solved in closed form for Rayleigh fading [135, eq. (5)]. In this section, we evaluate the integral for the latter case. We give an exact result for Nakagami-m fading, and tight upper and lower bounds for Rician fading, all in closed form. These results will be used to derive some bounds on $P_b(\alpha,\beta)$ in Section 6.6.

The average of the product of two Gaussian Q-functions over a fading distribution is given by

$$I = \int_0^\infty p_\gamma(\gamma) Q(A_1\sqrt{\gamma}) Q(A_2\sqrt{\gamma}) d\gamma, \quad A_1 \geq 0, A_2 \geq 0. \tag{6.32}$$

Here, $Q(x)$ is the Gaussian Q-function, given by [60]

$$Q(x) = \int_x^\infty \frac{e^{-t^2/2}}{\sqrt{2\pi}} dt = \frac{1}{2}\text{erfc}\left(\frac{x}{\sqrt{2}}\right) = \frac{1}{\pi}\int_0^{\pi/2} \exp\left(-\frac{x^2}{2\sin^2\theta}\right) d\theta. \tag{6.33}$$

The product $Q(x)Q(y)$ in (6.32) can be rewritten into a sum of two single finite-integrals by using a simple geometric approach. We assume that X and Y are two independent Gaussian random variables with zero mean and unit variance. Then the product $Q(x)Q(y)$ is the probability of (X,Y) lying in the shaded area $(X > x, Y > y)$ in Fig. 6.1. This probability can be obtained by computing the probability of (X,Y) lying in the unshaded areas P_1 and P_2 in the upper right

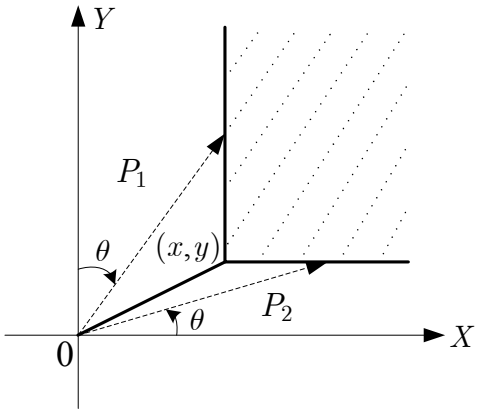

Fig. 6.1: Diagram of the evaluation of the product of two Gaussian Q-functions.

quadrant. This leads to

$$\begin{aligned}
&Q(x)Q(y) \\
&= \frac{1}{4} - \Pr[(X,Y) \in P_1] - \Pr[(X,Y) \in P_2] \\
&= \frac{1}{4} - \int_{\theta=0}^{\pi/2-\arctan(y/x)} \int_{r=0}^{x/\sin\theta} \frac{r}{2\pi} e^{-r^2/2} dr d\theta - \int_{\theta=0}^{\arctan(y/x)} \int_{r=0}^{y/\sin\theta} \frac{r}{2\pi} e^{-r^2/2} dr d\theta \\
&= \frac{1}{2\pi} \int_0^{\pi/2-\arctan(y/x)} \exp\left(-\frac{x^2}{2\sin^2\theta}\right) d\theta + \frac{1}{2\pi} \int_0^{\arctan(y/x)} \exp\left(-\frac{y^2}{2\sin^2\theta}\right) d\theta.
\end{aligned} \tag{6.34}$$

This result turns out to be the same as that in [5, eq. (4.8)].

Substituting (6.34) into (6.32), we can therefore rewrite the integral in (6.32) as

$$\begin{aligned}
I = &\frac{1}{2\pi} \int_0^{\pi/2-\arctan(A_2/A_1)} M_\gamma\left(-\frac{A_1^2}{2\sin^2\theta}\right) d\theta \\
&+ \frac{1}{2\pi} \int_0^{\arctan(A_2/A_1)} M_\gamma\left(-\frac{A_2^2}{2\sin^2\theta}\right) d\theta.
\end{aligned} \tag{6.35}$$

Using the MGFs given in Table 6.2, we can evaluate the average in (6.35) for various fading models.

6.5.1 Nakagami-m fading

For Nakagami-m fading, the MGF of γ is given by [5, eq. (2.22)]

$$M_\gamma(s) = (1 - s\bar{\gamma}/m)^{-m}, \qquad m \geq \frac{1}{2}. \tag{6.36}$$

Substituting (6.36) into (6.35) leads to

$$\begin{aligned} I_{Nakagami} = &\frac{1}{2\pi}\int_0^{\pi/2-\arctan(A_2/A_1)} \left[\frac{\sin^2\theta}{\sin^2\theta + A_1^2\bar{\gamma}/(2m)}\right]^m d\theta \\ &+ \frac{1}{2\pi}\int_0^{\arctan(A_2/A_1)} \left[\frac{\sin^2\theta}{\sin^2\theta + A_2^2\bar{\gamma}/(2m)}\right]^m d\theta. \end{aligned} \tag{6.37}$$

The integrals in (6.37) can be solved by using the formula in [5, eq. (5A.24)] which can be rewritten as

$$\begin{aligned} \frac{1}{\pi}\int_0^{\phi}\left(\frac{\sin^2\theta}{\sin^2\theta+\eta}\right)^m d\theta = &\frac{\phi}{\pi} - \frac{1}{\pi}\sum_{k=0}^{m-1}\binom{2k}{k}\frac{(\frac{\pi}{2}+\arctan\varphi)\varpi}{4^k(1+\eta)^k} \\ &- \frac{1}{\pi}\sum_{k=1}^{m-1}\sum_{i=1}^{k}\frac{T_{ik}\varphi\varpi}{(1+\varphi^2)^{k-i+1}(1+\eta)^k}, \ m \text{ integer,} \end{aligned} \tag{6.38}$$

where

$$\begin{aligned} \varpi &= \sqrt{\frac{\eta}{1+\eta}}\text{sign}\phi, \\ \varphi &= -\varpi\cot\phi, \\ T_{ik} &= \frac{\binom{2k}{k}}{\binom{2k-2i}{k-i}4^i(2k-2i+1)}. \end{aligned}$$

Applying (6.38) to (6.37), we obtain a closed-form result for (6.37) with integer m after some simplifications, namely,

$$\begin{aligned} I_{Nakagami} = &\frac{1}{4} - \frac{1}{2\pi}\sum_{k=0}^{m-1}\binom{2k}{k}\left[\frac{\lambda(c_1,c_2)}{4^k(1+c_1)^k} + \frac{\lambda(c_2,c_1)}{4^k(1+c_2)^k}\right] \\ &+ \frac{1}{2\pi}\sum_{k=1}^{m-1}\sum_{i=1}^{k}\frac{T_{ik}\sqrt{c_1c_2}[(1+c_1)^{-i}+(1+c_2)^{-i}]}{(1+c_1+c_2)^{k-i+1}}. \end{aligned} \tag{6.39}$$

Here, $c_1 = A_1^2\bar{\gamma}/(2m)$, $c_2 = A_2^2\bar{\gamma}/(2m)$, and the function $\lambda(x_1, x_2)$ is given by

$$\lambda(x_1, x_2) = \sqrt{\frac{x_1}{1+x_1}} \arctan\left(\sqrt{\frac{1+x_1}{x_2}}\right).$$

For the case of Rayleigh fading, i.e., $m = 1$, (6.39) reduces to

$$I_{Rayleigh} = \frac{1}{4} - \frac{\lambda(A_1^2\bar{\gamma}/2, A_2^2\bar{\gamma}/2) + \lambda(A_2^2\bar{\gamma}/2, A_1^2\bar{\gamma}/2)}{2\pi}. \tag{6.40}$$

The result in (6.40) turns out to be the same as that in [135, eq. (5)]. Our derivation has avoided computing the three-fold integral in (6.32) directly, and thus is much simpler than that in [135].

6.5.2 Rician Fading

For Rician fading, the MGF of γ is given by [5, eq. (2.17)]

$$M_\gamma(s) = \frac{1+K}{1+K-s\bar{\gamma}} \exp\left(\frac{Ks\bar{\gamma}}{1+K-s\bar{\gamma}}\right). \tag{6.41}$$

Substituting (6.41) into (6.35) gives

$$\begin{aligned} & I_{Rician} \\ &= \frac{1}{2\pi}\int_0^{\pi/2-\arctan(A_2/A_1)} \frac{\sin^2\theta}{\sin^2\theta + A_1^2\bar{\gamma}/(2+2K)} \exp\left(-\frac{KA_1^2\bar{\gamma}/(2+2K)}{\sin^2\theta + A_1^2\bar{\gamma}/(2+2K)}\right) d\theta \\ &\quad + \frac{1}{2\pi}\int_0^{\arctan(A_2/A_1)} \frac{\sin^2\theta}{\sin^2\theta + A_2^2\bar{\gamma}/(2+2K)} \exp\left(-\frac{KA_2^2\bar{\gamma}/(2+2K)}{\sin^2\theta + A_2^2\bar{\gamma}/(2+2K)}\right) d\theta. \end{aligned} \tag{6.42}$$

It is difficult to give closed-form results for the integrals in (6.42), but we can upper and lower bound these integrals by substituting, respectively, the upper and lower integral limits into the exponential integrands, i.e., using the inequalities

$$\begin{aligned} \int_0^\phi \frac{e^{-K}\sin^2\theta}{\sin^2\theta+\eta} d\theta &\le \int_0^\phi \frac{\sin^2\theta}{\sin^2\theta+\eta} \exp\left[-\frac{K\eta}{\sin^2\theta+\eta}\right] d\theta \\ &\le \exp\left[-\frac{K\eta}{\sin^2\phi+\eta}\right] \int_0^\phi \frac{\sin^2\theta}{\sin^2\theta+\eta} d\theta. \end{aligned} \tag{6.43}$$

The integral in the upper and lower bounds in (6.43) can be evaluated in closed form by using Mathematica or setting $m = 1$ in the formula in (6.38). Thus, we have

$$\int_0^{\phi} \frac{\sin^2\theta}{\sin^2\theta + \eta} d\theta = \phi - \sqrt{\frac{\eta}{1+\eta}} \arctan\left(\sqrt{\frac{1+\eta}{\eta}} \tan\phi\right). \tag{6.44}$$

Applying (6.43) to (6.42) leads to a closed-form upper bound on I_{Rician}, i.e.,

$$I_{Rician} \leq \frac{1}{2\pi} q(r_1, r_2) \exp\left[-\frac{K(r_1+r_2)}{1+r_1+r_2}\right], \tag{6.45}$$

and a closed-form lower bound on I_{Rician}, i.e.,

$$I_{Rician} \geq \frac{1}{2\pi} q(r_1, r_2) \exp(-K), \tag{6.46}$$

where $r_1 = A_1^2\bar{\gamma}/(2+2K)$, $r_2 = A_2^2\bar{\gamma}/(2+2K)$, and

$$q(x_1, x_2) = \frac{\pi}{2} - \lambda(x_1, x_2) - \lambda(x_2, x_1).$$

In (6.43), the equalities hold for $K = 0$ or $\eta \to \infty$. The second equality also holds for $\eta = 0$. Thus, the bounds on I_{Rician} in (6.45) and (6.46) equal the exact result in (6.42) when $K = 0$, i.e., reduce to $I_{Rayleigh}$ in (6.40). The upper bound is accurate when r_1 and r_2 approach infinity or zero. The lower bound grows tighter as r_1 and/or r_2 increase. Fig. 6.2 shows that at high SNR, both bounds converge to the exact value. For low SNR around $\bar{\gamma} = 0$dB, the upper bound is close to the exact value, and much tighter than the lower bound. If $\bar{\gamma}$ decreases further, the upper bound will merge with the exact value eventually.

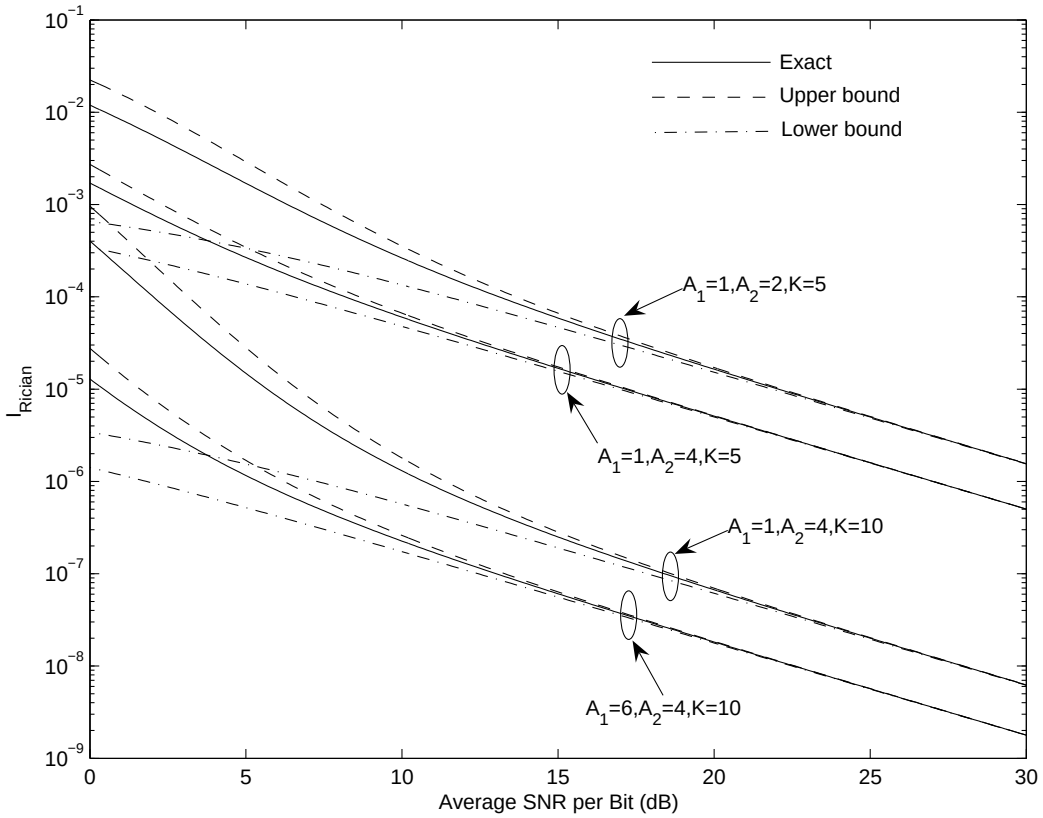

Fig. 6.2: Exact value of I_{Rician} in (6.42), its upper bound in (6.45) and its lower bound in (6.46) versus $\bar{\gamma}$.

6.6 Bounds on the Average Bit Error Probability Derived from the Simple Erfc Bounds on the First-Order Marcum Q-Function

We now apply the results in Section 6.5 to bounding the average bit error probability $P_b(\alpha, \beta)$ in (6.19). In Section 4.7, for the first-order Marcum Q-function, $Q(a, b)$, we have derived a simple upper erfc bound, i.e., UB3-KL in (4.43), and a simple lower erfc bound, i.e., LB3-KL in (4.44). Using the Gaussian Q-function in (6.33), these two erfc bounds can be rewritten as

$$Q_{UB3\text{-}KL}(a, b) = Q(b + a) + Q(b - a) + \frac{e^{-(b-a)^2/2} - e^{-(b+a)^2/2}}{a\sqrt{2\pi}}, \quad a > 0,\ b \geq 0, \tag{6.47}$$

and

$$Q_{LB3\text{-}KL}(a,b) = \left[Q\left(b+a\right) + Q\left(b-a\right)\right]\left[1-2Q\left(b\right)\right] + 2Q\left(b\right), \quad a \geq 0, b \geq 0. \tag{6.48}$$

Using (6.47) and (6.48) to bound the Marcum Q-functions in (6.19), we obtain a new upper bound on $P_b(\alpha,\beta)$, i.e.,

$$\begin{aligned} P_b(\alpha,\beta) &\leq \frac{1}{2} + \frac{1}{2}\int_0^\infty p_\gamma(\gamma)\left[Q_{UB3\text{-}KL}(\alpha\sqrt{\gamma},\beta\sqrt{\gamma}) - Q_{LB3\text{-}KL}(\beta\sqrt{\gamma},\alpha\sqrt{\gamma})\right]d\gamma \\ &= \int_0^\infty p_\gamma(\gamma)\Bigg\{Q((\beta-\alpha)\sqrt{\gamma}) + \frac{1}{2\alpha\sqrt{2\pi}\sqrt{\gamma}} \\ &\quad \cdot \left\{\exp\left[-\frac{(\beta-\alpha)^2\gamma}{2}\right] - \exp\left[-\frac{(\beta+\alpha)^2\gamma}{2}\right]\right\} \\ &\quad + [Q((\beta+\alpha)\sqrt{\gamma}) - Q((\beta-\alpha)\sqrt{\gamma})]Q(\alpha\sqrt{\gamma})\Bigg\}d\gamma, \end{aligned} \tag{6.49}$$

and a new lower bound

$$\begin{aligned} P_b(\alpha,\beta) &\geq \frac{1}{2} + \frac{1}{2}\int_0^\infty p_\gamma(\gamma)\left[Q_{LB3\text{-}KL}(\alpha\sqrt{\gamma},\beta\sqrt{\gamma}) - Q_{UB3\text{-}KL}(\beta\sqrt{\gamma},\alpha\sqrt{\gamma})\right]d\gamma \\ &= \int_0^\infty p_\gamma(\gamma)\Bigg\{Q((\beta-\alpha)\sqrt{\gamma}) + Q(\beta\sqrt{\gamma}) - \frac{1}{2\beta\sqrt{2\pi}\sqrt{\gamma}} \\ &\quad \cdot \left\{\exp\left[-\frac{(\beta-\alpha)^2\gamma}{2}\right] - \exp\left[-\frac{(\beta+\alpha)^2\gamma}{2}\right]\right\} \\ &\quad - [Q((\beta+\alpha)\sqrt{\gamma}) + Q((\beta-\alpha)\sqrt{\gamma})]Q(\beta\sqrt{\gamma})\Bigg\}d\gamma. \end{aligned} \tag{6.50}$$

In the following, we evaluate the right-hand sides of (6.49) and (6.50) for Nakagami-m and Rician fading.

6.6.1 Nakagami-m fading

For Nakagami-m fading, the PDF of γ is given by [5, eq. (2.21)]

$$p_\gamma(\gamma) = \frac{m^m \gamma^{m-1}}{\bar{\gamma}^m \Gamma(m)} \exp\left(-\frac{m\gamma}{\bar{\gamma}}\right), \qquad \gamma \geq 0. \tag{6.51}$$

The average of the Gaussian Q-function over Nakagami-m fading is given by

$$\begin{aligned}\int_0^\infty Q(c\sqrt{\gamma}) p_\gamma(\gamma) d\gamma &= \frac{1}{\pi} \int_0^\infty \int_0^{\pi/2} \exp\left(-\frac{c^2\gamma}{2\sin^2\theta}\right) d\theta p_\gamma(\gamma) d\gamma \\ &= \frac{1}{\pi} \int_0^{\pi/2} M_\gamma\left(-\frac{c^2}{2\sin^2\theta}\right) d\theta \\ &= \frac{1}{\pi} \int_0^{\pi/2} \left(1 + \frac{c^2\bar{\gamma}}{2m\sin^2\theta}\right)^{-m} d\theta. \end{aligned} \tag{6.52}$$

For integer m, the integral in the last step of (6.52) can be evaluated by using the formula in (6.38), and thus (6.52) becomes [5, eq. (5.18)]

$$\int_0^\infty Q(c\sqrt{\gamma}) p_\gamma(\gamma) d\gamma = \frac{1}{2}\left[1 - \sqrt{\frac{c^2\bar{\gamma}/(2m)}{1 + c^2\bar{\gamma}/(2m)}} \sum_{k=0}^{m-1} \binom{2k}{k} \frac{1}{4^k [1 + c^2\bar{\gamma}/(2m)]^k}\right], \quad m \text{ integer.} \tag{6.53}$$

The average of the exponential function over Nakagami-m fading can be obtained by using the definition of the Gamma function in (3.74), and thus is given by

$$\begin{aligned}\int_0^\infty \gamma^{-1/2} \exp\left(-\frac{c^2\gamma}{2}\right) p_\gamma(\gamma) d\gamma &= \int_0^\infty \frac{m^m \gamma^{m-3/2}}{\bar{\gamma}^m \Gamma(m)} \exp\left[-\left(\frac{c^2}{2} + \frac{m}{\bar{\gamma}}\right)\gamma\right] d\gamma \\ &= \frac{m^{1/2}\Gamma(m - \frac{1}{2})}{\bar{\gamma}^{1/2}\Gamma(m)\left[1 + c^2\bar{\gamma}/(2m)\right]^{m-1/2}}. \end{aligned} \tag{6.54}$$

Applying (6.53), (6.54) and (6.39) to the RHS of (6.49) leads to a closed-form

upper bound on $P_b(\alpha,\beta)$ for integer m, namely

$$\begin{aligned}
P_b(\alpha,\beta) &\le P_{b,UB\text{-}KL}(\alpha,\beta) \\
&= \frac{1}{2} - \frac{1}{2\pi}\sum_{k=0}^{m-1}\binom{2k}{k}\left[\frac{\pi\sqrt{e_1/(1+e_1)}-\lambda(e_1,e_3)}{4^k(1+e_1)^k}\right. \\
&\quad \left. + \frac{\lambda(e_2,e_3)}{4^k(1+e_2)^k} + \frac{\lambda(e_3,e_2)-\lambda(e_3,e_1)}{4^k(1+e_3)^k}\right] \\
&\quad + \frac{1}{2\pi}\sum_{k=1}^{m-1}\sum_{i=1}^{k}\left\{\frac{T_{ik}\sqrt{e_2e_3}[(1+e_2)^{-i}+(1+e_3)^{-i}]}{(1+e_2+e_3)^{k-i+1}}\right. \\
&\quad \left. - \frac{T_{ik}\sqrt{e_1e_3}[(1+e_1)^{-i}+(1+e_3)^{-i}]}{(1+e_1+e_3)^{k-i+1}}\right\} \\
&\quad + \frac{\Gamma(m-\frac{1}{2})}{4\sqrt{\pi e_3}\Gamma(m)}\left[(1+e_1)^{\frac{1}{2}-m}-(1+e_2)^{\frac{1}{2}-m}\right], \quad m \text{ integer},
\end{aligned} \tag{6.55}$$

where $e_1=(\beta-\alpha)^2\bar{\gamma}/(2m)$, $e_2=(\beta+\alpha)^2\bar{\gamma}/(2m)$, $e_3=\alpha^2\bar{\gamma}/(2m)$.

Similarly, applying (6.53), (6.54) and (6.39) to the RHS of (6.50), we obtain a closed-form lower bound on $P_b(\alpha,\beta)$ for integer m as

$$\begin{aligned}
P_b(\alpha,\beta) &\ge P_{b,LB\text{-}KL}(\alpha,\beta) \\
&= \frac{1}{2} - \frac{1}{2\pi}\sum_{k=0}^{m-1}\binom{2k}{k}\left[\frac{\pi\sqrt{e_1/(1+e_1)}-\lambda(e_1,e_4)}{4^k(1+e_1)^k}\right. \\
&\quad \left. + \frac{\pi\sqrt{e_4/(1+e_4)}-\lambda(e_4,e_2)-\lambda(e_4,e_1)}{4^k(1+e_4)^k} - \frac{\lambda(e_2,e_4)}{4^k(1+e_2)^k}\right] \\
&\quad - \frac{1}{2\pi}\sum_{k=1}^{m-1}\sum_{i=1}^{k}\left\{\frac{T_{ik}\sqrt{e_2e_4}[(1+e_2)^{-i}+(1+e_4)^{-i}]}{(1+e_2+e_4)^{k-i+1}}\right. \\
&\quad \left. + \frac{T_{ik}\sqrt{e_1e_4}[(1+e_1)^{-i}+(1+e_4)^{-i}]}{(1+e_1+e_4)^{k-i+1}}\right\} \\
&\quad - \frac{\Gamma(m-\frac{1}{2})}{4\sqrt{\pi e_4}\Gamma(m)}\left[(1+e_1)^{\frac{1}{2}-m}-(1+e_2)^{\frac{1}{2}-m}\right], \quad m \text{ integer},
\end{aligned} \tag{6.56}$$

where $e_4=\beta^2\bar{\gamma}/(2m)$.

6.6.2 Rician Fading

For Rician fading, the PDF of γ is given by [5, eq. (2.16)]

$$p_\gamma(\gamma) = \frac{(1+K)e^{-K-\frac{(1+K)\gamma}{\bar{\gamma}}}}{\bar{\gamma}} I_0\left(2\sqrt{\frac{K(1+K)\gamma}{\bar{\gamma}}}\right), \qquad \gamma \geq 0.$$

The average of the Gaussian Q-function over Rician fading can be solved by using the result in [132, eq. (19)], i.e.,

$$\int_0^\infty Q(c\sqrt{\gamma}) p_\gamma(\gamma) d\gamma = Q[u(d), v(d)] - \frac{w(d)}{2}\left[1 + \sqrt{\frac{d}{1+d}}\right],$$

where $d = c^2\bar{\gamma}/(2+2K)$, and

$$\begin{aligned} u(x) &= \sqrt{K\left[1 + 2x - 2\sqrt{x(1+x)}\right]/(2+2x)}, \\ v(x) &= \sqrt{K\left[1 + 2x + 2\sqrt{x(1+x)}\right]/(2+2x)}, \\ w(x) &= \exp\left[-K(1+2x)/(2+2x)\right] I_0\left[K/(2+2x)\right]. \end{aligned}$$

The average of the exponential function over Rician fading can be obtained by applying [124, eq. (6.618 4)]

$$\int_0^\infty \gamma^{-1/2} \exp\left(-\frac{c^2\gamma}{2}\right) p_\gamma(\gamma) d\gamma = \sqrt{\frac{(1+K)\pi}{\bar{\gamma}(1+d)}} w(d). \tag{6.57}$$

For the average of the two products of Gaussian Q-functions over Rician fading, to obtain an upper bound on $P_b(\alpha, \beta)$, we use the upper bound in (6.45) to bound the integral corresponding to the positive product and use the lower bound in (6.46) to bound the integral corresponding to the negative product. Thus, the RHS of (6.49) can be further upper bounded in closed form, and an

upper bound on $P_b(\alpha,\beta)$ can be given by

$$\begin{aligned} P_b(\alpha,\beta) &\le P_{b,UB\text{-}KL}(\alpha,\beta) \\ &= Q(u(d_1),v(d_1)) - \left[1+\sqrt{\frac{d_1}{1+d_1}} - \frac{1}{2\sqrt{d_3(1+d_1)}}\right] \\ &\quad \cdot \frac{w(d_1)}{2} - \frac{w(d_2)}{4\sqrt{d_3(1+d_2)}} + \frac{1}{2\pi}q(d_2,d_3) \\ &\quad \cdot \exp\left[-\frac{K(d_2+d_3)}{1+d_2+d_3}\right] - \frac{1}{2\pi}q(d_1,d_3)\exp(-K), \end{aligned} \tag{6.58}$$

where $d_1=(\beta-\alpha)^2\bar{\gamma}/(2+2K)$, $d_2=(\beta+\alpha)^2\bar{\gamma}/(2+2K)$, $d_3=\alpha^2\bar{\gamma}/(2+2K)$.

To obtain a lower bound on $P_b(\alpha,\beta)$, we use the upper bound in (6.45) to bound the averages of the two positive products of Gaussian Q-functions in (6.50). Thus, the RHS of (6.50) can be further lower bounded in closed form, and a lower bound on $P_b(\alpha,\beta)$ is given by

$$\begin{aligned} P_b(\alpha,\beta) &\ge P_{b,LB\text{-}KL}(\alpha,\beta) \\ &= Q(u(d_1),v(d_1)) + Q(u(d_4),v(d_4)) - \left[1+\sqrt{\frac{d_1}{1+d_1}} + \frac{1}{2\sqrt{d_4(1+d_1)}}\right] \\ &\quad \cdot \frac{w(d_1)}{2} - \left[1+\sqrt{\frac{d_4}{1+d_4}}\right]\frac{w(d_4)}{2} + \frac{w(d_2)}{4\sqrt{d_4(1+d_2)}} - \frac{1}{2\pi}q(d_2,d_4) \\ &\quad \cdot \exp\left[-\frac{K(d_2+d_4)}{1+d_2+d_4}\right] - \frac{1}{2\pi}q(d_1,d_4)\exp\left[-\frac{K(d_1+d_4)}{1+d_1+d_4}\right], \end{aligned} \tag{6.59}$$

where $d_4=\beta^2\bar{\gamma}/(2+2K)$.

6.7 Comparison and Numerical Results

In this section, we give some numerical results to show the tightness of our new upper and lower bounds derived in Sections 6.4 and 6.6 for the average bit error probability of QFRs for single-channel, differentially coherent and quadratic detections over Nakagami-m and Rician fading channels. We also compare the tightness of our new upper bounds with that of the existing upper bounds, i.e.,

$P_{b,UB\text{-}SA}(\alpha,\beta)$ in (6.22) and $P_{b,UB\text{-}AT}(\alpha,\beta)$ in (6.23).

6.7.1 Nakagami-m fading

In Section 6.4, we have derived a generic upper bound, i.e., $P_{b,GUB\text{-}KL}(\alpha,\beta)$ in (6.24), and a generic lower bound, i.e., $P_{b,GLB\text{-}KL}(\alpha,\beta)$ in (6.29), on the average bit error probability $P_b(\alpha,\beta)$ in (6.21). This pair of bounds was derived from our generic exponential bounds on $Q(a,b)$. They are given in terms of weighted sums of an arbitrarily large number of the MGFs of the SNR per bit, and are applicable to a variety of fading channel models. For Nakagami fading, they have the explicit expressions in (6.27) and (6.30). In Section 6.6.1, by using our simple erfc bounds on $Q(a,b)$, we have also derived another pair of bounds on $P_b(\alpha,\beta)$, i.e., the upper bound $P_{b,UB\text{-}KL}(\alpha,\beta)$ in (6.55), and the lower bound $P_{b,LB\text{-}KL}(\alpha,\beta)$ in (6.56). For different cases, the values of the parameters in the generic bounds, $P_{b,GUB\text{-}KL}(\alpha,\beta)$ in (6.27) and $P_{b,GLB\text{-}KL}(\alpha,\beta)$ in (6.30), required to achieve a satisfactory tightness may be different. For simplicity, in all our numerical results for these generic bounds, we set $G = H = M = 5$ and choose equispaced points for ϕ_k, θ_i and ω_j, i.e., $\phi_k = k\pi/G$, $\theta_i = \pi - \arcsin(\alpha/\beta) + i\arcsin(\alpha/\beta)/H$, and $\omega_j = \pi - \arcsin(\alpha/\beta) + j\arcsin(\alpha/\beta)/M$. The exact value of the average bit error probability $P_b(\alpha,\beta)$ in (6.21) is shown by the solid line. The new generic bounds $P_{b,GUB\text{-}KL}(\alpha,\beta)$ in (6.27) and $P_{b,GLB\text{-}KL}(\alpha,\beta)$ in (6.30) are shown by the dash-dotted lines. The new bounds $P_{b,UB\text{-}KL}(\alpha,\beta)$ in (6.55) and $P_{b,LB\text{-}KL}(\alpha,\beta)$ in (6.56) are shown by the dashed lines. The existing upper bounds $P_{b,UB\text{-}SA}(\alpha,\beta)$ in (6.22) and $P_{b,UB\text{-}AT}(\alpha,\beta)$ in (6.23) are shown by the dotted lines.

We first consider the case of DQPSK with Gray coding where $\alpha = \sqrt{2-\sqrt{2}}$ and $\beta = \sqrt{2+\sqrt{2}}$. Figs. 6.3, 6.4 and 6.5 show the results for Nakagami-m fading with $m = 1$, $m = 2$ and $m = 5$, respectively. The case of $m = 1$ shows the results for Rayleigh fading. We can see that our new lower bounds $P_{b,GLB\text{-}KL}(\alpha,\beta)$ and $P_{b,LB\text{-}KL}(\alpha,\beta)$ are tight. Our generic upper bound $P_{b,GUB\text{-}KL}(\alpha,\beta)$ is tighter than the existing bounds $P_{b,UB\text{-}SA}(\alpha,\beta)$ and $P_{b,UB\text{-}AT}(\alpha,\beta)$. Our upper bound

$P_{b,UB\text{-}KL}(\alpha,\beta)$ is tighter than the existing bound $P_{b,UB\text{-}SA}(\alpha,\beta)$, and for most cases also tighter than $P_{b,UB\text{-}AT}(\alpha,\beta)$. The bound $P_{b,UB\text{-}KL}(\alpha,\beta)$ is only looser than $P_{b,UB\text{-}AT}(\alpha,\beta)$ either at low SNR or for the case of $m=1$. Then we consider the case of binary correlated signals, where $\alpha=\sqrt{(1-\sqrt{1-|\varsigma|^2})/2}$ and $\beta=\sqrt{(1+\sqrt{1-|\varsigma|^2})/2}$. Figs. 6.6 and 6.7 show the results for $|\varsigma|=0.5$ and $|\varsigma|=0.95$, respectively, over Nakagami fading with $m=1$. Figs. 6.8 and 6.9 show the results for $|\varsigma|=0.5$ and $|\varsigma|=0.95$, respectively, over Nakagami fading with $m=5$. We can see that for this modulation scheme, our new lower bounds $P_{b,GLB\text{-}KL}(\alpha,\beta)$ and $P_{b,LB\text{-}KL}(\alpha,\beta)$ are also tight. Our generic upper bound $P_{b,GUB\text{-}KL}(\alpha,\beta)$ is tighter than the existing bounds $P_{b,UB\text{-}SA}(\alpha,\beta)$ and $P_{b,UB\text{-}AT}(\alpha,\beta)$. Our upper bound $P_{b,UB\text{-}KL}(\alpha,\beta)$ is tighter than the existing bound $P_{b,UB\text{-}SA}(\alpha,\beta)$, and also tighter than the existing bound $P_{b,UB\text{-}AT}(\alpha,\beta)$ when the magnitude of the correlation coefficient is large.

6.7.2 Rician fading

For Rician fading, the explicit expressions for the generic upper bound $P_{b,GUB\text{-}KL}(\alpha,\beta)$ and the generic lower bound $P_{b,GLB\text{-}KL}(\alpha,\beta)$ are given in (6.28) and (6.31), respectively. In Section 6.6.2, we have given another pair of bounds, i.e., the upper bound $P_{b,UB\text{-}KL}(\alpha,\beta)$ in (6.58), and the lower bound $P_{b,LB\text{-}KL}(\alpha,\beta)$ in (6.59). Here, we also set $G=H=M=5$ for the generic bounds $P_{b,GUB\text{-}KL}(\alpha,\beta)$ in (6.28) and $P_{b,GLB\text{-}KL}(\alpha,\beta)$ in (6.31), and choose equispaced points for ϕ_k, θ_i and ω_j, just as in the case of Nakagami-m fading.

Figs. 6.10 and 6.11 show the results for the case of DQPSK with Gray coding over Rician fading with $K=5$ and $K=15$, respectively. We can see that our new lower bounds $P_{b,GLB\text{-}KL}(\alpha,\beta)$ and $P_{b,LB\text{-}KL}(\alpha,\beta)$ are tight. Our generic upper bound $P_{b,GUB\text{-}KL}(\alpha,\beta)$ is tighter than the existing bounds $P_{b,UB\text{-}SA}(\alpha,\beta)$ and $P_{b,UB\text{-}AT}(\alpha,\beta)$. Our upper bound $P_{b,UB\text{-}KL}(\alpha,\beta)$ is tighter than the existing bound $P_{b,UB\text{-}SA}(\alpha,\beta)$, but only tighter than $P_{b,UB\text{-}AT}(\alpha,\beta)$ when K is large and SNR is neither very low nor very high. Figs. 6.12 and 6.13 show the results for

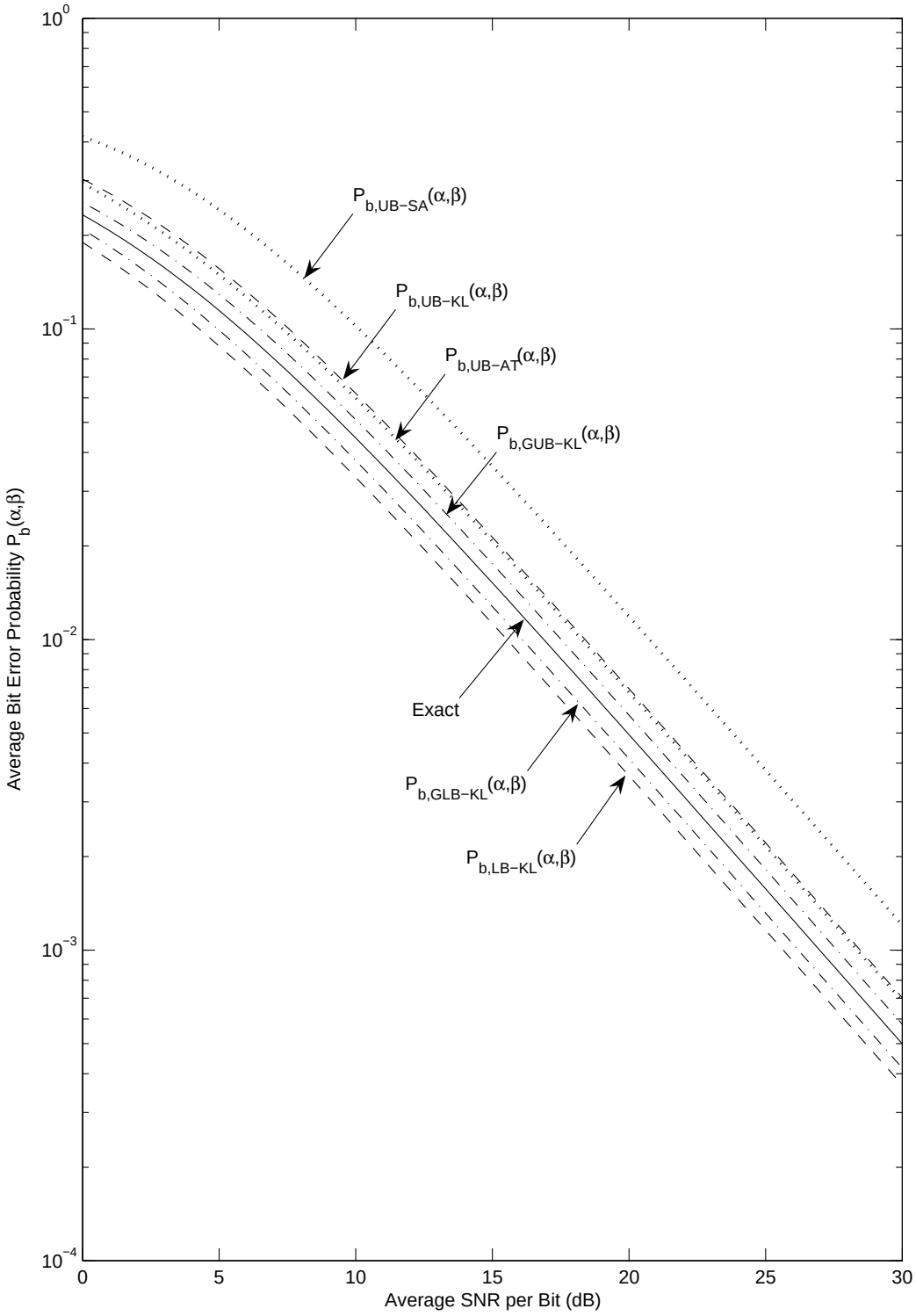

Fig. 6.3: The average bit error probability in (6.21) (solid line), the new upper bounds in (6.27) (dash-dotted line) and (6.55) (dashed line), the new lower bounds in (6.30) (dash-dotted line) and (6.56) (dashed line), and the existing upper bounds in (6.22) (dotted line) and (6.23) (dotted line) versus $\bar{\gamma}$ for the case of DQPSK with Gray coding, where $\alpha = \sqrt{2-\sqrt{2}}$ and $\beta = \sqrt{2+\sqrt{2}}$, over Nakagami fading with $m = 1$.

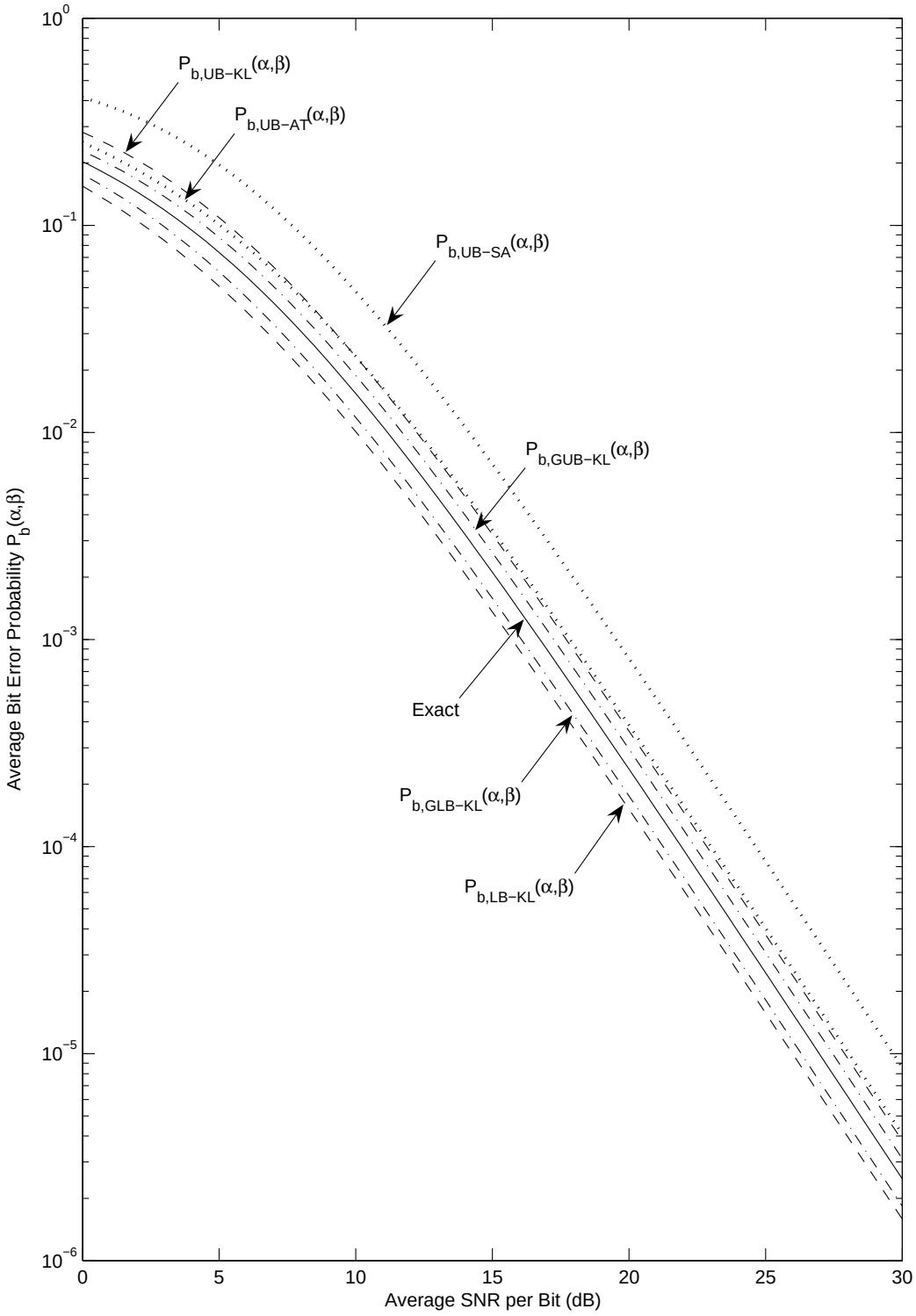

Fig. 6.4: The average bit error probability in (6.21) (solid line), the new upper bounds in (6.27) (dash-dotted line) and (6.55) (dashed line), the new lower bounds in (6.30) (dash-dotted line) and (6.56) (dashed line), and the existing upper bounds in (6.22) (dotted line) and (6.23) (dotted line) versus $\bar{\gamma}$ for the case of DQPSK with Gray coding, where $\alpha = \sqrt{2-\sqrt{2}}$ and $\beta = \sqrt{2+\sqrt{2}}$, over Nakagami fading with $m = 2$.

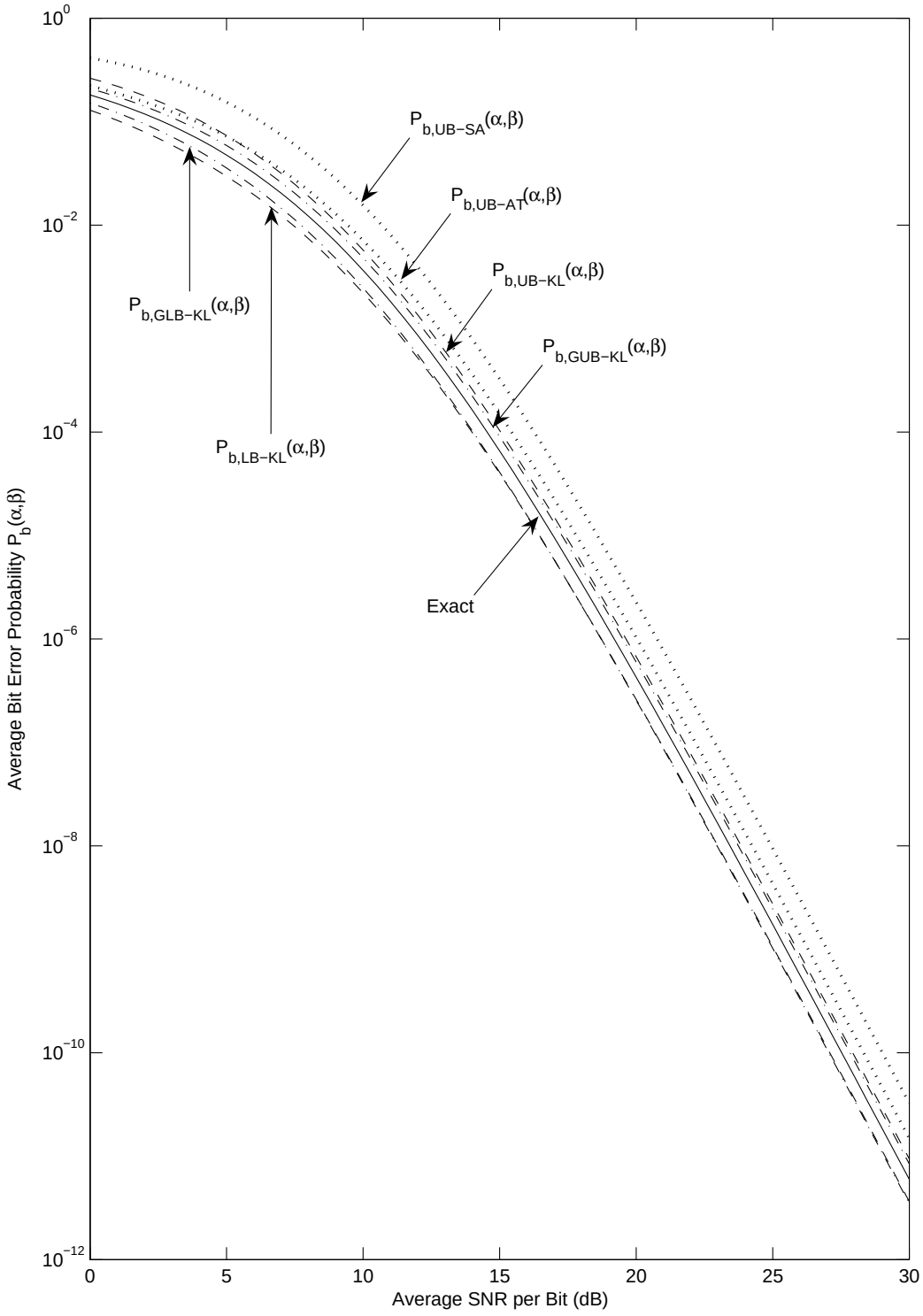

Fig. 6.5: The average bit error probability in (6.21) (solid line), the new upper bounds in (6.27) (dash-dotted line) and (6.55) (dashed line), the new lower bounds in (6.30) (dash-dotted line) and (6.56) (dashed line), and the existing upper bounds in (6.22) (dotted line) and (6.23) (dotted line) versus $\bar{\gamma}$ for the case of DQPSK with Gray coding, where $\alpha = \sqrt{2-\sqrt{2}}$ and $\beta = \sqrt{2+\sqrt{2}}$, over Nakagami fading with $m = 5$.

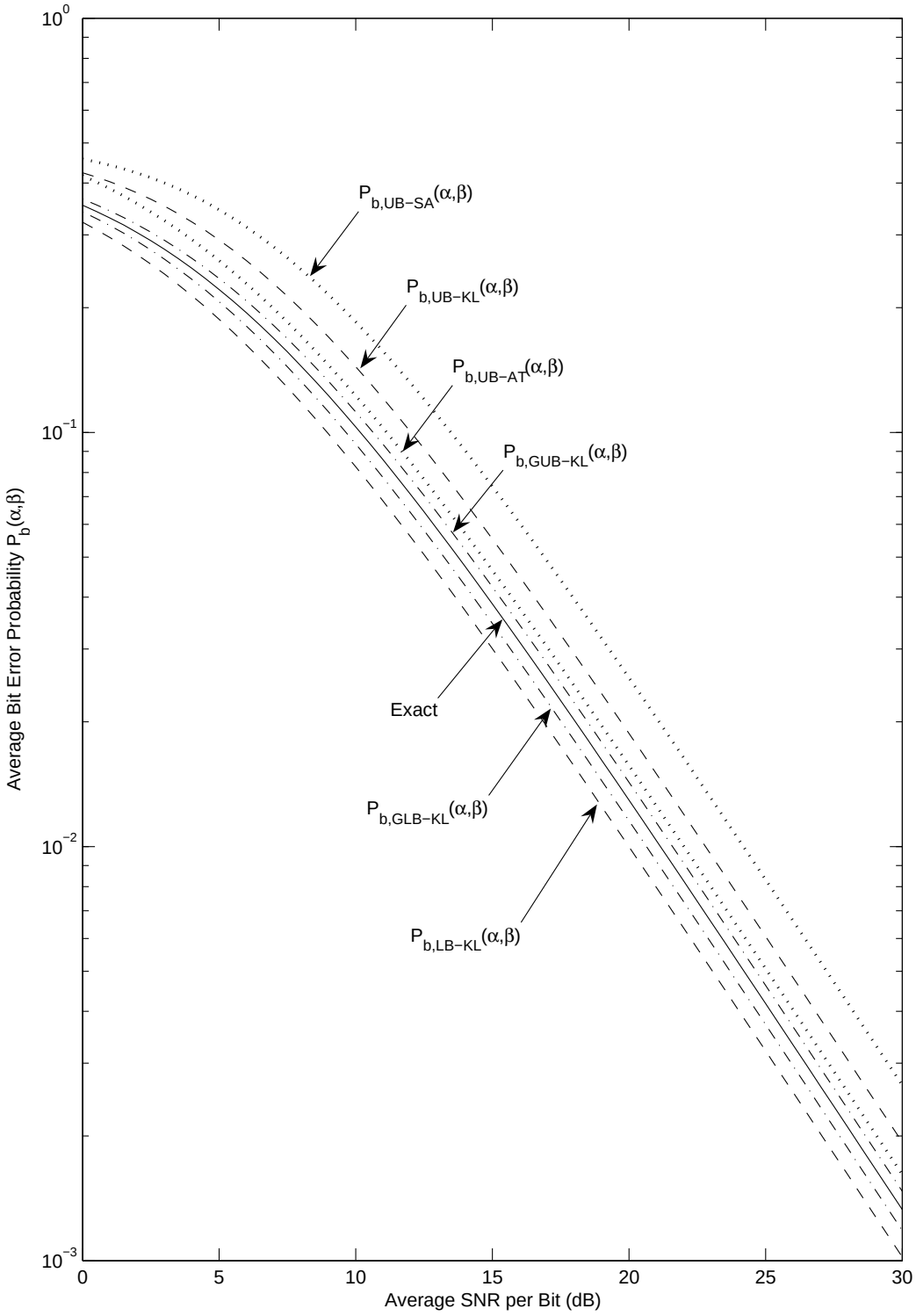

Fig. 6.6: The average bit error probability in (6.21) (solid line), the new upper bounds in (6.27) (dash-dotted line) and (6.55) (dashed line), the new lower bounds in (6.30) (dash-dotted line) and (6.56) (dashed line), and the existing upper bounds in (6.22) (dotted line) and (6.23) (dotted line) versus $\bar{\gamma}$ for the case of binary correlated signals, where $\alpha = \sqrt{(1-\sqrt{1-|\varsigma|^2})/2}$, $\beta = \sqrt{(1+\sqrt{1-|\varsigma|^2})/2}$, and $|\varsigma| = 0.5$, over Nakagami fading with $m = 1$.

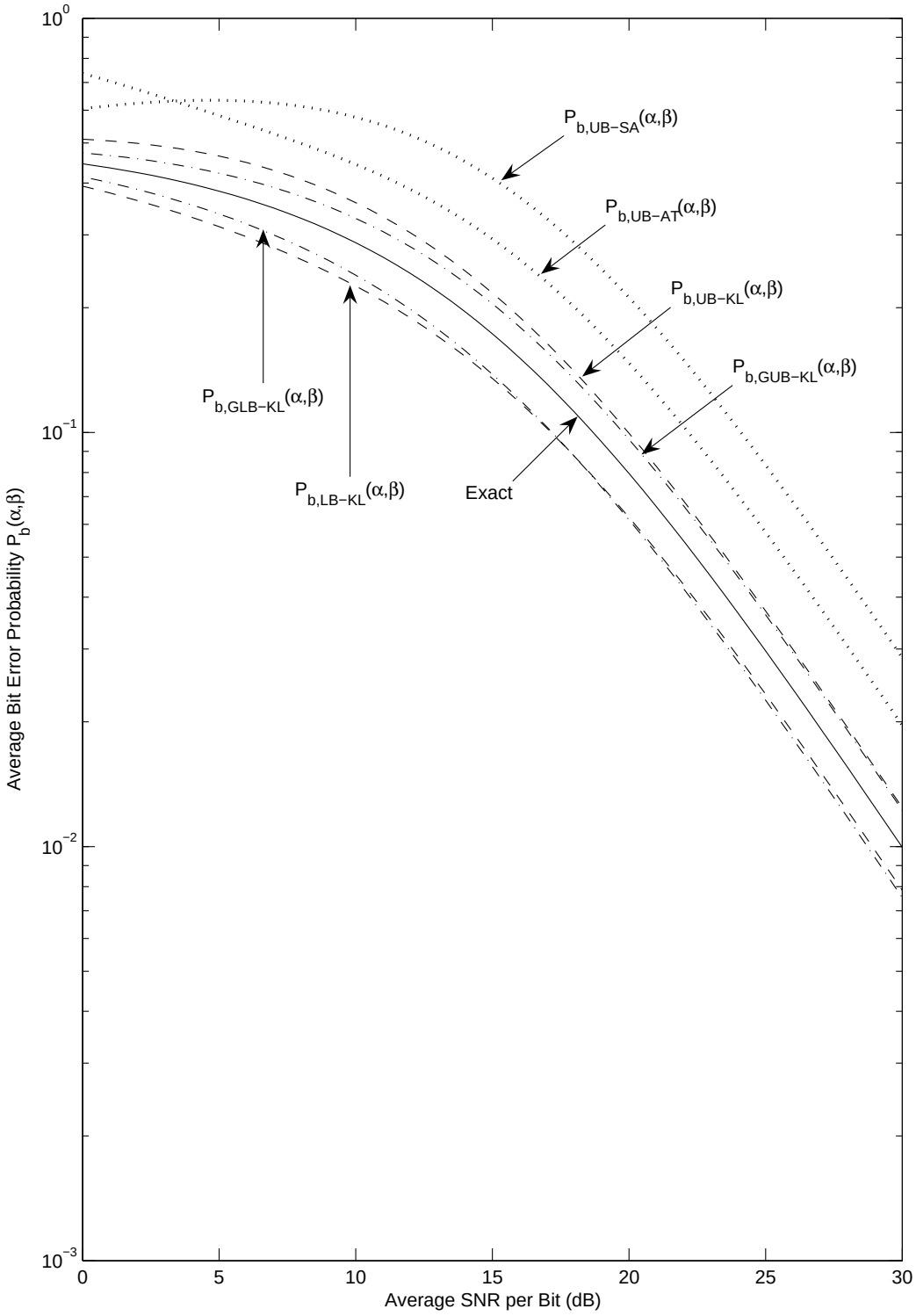

Fig. 6.7: The average bit error probability in (6.21) (solid line), the new upper bounds in (6.27) (dash-dotted line) and (6.55) (dashed line), the new lower bounds in (6.30) (dash-dotted line) and (6.56) (dashed line), and the existing upper bounds in (6.22) (dotted line) and (6.23) (dotted line) versus $\bar{\gamma}$ for the case of binary correlated signals, where $\alpha = \sqrt{(1-\sqrt{1-|\varsigma|^2})/2}$, $\beta = \sqrt{(1+\sqrt{1-|\varsigma|^2})/2}$, and $|\varsigma| = 0.95$, over Nakagami fading with $m = 1$.

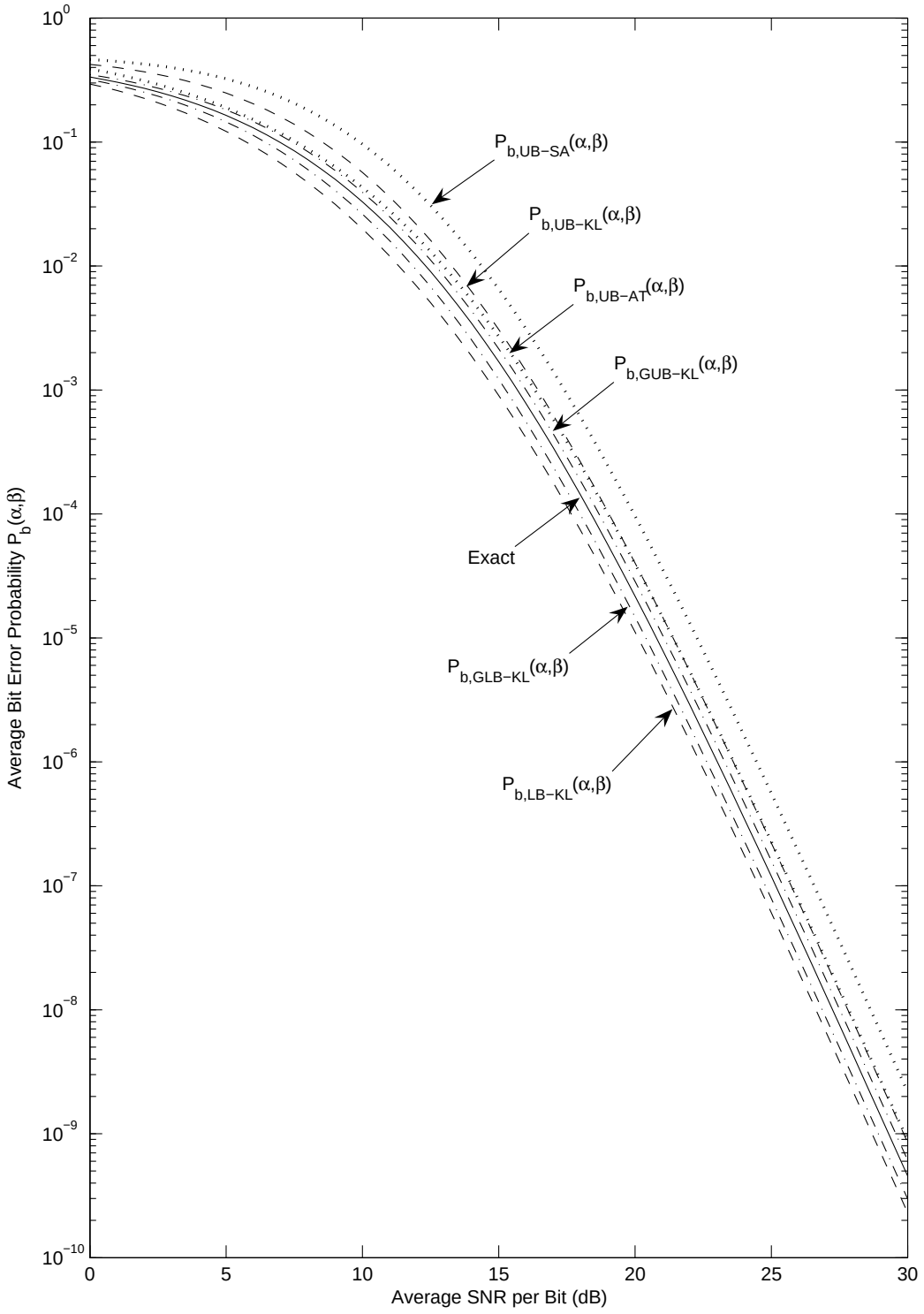

Fig. 6.8: The average bit error probability in (6.21) (solid line), the new upper bounds in (6.27) (dash-dotted line) and (6.55) (dashed line), the new lower bounds in (6.30) (dash-dotted line) and (6.56) (dashed line), and the existing upper bounds in (6.22) (dotted line) and (6.23) (dotted line) versus $\bar{\gamma}$ for the case of binary correlated signals, where $\alpha = \sqrt{(1-\sqrt{1-|\varsigma|^2})/2}$, $\beta = \sqrt{(1+\sqrt{1-|\varsigma|^2})/2}$, and $|\varsigma| = 0.5$, over Nakagami fading with $m = 5$.

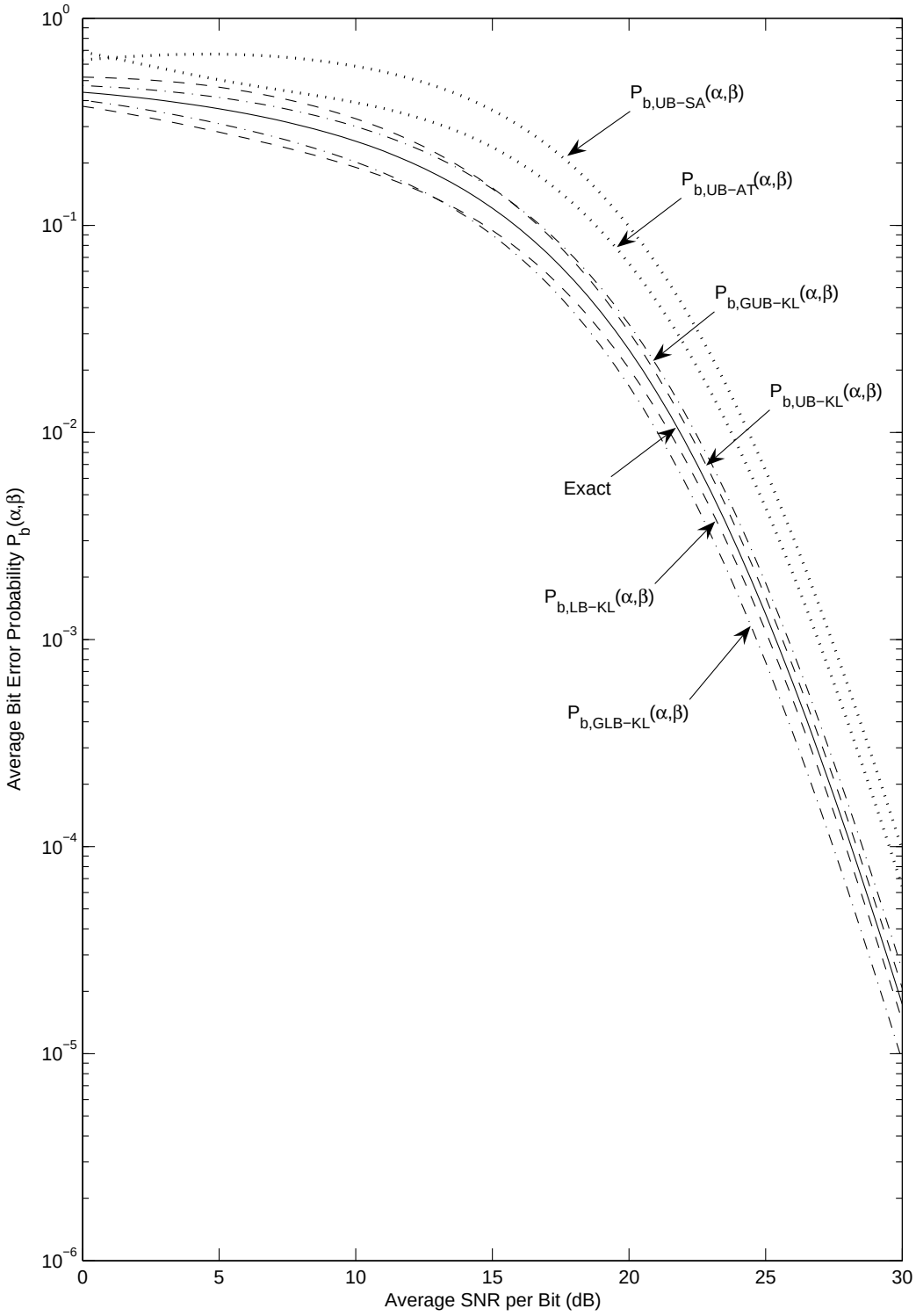

Fig. 6.9: The average bit error probability in (6.21) (solid line), the new upper bounds in (6.27) (dash-dotted line) and (6.55) (dashed line), the new lower bounds in (6.30) (dash-dotted line) and (6.56) (dashed line), and the existing upper bounds in (6.22) (dotted line) and (6.23) (dotted line) versus $\bar{\gamma}$ for the case of binary correlated signals, where $\alpha = \sqrt{(1-\sqrt{1-|\varsigma|^2})/2}$, $\beta = \sqrt{(1+\sqrt{1-|\varsigma|^2})/2}$, and $|\varsigma| = 0.95$, over Nakagami fading with $m = 5$.

the case of binary correlated signals with $|\varsigma| = 0.5$ and $|\varsigma| = 0.95$, respectively, over Rician fading with $K = 5$. Figs. 6.14 and 6.15 show the results for the case of binary correlated signals with $|\varsigma| = 0.5$ and $|\varsigma| = 0.95$, respectively, over Rician fading with $K = 15$. We can see that our generic upper bound $P_{b,GUB\text{-}KL}(\alpha, \beta)$ is tighter than the existing bounds $P_{b,UB\text{-}SA}(\alpha, \beta)$ and $P_{b,UB\text{-}AT}(\alpha, \beta)$, although for the case of small $|\varsigma|$ and large K, $P_{b,GUB\text{-}KL}(\alpha, \beta)$ may need a larger G to outperform $P_{b,UB\text{-}AT}(\alpha, \beta)$. For example, for the case of $|\varsigma| = 0.02$ and $K = 10$, $P_{b,GUB\text{-}KL}(\alpha, \beta)$ with $G = 5$ and $H = M = 2$ is looser than $P_{b,UB\text{-}AT}(\alpha, \beta)$, but $P_{b,GUB\text{-}KL}(\alpha, \beta)$ with $G = 8$ and $H = M = 2$ is tighter than the latter. Our upper bound $P_{b,UB\text{-}KL}(\alpha, \beta)$ is tighter than the existing bound $P_{b,UB\text{-}AT}(\alpha, \beta)$ at medium and high SNR for large $|\varsigma|$. This bound and $P_{b,LB\text{-}KL}(\alpha, \beta)$ are very close to the exact value at high SNR for large K and $|\varsigma|$.

6.8 Summary

In this chapter, we have shown the applications of our new representations, generic exponential bounds, and simple erfc bounds derived in Chapter 4 for the first-order Marcum Q-function, $Q(a, b)$, to error performance analysis of QFRs for a variety of single-channel, differentially coherent and quadratic detections. We have derived a new single-finite-integral expression for the average bit error probability of QFRs. This expression is applicable for various fading channel models, and is more robust than its counterpart in the literature. We have also derived a pair of generic upper and lower bounds on the average bit error probability of QFRs for a variety of fading channel models by using our generic exponential bounds on $Q(a, b)$. Besides, we have derived, for each of Nakagami-m fading and Rician fading, another pair of upper and lower bounds on the average bit error probability of QFRs by using our simple erfc bounds on $Q(a, b)$. Our new lower bounds are the only lower bounds available thus far, and they have been shown to be tight. Our generic upper bound on the average bit error probability of QFRs

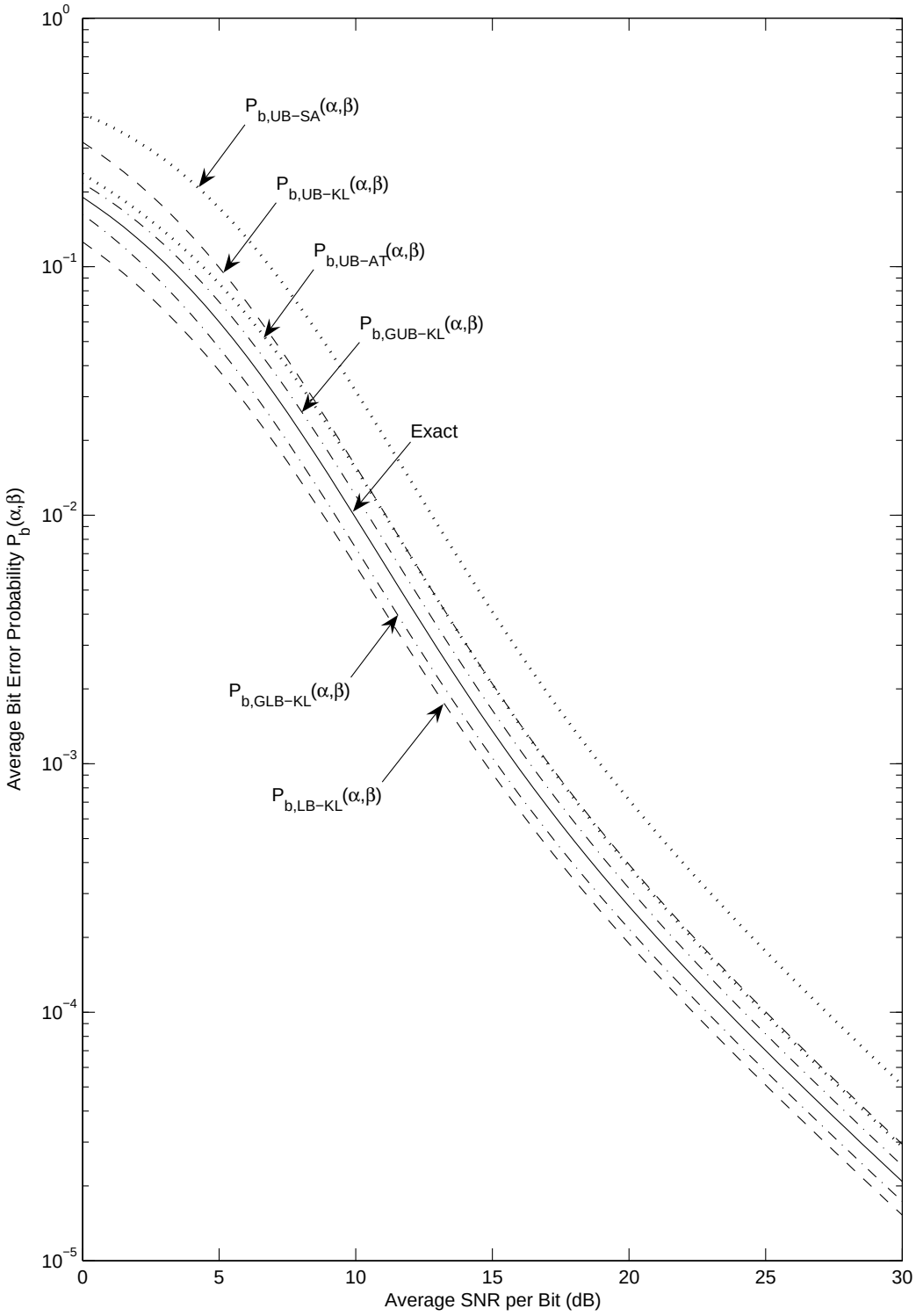

Fig. 6.10: The average bit error probability in (6.21) (solid line), the new upper bounds in (6.28) (dash-dotted line) and (6.58) (dashed line), the new lower bounds in (6.31) (dash-dotted line) and (6.59) (dashed line), and the existing upper bounds in (6.22) (dotted line) and (6.23) (dotted line) versus $\bar{\gamma}$ for the case of DQPSK with Gray coding, where $\alpha = \sqrt{2-\sqrt{2}}$ and $\beta = \sqrt{2+\sqrt{2}}$, over Rician fading with $K = 5$.

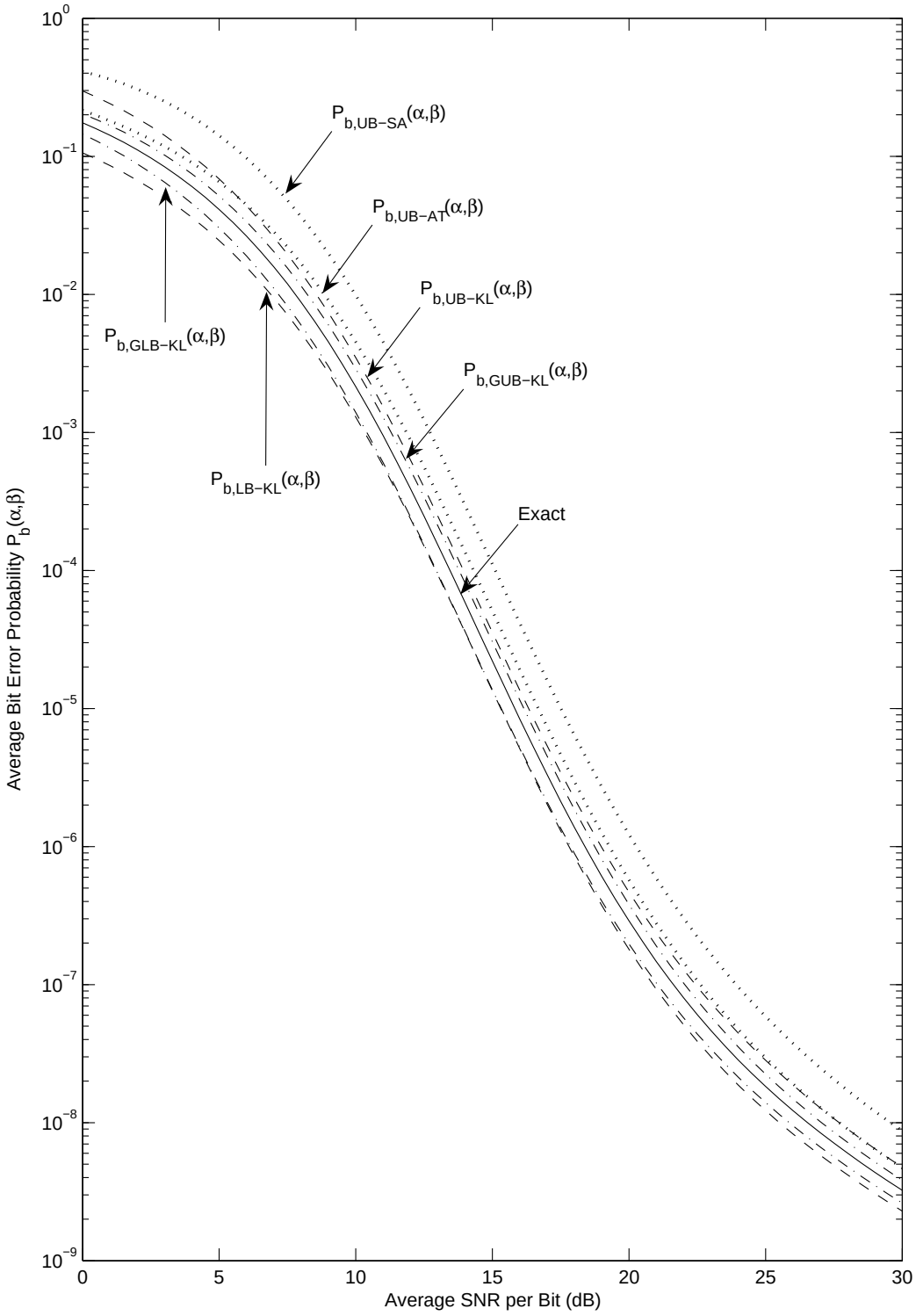

Fig. 6.11: The average bit error probability in (6.21) (solid line), the new upper bounds in (6.28) (dash-dotted line) and (6.58) (dashed line), the new lower bounds in (6.31) (dash-dotted line) and (6.59) (dashed line), and the existing upper bounds in (6.22) (dotted line) and (6.23) (dotted line) versus $\bar{\gamma}$ for the case of DQPSK with Gray coding, where $\alpha = \sqrt{2-\sqrt{2}}$ and $\beta = \sqrt{2+\sqrt{2}}$, over Rician fading with $K = 15$.

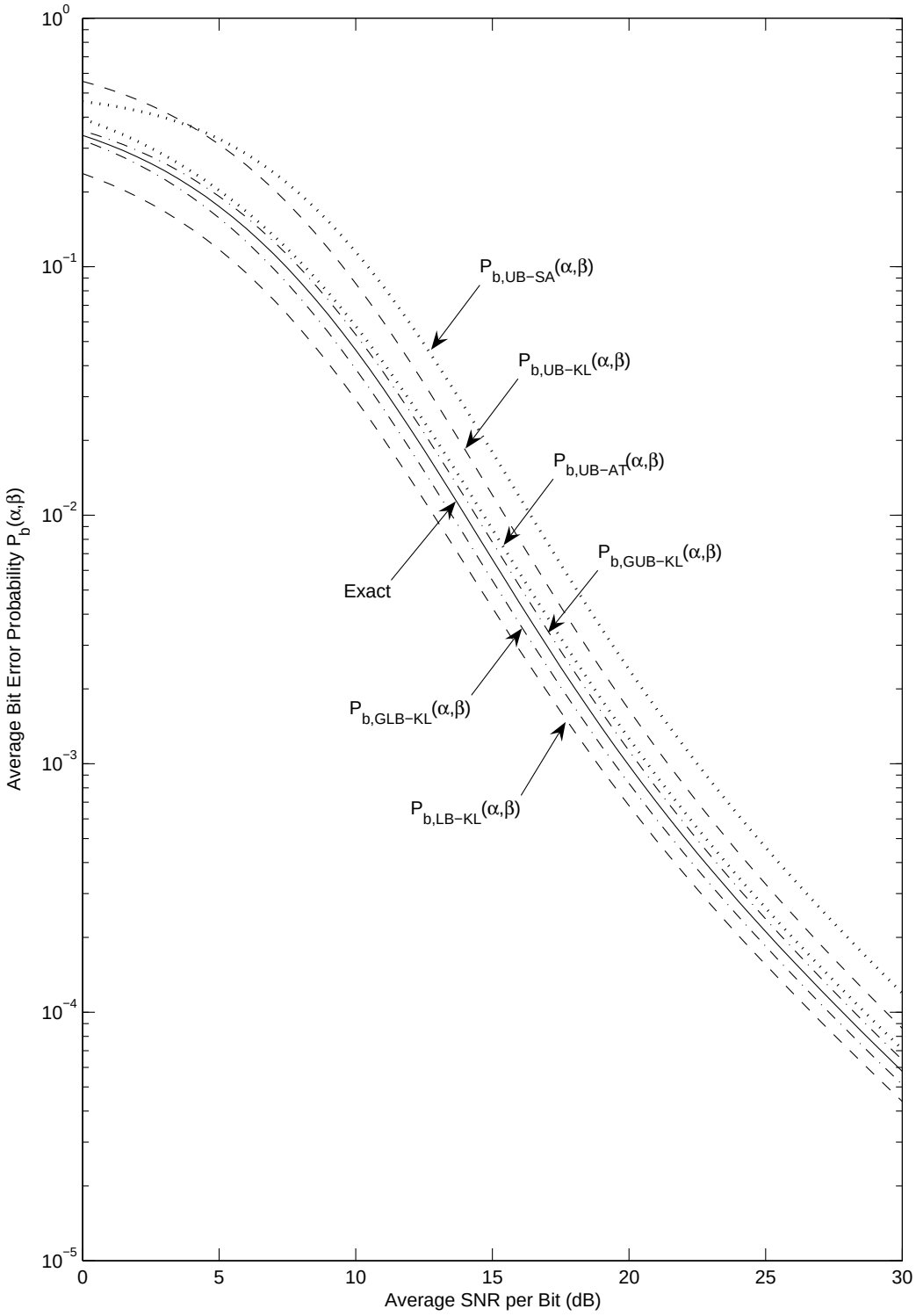

Fig. 6.12: The average bit error probability in (6.21) (solid line), the new upper bounds in (6.28) (dash-dotted line) and (6.58) (dashed line), the new lower bounds in (6.31) (dash-dotted line) and (6.59) (dashed line), and the existing upper bounds in (6.22) (dotted line) and (6.23) (dotted line) versus $\bar{\gamma}$ for the case of binary correlated signals, where $\alpha = \sqrt{(1-\sqrt{1-|\varsigma|^2})/2}$, $\beta = \sqrt{(1+\sqrt{1-|\varsigma|^2})/2}$, and $|\varsigma| = 0.5$, over Rician fading with $K = 5$.

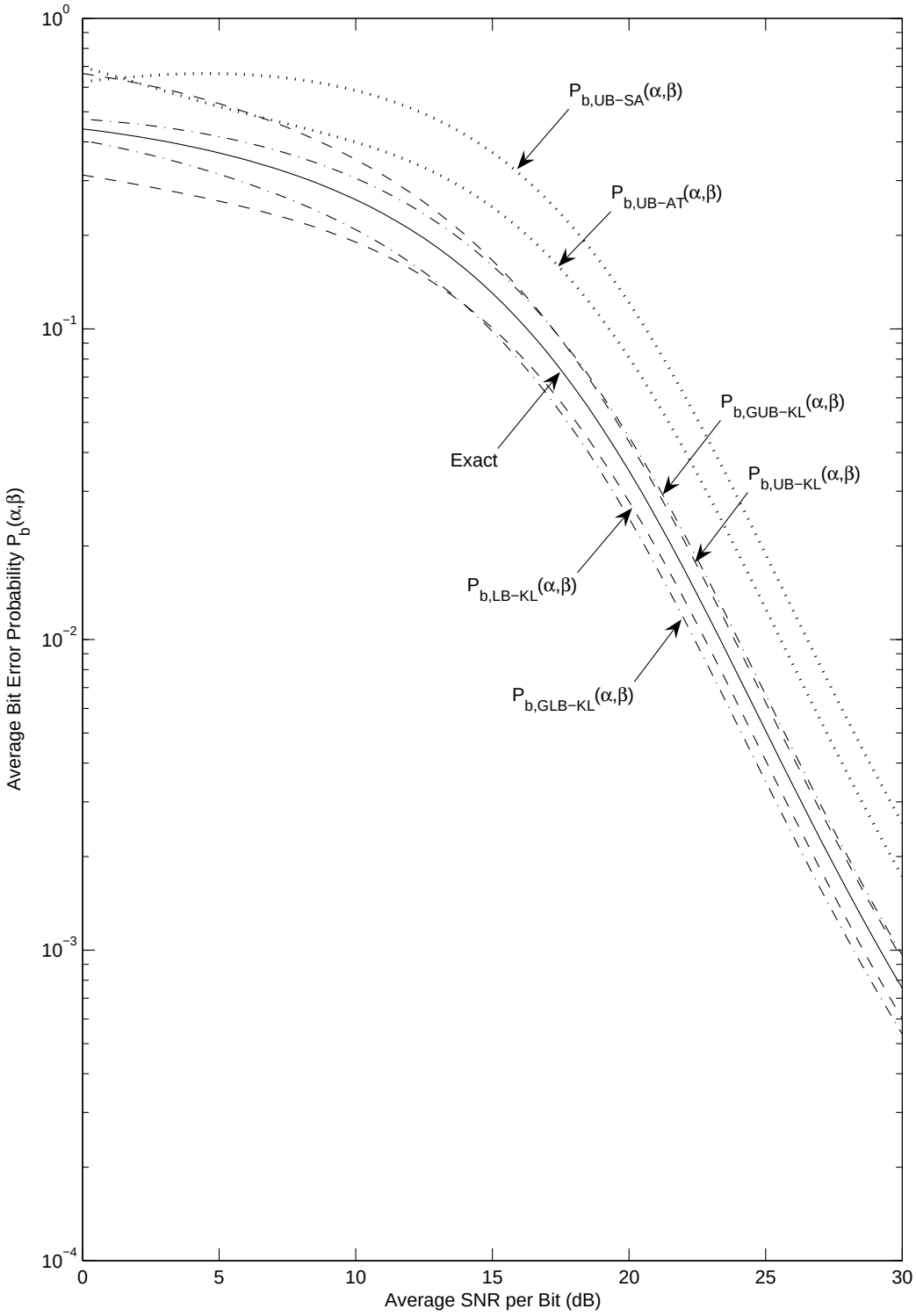

Fig. 6.13: The average bit error probability in (6.21) (solid line), the new upper bounds in (6.28) (dash-dotted line) and (6.58) (dashed line), the new lower bounds in (6.31) (dash-dotted line) and (6.59) (dashed line), and the existing upper bounds in (6.22) (dotted line) and (6.23) (dotted line) versus $\bar{\gamma}$ for the case of binary correlated signals, where $\alpha = \sqrt{(1-\sqrt{1-|\varsigma|^2})/2}$, $\beta = \sqrt{(1+\sqrt{1-|\varsigma|^2})/2}$, and $|\varsigma| = 0.95$, over Rician fading with $K = 5$.

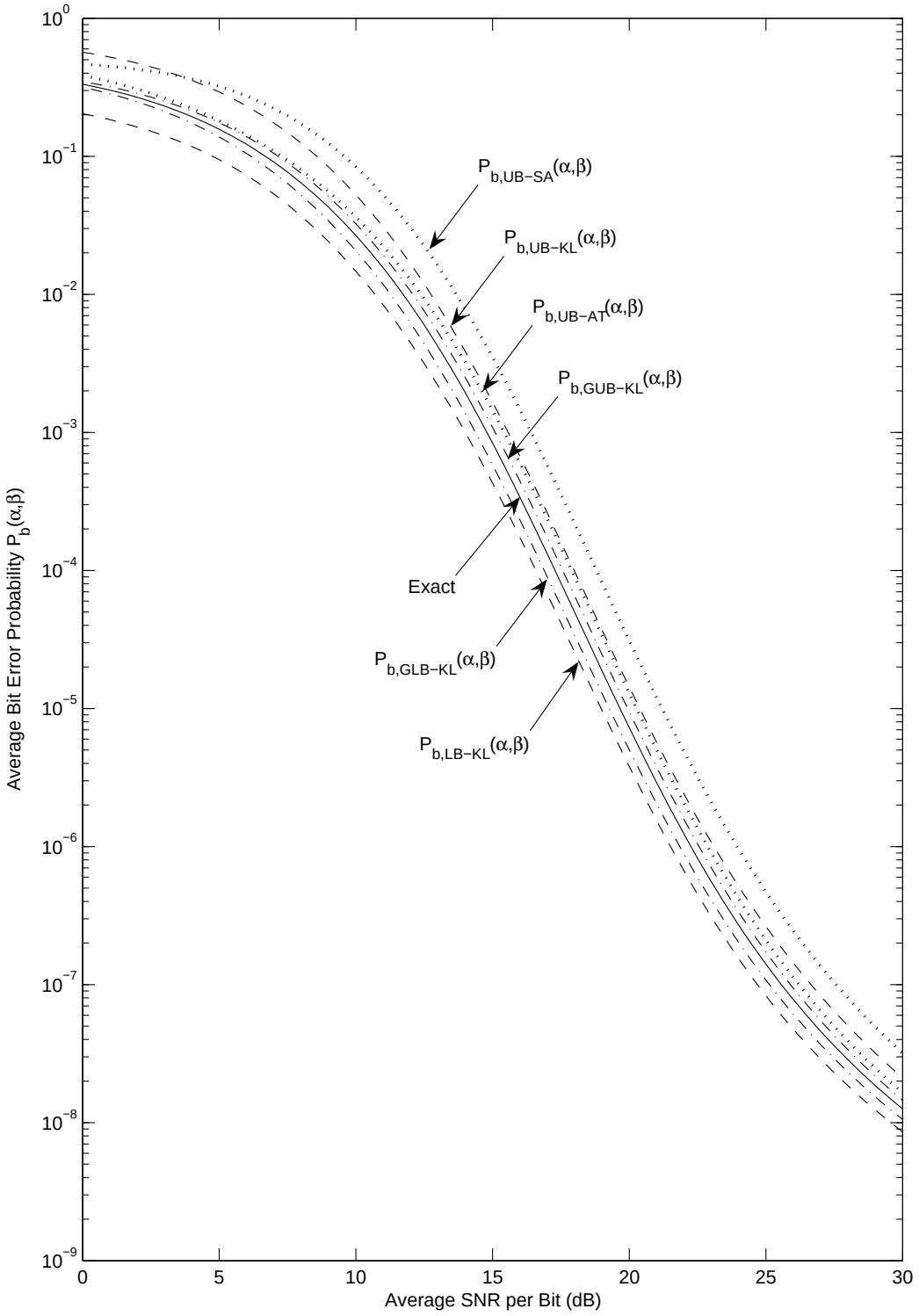

Fig. 6.14: The average bit error probability in (6.21) (solid line), the new upper bounds in (6.28) (dash-dotted line) and (6.58) (dashed line), the new lower bounds in (6.31) (dash-dotted line) and (6.59) (dashed line), and the existing upper bounds in (6.22) (dotted line) and (6.23) (dotted line) versus $\bar{\gamma}$ for the case of binary correlated signals, where $\alpha = \sqrt{(1-\sqrt{1-|\varsigma|^2})/2}$, $\beta = \sqrt{(1+\sqrt{1-|\varsigma|^2})/2}$, and $|\varsigma| = 0.5$, over Rician fading with $K = 15$.

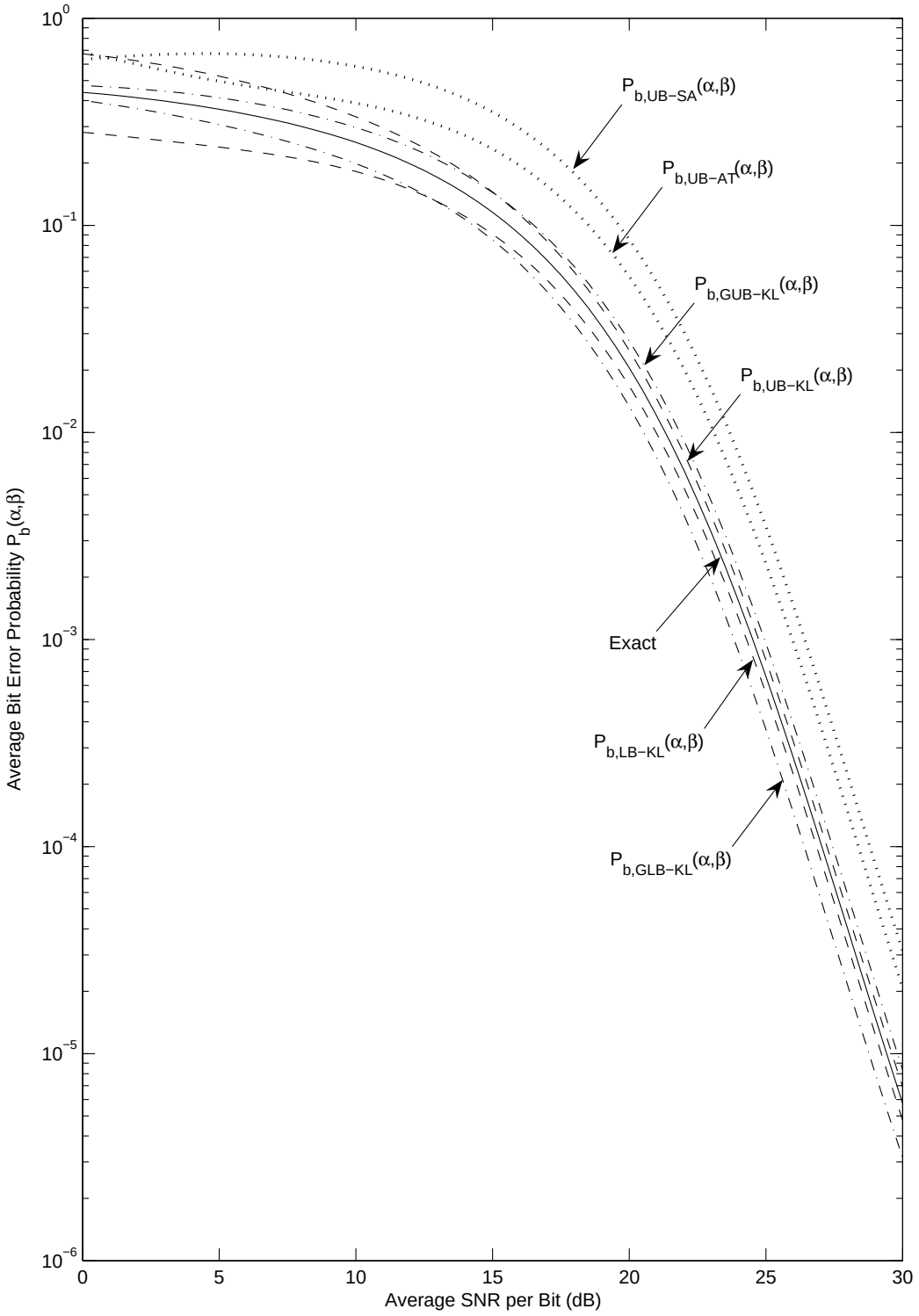

Fig. 6.15: The average bit error probability in (6.21) (solid line), the new upper bounds in (6.28) (dash-dotted line) and (6.58) (dashed line), the new lower bounds in (6.31) (dash-dotted line) and (6.59) (dashed line), and the existing upper bounds in (6.22) (dotted line) and (6.23) (dotted line) versus $\bar{\gamma}$ for the case of binary correlated signals, where $\alpha = \sqrt{(1-\sqrt{1-|\varsigma|^2})/2}$, $\beta = \sqrt{(1+\sqrt{1-|\varsigma|^2})/2}$, and $|\varsigma| = 0.95$, over Rician fading with $K = 15$.

when evaluated with a few terms has been shown to be tighter than the existing bounds available in the literature for Nakagami-m and Rician fading. Our upper bounds derived from the simple erfc bounds on $Q(a, b)$ have also been shown to be tighter than the existing bounds in some cases.

In addition, we have also evaluated the averages of the product of two Gaussian Q-functions over fading statistics. For Nakagami-m fading, an exact closed-form result has been derived. For Rician fading, a pair of closed-form, upper and lower bounds has been obtained and shown to be asymptotically tight. These results have been used in the derivation of the closed-form bounds on the average bit error probability of QFRs based on the simple erfc bounds on $Q(a, b)$.

Chapter 7

Conclusions and Future Work

7.1 Conclusions

QFRs are receivers which have quadratic-form decision metrics. They are commonly used in communication systems. In this dissertation, we have studied some topics on design and performance analysis of QFRs.

We started with the performance analysis of QRs in MIMO systems. As one type of QFRs, QRs are also referred to as square-law receivers, and are usually used when knowledge of the received carrier phase is not available at the receiver. MIMO systems have been widely accepted as a bandwidth-saving approach to increasing the capacity of wireless communication systems, and STC is a popular technique to achieve the capacity of MIMO systems. Among all the STC structures, USTM is the one that uses a QR to detect signals without CSI at either the transmitter or the receiver. For USTM, we have derived some simple, tight, upper and lower bounds on the PEP of the QR over the Rayleigh block-fading channel. Our analytical and numerical results have shown that these simple bounds are tighter than the existing bounds in the literature either over a particular SNR range or over the entire SNR range. They have also led to some modifications for the USTM constellation design criteria.

In addition to the performance analysis of the conventional QR for USTM,

we have also contributed to designing new receivers, i.e., the GQRs, to improve the error performance of USTM. For USTM, perfect knowledge of CSI at the receiver can bring about a 2–4 dB gain in SNR. To realize this large performance improvement potential, we have designed the GQRs to incorporate channel estimation into the receivers for various unitary space–time constellations, including the USTC-OD, OUSTC and general NOUSTC. These GQRs estimate the channel gains without the help of additional training signals, and thus conserve bandwidth resources. They exploit the channel memory to improve the channel estimation accuracy, and thus bridge the performance gap between the QR and the CR as the channel memory span exploited in channel estimation increases. For the GQR designed for the USTC-OD with two or four transmit antennas and the GQR designed for OUSTC, closed-form expressions of the PEP have been derived. The GQRs have been shown to work well in both slow and fast fading environments, and the improvement obtained by exploiting the channel memory decreases with the channel fade rate. The GQR for the USTC-OD with two or four transmit antennas have been simplified, and its complexity can be much less than those of the original form and the simplified form of the QR when the constellation size is large and the channel memory span exploited is small.

After analyzing the QR and deriving the GQRs for USTM, we extend our research to the performance analysis of a general QFR, whose decision metric is given in terms of a general quadratic form in complex Gaussian random variables. Receivers for a variety of coherent, differentially coherent, partially coherent, and quadratic detections with diversity can be written as a special case of this general QFR. The bit error probability of this general QFR has been given in the literature in terms of the first-order Marcum Q-function, $Q(a, b)$, and the generalized Marcum Q-function, $Q_m(a, b)$. To facilitate the error performance analysis of the general QFR over fading channels, we have studied the first-order Marcum Q-function and the generalized Marcum Q-function by using a geometric approach. We began with the first-order Marcum Q-function. By taking a geometric view of

$Q(a,b)$, we have derived some new representations and upper and lower bounds for $Q(a,b)$. Our new finite-integral representations of $Q(a,b)$ are simpler than their counterparts in the literature. Our new closed-form bounds include the generic and simple exponential bounds and the generic and simple erfc bounds. The generic bounds have been shown to approach the exact value of $Q(a,b)$ as the number of terms involved increases. The simple bounds have been shown to be tighter than the existing exponential bounds in most cases, especially when the arguments a and b are large. In addition to the closed-form bounds, we have also developed some generic and simple single-integral bounds which involve single finite integrals. These single-integral bounds may be tighter than the exponential bounds and the erfc bounds in some cases, but at a cost of involving single integrals.

Then we extended the geometric approach to the generalized Marcum Q-function. Based on a novel geometric view of $Q_m(a,b)$, we have derived a new closed-form representation of $Q_m(a,b)$ for m being an odd multiple of 0.5, which is the first closed-form representation of $Q_m(a,b)$ for this case, involving only simple exponential functions and erfc functions. We have also derived a pair of new finite-integral representations of $Q_m(a,b)$ for m being an integer, which are more robust than their counterparts in the literature. We have shown that $Q_{m+0.5}(a,b)$ and $Q_{m-0.5}(a,b)$ are, respectively, tight upper and lower bounds on $Q_m(a,b)$, and their average is a good approximation of $Q_m(a,b)$. Thus, for the case of m integer, $Q_{m+0.5}(a,b)$ and $Q_{m-0.5}(a,b)$ can be evaluated by using our new closed-form representation, and can be used to bound $Q_m(a,b)$ tightly. In addition to these two bounds, we have also derived some generic exponential bounds and erfc bounds on $Q_m(a,b)$ of integer order m. These generic bounds approach the exact value of $Q_m(a,b)$ as the number of terms involved increases. When evaluated with a few terms, our generic upper bounds can be tighter than the existing bounds in some cases. Our generic lower bounds can be tighter than the existing exponential bounds for a wide range of values of the arguments, and

can be even tighter than the existing I_k-bounds when b is less than a.

With these new representations and bounds for the Marcum Q-functions, we can obtain some new results for the error performance analysis of the general QFR over fading channels. In the literature, receivers in a variety of single-channel, differentially coherent and quadratic detections have been shown as spacial cases of the general QFR whose conditional bit error probability involves only the first-order Marcum Q-functions with both the arguments being proportional to the square root of the instantaneous SNR. For this type of QFRs, we have illustrated some applications of our results for $Q(a, b)$ to evaluating the average bit error probability. By using the new representations of $Q(a, b)$, we have derived a new single-finite-integral expression for the average bit error probability of QFRs over generalized fading channels, which is more robust than its counterpart in the literature. By using our generic exponential bounds on $Q(a, b)$, we have derived a pair of generic upper and lower bounds on the average bit error probability of QFRs over generalized fading channels, which approach the exact value of the average bit error probability as the number of terms involved increases. By using our simple erfc bounds on $Q(a, b)$, we have derived, for each of Nakagami-m fading and Rician fading, a pair of upper and lower bounds on the average bit error probability of QFRs. Our new lower bounds on the average bit error probability of QFRs are the only lower bounds available thus far, and they have been shown to be tight. When evaluated with a few terms, our generic upper bound on the average bit error probability of QFRs has been shown to be tighter than the existing bounds for Nakagami-m and Rician fading. Our upper bounds derived from the simple erfc bounds on $Q(a, b)$ have also been shown to be tighter than the existing bounds in some cases. As a basis of applying our simple erfc bounds on $Q(a, b)$ to evaluating the average bit error probability of QFRs, we have also evaluated the averages of the product of two Gaussian Q-functions over fading statistics. For Nakagami-m fading, an exact closed-form result has been derived. For Rician fading, a pair of closed-form, upper and lower bounds has

been obtained and shown to be asymptotically tight.

7.2 Future Work

7.2.1 Applications of New Representations and Bounds for the Generalized Marcum Q-Function

In this dissertation, we have shown some applications of our new representations and bounds for $Q(a, b)$ to the error performance analysis of QFRs for a variety of single-channel, differentially coherent and quadratic detections. In our future work, we will also work on the applications of our new representations and bounds on $Q_m(a, b)$ to the error performance analysis of QFRs for multichannel reception. In the case of multichannel reception, to obtain the average error probability of QFRs over fading channels, we need to average the conditional error probability of QFRs over the distribution of the total instantaneous SNR at the output of the diversity combiner. This distribution depends on the combining technique used in detection, and in some cases it may be very complicated [5, 118, 143]. Averaging the conditional error probability of QFRs over these complicated distributions may be difficult. Thus, we still have a lot of work to do to obtain closed-form, exact expressions or tight bounds for the average error probability of QFRs for multichannel reception.

7.2.2 Extension of the Generalized Marcum Q-Function and Performance Analysis of QFRs

In Chapter 5, we have shown that if the real Gaussian random variables $\{z_i\}_{i=1}^n$ are independent and have means $\{p_i\}_{i=1}^n$ and variances 1, i.e., z_i is $\mathcal{N}(p_i, 1)$ distributed, then the generalized Marcum Q-function gives the tail probability of

the sum of the noncentral chi-square random variables $\{z_i^2\}_{i=1}^n$, i.e., we have

$$Q_m(a,b) = \Pr\left(\sum_{i=1}^{n} z_i^2 > b^2\right), \tag{7.1}$$

where $a^2 = \sum_{i=1}^n p_i^2$. In Chapter 6, we have discussed the general quadratic form in complex Gaussian random variables

$$D = \sum_{k=1}^{N} (A|X_k|^2 + B|Y_k|^2 + CX_kY_k^* + C^*X_k^*Y_k), \tag{7.2}$$

where X_k's are independent $\mathcal{CN}(\bar{X}_k, 2\mu_{xx})$ distributed, Y_k's are independent $\mathcal{CN}(\bar{Y}_k, 2\mu_{yy})$ distributed, and we have $\mathrm{E}[(X_k - \bar{X}_k)(Y_k - \bar{Y}_k)^*] = 2\mu_{xy}$, $\mathrm{E}[(X_k - \bar{X}_k)(Y_i - \bar{Y}_i)^*] = 0$ for $k \neq i$. Here, the variances, μ_{xx} and μ_{yy}, and the covariance, μ_{xy}, are independent of the channel index k. The probability of D being negative has been shown to be given by

$$\begin{aligned}\Pr(D<0) = {} & \frac{(v_2/v_1)^N}{(1+v_2/v_1)^{2N-1}} \sum_{k=1}^{N} \binom{2N-1}{N-k} \\ & \cdot \left\{ \left(\frac{v_1}{v_2}\right)^k Q_k(a,b) - \left(\frac{v_2}{v_1}\right)^{k-1} Q_k(b,a) + \left(\frac{v_2}{v_1}\right)^{k-1} \right\}. \end{aligned} \tag{7.3}$$

Comparing the expression of D in (7.2) with the quantity in the brackets in (7.1), it is easy to understand why the probability $\Pr(D<0)$ can be given in terms of the generalized Marcum Q-functions.

An extension of the general quadratic form in (7.2) can be given by

$$D_g = \sum_{k=1}^{N} (A_k|X_k|^2 + B_k|Y_k|^2 + C_kX_kY_k^* + C_k^*X_k^*Y_k). \tag{7.4}$$

Here, X_k's and Y_k's have the same definitions as those in (7.2). The constant coefficients A_k, B_k and C_k now are dependent on the channel index k. The variances, μ_{xx} and μ_{yy}, and the covariance, μ_{xy}, are still assumed to be independent of the channel index k, since the effect of X_k's and Y_k's having different variances and

covariances for different k can be reflected by the coefficients A_k's, B_k's and C_k's and the corresponding changes in the values of $\bar{X}_k$'s and $\bar{Y}_k$'s.

Another general quadratic form in complex Gaussian random variables discussed a lot in the literature is given by

$$D_f = \mathbf{r}^\dagger \mathbf{F} \mathbf{r}. \tag{7.5}$$

This is an indefinite Hermitian quadratic form of the N-dimensional complex Gaussian random vector $\mathbf{r}$. Here, $\mathbf{F}$ is an $N \times N$ Hermitian matrix, i.e., we have $\mathbf{F} = \mathbf{F}^\dagger$, and $\mathbf{r}$ is $\mathcal{CN}(\mathbf{m}_r, \mathbf{V}_r)$ distributed. This general quadratic form also generalizes decision metrics of a variety of coherent, differentially coherent, partially coherent, and quadratic detections, and applies to various detections by using different definitions for the Gaussian random vector $\mathbf{r}$ and the Hermitian matrix $\mathbf{F}$ [20, 34–38]. In [36] and [20, Appendix B], the indefinite quadratic form in (7.5) was shown to be equivalent to a weighted sum of norm squares of independent complex Gaussian random variables with different nonzero means and identical variances, i.e., we have

$$D_f = \sum_{k=1}^{N} \alpha_k |q_k|^2. \tag{7.6}$$

Here, $\mathbf{q} = [q_1,\ q_2, \cdots, q_N]$ is $\mathcal{CN}(\mathbf{U}^\dagger \mathbf{L}^{-1} \mathbf{m}_r, \mathbf{I}_N)$ distributed; $\mathbf{L}$ is any nonsingular factorization of $\mathbf{V}_r$ such that $\mathbf{V}_r = \mathbf{L}\mathbf{L}^\dagger$; $\mathbf{\Delta} = \mathrm{diag}(\alpha_1,\ \alpha_2,\ \cdots,\ \alpha_N)$ is the diagonal real eigenvalue matrix of $\mathbf{L}^\dagger \mathbf{F} \mathbf{L}$, and $\mathbf{U}$ is the corresponding unitary eigenvector matrix. Comparing (7.6) with (7.4), we can see that the quadratic form in (7.5) or the difference of two such quadratic forms can be regarded as a special case of the quadratic form in (7.4).

For the case of $\bar{X}_k = \bar{Y}_k = 0, k = 1, \cdots, n$, the CF and the CDF of the general quadratic form in (7.4) have been evaluated in [29]. However, even for this zero-mean case, the CDF was just given in an implicit residue form, and is not easy to use. Thus, evaluating the CDF of D_g in (7.4) in explicit closed form

for both the nonzero-mean and zero-mean cases is still an open problem.

From (7.3), we can see that the probability of D being negative can be given in terms of the weighted differences of two generalized Marcum Q-functions with the arguments in the reverse order. This result inspires us to investigate in our future work the possibility of expressing the probability of D_g being negative in terms of some weighted differences of two super generalized Marcum Q-functions. This super generalized Marcum Q-function can be regarded as an extension of the generalized Marcum Q-function in (7.1), and can be defined as the tail probability of the weighted sum of the noncentral chi-square random variables $\{z_i^2\}_{i=1}^n$, namely

$$Q_m\left(a, b, \mathbf{\Lambda}\right) = \Pr\left(\sum_{i=1}^{n} \lambda_i z_i^2 > b^2\right). \tag{7.7}$$

Here, $\{z_i\}_{i=1}^n$ are independent Gaussian random variables with $\mathcal{CN}(p_i, 1)$ distribution, and we have $\lambda_i > 0$, $\mathbf{\Lambda} = \mathrm{diag}\{\lambda_1, \cdots, \lambda_n\}$ and $a^2 = \sum_{i=1}^n p_i^2$. The complement of this super generalized Marcum Q-function, i.e, $1 - Q_m\left(a, b, \mathbf{\Lambda}\right) = \Pr\left(\sum_{i=1}^{n} \lambda_i z_i^2 < b^2\right)$, has been studied a lot in the literature, such as in [39, 144–147]. We can also extend our geometric approach to the evaluation of the right-hand side of (7.7) to see whether we can obtain some new representations and bounds for $Q_m\left(a, b, \mathbf{\Lambda}\right)$. If we can express the probability of D_g being negative in terms of the super generalized Marcum Q-functions compactly, we can give some explicit, compact, closed-form results for the error performance of QFRs for a variety of coherent, differentially coherent, partially coherent, and quadratic detections.

Bibliography

[1] J. G. Proakis, *Digital Communications*, 4th ed. New York, NY: McGraw-Hill, 2001.

[2] G. J. Foschini and M. J. Gans, "On limits of wireless communications in a fading environment when using multiple antennas," *Wireless Personal Commun.*, vol. 6, no. 3, pp. 311–335, Mar. 1998.

[3] I. E. Telatar, "Capacity of multi-antenna Gaussian channels," *European Trans. on Telecommun.*, vol. 10, no. 6, pp. 585–595, Nov./Dec. 1999.

[4] B. Vucetic and J. Yuan, *Space–Time Coding*. New York: John Wiley & Sons, Inc., 2003.

[5] M. K. Simon and M.-S. Alouini, *Digital Communication over Fading Channels: A Unified Approach to Performance Analysis*, 2nd ed. Hoboken, NJ: John Wiley & Sons, Inc., 2004.

[6] V. Tarokh, N. Seshadri, and A. R. Calderbank, "Space–time codes for high data rate wireless communications: Perfrmance criterion and code construction," *IEEE Trans. Inform. Theory*, vol. 44, no. 2, pp. 744–765, Mar. 1998.

[7] V. Tarokh, H. Jafarkhani, and A. R. Calderbank, "Space–time block codes from orthogonal designs," *IEEE Trans. Inform. Theory*, vol. 45, no. 5, pp. 1456–1467, July 1999.

[8] T. L. Marzetta, "Blast training: Estimating channel characteristics for high-capacity space-time wireless," in *Proc. 37th Annual Allerton Conf. on Commun., Control, and Computing*, Monticello, IL, Sept. 22–24, 1999, pp. 958–966.

[9] B. Hassibi and B. M. Hochwald, "How much training is needed in multiple-antenna wireless links?" *IEEE Trans. Inform. Theory*, vol. 49, no. 4, pp. 951–963, Apr. 2003.

[10] P. Dayal, M. Brehler, and M. K. Varanasi, "Leveraging coherent space–time codes for noncoherent communication via training," *IEEE Trans. Inform. Theory*, vol. 50, no. 9, pp. 2058–2080, Sept. 2004.

[11] P. Garg, R. K. Mallik, and H. M. Gupta, "Performance analysis of space–time coding with imperfect channel estimation," *IEEE Trans. Wireless Commun.*, vol. 4, no. 1, pp. 257–265, Jan. 2005.

[12] G. Taricco and E. Biglieri, "Space–time decoding with imperfect channel estimation," *IEEE Trans. Wireless Commun.*, vol. 4, no. 4, pp. 1874–1888, July 2005.

[13] P. Y. Kam and C. H. Teh, "Reception of PSK signals over fading channels via quadrature amplitude estimation," *IEEE Trans. Commun.*, vol. 31, no. 8, pp. 1024–1027, Aug. 1983.

[14] ——, "An adaptive receiver with memory for slowly fading channels," *IEEE Trans. Commun.*, vol. 32, no. 6, pp. 654–659, June 1984.

[15] P. Y. Kam, "Maximum likelihood carrier phase recovery for linear suppressed-carrier digital data modulations," *IEEE Trans. Commun.*, vol. 34, no. 6, pp. 522–527, June 1986.

[16] ——, "Optimal detection of digital data over the nonselective Rayleigh fading channel with diversity reception," *IEEE Trans. Commun.*, vol. 39, no. 2, pp. 214–219, Feb. 1991.

[17] V. Tarokh and H. Jafarkhani, "A differential detection scheme for transmit diversity," *IEEE J. Select. Areas Commun.*, vol. 18, no. 7, pp. 1169–1174, July 2000.

[18] B. L. Hughes, "Differential space–time modulation," *IEEE Trans. Inform. Theory*, vol. 46, pp. 2567–2578, Nov. 2000.

[19] B. M. Hochwald and W. Sweldens, "Differential unitary space–time modulation," *IEEE Trans. Commun.*, vol. 48, no. 12, pp. 2041–2052, Dec. 2000.

[20] M. Schwartz, W. R. Bennett, and S. Stein, *Communication Systems and Techniques*, IEEE Press ed. New York, NY: IEEE, Inc., 1996.

[21] B. M. Hochwald and T. L. Marzetta, "Unitary space–time modulation for multiple–antenna communications in Rayleigh flat fading," *IEEE Trans. Inform. Theory*, vol. 46, no. 2, pp. 543–564, Mar. 2000.

[22] S. Stein, "Unified analysis of certain coherent and noncoherent binary communications systems," *IEEE Trans. Inform. Theory*, vol. 10, no. 1, pp. 43–51, Jan. 1964.

[23] P. Y. Kam, "Tight bounds on Rician-type error probabilities and some applications," *IEEE Trans. Commun.*, vol. 42, no. 12, pp. 3119–3128, Dec. 1994.

[24] P. A. Bello and B. D. Nelin, "Predetection diversity combining with selectively fading channels," *IRE Trans. Commun. Systems*, vol. 10, pp. 32–42, Mar. 1962.

[25] P. A. Bello, "Binary error probabilities over selectively fading channels containing specular components," *IEEE Trans. Commun. Technol.*, vol. 14, no. 4, pp. 400–406, Aug. 1966.

[26] G. D. Hingorani, "Error rates for a class of binary receivers," *IEEE Trans. Commun. Technol.*, vol. 15, no. 2, pp. 209–215, Apr. 1967.

[27] J. G. Proakis, "On the probability of error for multichannel reception of binary signals," *IEEE Trans. Commun. Technol.*, vol. 16, no. 1, pp. 68–71, Feb. 1968.

[28] K. H. Biyari and W. C. Lindsey, "Statistical distributions of Hermitian quadratic forms in complex Gaussian variables," *IEEE Trans. Inform. Theory*, vol. 39, no. 3, pp. 1076–1082, May 1993.

[29] J. K. Cavers, "Analysis of the error performance of trellis-coded modulations in Rayleigh-fading channels," *IEEE Trans. Commun.*, vol. 40, no. 1, pp. 74–83, Jan. 1992.

[30] R. Price, "Some non-central F-distributions expressed in closed form," *Biometrika*, vol. 51, no. 1/2, pp. 107–122, June 1964.

[31] M. K. Simon and M.-S. Alouini, "A unified approach to the probability of error for noncoherent and differentially coherent modulations over generalized fading channels," *IEEE Trans. Commun.*, vol. 46, no. 12, pp. 1625–1638, Dec. 1998.

[32] D. A. Shnidman, "Two noncentral chi-square generalizations," *IEEE Trans. Inform. Theory*, vol. 42, no. 1, pp. 283–285, Jan. 1996.

[33] M. K. Simon and M.-S. Alouini, "On the difference of two chi-square variates with application to outage probability computation," *IEEE Trans. Commun.*, vol. 49, no. 11, pp. 1946–1954, Nov. 2001.

[34] G. L. Turin, "The characteristic function of Hermitian quadratic forms in complex normal variables," *Biometrika*, vol. 47, no. 1/2, pp. 199–201, June 1960.

[35] M. J. Barrett, "Error probability for optimal and suboptimal quadratic receivers in rapid Rayleigh fading channels," *IEEE J. Select. Areas Commun.*, vol. 5, no. 2, pp. 302–304, Feb. 1987.

[36] D. Raphaeli, "Distribution of noncentral indefinite quadratic forms in complex normal variables," *IEEE Trans. Inform. Theory*, vol. 42, no. 3, pp. 1002–1007, May 1996.

[37] M. Brehler and M. K. Varanasi, "Asymptotic error probability analysis of quadratic receivers in Rayleigh-fading channels with applications to a unified analysis of coherent and noncoherent space–time receivers," *IEEE Trans. Inform. Theory*, vol. 47, no. 6, pp. 2383–2399, Sept. 2001.

[38] C. B. Peel and A. L. Swindlehurst, "Performance of space–time modulation for a generalized time-varying Rician channel model," *IEEE Trans. Wireless Commun.*, vol. 3, no. 3, pp. 1003–1012, May 2004.

[39] A. M. Mathai and S. B. Provost, *Quadratic Forms in Random Variables: Theory and Applications*. New York: Marcel Dekker, Inc, 1992.

[40] J. M. Wozencraft and I. M. Jacobs, *Principles of Communication Engineering*. New York, NY: John Wiley & Sons, Inc., 1965.

[41] P. Y. Kam, "Binary orthogonal signaling over the Gaussian channel with unknown phase/fading: New results and interpretations," *IEEE Trans. Commun.*, vol. 38, no. 10, pp. 1686–1692, Oct. 1990.

[42] P. Y. Kam, P. Sinha, and Y. K. Some, "Generalized quadratic receivers for orthogonal signals over the Gaussian channel with unknown phase/fading," *IEEE Trans. Commun.*, vol. 43, no. 6, pp. 2050–2059, June 1995.

[43] S. M. Alamouti, "A simple transmit diversity technique for wireless communications," *IEEE J. Select. Areas Commun.*, vol. 16, no. 8, pp. 1451–1458, Oct. 1998.

[44] V. Tarokh, A. Naguib, N. Seshadri, and A. R. Calderbank, "Space–time codes for high data rate wireless communications: Performance criterion in the presence of channel estimation errors, mobility, and multiple paths," *IEEE Trans. Commun.*, vol. 47, no. 2, pp. 199–207, Feb. 1999.

[45] T. L. Marzetta and B. M. Hochwald, "Capacity of a mobile multiple antenna communication link in Rayleigh flat fading," *IEEE Trans. Inform. Theory*, vol. 45, no. 1, pp. 139–157, Jan. 1999.

[46] L. Zheng and D. N. C. Tse, "Diversity and multiplexing: A fundamental tradeoff in multiple-antenna channels," *IEEE Trans. Inform. Theory*, vol. 49, no. 5, pp. 1073–1096, May 2003.

[47] H. Yao and G. W. Wornell, "Structured space-time block codes with optimal diversity-multiplexing tradeoff and minimum delay," in *Proc. IEEE Global Telecommun. Conf.*, vol. 4, San Francisco, CA, USA, Dec. 1–5, 2003, pp. 1941–1945.

[48] R. Narasimhan, A. Ekbal, and J. M. Cioffi, "Finite-SNR diversity-multiplexing tradeoff of space-time codes," in *Proc. IEEE Intern. Conf. on Commun.*, vol. 1, Seoul, Korea, May 16–20, 2005, pp. 458–462.

[49] P. Elia, K. R. Kumar, S. A. Pawar, P. V. Kumar, and L. Hsiao-feng, "Explicit space-time codes that achieve the diversity-multiplexing gain tradeoff," in *Proc. IEEE Intern. Symposium on Inform. Theory*, Adelaide, Australia, Sept. 4–9, 2005, pp. 896–900.

[50] R. Vaze and B. S. Rajan, "On space-time trellis codes achieving optimal diversity multiplexing tradeoff," in *Proc. IEEE Intern. Conf. on Commun.*, vol. 3, Istanbul, Turkey, June 11–15, 2006, pp. 1277–1282.

[51] C. Shan, P. Y. Kam, and A. Nallanathan, "On the performance of space-time block coded systems with channel estimation," in *Proc. IEEE Veh. Technol. Conf.*, Los Angeles, CA, USA, Sept. 26–29, 2004, pp. 2439–2443.

[52] ——, "Theoretical performance of space-time block coded systems with channel estimation," in *Proc. IEEE Global Telecommun. Conf.*, Dallas, Texas, USA, Nov. 29–Dec. 3, 2004, pp. 3666–3670.

[53] ——, "A symbol-by-symbol channel estimation receiver for space-time block coded systems and its performance analysis," *IEEE Trans. Commun.*, accepted for publication.

[54] B. M. Hochwald, T. L. Marzetta, T. J. Richardson, W. Sweldens, and R. Urbanke, "Systematic design of unitary space–time constellations," *IEEE Trans. Inform. Theory*, vol. 46, no. 6, pp. 1962–1973, Sept. 2000.

[55] B. M. Hochwald, T. L. Marzetta, and B. Hassibi, "Space–time autocoding," *IEEE Trans. Inform. Theory*, vol. 47, no. 7, pp. 2761–2781, Nov. 2001.

[56] T. L. Marzetta, B. Hassibi, and B. M. Hochwald, "Space–time autocoding constellations with pairwise-independent signals," in *Proc. IEEE Intern. Symposium on Inform. Theory*, Washington, D.C., June 24–29, 2001, p. 326.

[57] ——, "Structured unitary space–time autocoding constellations," *IEEE Trans. Inform. Theory*, vol. 48, no. 4, pp. 942–950, Apr. 2002.

[58] N. Chiurtu and T. L. Marzetta, "Random coding exponents for unitary space–time modulation," in *Proc. IEEE Intern. Symposium on Inform. Theory*, Lausanne Switzerland, June 30–July 5, 2002, p. 301.

[59] H. feng Lu, Y. Wang, P. V. Kumar, and K. M. Chugg, "Remarks on space–time codes including a new lower bound and an improved code," *IEEE Trans. Inform. Theory*, vol. 49, no. 10, pp. 2752–2757, Oct. 2003.

[60] J. W. Craig, "A new, simple and exact result for calculating the probability of error for two-dimensional signal constellations," in *Proc. IEEE Military Commun. Conf.*, vol. 2, McLean, VA, Nov. 4–7, 1991, pp. 571–575.

[61] D. Agrawal, T. J. Richardson, and R. Urbanke, "Multiple-antenna signal constellations for fading channels," *IEEE Trans. Inform. Theory*, vol. 47, no. 6, pp. 2618–2626, Sept. 2001.

[62] J. R. Guangyue Han, "A numerical approach for designing unitary space time codes with large diversity product and diversity sum," in *Proc. IEEE Intern. Symposium on Inform. Theory*, June 29–July 4, 2003, p. 178.

[63] M. L. McCloud, M. Brehler, and M. K. Varanasi, "Signal design and convolutional coding for noncoherent space–time communication on the block-Rayleigh-fading channel," *IEEE Trans. Inform. Theory*, vol. 48, no. 5, pp. 1186–1194, May 2002.

[64] Y. Jing and B. Hassibi, "Unitary space–time modulation via cayley transform," *IEEE Trans. Signal Processing*, vol. 51, no. 11, pp. 2891–2904, Nov. 2003.

[65] V. Tarokh and K. Il-Min, "Existence and construction of noncoherent unitary space–time codes," *IEEE Trans. Inform. Theory*, vol. 48, no. 12, pp. 3112–3117, Dec. 2002.

[66] W. Zhao, G. Leus, and G. B. Giannakis, "Algebraic design of unitary space–time constellations," in *Proc. IEEE Intern. Conf. on Commun.*, vol. 5, Anchorage, Alaska, May 11–15, 2003, pp. 3180–3184.

[67] ——, "Orthogonal design of unitary constellations for uncoded and trellis-coded noncoherent space–time systems," *IEEE Trans. Inform. Theory*, vol. 50, no. 6, pp. 1319–1327, June 2004.

[68] B. Hassibi and M. Khorrami. (2000, Oct.) Fully-diverse multiple-antenna signal constellations and fixed-point-free Lie groups. lie.pdf. Bell Laboratories, Lucent Technologies. 600 Mountain Avenue, Murray Hill, NJ 07974. [Online]. Available: http://mars.bell-labs.com/cm/ms/what/mars/papers/lie/

[69] E. G. Larsson, "Unitary nonuniform space–time constellations for the broadcast channel," *IEEE Commun. Lett.*, vol. 7, no. 1, pp. 21–23, Jan. 2003.

[70] Y. Wu, K. Ruotsalainen, and M. Juntti, "A novel design of unitary space-time constellations," in *Proc. IEEE Intern. Conf. on Commun.*, vol. 2, Seoul, Korea, May 16–20, 2005, pp. 825–829.

[71] J. Wang and X. Wang, "Optimum design of noncoherent cayley unitary space-time codes," *IEEE Trans. Wireless Commun.*, vol. 5, no. 7, pp. 1942–1951, July 2006.

[72] G. Han and J. Rosenthal, "Geometrical and numerical design of structured unitary space–time constellations," *IEEE Trans. Inform. Theory*, vol. 52, no. 8, pp. 3722–3735, Aug. 2006.

[73] C. B. Peel and A. L. Swindlehurst, "Effective SNR for space–time modulation over a time–varying Rician channel," *IEEE Trans. Commun.*, vol. 52, no. 1, pp. 17–23, Jan. 2004.

[74] B. L. Hughes, "Optimal space–time constellations from groups," *IEEE Trans. Inform. Theory*, vol. 49, no. 2, pp. 401–410, Feb. 2003.

[75] A. Shokrollahi, B. Hassibi, B. Hochwald, and W. Sweldens, "Representation theory for high-rate multiple-antenna code design," *IEEE Trans. Inform. Theory*, vol. 47, no. 6, pp. 2335–2367, Sept. 2001.

[76] A. Shokrollahi, "Design of unitary space–time codes from representations of SU(2)," in *Proc. IEEE Intern. Symposium on Inform. Theory*, June 24–29, 2001, p. 241.

[77] ——, "Computing the performance of unitary space–time group codes from their character table," *IEEE Trans. Inform. Theory*, vol. 48, no. 6, pp. 1355–1371, June 2002.

[78] K. L. Clarkson, W. Sweldens, and A. Zhang, "Fast multiple-antenna differential decoding," *IEEE Trans. Commun.*, vol. 49, no. 2, pp. 253–261, Feb. 2001.

[79] B. Bhukania and P. Schniter, "Decision-feedback detection of differential unitary space–time modulation in fast Rayleigh-fading channels," in *Proc. IEEE Allerton Conf. on Commun., Control, and Computing*, Monticello, Illinois, Oct. 2002.

[80] R. Schober and L. H.-J. Lampe, "Noncoherent receivers for differential space–time modulation," *IEEE Trans. Commun.*, vol. 50, no. 5, pp. 768–777, May 2002.

[81] B. Hassibi and B. Hochwald, "Cayley differential unitary space–time codes," *IEEE Trans. Inform. Theory*, vol. 48, no. 6, pp. 1485–1503, June 2002.

[82] D. Warrier and U. Madhow, "Spectrally efficient noncoherent communication," *IEEE Trans. Inform. Theory*, vol. 48, no. 3, pp. 651–668, Mar. 2002.

[83] J. Wang, M. P. Fitz, and K. Yao, "Differential unitary space–time modulation for a large number of receive antennas," in *Conference Record of the Thirty-Sixth Asilomar Conference on Signals, Systems and Computers*, vol. 1, Nov. 3–6, 2002, pp. 565–569.

[84] J. Wang and K. Yao, "Differential unitary space-time-frequency coding for MIMO OFDM systems," in *Conference Record of the Thirty-Sixth Asilomar Conference on Signals, Systems and Computers*, vol. 2, Nov. 3–6, 2002, pp. 1867–1871.

[85] J. Wang, M. K. Simon, and K. Yao, "On the optimum design of differential unitary space–time modulation," in *Proc. IEEE Global Telecommun. Conf.*, vol. 4, Dec. 1–5, 2003, pp. 1968–1972.

[86] ——, "On the optimum design of unitary cyclic group space–time codes," *IEEE Trans. Commun.*, vol. 52, no. 5, pp. 706–710, May 2004.

[87] X.-B. Liang and X.-G. Xia, "Unitary signal constellations for differential space–time modulation with two transmit antennas: Parametric codes, optimal designs and bounds," *IEEE Trans. Inform. Theory*, vol. 48, no. 8, pp. 2291–2322, Aug. 2002.

[88] H. Wang, G. Wang, and X.-G. Xia, "A design of 2 by 2 unitary space–time codes from sphere packing theory with optimal diversity product of code size 6," in *Proc. IEEE Intern. Symposium on Inform. Theory*, June 29–July 4, 2003, p. 104.

[89] T. Konishi, "Unitary subgroup space–time codes using Bruhat decomposition and Weyl groups," *IEEE Trans. Inform. Theory*, vol. 49, no. 10, pp. 2713–2716, Oct. 2003.

[90] Y. Jing and B. Hassibi, "Design of fully-diverse multi-antenna codes based on Sp(2)," in *Proc. IEEE Intern. Conf. on Acoustics, Speech, and Signal Processing*, vol. 4, Apr. 6–10, 2003, pp. 33–36.

[91] Z. Du and J. Zhu, "Improved differential unitary space–time codes with multiple amplitude modulation," in *Proc. IEEE Veh. Technol. Conf.*, vol. 2, Apr. 22–25, 2003, pp. 1104–1108.

[92] C. Ling, K. H. Li, A. C. Kot, and Q. T. Zhang, "Multisampling decision-feedback linear prediction receivers for differential space–time modulation over Rayleigh fast-fading channels," *IEEE Trans. Commun.*, vol. 51, no. 7, pp. 1214–1223, July 2003.

[93] C. Ling, K. Li, and A. C. Kot, "Noncoherent sequence detection of differential space–time modulation," *IEEE Trans. Inform. Theory*, vol. 49, no. 10, pp. 2727–2734, Oct. 2003.

[94] C. B. Peel and A. L. Swindlehurst, "Pairwise probability of error for differential space–time modulation over a time-varying Rician channel," in *Proc. IEEE Intern. Conf. on Commun.*, vol. 4, May 11–15, 2003, pp. 2698–2702.

[95] C. Shan, A. Nallanathan, and P. Y. Kam, "A new class of signal constellations for differential unitary space–time modulation (DUSTM)," *IEEE Commun. Lett.*, vol. 8, no. 1, pp. 1–3, Jan. 2004.

[96] B. Bhukania and P. Schniter, "On the robustness of decision-feedback detection of DPSK and differential unitary space–time modulation in Rayleigh-fading channels," *IEEE Trans. Wireless Commun.*, vol. 3, no. 5, pp. 1481–1489, Sept. 2004.

[97] A. L. Moustakas, S. H. Simon, and T. L. Marzetta, "Capacity of differential versus nondifferential unitary spacectime modulation for MIMO channels," *IEEE Trans. Inform. Theory*, vol. 52, no. 8, pp. 3622–3634, Aug. 2006.

[98] H. Jafarkhani and V. Tarokh, "Multiple transmit antenna differential detection from generalized orthogonal designs," *IEEE Trans. Commun.*, vol. 47, no. 6, pp. 2626–2631, Sept. 2001.

[99] G. Ganesan and P. Stoica, "Differential modulation using space-time block codes," *IEEE Signal Processing Lett.*, vol. 9, no. 2, pp. 57–60, Feb. 2002.

[100] X. Shao and J. Yuan, "A new differential space-time block coding scheme," *IEEE Commun. Lett.*, vol. 7, no. 9, pp. 437–439, Sept. 2003.

[101] C. Hwang, S. H. Nam, J. Chung, and V. Tarokh, "Differential space time block codes using nonconstant modulus constellations," *IEEE Trans. Signal Processing*, vol. 51, no. 11, pp. 2955–2964, Nov. 2003.

[102] Z. Liu, G. B. Giannakis, and B. L. Hughes, "Double differential space-time block coding for time-selective fading channels," *IEEE Trans. Commun.*, vol. 49, no. 9, pp. 1529–1539, Sept. 2001.

[103] J. I. Marcum, "A statistical theory of target detection by pulsed radar," *IEEE Trans. Inform. Theory*, vol. IT-6, pp. 59–267, Apr. 1960.

[104] ——, "Table of Q functions," Rand Corporation, Santa Monica, CA, ASTIA Document AD 1165451, Jan. 1950.

[105] D. A. Shnidman, "Evaluation of the Q function," *IEEE Trans. Commun.*, vol. 22, no. 3, pp. 342–346, Mar. 1974.

[106] ——, "Efficient evaluation of probabilities of detection and the generalized Q-function," *IEEE Trans. Inform. Theory*, vol. IT-22, pp. 746–751, Nov. 1976.

[107] S. Parl, "A new method of calculating the generalized Q function," *IEEE Trans. Inform. Theory*, vol. IT-26, pp. 121–124, Jan. 1980.

[108] P. E. Cantrell, "On the calculation of the generalized Q function via Parls method," *IEEE Trans. Inform. Theory*, vol. IT-32, pp. 817–824, Nov. 1986.

[109] P. E. Cantrell and A. K. Ojha, "Comparison of generalized Q-function algorithms," *IEEE Trans. Inform. Theory*, vol. IT-33, pp. 591–596, July 1987.

[110] D. A. Shnidman, "The calculation of the probability of detection and the generalized Marcum Q-function," *IEEE Trans. Inform. Theory*, vol. 35, pp. 389–400, Mar. 1989.

[111] ——, "Note on "The calculation of the probability of detection and the generalized Marcum Q-function"," *IEEE Trans. Inform. Theory*, vol. 37, p. 1233, July 1991.

[112] C. W. Helstrom, "Computing the generalized Marcum Q-function," *IEEE Trans. Inform. Theory*, vol. 38, pp. 1422–1428, July 1992.

[113] ——, *Elements of Signal Detection and Estimation.* Englewood Cliffs, NJ: Prentice-Hall, 1995.

[114] M. K. Simon, "A new twist on the Marcum Q-function and its application," *IEEE Commun. Lett.*, vol. 2, no. 2, pp. 39–41, Feb. 1998.

[115] R. F. Pawula, "A new formula for MDPSK symbol error probability," *IEEE Commun. Lett.*, vol. 2, pp. 271–272, Oct. 1998.

[116] M. Chiani, "Integral representation and bounds for Marcum Q-function," *IEEE Electronics Lett.*, vol. 35, no. 6, pp. 445–446, Mar. 1999.

[117] M. K. Simon and M.-S. Alouini, "A unified performance analysis of digital communication with dual selective combining diversity over correlated Rayleigh and Nakagami-m fading channels," *IEEE Trans. Commun.*, vol. 47, no. 1, pp. 33–43, Jan. 1999.

[118] S. Gaur and A. Annamalai, "Some integrals involving the $Q_m(a\sqrt{x}, b\sqrt{x})$ with application to error probability analysis of diversity receivers," *IEEE Trans. Veh. Technol.*, vol. 52, no. 6, pp. 1568–1575, Nov. 2003.

[119] A. Annamalai, C. Tellambura, and V. K. Bhargava, "A general method for calculating error probabilities over fading channels," *IEEE Trans. Commun.*, vol. 53, no. 5, pp. 841–852, May 2005.

[120] M. K. Simon and M.-S. Alouini, "Exponential-type bounds on the generalized Marcum Q-function with application to error probability analysis over fading channels," *IEEE Trans. Commun.*, vol. 48, no. 3, pp. 359–366, Mar. 2000.

[121] A. Annamalai and C. Tellambura, "Cauchy-schwarz bound on the generalized Marcum Q-function," *Wirel. Commun. Mob. Comput.*, vol. 1, pp. 243–253, 2001.

[122] G. E. Corazza and G. Ferrari, "New bounds for the Marcum Q-function," *IEEE Trans. Inform. Theory*, vol. 48, pp. 3003–3008, Nov. 2002.

[123] M.-K. Byun and B. G. Lee, "New bounds of pairwise error probability for space–time codes in Rayleigh fading channels," in *Proc. IEEE Wireless Commun. and Networking Conf.*, vol. 1, Mar. 17–21, 2002, pp. 89–93.

[124] I. S. Gradshteyn and I. M. Ryzhik, *Table of Integrals, Series, and Products*, 5th ed. Academic Press, Inc., 1994.

[125] C. D. Meyer, *Matrix Analysis and Applied Linear Algebra*. Philadelphia: Society for Industrial and Applied Mathematics, 2000.

[126] P. Garg, R. K. Mallik, and H. M. Gupta, "Exact error performance of square orthogonal space–time block coding with channel estimation," *IEEE Trans. Commun.*, vol. 54, no. 3, pp. 430–437, Mar. 2006.

[127] B. Farhang-Boroujeny, *Adaptive Filters Theory and Applications*. New York, NY: John Wiley & Sons, Inc., 1998, ch. 3.

[128] W. C. Jakes, *Microwave Mobile Communications*. Piscataway, NJ: IEEE Press, 1993.

[129] P. Y. Kam, "New, upper and lower expotential bounds on the generalized Marcum Q-function and some applications," in *Proc. Second Int. Conf. on Inform., Commun., and Signal Processing*, Singapore, 1999.

[130] E. Kreyszig, *Advanced Engineering Mathematic*, 7th ed. New York: Wiley, 1993.

[131] M. Chiani, D. Dardari, and M. K. Simon, "New exponential bounds and approximations for the computation of error probability in fading channels," *IEEE Trans. Wireless Commun.*, vol. 2, no. 4, pp. 840–845, July 2003.

[132] W. C. Lindsey, "Error probabilities for Rician fading multichannel reception of binary and n-ary signals," *IEEE Trans. Inform. Theory*, vol. 10, no. 4, pp. 339–350, Oct. 1964.

[133] C. H. Ong, "Computation and simulation of bounds on Marcum's Q-function," B. Eng. thesis, National University of Singapore, Singapore, 2003/04, supervised by P. Y. Kam.

[134] P. Y. Kam and R. Li, "A new geometric view of the first-order Marcum Q-function and some simple tight erfc-bounds," in *Proc. IEEE Veh. Technol. Conf.*, vol. 5, Melbourne, Australia, May 7–10, 2006, pp. 2553–2557.

[135] N. C. Beaulieu, "A useful integral for wireless communication theory and its application to rectangular signaling constellation error rates," *IEEE Trans. Commun.*, vol. 54, no. 5, pp. 802–805, May 2006.

[136] E. J. Wegman. (2003) Geometric methods in statistics. Center for Computational Statistics, George Mason University. Fairfax, VA 22030-4444. [Online]. Available: http://www.galaxy.gmu.edu/stats/syllabi/csi877/Geowithpics.pdf

[137] D. M. Y. Sommerville, *An Introduction to the Geometry of N Dimensions*. New York: Dover Publications, Inc., 1958.

[138] H. Ruben, "Probability content of regions under spherical normal distribution, I," *Ann. Math. Stat.*, vol. 31, no. 3, pp. 598–618, Sept. 1960.

[139] E. W. Weisstein. Ball. MathWorld–A Wolfram Web Resource. [Online]. Available: http://mathworld.wolfram.com/Ball.html

[140] V. V. Prasolov and V. M. Tikhomirov, *Geometry*. Providence, Rhode Island: American Mathematical Society, 2001, vol. 200.

[141] E. W. Weisstein. Spherical sector. MathWorld–A Wolfram Web Resource. [Online]. Available: http://mathworld.wolfram.com/SphericalSector.html

[142] ——. Spherical shell. MathWorld–A Wolfram Web Resource. [Online]. Available: http://mathworld.wolfram.com/SphericalShell.html

[143] M. K. Simon and M.-S. Alouini, "Some new results for integrals involving the generalized Marcum Q function and their application to performance evaluation over fading channels," *IEEE Trans. Wireless Commun.*, vol. 2, no. 4, pp. 611–615, July 2003.

[144] H. Ruben, "Probability content of regions under spherical normal distribution, IV: The distribution of homogeneous and non-homogeneous quadratic functions of normal variables," *Ann. Math. Stat.*, vol. 33, no. 2, pp. 542–570, June 1962.

[145] ——, "A new result on the distribution of quadratic forms," *Ann. Math. Stat.*, vol. 34, no. 4, pp. 1582–1584, Dec. 1963.

[146] S. J. Press, "Linear combinations of non-central chi-square variates," *Ann. Math. Stat.*, vol. 37, no. 2, pp. 480–487, Apr. 1966.

[147] A. Castaño-Martínez and F. López-Blázquez, "Distribution of a sum of weighted noncentral chi-square variables," *Test*, vol. 14, no. 2, pp. 397–415, 2005.

List of Publications

[1] R. Li and P. Y. Kam, "New tight bounds on the pairwise error probability for unitary space-time modulations," *IEEE Commun. Lett.*, vol. 9, no. 4, pp. 289–291, Apr. 2005.

[2] ——, "Averages of the product of two Gaussian Q-functions over fading statistics and applications," *IEEE Commun. Lett.*, vol. 11, no. 1, pp. 58–60, Jan. 2007.

[3] ——, "Generalized quadratic receivers for unitary space–time modulation over Rayleigh fading channels," *IEEE Trans. Commun.*, vol. 55, no. 10, Oct. 2007.

[4] P. Y. Kam and R. Li, "Computing and bounding the first-order Marcum Q-function—a geometric approach," *IEEE Trans. Commun.*, to be published.

[5] R. Li and P. Y. Kam, "Computing and bounding the generalized Marcum Q-function—a geometric approach," *IEEE Trans. Commun.*, submitted for publication.

[6] ——, "New expression and bounds for the average bit error probability of quadratic-form receivers over fading channels," *IEEE Commun. Lett.*, submitted for publication.

[7] R. Li, "Effect of array configuration on multiuser diversity with opportunistic beamforming," in *Proc. IEEE Veh. Technol. Conf.*, Dallas, Texas, USA, Sept. 25–28, 2005, pp. 598–602.

[8] R. Li and P. Y. Kam, "Generalized quadratic receivers for unitary space–time constellations with orthogonal design over Rayleigh fading channels," in *Proc. IEEE Global Telecommun. Conf.*, St. Louis, Missouri, USA, Nov. 28–Dec. 2, 2005, session CT17.5.

[9] P. Y. Kam and R. Li, "A new geometric view of the first-order Marcum Q-function and some simple tight erfc-bounds," in *Proc. IEEE Veh. Technol. Conf.*, vol. 5, Melbourne, Australia, May 7–10, 2006, pp. 2553–2557.

[10] R. Li and P. Y. Kam, "Generalized quadratic receivers for orthogonal and nonorthogonal unitary space–time constellations over Rayleigh fading channels," in *Proc. IEEE Intern. Conf. on Commun.*, vol. 3, Istanbul, Turkey, June 11–15, 2006, pp. 1427–1432.

[11] P. Y. Kam and R. Li, "Simple tight exponential bounds on the first-order Marcum Q-function via the geometric approach," in *Proc. IEEE Intern. Symposium on Inform. Theory*, Seattle, Washington, USA, July 9–14, 2006, session 2.3.8.

[12] R. Li and P. Y. Kam, "Computing and bounding the generalized Marcum Q-function via a geometric approach," in *Proc. IEEE Intern. Symposium on Inform. Theory*, Seattle, Washington, USA, July 9–14, 2006, session 2.3.8.

[13] P. Y. Kam and R. Li, "Generic exponential bounds and erfc-bounds on the Marcum Q-function via the geometric approach," in *Proc. IEEE Global Telecommun. Conf.*, San Francisco, California, USA, Nov. 27–Dec. 1, 2006, session WLC10-1.

[14] R. Li and P. Y. Kam, "Generic exponential bounds on the generalized Marcum Q-function via the geometric approach," in *Proc. IEEE Global Telecommun. Conf.*, Washington, D.C., USA, Nov. 26–30, 2007.